Studies on Stereochemistry, Spectroscopy, and Catalytic Reactivity of Rhenium(V) Complexes with Asymmetrical Ligands

Tetuya Ohashi
(Doctoral Program in Chemistry)

Submitted to the Graduate School of
Pure and Applied Sciences
in Partial Fulfillment of the Requirements
for the Degree of Doctor of Philosophy in
Science

at the
University of Tsukuba

Contents

Chapter I. General Introduction

Rhenium ([Xe]$6s^2 5d^5$), which is named for the river Rhine, occurs in very low abundance (0.7 ppb) in the crust of the earth. Moreover, rhenium is the last stable elements, which was discovered in 1925. The chemistry of rhenium, which lies in the boundary between early period and late period and spans the oxidation state from -I to +VII, has been investigated actively since 1960s (Schemes I-1 and I-2).[1] In rhenium(I), many organometallic complexes have been reported.[2,3] In particular, $[Re^{I}X(CO)_3(L)]$ type tricarbonyl complexes (X = halide ion, L = 2,2'-bipyridine derivatives) have gotten much attention from the standpoint of the catalysts for the reduction of CO_2 to CO both photochemically and electrochemically (Scheme I-1 (a)).[4,5] In rhenium(III), a large number of mononuclear octahedral complexes have been reported.[6] It also forms dinuclear complexes having metal–metal multiple bonds such as a quadruple bond[7] (b) and trinuclear (c) or hexanuclear cluster compounds (d).[8] Since 1999, the hexarhenium(III) clusters, $[Re^{III}_6(\mu_3\text{-}E)_8(L)_6]^z$ (E = S, Se, Te; L = halide ion, CN^-, NCS^-, or σ-donor ligand), have received attention, because they show room temperature emission both in solution and in crystalline phases.[9,10] The most distinctive feature of rhenium(V) is the existence of many stable and diamagnetic complexes in which the metal forms multiple bonds to oxygen, nitrogen, or sulfur.[1,11] These complexes are mostly octahedral and contain one of the $[Re^{V}{=}O]^{3+}$, $[O{=}Re^{V}{=}O]^{+}$, $[O{=}Re^{V}{-}O{-}Re^{V}{=}O]^{4+}$, $[Re^{V}{\equiv}N]^{2+}$, $[Re^{V}{=}NR]^{3+}$, or $[Re^{V}{=}S]^{3+}$ moieties (Scheme I-2). The basic structures and spectroscopic properties of oxorhenium(V) complexes have been reported actively since the coordination chemistry of oxorhenium(V) was reported by Wilkinson et al. in 1960s.[12-15]

Scheme I-1

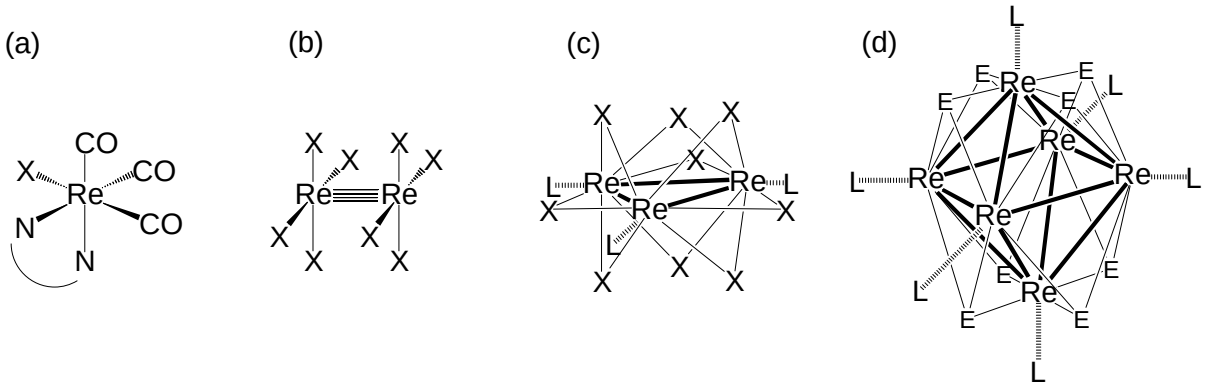

$[Re^{I}X(CO)_3(L)]$ $[X_4Re^{III}{\equiv}Re^{III}X_4]^{2-}$ $[Re^{III}_3(\mu_2\text{-}X)_9(L)_3]^z$ $[Re^{III}_6(\mu_3\text{-}E)_8(L)_6]^z$

Scheme I-2

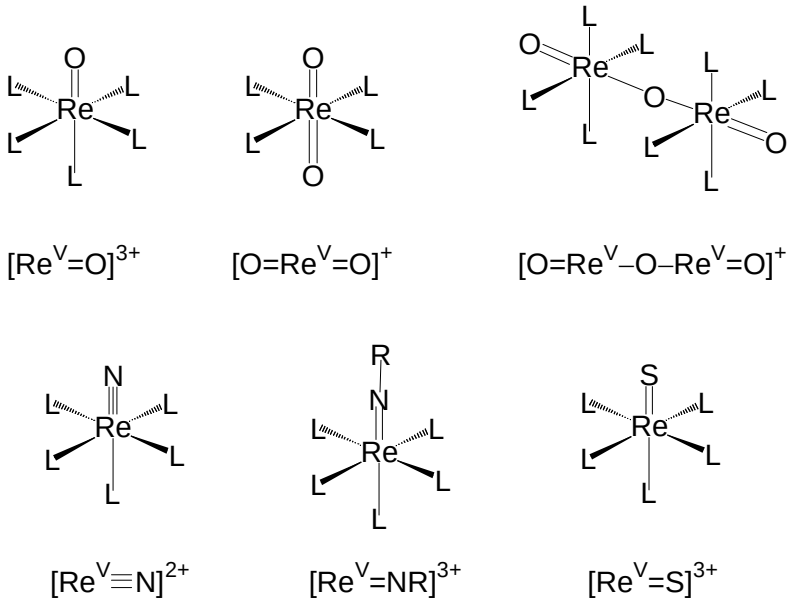

In recent years, the chemistry of rhenium complexes receives much attention from the standpoint of practical use, and it has been energetically investigated. For example, the radionuclides of rhenium are suitable for therapeutic applications, since they have high β-particle energy and short half-life (^{186}Re: β_{max} = 1.07 MeV, $t_{1/2}$ = 90 h; ^{188}Re: β_{max} = 2.12 MeV, $t_{1/2}$ = 17 h), which can target large tumors and have reasonably fast clearance from the blood and other nontarget tissues.[16,17] The fact that ^{99m}Tc (the most widely used radionuclide for diagnostic imaging in nuclear medicine) is chemical congener of rhenium makes the chemistry of both technetium and rhenium the same or near, and it adds value to $^{186/188}$Re-labeled drugs. Thus, when the chemistry of these radionuclides is similar, the ^{99m}Tc agent can be used as the "matched pair" for the corresponding $^{186/188}$Re agent. That is to say, the patients can be assessed by the excellent diagnostic imaging obtained from ^{99m}Tc agents, and the patients can be treated with therapeutic $^{186/188}$Re analogous accurately. Therefore, the coordination chemistry of rhenium is of very interest in this field. In particular, the oxorhenium(V) compounds are actively investigated for design of radiopharmaceuticals because of the convenience of handling that the oxorhenium(V) compounds are easily obtained from the reduction of perrhenate(VII) and are easily stabilized by coordinating with variety of ligands.[18-23]

Furthermore in some oxorhenium(V) or (VII) complexes, especially methylated complexes, the oxygen atom transfer (OAT) catalytic reactivity (Eq. I-1) by using the change of the oxidation number between +V and +VII is reported, and it is of interest from the viewpoint of the application for biological systems, organic synthesis, and industrial processes.[24-38] This Re(V/VII) redox system is isoelectronic with the redox system between the +IV (d^2) and +VI (d^0) oxidation state of active site of

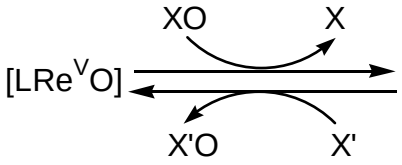

(I-1)

molybdenum or tungsten enzymes which is known for good OAT catalyst in biological systems. It is reported that the OAT catalytic property of some oxorhenium(V) complexes is much superior to that of the molybdenum[39-48] or tungsten[49-53] enzyme models. Rhenium is not an essential trace element, but modeling for the active site of molybdenum and tungsten enzymes by rhenium has received much attention because of the effecting OAT catalytic reaction from oxygen donor to tertiary phosphines.[30-33,54,55] Therefore, the study of structures and reactivity of oxorhenium(V) complexes is one of the most interesting catalysis in these OAT reactions.

Thus, so far many oxorhenium(V) complexes, which are coordinated with symmetrical didentate ligands 2,2'-bipyridine, 1,10-phenantrorine, 1,2-diol, 1,2-dithiol, etc., have been synthesized, and their structures and properties have been investigated.[31,34,55-65] Different from symmetrical didentate ligand, the introduction of the asymmetrical didentate ligands would be easy to control the coordination geometry. Accordingly, the studies of oxorhenium(V) complexes containing the asymmetrical didentate ligands are effective for the collection of meaningful data for application of oxorhenium(V) complexes to radiopharmaceutical or catalyst.

In this thesis, quinoline derivatives which have an amino, hydroxyl, or mercapto group on 8-position are used as asymmetrical didentate ligands for oxorhenium(V) complexes (Scheme I-3). The oxorhenium(V) complexes with quinoline derivatives are synthesized systematically, and their complexes are investigated for the structures, spectroscopic properties, and reactivity. Firstly, 8-aminoquinoline derivatives (8-amino-2-methylquinoline, H_2amq; 8-aminoquinoline, H_2aq) are used as asymmetrical didentate ligands. The amino group can make three types of bonding pattern (amino,[64] amide,[66,67] and imide[68,69]), when it coordinates to metal ion. The oxorhenium(V) complexes, which are coordinated by soft base ligands, alkyl or thiolate, or the ligand which makes multiple bond with metal center, prefer a five-coordination state.[47,55,70,71] Therefore, if the amino group is partially-deprotonated

Scheme I-3

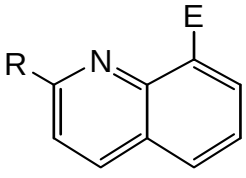

E = NH_2, R = Me; 8-amino-2-methylquinoline (H_2amq)
E = NH_2, R = H; 8-aminoquinoline (H_2aq)
E = OH, R = Me; 8-hydroxy-2-methylquinoline (Hhmq)
E = SH, R = H; 8-mercaptoquinoline (HSq)

and coordinated as amide which has multiple bonding character, it is expected that the metal center may release one ligand to be the five-coordinated state and have the vacant site which can act as a reactive site. Actually, when the aminoquinoline derivatives are reacted with oxorhenium(V) precursor [$ReOCl_3(PPh_3)_2$], the amine ligand coordinated as quinolinylamide. The quinolinylamido complexes showed release property of PPh_3 ligand as expectation. In Chapter II, by using the reactivity of the quinolinylamido complex, the monodentate ligand substituted complexes are synthesized, and the structures and spectroscopic properties of these complexes are investigated. Moreover, the application of the reactivity to OAT catalyst is attempted. In Chapter III, the catechol derivatives (catechol, H_2cat; tetrachlorocatechol, H_2Cl_4cat; tetrabromocatechol, H_2Br_4cat: Scheme I-4) instead of two chloride ions are introduced in the quinolinylamido complex for stabilizing the complex by chelate effects, and their complexes are synthesized. The quinolinylamido complexes with catecholate derivatives are also investigated for the substitution reactivity of monodentate ligands, structures, spectroscopic properties, and OAT catalytic property. In Chapter IV, the didentate-*N*,*O* ligand 8-hydroxy-2-methylquinoline (Hhmq) is chosen as an asymmetrical didentate ligand, instead of the didentate-*N*,*N* ligand H_2amq in the previous chapter. The structures and properties of the quinolinolato complexes are compared with those of the quinolinylamido complexes. The substitution reactivity of monodentate ligand and OAT catalytic reaction of the quinolinolato complexes are also attempted. In Chapter V, the oxorhenium(V) complexes with the didentate-*N*,*S* ligand 8-mercaptoquinoline (HSq) and catecholate derivatives are synthesized for comparing the properties with the corresponding quinolinylamido complexes. The quinolinethiolato complexes with catecholate derivatives are investigated for the substitution reactivity, structures, spectroscopic properties, and OAT catalytic property.

Scheme I-4

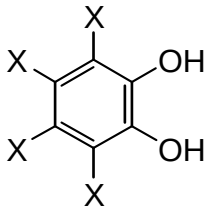

X = H; catechol (H_2cat)

X = Cl; tetrachlorocatechol (H_2Cl_4cat)

X = Br; tetrabromocatechol (H_2Br_4cat)

References

1 G. Rouschias, *Chem. Rev.*, **74**, 531 (1974).

2 M. Wrighton and D. L. Morse, *J. Am. Chem. Soc.*, **96**, 998 (1974).

3 A. T. Patton, C. E. Strouse, C. B. Knobler, and J. A. Gladysz, *J. Am. Chem. Soc.*, **105**, 5804 (1983).

4 Y. Hayashi, S. Kita, B. S. Brunschwig, and E. Fujita, *J. Am. Chem. Soc.*, **125**, 11976 (2003).

5 F. P. A. Johnson, M. W. George, F. Hartl, and J. J. Turner, *Organometallics*, **15**, 3374 (1996).

6 G. Rouschias and G. Wilkinson, *J. Chem. Soc.*, *A*, 993 (1967).

7 F. A. Cotton and R. A. Walton, Multiple Bonds Between Metal Atoms, Wiley-Interscience, New York (1982).

8 F. A. Cotton, S. J. Lippard, and J. T. Mague, *Inorg. Chem.*, **4**, 508 (1965).

9 N. Kitamura, Y. Ueda, S. Ishizuka, K. Yamada, M. Aniya, and Y. Sasaki, *Inorg. Chem.*, **44**, 6308 (2005).

10 T. G. Gray, C. M. Rudzinski, D. G. Nocera, and R. H. Holm, *Inorg. Chem.*, **38**, 5932 (1999).

11 M. Li, A. Ellern, and J. H. Espenson, *J. Am. Chem. Soc.*, **127**, 10436 (2005).

12 N. P. Johnson, C. J. L. Lock, and G. Wilkinson, *J. Chem. Soc.*, 1054 (1964).

13 N. P. Johnson, F. I. M. Taha, and G. Wilkinson, *J. Chem. Soc.*, 2614 (1964).

14 D. E. Grove and G. Wilkinson, *J. Chem. Soc.*, *A*, 1224 (1966).

15 N. P. Johnson, C. J. L. Lock, and G. Wilkinson, *Inorg. Synth.*, **9**, 145 (1967).

16 M. Gielen and E. R. T. Tiekink, Eds, Metallotherapeutic Drugs and Metal-Based Diagnostic Agents: The Use of Metals in Medicine, John Wiley & Sons, Ltd (2005)

17 W. A. Volkert and T. J. Hoffman, *Chem. Rev.*, **99**, 2269 (1999).

18 L. Hansen, R. Cini, A. J. Taylor, and L. G. Marzilli, *Inorg. Chem.*, **31**, 2801 (1992).

19 P. J. Blower, A. S. K. Lam, M. J. O'Doherty, A. G. Kettle, and F. F. Knapp Jr, *Eur. J. Nucl. Med.*, **25**, 613 (1998).

20 P. J. Blower, A. G. Kettle, M. J. O'Doherty, A. J. Coakley, and F. F. Knapp Jr, *Eur. J. Nucl. Med.*, **27**, 1405 (2000).

21 S. Prakash, M. J. Went, and P. J. Blower, *Nucl. Med. Biol.*, **23**, 543 (1996).

22 S. Guhlke, A. Schaffland, P. O. Zamora, J. Sartor, D. Diekmann, H. Bender, F. F. Knapp, and H. J. Biersack, *Nucl. Med. Biol.*, **25**, 621 (1998).

23 C.-B. Liu, G.-Z. Liu, N. Liu, Y.-M. Zhang, J. He, M. Rusckowski, and D. J. Hnatowich, *Nucl. Med. Biol.*, **30**, 207 (2003).

24 M. M. Abu-Omer and J. H. Espenson, *Inorg. Chem.*, **34**, 6239 (1995).

25 M. M. Abu-Omer, E. H. Appelman, and J. H. Espenson, *Inorg. Chem.*, **35**, 7751 (1996).

26 H. R. Tetzlaff and J. H. Espenson, *Inorg. Chem.*, **38**, 881 (1999).

27 M. D. Eager and J. H. Espenson, *Inorg. Chem.*, **38**, 2533 (1999).

28 J. H. Espenson and D. T. Y. Yiu, *Inorg. Chem.*, **39**, 4113 (2000).

29 G. Lente and J. H. Espenson, *Inorg. Chem.*, **39**, 4809 (2000).

30 R. Huang and J. H. Espenson, *Inorg. Chem.*, **40**, 994 (2001).

31 Y. Cai, A. Ellern, and J. H. Espenson, *Inorg. Chem.*, **44**, 2560 (2005).

32 Y. Wang and J. H. Espenson, *Inorg. Chem.*, **41**, 2266 (2002).

33 N. Koshino and J. H. Espenson, *Inorg. Chem.*, **42**, 5735 (2003).

34 K. A. Brittingham and J. H. Espenson, *Inorg. Chem.*, **40**, 2730 (2001).

35 A. Deloffre, S. Halut, L. Salles, J. M. Brégeault, J. R. Gregorio, B. Denise, and H. Rudler, *J. Chem. Soc., Dalton Trans.*, 2897 (1999).

36 K. P. Gable and E. C. Brown, *Organometallics*, **19**, 944 (2000).

37 J. H. Espenson, *Coord. Chem. Rev.*, **249**, 329 (2005).

38 M. J. Sabater, M. E. Domine, and A. Corma, *J. Catal.*, **210**, 192 (2002).

39 B. E. Schultz and R. H. Holm, *Inorg. Chem.*, **32**, 4244 (1993).

40 L. J. Laughlin and C. G. Young, *Inorg. Chem.*, **35**, 1050 (1996).

41 Z. Xiao, M. A. Bruck, J. H. Enemark, C. G. Young, and A. G. Wedd, *Inorg. Chem.*, **35**, 7508 (1996).

42 V. N. Nemykin and P. Basu, *Inorg. Chem.*, **44**, 7494 (2005).

43 J. P. Caradonna, P. R. Reddy, and R. H. Holm, *J. Am. Chem. Soc.*, **110**, 2139 (1988).

44 B. E. Schultz, R. Hille, and R. H. Holm, *J. Am. Chem. Soc.*, **117**, 827 (1995).

45 P. D. Smith, A. J. Millar, C. G. Young, A. Ghosh, and P. Basu, *J. Am. Chem. Soc.*, **122**, 9298 (2000).

46 B. S. Lim, M. W. Willer, M. Miao, and R. H. Holm, *J. Am. Chem. Soc.*, **123**, 8343 (2001).

47 J. P. McNamara, J. A. Joule, I. H. Hillier, and C. D. Garner, *Chem. Commun.*, 177 (2005).

48 A. J. Millar, C. J. Doonan, P. D. Smith, V. N. Nemykin, P. Basu, and C. G. Young, *Chem. Eur. J.*, **11**, 3255 (2005).

49 J.-J. Wang, O. P. Kryatova, E. V. Rybak-Akimova, and R. H. Holm, *Inorg. Chem.*, **43**, 8092 (2004).

50 J. Jiang and R. H. Holm, *Inorg. Chem.*, **44**, 1068 (2005).

51 C. Lorber, J. P. Donahue, C. A. Goddard, E. Nordlander, and R. H. Holm, *J. Am. Chem. Soc.*,

120, 8102 (1998).

52 K.-M. Sung and R. H. Holm, *J. Am. Chem. Soc.*, **123**, 1931 (2001).

53 J. J. G. Moura, C. D. Brondino, J. Trincão, and M. J. Romão, *J. Biol. Inorg. Chem*, **9**, 791 (2004).

54 J. C. Bryan, R. E. Stenkamp, T. H. Tulip, and J. M. Mayer, *Inorg. Chem.*, **26**, 2283 (1987).

55 X. Shan, A. Ellern, I. A. Guzei, and J. H. Espenson, *Inorg. Chem.*, **43**, 3854 (2004).

56 S. Fortin and A. L. Beauchamp, *Inorg. Chem.*, **39**, 4886 (2000).

57 S. Fortin and A. L. Beauchamp, *Inorg. Chem.*, **40**, 105 (2001).

58 J. H. Espenson, X. Shan, D. W. Lahti, T. M. Rockey, B. Saha, and A. Ellern, *Inorg. Chem.*, **40**, 6717 (2001).

59 M. Papachristou, I. C. Pirmettis, C. Tosukalas, D. Papagiannopoulou, C. Raptopoulou, A. Terzis, C. I. Stassinopoulou, E, Chiotellis, M. Pelecanou, and M. Papadopoulos, *Inorg. Chem.*, **42**, 5778 (2003).

60 C. F. Edwards, W. P. Griffith, A. J. P. White, and D. J. Williams, *J. Chem. Soc.*, *Dalton Trans.*, 957 (1992).

61 J. H. Jung, T. A. Albright, D. M. Hoffman, and T. R. Lee, *J. Chem. Soc.*, *Dalton Trans.*, 4487 (1999).

62 R. Chiozzone, R. González, C. Kremer, G. De Munno, and J. Faus, *Inorg. Chim. Acta*, **325**, 203 (2001).

63 H. Sugimoto and Y. Sasaki, *Chem. Lett.*, 541 (1997).

64 S. D. Orth, J. Barrera, M. Sabat, and W. D. Harman, *Inorg. Chem.*, **32**, 594 (1993).

65 J. T. Goodman, S. Inomata, and T. B. Rauchfuss, *J. Am. Chem. Soc.*, **118**, 11647 (1996).

66 M. T. Ahmet, B. Coutinho, J. R. Dilworth, J. R. Miller, S. J. Parrott, Y, Zheng, M. Harman, M. B. Hursthouse, and A. Malik, *J. Chem. Soc.*, *Dalton Trans.*, 3041 (1995).

67 G. Bandoli, A. Dolmella, T. I. A. Gerber, J. Perils, and J. G. H. du Preez, *Inorg. Chim. Acta*, **303**, 24 (2000).

68 H. Luo, I. Setyawati, S. J. Rettig, and C. Orvig, *Inorg. Chem.*, **34**, 2287 (1995).

69 G. Bandoli, T. I. A. Gerber, J. Perils, and J. G. H. du Preez, *Inorg. Chim. Acta*, **278**, 96 (1998).

70 J. Jacob, I. A. Guzei, and J. H. Espenson, *Inorg. Chem.*, **38**, 1040 (1999).

71 D. W. Lahti and J. H. Espenson, *J. Am. Chem. Soc.*, **123**, 6014 (2001).

Chapter II. Structures, Spectroscopy, and Reactivity of Rhenium(V) Complexes with Quinoline Derivatives

II-i. Introduction

At the first setout, 8-amino-2-methylquinoline (H_2amq) and 8-aminoquinoline (H_2aq), which contains two types of nitrogen donor atoms, were used as an asymmetrical didentate-*N*,*N* ligand in order to investigate the stereochemistry, spectroscopy, and reactivity of rhenium(V) complexes. This asymmetrical ligand is expected to act as the stereoselective coordination ligand, different from the case of symmetrical didentate-*N*,*N* ligands such as bipyridine and biimidazole derivatives.[1-8] Furthermore, the arylamine ligand is interesting from the viewpoint of structure and reactivity of metal center, because it can take three types of coordination modes, amine, amide, and imide, by deprotonation and it arises multiple bonding character with metal center. In the case of rhenium complexes with amine ligands, some amino, amido, and imido complexes are reported as shown in Chapter I.[8-18] $[Re^{V}O(Haq)_2(PPh_3)]BPh_4$, which was synthesized by the reaction between the oxorhenium(V) precursor $[Re^{V}OCl_3(PPh_3)_2]$ and two equiv of H_2aq as didentate quinolinylamide (amino group is partially deprotonated), was reported by Malik et al. in 1995.[15] On the other hand, $[Re^{V}Cl_3(aq)(PPh_3)]$ **5b**, which was synthesized by the reaction between the oxorhenium(V) precursor and one H_2aq as a didentate quinolinylimide (amino group is fully deprotonated) with deoxidation on oxorhenium(V) core, was reported by Okamoto et al.[18] In oxorhenium(V) complexes with soft base ligand or multiple bonds, the sixth coordination bond become weaker by strong *trans* influence. Then, some of these complexes release the sixth coordination ligand and have the five-coordinated state. The oxygen atom transfer (OAT) catalytic property on the vacant site (sixth coordination site) have been observed in some of these five-coordinated state oxorhenium(V) complexes with soft base ligand, especially methyl ligand.[19-38] Therefore, if the amino group of aminoquinoline derivatives is partially deprotonated and is coordinated as amide which has a multiple bonding character, it is expected that the obtained complex may have the five-coordinated state. Furthermore, it may show an interesting reactivity such as OAT catalytic reactivity.

In this chapter, at first the syntheses, stereochemistry, spectroscopy, and reactivity of $[ReOX_2(Hamq)(PPh_3)]$ (X = Cl, **1**; Br, **2**) and $[ReOX_2(Haq)(PPh_3)]$ (X = C1, **5**; Br, **6**) are investigated. Monodentate ligand substituted complexes $[ReOX_2(Hamq)(OPPh_3)]$ (X = Cl, **3**; Br, **4**), $[ReOX_2(Haq)(OPPh_3)]$ (X = C1, **7**; Br, **8**), and $[ReOCl_2(Hamq)(L)]$ (L = py, **9**; 4-Mepy, **10**; 4-*t*-Bupy,

11; 4-Clpy, **12**) are synthesized by using the unusual substitution reactivity which was revealed from spectroscopic study. They are characterized by stereochemistry, spectroscopy, and reactivity (Scheme II-1). In addition, the OAT catalytic property of **1** is discussed by exploiting the unusual reactivity. This chapter reveals the peculiar reactivity of oxorhenium(V) complexes with quinolinylamide.

Scheme II-1

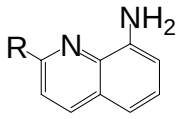

R = Me; H_2amq
R = H; H_2aq

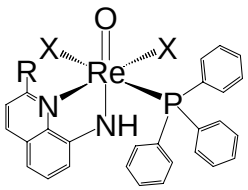

$[ReOX_2(HL)(PPh_3)]$
L = amq (R = Me), X = Cl; **1**
L = amq (R = Me), X = Br; **2**
L = aq (R = H), X = Cl; **5**
L = aq (R = H), X = Br; **6**

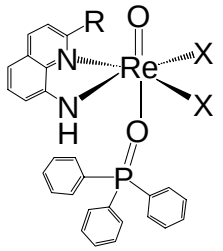

$[ReOX_2(HL)(OPPh_3)]$
L = amq (R = Me), X = Cl; **3**
L = amq (R = Me), X = Br; **4**
L = aq (R = H), X = Cl; **7**
L = aq (R = H), X = Br; **8**

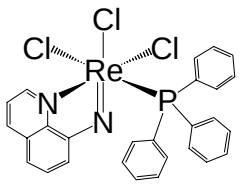

$[ReCl_3(aq)(PPh_3)]$ **5b**

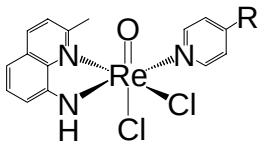

$[ReOCl_2(Hamq)(4\text{-}R\text{-}py)]$
R = H (py); **9**
R = Me (4-Mepy); **10**
R = *t*-Bu (4-*t*-Bupy); **11**
R = Cl (4-Clpy); **12**

II-ii. Experimental

Materials

Rhenium was purchased from Soekawa Chemical Co., Ltd. Triphenylphosphine oxide, 4-*t*-buthylpyridine (4-*t*-Bupy), and 4-chloropyridine monohydrochloride (4-Clpy·HCl) were purchased from Aldrich Chemical Co., Inc. 8-Amino-2-methylquinoline (H_2amq), 8-aminoquinoline (H_2aq), 4-methylpyridine (4-Mepy), and pyridine-*N*-oxide (pyO) were purchased from Tokyo Kasei Kogyo Co., Ltd. The other materials were purchased from Wako Pure Chemical Ind., Ltd. All the chemicals were used without further purification. The starting materials $[ReOX_3(PPh_3)_2]$ (X = Cl, Br),[39]

$[ReOCl_2(OEt)(PPh_3)_2]$,[40] and $[ReOCl_3(SMe_2)(OPPh_3)]$[41] were prepared according to the literature.

Syntheses of Complexes

$[ReOCl_2(Hamq)(PPh_3)]$ 1. To a suspension containing $[ReOCl_3(PPh_3)_2]$ (515 mg, 0.618 mmol) in CH_2Cl_2 (35 cm^3) was added a solution containing H_2amq (190 mg, 1.20 mmol) in $C_6H_5CH_3$ (15 cm^3). The mixture was stirred for 1 h, whereupon the color of the suspension turned from light green to dark brown. After yellow insoluble materials (mainly H_3amqCl) were filtered off, the filtrate was concentrated to 10 cm^3 under vacuum. The resulting dark brown precipitate was collected by filtration and washed with H_2O and $(C_2H_5)_2O$. Yield 314 mg, 73%. The precipitate was recrystallized from $CH_2Cl_2/C_6H_5CH_3$ to yield the dark brown prismatic crystals (**1**, major product) and dark brown octahedral crystals (**3**, minor product). **3** can be removed to a certain extent by washing with C_2H_5OH.

The complex was also synthesized from a solution of starting complex $[ReOCl_2(OEt)(PPh_3)_2]$ (54.6 mg, 0.0648 mmol) in CH_2Cl_2 (30 cm^3) and H_2amq (21.1 mg, 0.133 mmol) in $C_6H_5CH_3$ (10 cm^3). The mixture was treated as described above. The yield of **1** was 19.6 mg, 44%. Anal. Found: C, 48.54; H, 3.32; N, 4.15%. $[ReOCl_2(C_{10}H_9N_2)P(C_6H_5)_3]$ requires C, 48.56; H, 3.49; N, 4.04%. IR (KBr) 3292m (N–H) and 908s (Re=O) cm^{-1}. far-IR (Nujol) 334s and 270s (Re–Cl) cm^{-1}. $^{31}P\{^1H\}$ NMR δ -7.6. H_3amqCl was also obtained by treatment of H_2amq with HCl. This formula was confirmed by elemental analysis and IR spectra.

$[ReOBr_2(Hamq)(PPh_3)]$ 2. The bromo complex **2** was synthesized from $[ReOBr_3(PPh_3)_2]$ by a similar method to the chloro complex **1**. To a suspension containing $[ReOBr_3(PPh_3)_2]$ (500 mg, 0.517 mmol) in CH_2Cl_2 (130 cm^3) was added a solution containing H_2amq (160 mg, 1.01 mmol) in $C_6H_5CH_3$ (20 cm^3). The mixture was stirred for 1 h, whereupon the color of the suspension turned from yellow to dark brown. After insoluble materials were filtered off, the filtrate was concentrated to 10 cm^3 under vacuum. The resulting dark brown precipitate was collected by filtration and washed with H_2O and $(C_2H_5)_2O$. Yield 331 mg, 82%. The precipitate was recrystallized from $CH_2Cl_2/C_6H_5CH_3$ to yield the dark brown microcrystals (**2**, major product) and dark brown octahedral crystals (**4**, minor product). Anal. Found: C, 42.52; H, 2.93; N, 3.83%. $[ReOBr_2(C_{10}H_9N_2)P(C_6H_5)_3]$ requires C, 43.03; H, 3.10; N, 3.58%. IR (KBr) 3254m (N–H) and 915s (Re=O) cm^{-1}. far-IR (Nujol) 224w and 202w (Re–Br) cm^{-1}. $^{31}P\{^1H\}$ NMR δ -7.5.

[$ReOCl_2(Hamq)(OPPh_3)$] 3. To a suspension containing **1** (90.2 mg, 0.130 mmol) in the mixed solvent of CH_2Cl_2 (60 cm^3) and $C_6H_5CH_3$ (60 cm^3) was added $OPPh_3$ (383 mg, 1.38 mmol) and stirred for 10 min. The dark brown solution was filtered to remove insoluble materials and the filtrate was concentrated to 10 cm^3 under vacuum. After the resulting brown precipitate was collected by filtration and washed with $(C_2H_5)_2O$, the precipitate was redissolved in the mixed solvent of CH_2Cl_2 (60 cm^3) and $C_6H_5CH_3$ (10 cm^3). To the solution was added $OPPh_3$ (370 mg, 1.33 mmol). It was filtered and concentrated to 10 cm^3 under vacuum again. The resulting reddish brown precipitate was filtered and washed with a small amount of C_2H_5OH and $(C_2H_5)_2O$. Yield 57.6 mg, 62%.

The complex was also synthesized from $[ReOCl_3(SMe_2)(OPPh_3)]$. The solution of $[ReOCl_3(SMe_2)(OPPh_3)]$ (50.6 mg, 0.0780 mmol) in CH_2Cl_2 (30 cm^3) was added a solution containing H_2amq (27.0 mg, 0.171 mmol) in 10 cm^3 of $C_6H_5CH_3$ and stirred for 50 min. The brown solution was concentrated to 10 cm^3 under vacuum. The resulting reddish brown precipitate was collected by filtration and washed with H_2O and $(C_2H_5)_2O$. Yield 31.6 mg, 57%. Anal. Found: C, 47.51; H, 3.47; N, 3.85%. $[ReOCl_2(C_{10}H_9N_2)OP(C_6H_5)_3]$ requires C, 47.46; H, 3.41; N, 3.95%. IR (KBr) 3316m (N–H) and 973s (Re=O) cm^{-1}. far-IR (Nujol) 316s and 280s (Re–Cl) cm^{-1}. $^{31}P\{^1H\}$ NMR δ 27.8. $^{31}P\{^1H\}$ CP-MAS NMR δ 38.4.

[$ReOBr_2(Hamq)(OPPh_3)$] 4. The bromo complex **4** was synthesized from **2** by a similar method to the chloro complex **3**. After **2** (98.2 mg, 0.126 mmol) was reacted with $OPPh_3$ (360 mg, 1.29 mmol) in the mixed solvent of CH_2Cl_2 (60 cm^3) and $C_6H_5CH_3$ (10 cm^3), the reaction mixture was concentrated under vacuum and the brown precipitate was collected by filtration. The precipitate was redissolved in the mixed solvent and reacted with $OPPh_3$ (368 mg, 1.32 mmol) again. After the solution was concentrated, the resulting reddish brown precipitate was filtered and washed with a small amount of C_2H_5OH and $(C_2H_5)_2O$. Yield 42.3 mg, 42%. Anal. Found: C, 42.14; H, 2.87; N, 3.65%. $[ReOBr_2(C_{10}H_9N_2)OP(C_6H_5)_3]$ requires C, 42.17; H, 3.03; N, 3.51%. IR (KBr) 3311m (N–H) and 972s (Re=O) cm^{-1}. far-IR (Nujol) 231w and 210w (Re–Br) cm^{-1}. $^{31}P\{^1H\}$ NMR δ 27.7 $^{31}P\{^1H\}$ CP-MAS NMR δ 39.7.

Quinolinylamido complexes mixture 5a. Though the quinolinylamido complex $[ReOCl_2(Haq)(PPh_3)]$ **5** was attempt to synthesis by a similar method to the corresponding methylquinolinylamido complex **1**, the quinolinylamido complexes mixture **5a** was obtained instead of **5**. To a suspension containing $[ReOCl_3(PPh_3)_2]$ (518 mg, 0.622 mmol) in CH_2Cl_2 (130 cm^3) was added

a solution containing H_2aq (90.8 mg, 0.630 mmol) in $C_6H_5CH_3$ (15 cm^3) and stirred for 80 min. After insoluble materials were filtered off, the filtrate was concentrated to 10 cm^3 under vacuum. The resulting brown precipitate was collected by filtration and washed with H_2O and $(C_2H_5)_2O$. Yield 220 mg. IR (KBr) 3336w, 3199w (N–H) and 951m, 901m (Re=O) cm^{-1}.

[$ReCl_3$(aq)(PPh_3)] 5b. The deoxo complex **5b** was synthesized by a modified method of litelature,[18] and it is a nearly same method to **5a** except that the precipitate was obtained by slow evaporation. To a suspension containing [$ReOCl_3(PPh_3)_2$] (1000 mg, 1.20 mmol) in CH_2Cl_2 (300 cm^3) was added a solution containing H_2aq (220 mg, 1.52 mmol) in $C_6H_5CH_3$ (50 cm^3) and stirred for 1 d. After insoluble materials were filtered off, the filtrate was allowed to stand and slowly evaporated to 30 cm^3. The resulting dark brown crude crystals were obtained. Yield 386 mg. The crystals (100 mg) were recrystallized from CH_2Cl_2 (90 cm^3)/$C_6H_5CH_3$ (10 cm^3) to yield the dark brown crystals. Yield 16.1 mg, 16%. Anal. Found: C, 46.95; H, 3.16; N, 3.95%. [$ReCl_3(C_9H_6N_2)P(C_6H_5)_3$] requires C, 46.53; H, 3.04; N, 4.02%. $^{31}P\{^1H\}$ NMR δ -26.9.

[$ReOBr_2$(Haq)(PPh_3)] 6. The bromo complex **6** was synthesized from [$ReOBr_3(PPh_3)_2$] by a similar method to the corresponding methylquinolinylamido complex **2**. To a suspension containing [$ReOBr_3(PPh_3)_2$] (510 mg, 0.528 mmol) in CH_2Cl_2 (100 cm^3) was added a solution containing H_2aq (140 mg, 0.971 mmol) in $C_6H_5CH_3$ (30 cm^3) and stirred for 1 h. After insoluble materials were filtered off, the filtrate was concentrated to 10 cm^3 under vacuum. The resulting deep greenish brown precipitate was collected by filtration and washed with H_2O and $(C_2H_5)_2O$. Yield 220 mg, 54%. Anal. Found: C, 42.05; H, 2.78; N, 4.08%. [$ReOBr_2(C_9H_7N_2)$ $P(C_6H_5)_3$] requires C, 42.26; H, 2.89; N, 3.65%. IR (KBr) 3192m (N–H) and 909s (Re=O) cm^{-1}. far-IR (Nujol) 237w and 202w (Re–Br) cm^{-1}. $^{31}P\{^1H\}$ NMR δ -7.3.

[$ReOCl_2$(Haq)($OPPh_3$)] 7. The chloro complex **7** was synthesized from the quinolinylamido complexes mixture **5a** by a similar method to the corresponding methylquinolinylamido complex **3**. To a suspension containing **5a** (214 mg) in the mixed solvent of CH_2Cl_2 (150 cm^3) and $C_6H_5CH_3$ (20 cm^3) was added $OPPh_3$ (998 mg, 3.59 mmol) and stirred for 10 min. The dark brown solution was filtered to remove insoluble materials and the filtrate was concentrated to 10 cm^3 under vacuum. After the resulting brown precipitate was collected by filtration and washed with $(C_2H_5)_2O$, the precipitate was redissolved in the mixed solvent of CH_2Cl_2 (100 cm^3) and $C_6H_5CH_3$ (20 cm^3). To the solution was

added $OPPh_3$ (980 mg, 3.52 mmol). It was filtered and concentrated to 10 cm^3 under vacuum again. The resulting reddish brown precipitate was filtered and washed with a small amount of C_2H_5OH and $(C_2H_5)_2O$. Yield 102 mg. Anal. Found: C, 46.56; H, 3.05; N, 4.07%. $[ReOCl_2(C_9H_7N_2)OP(C_6H_5)_3]$ requires C, 46.69; H, 3.19; N, 4.03%. IR (KBr) 3307m (N–H) and 968s (Re=O) cm^{-1}. far-IR (Nujol) 326w and 276w (Re–Cl) cm^{-1}. $^{31}P\{^1H\}$ NMR δ 28.5. $^{31}P\{^1H\}$ CP-MAS NMR δ 38.1.

$[ReOBr_2(Haq)(OPPh_3)]$ 8. The bromo complex **8** was synthesized from **6** by a similar method to the corresponding methylquinolinylamido complex **4**. After **6** (88.1 mg, 0.115 mmol) was reacted with $OPPh_3$ (428 mg, 1.54 mmol) in the mixed solvent of CH_2Cl_2 (60 cm^3) and $C_6H_5CH_3$ (10 cm^3), the reaction mixture was concentrated under vacuum and the brown precipitate was collected by filtration. The precipitate was redissolved in the mixed solvent and reacted with $OPPh_3$ (324 mg, 1.16 mmol) again. After the solution was concentrated, the resulting brown precipitate was filtered and washed with a small amount of C_2H_5OH and $(C_2H_5)_2O$. Yield 52.1 mg, 58%. Anal. Found: C, 41.02; H, 2.67; N, 3.78%. $[ReOBr_2(C_9H_7N_2)OP(C_6H_5)_3]$ requires C, 41.39; H, 2.83; N, 3.58%. IR (KBr) 3292m (N–H) and 968s (Re=O) cm^{-1}. far-IR (Nujol) 245w and 199w (Re–Br) cm^{-1}. $^{31}P\{^1H\}$ NMR δ 26.8. $^{31}P\{^1H\}$ CP-MAS NMR δ 40.0.

$[ReOCl_2(Hamq)(py)]$ 9. To a suspension containing **1** (298 mg, 0.430 mmol) in $C_6H_5CH_3$ (150 cm^3) was added py (42.5 mg, 0.477 mmol) in $C_6H_5CH_3$ (20 cm^3) and stirred for 1 h. The dark brown suspension was filtered to collect reddish brown precipitate and the precipitate was washed with $(C_2H_5)_2O$. Yield 104 mg, 48%. Anal. Found: C, 35.60; H, 2.88; N, 8.11%. $[ReOCl_2(C_{10}H_9N_2)(C_5H_5N)]$ requires C, 35.37; H, 2.77; N, 8.25%. IR (KBr) 3325s (N–H) and 940s (Re=O) cm^{-1}. far-IR (Nujol) 342s and 277s (Re–Cl) cm^{-1}.

$[ReOCl_2(Hamq)(4\text{-}Mepy)]$ 10. To a suspension containing **1** (98.4 mg, 0.142 mmol) in $C_6H_5CH_3$ (40 cm^3) was added 4-Mepy (14.8 mg, 0.159 mmol) in $C_6H_5CH_3$ (10 cm^3) and stirred for 1 h. After insoluble materials were filtered off, the filtrate was concentrated to 10 cm^3 under vacuum. The resulting reddish brown precipitate was collected by filtration and washed with $(C_2H_5)_2O$. Yield 40.2 mg, 54%. Anal. Found: C, 36.55; H, 3.35; N, 7.88%. $[ReOCl_2(C_{10}H_9N_2)(C_5H_4NCH_3)]$ requires C, 36.71; H, 3.08; N, 8.03%. IR (KBr) 3326s (N–H) and 947s (Re=O) cm^{-1}. far-IR (Nujol) 330s and 264m (Re–Cl) cm^{-1}.

[$ReOCl_2$(Hamq)(4-*t*-Bupy)] 11. To a suspension containing **1** (101 mg, 0.145 mmol) in $C_6H_5CH_3$ (40 cm^3) was added 4-*t*-Bupy (22.3 mg, 0.165 mmol) in $C_6H_5CH_3$ (10 cm^3) and stirred for 1.5 h. After insoluble materials were filtered off by filtration, the filtrate was concentrated to 10 cm^3 under vacuum. The resulting brown precipitate was collected by filtration and washed with $(C_2H_5)_2O$. Yield 55 mg, 66.5%. Anal. Found: C, 40.46; H, 3.98; N, 7.36%. [$ReOCl_2(C_{10}H_9N_2)(C_5H_4NC_4H_9)$] requires C, 40.35; H, 3.92; N, 7.43%. IR (KBr) 3292s (N–H) and 938s (Re=O) cm^{-1}. far-IR (Nujol) 332s and 261m (Re–Cl) cm^{-1}.

[$ReOCl_2$(Hamq)(4-Clpy)] 12. To a solution of $KHCO_3$ (100 mg, 1.00 mmol) in H_2O (10 cm^3) was added 4-Clpy·HCl (150mg, 1.00 mmol) on an ice bath. The free base 4-Clpy recovered by extraction with CH_2Cl_2 (10 cm^3 × 3) was concentrated to 5 cm^3 and was then dissolved in the mixed solvent $(CH_3)_2CO$ (15 cm^3) and $C_6H_5CH_3$ (5 cm^3). To the 4-Clpy solution was added **1** (100 mg, 0.145 mmol) and stirred for 2 h. After removing insoluble materials by filtration, the filtrate was concentrated to 5 cm^3 under vacuum. The resulting brown precipitate was collected by filtration and washed with H_2O and $(C_2H_5)_2O$. Yield 49.0 mg, 62%. Anal. Found: C, 32.72; H, 3.01; N, 7.23%. [$ReOCl_2(C_{10}H_9N_2)(C_5H_4NCl)$] requires C, 33.13; H, 2.41; N, 7.73%. IR (KBr) 3289m (N–H) and 940s (Re=O) cm^{-1}. far-IR (Nujol) 325s (Re–Cl) cm^{-1}.

Measurements

Elemental analyses (C, H, N) were performed by the Research Facility Center for Science and Technology or Department of Chemistry of the University of Tsukuba. IR spectra were recorded as KBr pellets on a JASCO FT/IR-550 spectrometer in the range of 4000–400 cm^{-1} and far-IR spectra were recorded as Nujol mull method in the range of 650–50 cm^{-1} at room temperature. The electronic absorption spectra were recorded with a JASCO V-560 spectrophotometer. The diffuse reflectance spectra were recorded on a JASCO V-570 spectrophotometer equipped with an integrating sphere apparatus (JASCO ISN-470). The ^1H and $^{31}P\{^1H\}$ NMR spectra were obtained on a BRUKER AVANCE 600 spectrometer with $SiMe_4$ as an internal reference and PPh_3 as an external reference respectively (in $CDCl_3$ PPh_3 resonates at δ -7.42 with respect to 85% H_3PO_4 in D_2O).[14] The $^{31}P\{^1H\}$ CP-MAS NMR spectra were obtained at 243 MHz with the BRUKER AVANCE 600 spectrometer equipped with a PHMAS 4BL VTN instrument by using $NH_4H_2PO_4$ as an external reference (δ 1.0).

Crystallography

Single crystals of **1**·CH_2Cl_2, **3**, **4**, **5b**·0.5$C_6H_5CH_3$, **6**·0.5$C_6H_5CH_3$, **7,** and **9** were used for data collection on a Rigaku AFC-7S four-circle diffractometer with graphite-monochromatized MoKα (0.71069 Å) radiation. The intensity data were collected by the ω–2θ scan technique up to 55° at 296 K. For **5b**, the intensity data were collected by the ω–2θ scan technique up to 40° at 296 K, since the crystal decayed during the measurement. An empirical absorption correction was applied. The crystal data and experimental parameters are listed in Tables II-1, II-2, and II-3. The positions of most non-hydrogen atoms were determined by direct methods (SIR92[42] in **1**, **3**, **4**, and **5b**, and SIR88[43] in **6** and **7**) and some remaining atoms positions were found by successive difference Fourier techniques.[44] The structures were refined by full-matrix least-squares techniques using anisotropic thermal parameters for non-hydrogen atoms. For **1**, **3**, **4**, **5b**, and **9**, all the hydrogen atoms were included in the refinement but constrained to ride on the atoms (C–H = N–H = 0.95 Å, U(H) = 1.2U(C, N)). On the other hand, for **6** and **7**, the hydrogen atoms were not included in the refinement because of weak reflections. All of the calculations were performed using the teXsan crystallographic software package.[45] Different from the literature,[18] crystal packing of **5b** contained $C_6H_5CH_3$ molecular, and evaporation of $C_6H_5CH_3$ during X-ray measurement made the R_w value of **5b** worse. High R_w value was also observed in **9** because of a positional disorder.

Single crystals of **10**, **11**, and **12** were used for data collection on a Rigaku/MSC Mercury CCD system with graphite-monochromatized MoKα (0.71069 Å) radiation. The intensity data were collected to a maximum 2θ value of 55° at 296 K. Data were collected and were processed using CrystalClear.[46] An empirical absorption correction was applied. The crystal data and experimental parameters are listed in Table II-3. The positions of most non-hydrogen atoms were determined by direct methods (SIR92[42] in **10**, SAPI91[47] in **11**, and SIR88[43] in **12**) and some remaining atoms positions were found by successive difference Fourier techniques.[48] The structures were refined by full-matrix least-squares techniques using anisotropic thermal parameters for non-hydrogen atoms. For **10** and **11**, all the hydrogen atoms were included in the refinement but constrained to ride on the atoms (C–H = N–H = 0.95 Å, U(H) = 1.2U(C, N)). On the other hand, for **12**, the hydrogen atoms were not included in the refinement because of high disorder. The calculations on **10**, **11**, and **12** were performed using the CrystalStructure crystallographic software package.[49,50] The high R_w value was observed in **12** because of a positional disorder similar to the case of **9**.

Table II-1 Crystal data and experimental parameters for $[ReOCl_2(Hamq)(PPh_3)]\cdot CH_2Cl_2$ **1**·CH_2Cl_2, $[ReOCl_2(Hamq)(OPPh_3)]$ **3**, and $[ReOBr_2(Hamq)(OPPh_3)]$ **4**

	1·CH_2Cl_2	**3**	**4**
Formula	$C_{29}H_{26}Cl_4N_2OPRe$	$C_{28}H_{24}Cl_2N_2O_2PRe$	$C_{28}H_{24}Br_2N_2O_2PRe$
Formula weight	777.53	708.60	797.50
Cryst. system	triclinic	monoclinic	monoclinic
Space group	*P*-1 (No. 2)	$P2_1/n$ (No. 14)	$P2_1/n$ (No. 14)
a, Å	11.551(2)	14.90(1)	15.127(3)
b, Å	14.105(2)	17.272(4)	17.376(4)
c, Å	10.133(1)	10.485(2)	10.569(2)
α, °	91.258(9)		
β, °	109.252(10)	95.46(4)	96.56(2)
γ, °	75.30(1)		
V, Å^3	1504.2(3)	2685(2)	2759.6(10)
Z	2	4	4
D_{calc}, g cm^{-3}	1.717	1.753	1.919
μ (Mo Kα), cm^{-1}	44.74	48.14	73.96
Reflections collected	7390	6722	6901
Unique reflections	6902	6180	6347
R_{int}	0.018	0.037	0.038
Observations ($I > 1.5\sigma(I)$)	5685	4862	4058
Variable parameters	343	325	325
R[a]	0.052	0.068	0.074
R_w[b]	0.085	0.106	0.116
GOF	1.02	1.40	1.11

[a] $R = \Sigma||F_o| - |F_c||/\Sigma|F_o|$. [b] $R_w = [\Sigma w(F_o^2 - F_c^2)^2/\Sigma w(F_o^2)^2]^{1/2}$, where $w = 1/\sigma^2(F_o^2)$.

Table II-2 Crystal data and experimental parameters for $[ReCl_3(aq)(PPh_3)]\cdot 0.5C_6H_5CH_3$ **5b**$\cdot 0.5C_6H_5CH_3$, $[ReOBr_2(Haq)(PPh_3)]\cdot 0.5C_6H_5CH_3$ **6**$\cdot 0.5C_6H_5CH_3$, and $[ReOCl_2(Haq)(OPPh_3)]$ **7**

	5b$\cdot 0.5C_6H_5CH_3$	**6**$\cdot 0.5C_6H_5CH_3$	**7**
Formula	$C_{30.5}H_{25}Cl_3N_2PRe$	$C_{30.5}H_{26}Br_2N_2OPRe$	$C_{27}H_{22}Cl_2N_2O_2PRe$
Formula weight	743.09	813.54	694.57
Cryst. system	triclinic	triclinic	triclinic
Space group	*P*-1 (No. 2)	*P*-1 (No. 2)	*P*-1 (No. 2)
a, Å	10.34(1)	12.136(7)	10.768(9)
b, Å	15.57(1)	12.668(4)	12.444(6)
c, Å	10.29(1)	10.600(4)	10.364(3)
α, °	98.91(8)	90.91(3)	100.43(3)
β, °	115.70(8)	115.81(3)	103.33(4)
γ, °	91.87(9)	92.38(4)	74.97(4)
V, Å^3	1465(2)	1464(1)	1294(1)
Z	2	2	2
D_{calc}, g cm^{-3}	1.684	1.844	1.782
μ (Mo Kα), cm^{-1}	44.98	69.62	49.92
Reflections collected	2240	7212	6333
Unique reflections	2117	6748	5936
R_{int}	0.060	0.060	0.019
Observations ($I > 1.5\sigma(I)$)	1905[c]	3270	3414
Variable parameters	319	334	406
R[a]	0.120	0.154	0.085
R_w[b]	0.154	0.210	0.150
GOF	2.57	1.87	1.62

[a] $R = \Sigma||F_o| - |F_c||/\Sigma|F_o|$. [b] $R_w = [\Sigma w(F_o^2 - F_c^2)^2/\Sigma w(F_o^2)^2]^{1/2}$, where $w = 1/\sigma^2(F_o^2)$. [c] $I > 3\sigma(I)$.

Table II-3 Crystal data and experimental parameters for [$ReOCl_2$(Hamq)(py)] **9**, [$ReOCl_2$(Hamq)(4-Mepy)] **10**, [$ReOCl_2$(Hamq)(4-*t*-Bupy)] **11**, and [$ReOCl_2$(Hamq)(4-Clpy)] **12**

	9	**10**	**11**	**12**
Formula	$C_{15}H_{14}Cl_2N_3ORe$	$C_{16}H_{16}Cl_2N_3ORe$	$C_{19}H_{22}Cl_2N_3ORe$	$C_{15}H_{13}Cl_3N_3ORe$
Formula weight	509.41	523.43	565.52	543.85
Cryst. system	monoclinic	monoclinic	monoclinic	triclinic
Space group	$P2_1/c$ (No. 14)	$P2_1/c$ (No. 14)	$P2_1/c$ (No. 14)	P-1 (No. 2)
a, Å	16.184(4)	7.258(4)	10.252(6)	8.872(11)
b, Å	7.5110(10)	7.975(4)	21.624(12)	9.728(12)
c, Å	15.112(5)	30.17(2)	18.390(10)	10.429(13)
α, °				80.86(4)
β, °	117.38(2)	92.860(7)	100.197(7)	84.32(4)
γ, °				81.43(4)
V, Å^3	1631.2(7)	1744.4(16)	4012.5(1)	876.1(19)
Z	4	4	8	2
D_{calc}, g cm^{-3}	2.074	1.993	1.872	2.061
μ (Mo Kα), cm^{-1}	77.83	72.81	63.38	74.00
Reflections collected	4240	14393	33457	6950
Unique reflections	4008	3970	9171	3492
R_{int}	0.054	0.055	0.124	0.072
Observations ($I > 3\sigma(I)$)	2358	2644	5462[c]	3101
Variable parameters	199	224	469	208
R[a]	0.093	0.041	0.128	0.166
R_w[b]	0.346	0.100	0.321	0.182
GOF	1.615	1.007	1.000	6.91

[a] $R = \Sigma||F_o| - |F_c||/\Sigma|F_o|$. [b] $R_w = [\Sigma w(F_o^2 - F_c^2)^2/\Sigma w(F_o^2)^2]^{1/2}$, where $w = 1/\sigma^2(F_o^2)$. [c] $I > 2\sigma(I)$.

II-iii. Syntheses

II-iii-i. $[ReOX_2(Hamq)(L)]$ (X = Cl, L = PPh_3, **1**; X = Br, L = PPh_3, **2**; X = Cl, L = $OPPh_3$, **3**; X = Br, L = $OPPh_3$, **4**) and $[ReOCl_2(Hamq)(L')]$ (L' = py, **9**; 4-Mepy, **10**; 4-*t*-Bupy, **11**; 4-Clpy, **12**)

$[ReOCl_2(Hamq)(L)]$ (L = PPh_3, 1; $OPPh_3$, 3) The reactions of the oxorhenium(V) precursor $[ReOCl_3(PPh_3)_2]$ with 8-amino-2-methylquinoline (H_2amq) as 1:2 molar ratio in the $CH_2Cl_2/C_6H_5CH_3$ mixed solvent gave selectively the dark brown precipitate $[ReOCl_2(Hamq)(PPh_3)]$ **1** as main products (Eq. II-1). In spite of the addition of two equivalents of H_2amq, any complexes which have two quinolinylamide

$$[ReOCl_3(PPh_3)_2] + 2H_2amq \longrightarrow [ReOCl_2(Hamq)(PPh_3)]\ \mathbf{1} + PPh_3 + H_3amqCl \quad (II\text{-}1)$$

ligands like $[ReO(Haq)_2(PPh_3)]^{+}$ [15] could not be obtained. The yellow precipitate H_3amqCl, which can be removed by washing with H_2O, accompanied the reaction (Eq. II-1). Therefore, this reaction needs two equivalents of H_2amq. If only one equivalent of H_2amq is added, yield will reduced by half. Since the bis type complex $[ReO(Haq)_2(PPh_3)]^{+}$ [15] was obtained from the reaction with excess of H_2aq, H_2amq and H_2aq seem to act to extract the chloride ion from the starting materials. The complex **1** can be also synthesized from $[ReOCl_2(OEt)(PPh_3)_2]$ and H_2amq. In this case, a chloride ion is not released from the precursor and then the formation of H_3amqCl was not observed (Eq. II-2). Therefore, this reaction needs only one equivalent of H_2amq.

$$[ReOCl_2(OEt)(PPh_3)_2] + H_2amq \longrightarrow [ReOCl_2(Hamq)(PPh_3)]\ \mathbf{1} + PPh_3 + EtOH \quad (II\text{-}2)$$

The recrystallization of the dark brown precipitate gave two types of crystals. Although most of them were the dark brown prismatic-shaped crystals, the small amounts of dark brown octahedral-shaped crystals were also formed. From X-ray analyses and IR spectra, the major crystals were *trans* O=Re–N (amido) type complexes, $[ReOCl_2(Hamq)(PPh_3)]$ **1**, whereas the minor crystals were *trans* O=Re–$OPPh_3$ type complexes, $[ReOCl_2(Hamq)(OPPh_3)]$ **3**. The formation of **3** may be caused by the ligand replacement from PPh_3 to $OPPh_3$ during the recrystallization from these results. Therefore, it is suggested that the $OPPh_3$ coordinated complex **3** can be synthesized by the ligand substitution reaction. In practice, the reaction of **1** with excess of free $OPPh_3$ afforded **3**. These reactions can be reversed from **3** to **1** by adding excess of free PPh_3 (Eq. II-3). The $OPPh_3$ coordinated complex **3** can be also synthesized from $[ReOCl_3(Me_2S)OPPh_3]$

and H_2amq. In this case, H_3amqCl was observed (Eq. II-4). Therefore two equivalents of H_2amq need for the reaction similarly to Eq. II-1.

$$[ReOCl_2(Hamq)(PPh_3)]\ \mathbf{1} + OPPh_3 \rightleftharpoons [ReOCl_2(Hamq)(OPPh_3)]\ \mathbf{3} + PPh_3 \quad \text{(II-3)}$$

$$[ReOCl_3(SMe_2)(OPPh_3)] + 2H_2amq \longrightarrow [ReOCl_2(Hamq)(OPPh_3)]\ \mathbf{3} + SMe_2 + H_3amqCl \quad \text{(II-4)}$$

Although **1** and **3** are stable in solid state even under air, it is suspected that they release PPh_3 or $OPPh_3$ in solution from electronic absorption and $^{31}P\{^1H\}$ NMR spectroscopy (vide infra). Therefore, it is suggested that the formation of the minor product **3** obtained during recrystallization of **1** would be caused by the oxidation of the released PPh_3 due to dissolved oxygen. As a result of stirring the PPh_3 coordinated complex **1** in CH_2Cl_2 solution under an oxygen atmosphere for 1 d, the formation of a small amount of the $OPPh_3$ coordinated complex **3** was observed. This preliminary experiment supports above suggestion (Scheme II-2). Although many reported oxorhenium(V) complexes with $OPPh_3$ were synthesized from the precursors which have $OPPh_3$ like $[ReOCl_3(Me_2S)(OPPh_3)]$,[2,51-53] it can be said that the present easy substitution property is very unusual and interesting.

Scheme II-2

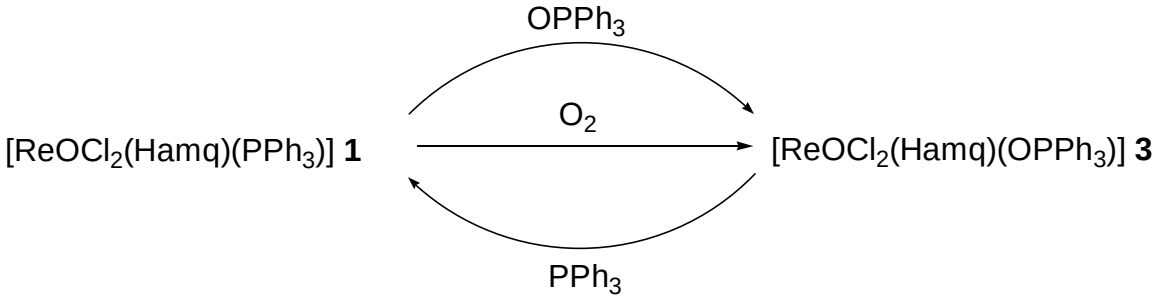

$[ReOBr_2(Hamq)(L)]$ (L = PPh_3, 2; $OPPh_3$, 4) The bromo complexes $[ReOBr_2(Hamq)(PPh_3)]$ **2** and $[ReOBr_2(Hamq)(OPPh_3)]$ **4** were synthesized by similar methods to the corresponding chloro complexes **1** and **3**, respectively. These complexes are also showed unusual PPh_3 or $OPPh_3$ release and easy substitution property in solution (Eqs. II-5 and II-6).

$[ReOBr_3(PPh_3)_2] + 2H_2amq \longrightarrow$

$[ReOBr_2(Hamq)(PPh_3)]$ **2** $+ PPh_3 + H_3amqBr$ (II-5)

$[ReOBr_2(Hamq)(PPh_3)]$ **2** $+ OPPh_3 \rightleftharpoons$

$[ReOBr_2(Hamq)(OPPh_3)]$ **4** $+ PPh_3$ (II-6)

$[ReOCl_2(Hamq)(L')]$ (L' = py, 9; 4-Mepy, 10; 4-*t*-Bupy, 11; 4-Clpy, 12) The unusual reactivity of the methylquinolinylamido complexes was applied for the substitution reaction of PPh_3 or $OPPh_3$. Then no charged monodentate ligands pyridine derivatives (py, 4-Mepy, 4-*t*-Bupy, 4-Clpy) were used

Scheme II-3

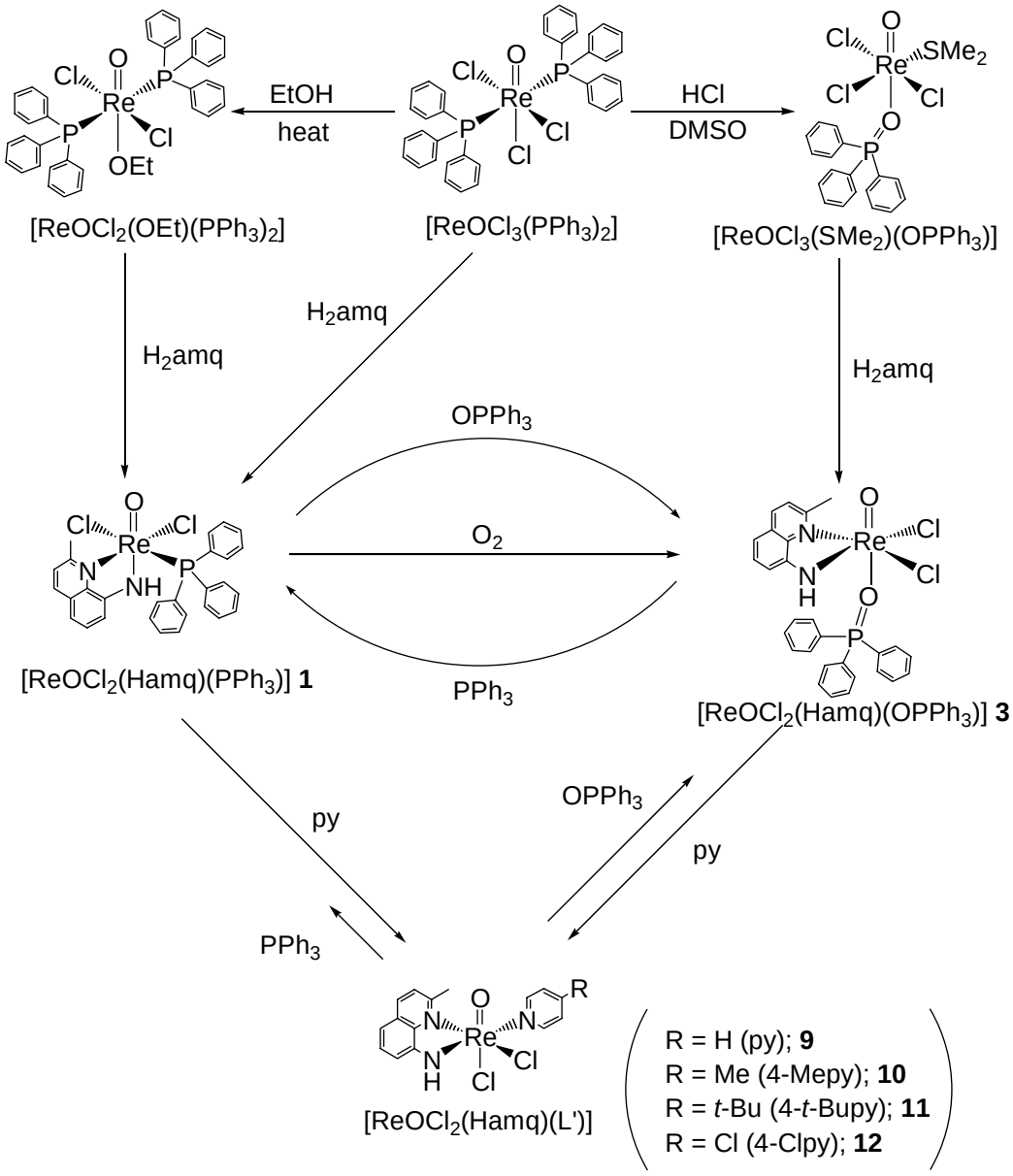

for substituent group. Though the reaction of the PPh_3 coordinated complex **1** with pyridine derivatives easily gave the pyridine coordinated complexes $[ReOCl_2(Hamq)(L')]$ (L' = py, **9**; 4-Mepy, **10**; 4-*t*-Bupy, **11**; 4-Clpy, **12)**, it was observed little reverse reaction, the pyridine coordinated complexes **9**–**12** to the PPh_3 coordinated complex **1** (Scheme II-3). The reaction of the $OPPh_3$ coordinated complex **3** with pyridine derivatives also gave the pyridine coordinated complexes **9**–**12** (Scheme II-3). Different from PPh_3, the reverse reaction, the pyridine coordinated complexes **9**–**12** to the $OPPh_3$ coordinated complex **3**, was a little observed.

The summary of the reactivity of the methylquinolinylamido complexes with chloride ion system are shown in Scheme II-3. The complex **1** can be prepared from the starting complex $[ReOCl_3(PPh_3)_2]$. The complexes **1** and **3** can be also synthesized from $[ReOCl_2(OEt)(PPh_3)_2]$ and $[ReOCl_3(Me_2S)OPPh_3]$, respectively. The ligands PPh_3 and $OPPh_3$ in **1** and **3** are easily replaced which is accompanied by changing geometry around the rhenium(V) ion. The pyridine coordinated complexes **9**–**12** can be also synthesized from the substitution reactions which are accompanied by changing geometry around the rhenium(V) ion. These easy replacement property is not observed in the other oxorhenium(V) complexes with didentate-*N*,*N* ligands.[2-5] Therefore, it can be said that the unusual reactivity observed this time is characteristic of the oxorhenium(V) complexes with quinolinylamide derivatives which have two types of coordination nitrogen atoms.

II-iii-ii. $[ReOX_2(Haq)(L)]$ (X = Cl, L = PPh_3, **5a**; X = Br, L = PPh_3, **6**; X = Cl, L = $OPPh_3$, **7**; X = Br, L = $OPPh_3$, **8**) and $[ReCl_3(aq)(PPh_3)]$ **5b**

The quinolinylamido complexes $[ReOBr_2(Haq)(PPh_3)]$ **6** and $[ReOBr_2(Haq)(OPPh_3)]$ **8** were synthesized by a similar method to the corresponding methylquinolinylamido complexes **2** and **4**, respectively. These complexes also showed unusual PPh_3 or $OPPh_3$ release and easy substitution property in solution (Eqs. II-7 and II-8).

$$[ReOBr_3(PPh_3)_2] + 2H_2aq \longrightarrow [ReOBr_2(Haq)(PPh_3)]\ \mathbf{6} + PPh_3 + H_3aqBr \quad \text{(II-7)}$$

$$[ReOBr_2(Haq)(PPh_3)]\ \mathbf{6} + OPPh_3 \rightleftharpoons [ReOBr_2(Haq)(OPPh_3)]\ \mathbf{8} + PPh_3 \quad \text{(II-8)}$$

On the other hand, the chloro complexes $[ReOCl_2(Haq)(PPh_3)]$ **5** and $[ReOCl_2(Haq)(OPPh_3)]$ **7** showed different reactivity from the complexes **6** and **8**. Though the complex **5** was attempted to be synthesized by a similar method to the corresponding methylquinolinylamido complex **1**, the quinolinylamido complexes mixture **5a** was obtained instead of **5**. Isolation of **5** was not succeeded. On the other hand, recrystallization of crude compound, which was obtained from spontaneous evaporation of mother liquor, gave crystals of the deoxo complex $[ReCl_3(aq)(PPh_3)]$ **5b** reported by Okamoto et al., previously.[18] The result of the experiment, that the mother liquor was forcibly evaporated by vacuum line after stirred for 3 d, showed the formation of the deoxo complex **5b**. Therefore, it is suggested that the difference in formation between **5a** and **5b** depends on reaction time, not evaporation velocity (Scheme II-4). Though the same preliminary experiment was conducted in **1**, the formation of the corresponding deoxo complex was not observed. Therefore, it can be said that the reactivity is characteristic of the complex containing 8-aminoquinoline with chloride ion. The $OPPh_3$ coordinated complex **7** was synthesized from the reaction of **5a** with excess of $OPPh_3$ similar to **3** (Scheme II-4). The reverse reaction, the $OPPh_3$ coordinated complex **7** to the PPh_3 coordinated complex **5a**, was also observed similar to the other methylquinolinylamido or quinolinylamido complexes (Scheme II-4). On the other hand, the deoxo complex **5b** was not reacted with $OPPh_3$, then **5b** is stable different from other methylquinolinylamido or quinolinylamido complexes. Further, **5b** could not be obtained from **5a**, even that **5a** was stirred for a few days. From the results of observed above and spectroscopic measurements, **5a** would be a mixture of geometrical isomers of **5** ($[ReOCl_2(Haq)(PPh_3)]$). Then the reversible reaction between **5a** and **7** can be explained. In addition, the fact that **5b** could not be obtained from **5a** can be also explained from lack of chloride ion.

Scheme II-4

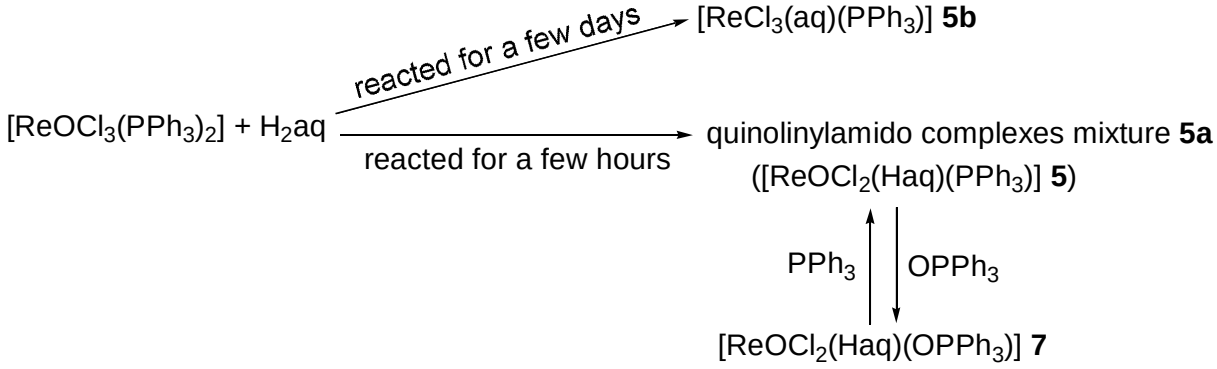

II-iv. Crystal Structures

II-iv-i. Crystal Structures of **1**, **3**, **4**, **9**–**12**

[$ReOCl_2$(Hamq)(PPh_3)] 1 An X-ray crystal analysis for **1** revealed the presence of a complex molecule and a CH_2Cl_2 molecule in an asymmetric unit. A perspective drawing of the complex molecule **1** is shown in Figure II-1 and its selected bond distances and angles are listed in Table II-4. The coordination geometry around rhenium atom is distorted octahedral with an oxo ligand, two nitrogen atoms from the asymmetrical didentate-*N*,*N* ligand, two chloride ions and one phosphorus atom from the PPh_3 ligand. The oxo ligand and aromatic amido nitrogen atom N2 lie in the *trans* position (axial direction), whereas the heterocyclic nitrogen atom N1, the phosphorus atom, and two chloride ions occupy the *cis* positions (equatorial plane).

Although the Re1–N1 distance (2.165(4) Å) in **1** is within the reported Re–N (heterocyclic) distances in the oxorhenium(V) complexes (2.11–2.17 Å),[2,54-57] the Re1–N2 distance (2.000(4) Å) is significantly shorter than the Re1–N1 distance and this distance agrees with the Re–N (amido) distance (1.93–2.05 Å) (Table II-4).[14-16] Further, the Re1–N2–C8 angle (120.7(3)°) is similar to the corresponding angles of the complexes with the amido-type Haq.[15] Therefore, it is suggested that N2 amine group is partially deprotonated and the Re1–N2 bond has a multiple bonding character.[14-16] The Re1–O1 distance (1.724(4) Å), which occupies the *trans* position to the Re1–N2 (amido) bond, lies at the long end of the range found for the Re=O double bond in the oxorhenium(V) complexes (1.63–1.71 Å).[15,27,54-64] The oxorhenium(V) complex [ReO(PPh_2(C_6H_4NH-2))$_2$Cl] reported by Refosco et al. has a surprisingly long Re=O distance (1.767(7) Å), which also occupied the *trans* position to the partially deprotonated aromatic amide.[14] It is suggested, therefore, that the reason of the long Re=O distance in **1** is the result of the *trans* influence of the Re1–N2 (amido) bond. These characters are similar to the bisquinolinylamido complex [ReO(Haq)$_2$(PPh_3)]$^+$.[15] The *trans* influence of P1 atom is also observed in **1**. The Re1–Cl2 distance (2.452(1) Å), which occupies the *trans* position to P1 atom, is 0.115 Å longer than the Re1–Cl1 distance (2.337(1) Å), which occupies the *cis* position to P1 atom. Similar behavior was also observed for the rhenium complexes with phosphine ligands such as [$Re^V OCl_3$(L)(PPh_3)] (HL = 5,7-substituted-8-hydroxyquinoline),[63,65] [$Re^V OCl_2$(OC_6H_4CHNH)(PPh_3)][66], and [$Re^V LCl_3$(PPh_3)] (L = pyridine-2-aldimine).[67]

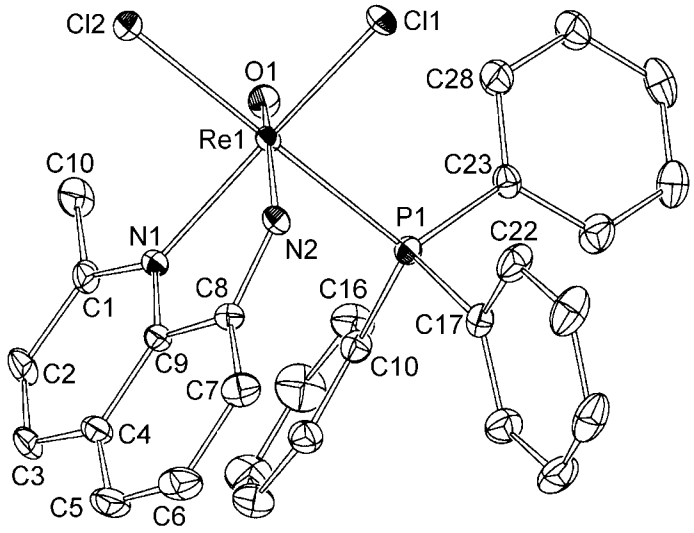

Figure II-1 An ORTEP view of $[ReOCl_2(Hamq)(PPh_3)]$ **1** with numbering scheme. Hydrogen atoms have been omitted for clarity.

Table II-4 Selected bond distances (Å) and angles (°) for $[ReOCl_2(Hamq)(PPh_3)]$ **1**

Re1–O1	1.724(4)	Re1–N1	2.165(4)
Re1–N2	2.000(4)	Re1–P1	2.455(1)
Re1–Cl1	2.337(1)	Re1–Cl2	2.452(1)
O1–Re1–N1	94.8(2)	N2–Re1–N1	75.3(2)
O1–Re1–P1	82.4(1)	N2–Re1–P1	86.6(1)
O1–Re1–Cl1	103.9(1)	N2–Re1–Cl1	86.9(1)
O1–Re1–Cl2	96.0(1)	N2–Re1–Cl2	95.0(1)
O1–Re1–N2	164.9(2)	N1–Re1–Cl1	161.0(1)
P1–Re1–Cl2	178.34(5)	N1–Re1–P1	92.9(1)
N1–Re1–Cl2	87.7(1)	P1–Re1–Cl1	92.43(5)
Cl1–Re1–Cl2	87.46(5)	Re1–N2–C8	120.7(3)

As often observed in oxorhenium(V) systems, the equatorial ligand are displaced away from the Re=O group. That is to say, the L_{eq}–Re1–N2 angles are smaller than the L_{eq}–Re1=O1 angles, except for the P1–Re1–N2 and P1–Re1=O1 angles. The P1–Re1–Cl1 moiety is almost linear (178.34(5)°), whereas the O1–Re1–N2 and N1–Re1–Cl1 angles (161–165°) deviates from 180° for an ideal octahedral structure (Table II-4). The principal distortions are the result of the bite angle of the didentate ligand (N1–Re1–N2; 75.3(2)°).

The C11–C16 phenyl ring of PPh_3 is approximately parallel to the quinoline ring (dihedral angle = 22.7(2)°) and the inter-ring average distances are 3.67(1) Å. In addition, the C11–C16 phenyl ring

position is not just above the quinoline ring (torsion angle; N1–Re1–P1–C11 = -29.7(2)°), but it is over between the methyl group C10 and the edge of the quinoline ring C1 (Figure II-2). Consequently, it is suggested that the intramolecular π–π and/or CH–π stacking interactions exist between two planes.[52]

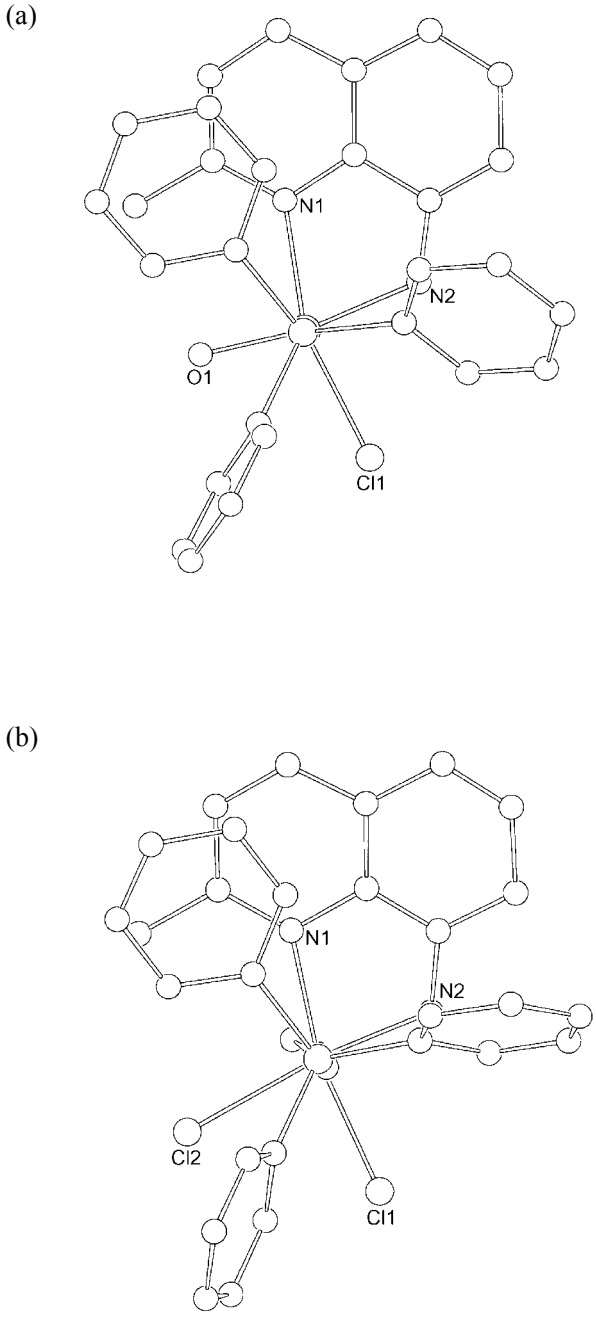

Figure II-2 Crystal structures of $[ReOCl_2(Hamq)(PPh_3)]$ **1** (a) and $[ReOCl_2(Hamq)(OPPh_3)]$ **3** (b) viewed from P–Re axis.

The intermolecular interactions are also considered from the crystal packing (Figure II-3). The quinoline rings of adjacent molecules are overlapped in axial direction, and the complex molecules take a dimeric structure in the crystal packing of **1**. The interplane distances (average 3.46(8) Å) between two planes of neighboring amq moieties are within the range of the intermolecular π–π stacking.[68,69] Although the CH_2Cl_2 molecule is also incorporated in the crystal packing, it does not participate in any intermolecular interactions.

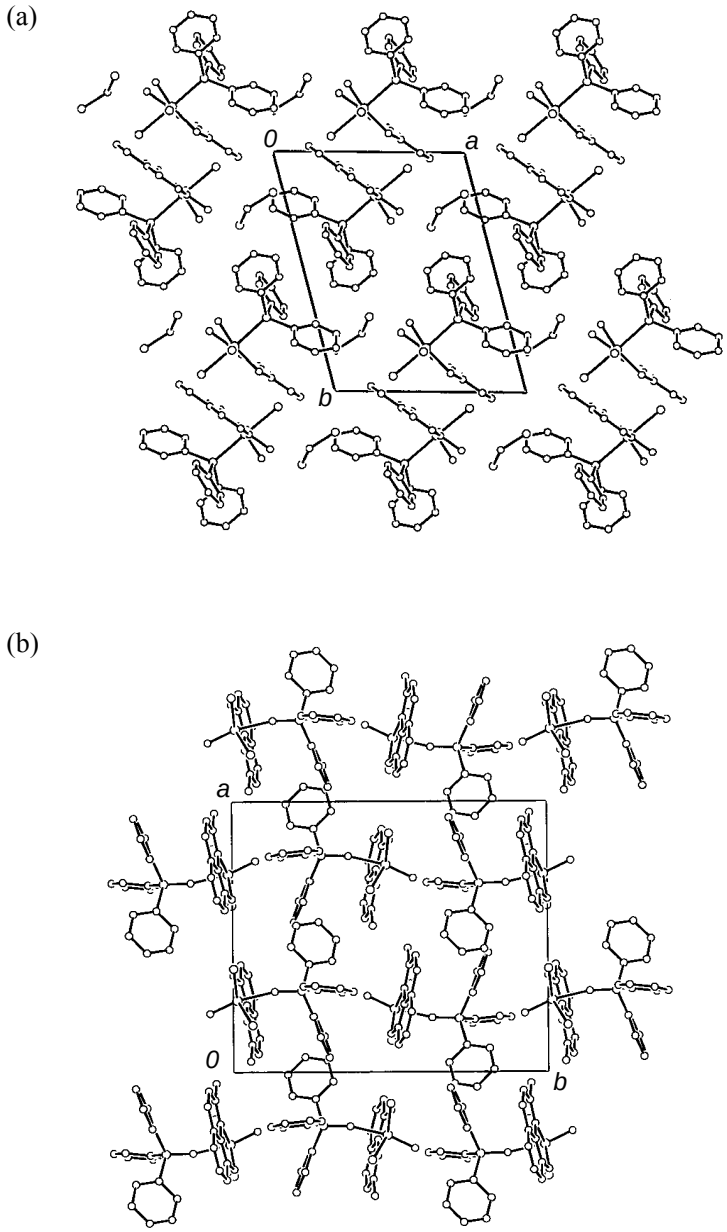

Figure II-3 Projection of crystal packing for $[ReOCl_2(Hamq)(PPh_3)]\cdot CH_2Cl_2$ **1**·CH_2Cl_2 (a) and $[ReOCl_2(Hamq)(OPPh_3)]$ **3** (b).

[$ReOX_2$(Hamq)($OPPh_3$)] 3 (X = Cl), **4** (X = Br) X-ray crystal analyses for **3** and **4** revealed the presence of only a complex molecule. As shown in Figure II-4 and Table II-5, the rhenium atom in **3** also situated in a distorted octahedral environment as in **1**. Although the PPh_3 group of **1** is substituted by the $OPPh_3$ group in **3**, it is noted that the coordination geometry of **3** is changed from that of **1**. That is to say, the PPh_3 group lies in the *cis* position to the oxo ligand, whereas the $OPPh_3$ ligand does the *trans* position. A similar tendency, which the *trans* position of the oxo ligand is occupied with the oxygen atom as observed in **3**, was also observed generally for analogous $OPPh_3$ coordinated complexes.[51-53]

The Re1–N1 distance (2.156(6) Å) in **3** is within the normal single bond,[2,54-57] whereas the short Re1–N2 distance (1.952(7) Å) and the Re1–N2–C8 angle (116.9(7)°) are similar to the corresponding distance and angle in **1** (Table II-5). Therefore, it is suggested that the N2 amine group is also partially deprotonated and the Re1–N2 bond has a multiple bonding character (amide), as in the case of **1**. The Re1–O1 distance (1.670(5) Å) is normal for double bonds in oxorhenium(V) complexes.[15,27,54-64] Since the oxygen atom of $OPPh_3$ lies the *trans* position to the oxo ligand, it seems that no special *trans* influence for the oxo ligand exist. On the other hand, the Re1–Cl2 distance (2.447(2) Å) lies the *trans* position to the Re1–N2 (amide) bond and exhibits *trans* influence. The *trans* influence make the Re1–Cl2 distance become longer than the Re1–Cl1 distance (2.363(2) Å). The bond distances and angles in **4** are approximately the same as those of **3**, except that the Re–Br distances are longer than the Re–Cl distances about 0.15 Å.

In **3**, the equatorial ligand are also displaced away from the Re=O group. In other words, the L_{eq}–Re1–O2 angles are smaller than the L_{eq}–Re1=O1 angles. All axes (O1–Re1–O2, N1–Re1–Cl1, and N2–Re1–Cl2) are bent (162–168°) and deviates from 180° for an ideal octahedral structure (Table II-5). The principal distortions are the result of the bite angle of the didentate-*N*,*N* ligand (N1–Re1–N2; 79.2(3)°).

The C11–C16 phenyl ring of the PPh_3 ligand is approximately parallel to the quinoline ring (dihedral angle = 10.8(3)°) and the inter-ring average distances are 3.75(2) Å. The smaller dihedral angle may be caused by the O2 atom which works as a joint (Re1–O2–P1 angle = 167.6(3)°). In addition, the C11–C16 phenyl ring position is not just above the amq ring, but it is over between the methyl group C10 and the edge of the quinoline ring C1 as in **1** (Figure II-2). Consequently, it is suggested that the intramolecular π–π and/or CH–π stacking interactions exist between two planes.[52] The intermolecular interactions are also considered from the crystal packing (Figure II-3). The molecules align according to the Re=O axis and no intermolecular π–π interaction is observed in the

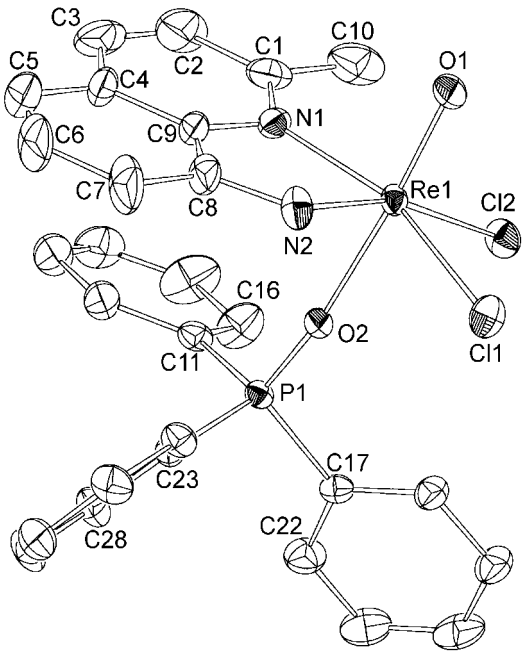

Figure II-4 An OPTEP view of $[ReOCl_2(Hamq)(OPPh_3)]$ **3** with numbering scheme. Hydrogen atoms have been omitted for clarity. The numbering scheme of $[ReOBr_2(Hamq)(OPPh_3)]$ **4** is the same as that of **3**.

Table II-5 Selected bond distances (Å) and angles (°) for $[ReOX_2(Hamq)(OPPh_3)]$ **3** (X = Cl) and **4** (X = Br)

	3	**4**		**3**	**4**
Re1–O1	1.670(5)	1.665(7)	Re1–O2	2.116(4)	2.125(7)
Re1–N1	2.156(6)	2.170(10)	Re1–N2	1.952(7)	1.938(9)
Re1–X1	2.363(2)	2.509(1)	Re1–X2	2.447(2)	2.600(1)
O1–Re1–N1	91.6(2)	92.9(4)	O2–Re1–N1	79.7(2)	80.0(3)
O1–Re1–N2	103.3(3)	104.0(4)	O2–Re1–N2	84.2(2)	84.3(3)
O1–Re1–X1	102.6(2)	101.7(3)	O2–Re1–X1	87.7(1)	87.5(2)
O1–Re1–X2	92.6(2)	91.2(3)	O2–Re1–X2	80.9(1)	81.3(2)
O1–Re1–O2	167.4(2)	167.9(4)	N1–Re1–X1	162.5(2)	161.3(3)
N2–Re1–X2	163.8(2)	164.3(3)	Re1–O2–P1	167.6(3)	166.7(5)
N1–Re1–N2	79.2(3)	78.5(4)	N1–Re1–X2	103.9(2)	105.0(3)
N2–Re1–X1	87.5(2)	86.6(3)	X1–Re1–X2	85.77(9)	86.54(5)
Re1–N2–C8	116.9(7)	119.6(9)			

crystal packing of **3**. The crystal packing property of **4** such as the intermolecular π–π stacking interaction and the intramolecular π–π and/or CH–π stacking interaction (dihedral angle = 9.4(5)°) is almost the same as that of **3**. Consequently, it seems to be indicated that the differences of coordination geometry depending on the substitution of PPh_3 for $OPPh_3$ also influence the crystal packing.

[$ReOCl_2$(Hamq)(4-R-py)] 9 (R = H), **10** (R = Me), **11** (R = *t*-Bu), **12** (R = Cl) The results of the X-ray crystal analyses of **9**–**12** revealed their geometrical structures and the structure of **9** is shown in Figure II-5 (two crystallographically independent complex molecules are observed in **11**). Selected bond distances and angles for all complexes are given in Table II-6. The coordination geometry around the rhenium atom is distorted octahedral with the oxo ligand, three nitrogen atoms from the asymmetrical didentate-*N*,*N* ligand and the pyridine ligand, and two chloride ions. In **9**, different from **1** and **3**, the oxo ligand and chloride ion Cl2 lie in the *trans* position. The heterocyclic nitrogen atom N1 and chloride ion Cl1, and the aromatic amido nitrogen atom N2 and pyridine nitrogen atom N3 occupy the *cis* position, respectively. The coordination geometries around rhenium atom of the other quinolinylamido complexes **10**–**12** with pyridine derivatives are roughly the same as that of **9**.

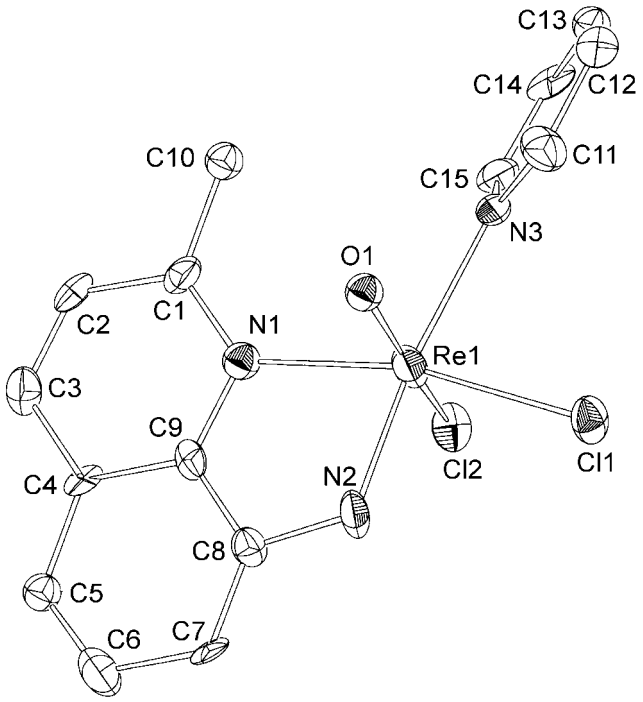

Figure II-5 An ORTEP view of [$ReOCl_2$(Hamq)(py)] **9** with numbering scheme. Hydrogen atoms have been omitted for clarity. The numbering scheme of [$ReOCl_2$(Hamq)(L)] (L = 4-Mepy, **10**; 4-*t*-Bupy, **11**, 4-Clpy, **12**) are the same as that of **9**.

Table II-6. Selected bond distances (Å) and angles (°) for [$ReOCl_2$(Hamq)(4-R-py)] (**9**–**12**)

	[$ReOCl_2$(Hamq)(py)] **9**	[$ReOCl_2$(Hamq)(4-Mepy)] **10**	[$ReOCl_2$(Hamq)(4-*t*-Bupy)] **11**[a]		[$ReOCl_2$(Hamq)(4-Clpy) **12**
bond distances					
Re1–O1	1.901(7)	1.702(6)	1.75(2)	1.76(2)	1.842(11)
Re1–N1	2.15(2)	2.179(6)	2.16(2)	2.13(2)	2.20(2)
Re1–N2	1.94(2)	1.940(7)	1.91(2)	1.90(2)	1.93(2)
Re1–N3	2.25(2)	2.274(7)	2.27(2)	2.27(3)	2.31(2)
Re1–Cl1	2.365(6)	2.345(3)	2.340(7)	2.344(7)	2.348(6)
Re1–Cl2	2.279(7)	2.447(2)	2.454(7)	2.419(8)	2.395(7)
bond angles					
O1–Re1–N1	90.8(5)	92.7(3)	92.2(8)	92.4(9)	88.0(7)
Cl2–Re1–N1	83.5(4)	79.7(2)	81.4(7)	80.9(7)	84.1(5)
O1–Re1–N2	99.4(8)	103.6(3)	100.3(10)	96.7(10)	98.1(10)
Cl2–Re1–N2	88.1(8)	90.5(2)	91.8(8)	93.3(8)	92.7(9)
O1–Re1–N3	89.1(6)	83.1(3)	86.0(8)	85.2(8)	86.3(6)
Cl2–Re1–N3	84.0(5)	83.8(2)	82.4(6)	84.9(6)	84.3(5)
O1–Re1–Cl1	96.9(4)	102.0(2)	100.6(6)	100.6(6)	100.2(5)
Cl2–Re1–Cl1	90.6(3)	88.51(9)	88.2(3)	87.8(3)	90.3(3)
O1–Re1–Cl2	169.4(4)	162.3(2)	165.0(6)	166.6(6)	165.1(5)
N1–Re1–N2	77.8(8)	78.2(3)	79.3(9)	78.5(11)	78.6(8)
N2–Re1–Cl1	89.2(6)	89.4(2)	89.6(7)	92.3(8)	88.6(6)
N3–Re1–Cl1	86.1(5)	84.5(2)	86.0(6)	86.5(6)	84.3(5)
N1–Re1–N3	106.0(8)	106.5(3)	103.9(8)	102.3(9)	108.1(8)
N1–Re1–Cl1	165.8(5)	162.7(2)	164.5(6)	164.9(6)	165.8(6)
N2–Re1–N3	170.7(8)	171.8(3)	172.9(9)	177.9(10)	172.2(7)

[a] There are two crystallographically independent complex molecules in the asymmetric unit.

In the 4-Mepy coordinated complex **10**, the Re1−O1 distance (1.702(6) Å) is normal for double bonds in the oxorhenium(V) complexes as described above (Table II-6).[15,27,54-64] The longer Re1−Cl2 distance than the Re1−Cl1 distance will arise from the *trans* influence of the Re=O double bond, and the Re1−N3 distance, which is fairly long in comparison with reported Re-N (heterocyclic) distances (2.11–2.17 Å),[2,54-57] will also arise from *trans* influence of the Re1−N2 (amide) bond. The Re1−O1 distance (1.75(2) Å) of 4-*t*-Bupy coordinated complex **11** can be classed as the longest Re=O double bond. The tendency of other bond distances around rhenium atom in **11** is similar to **10**. On the other hand, the Re1−O1 distances of the pyridine coordinated complex **9** (1.901(7) Å) and 4-Clpy coordinated complex **12** (1.842(11) Å) are too long as Re=O double bond (Table II-6). These distances agree with those of Re−O single bond such as alcoholate. On the other hand, the Re1−Cl2 distances (**9**, 2.279(7); **12**, 2.395(7) Å) are too short. These results do not agree with other results, which were observed in **10** and **11**. Firstly, if it is assumed that O1 is hydroxyl oxygen atom, rhenium core will be +IV. The magnetic susceptibility, however, indicated diamagnetism suggesting presence of the oxorhenium(V) core. Secondly, IR and far-IR spectra (see below section) show that Re=O and Re−Cl distances will be middle between **1** and **3**. Therefore, it is anticipated that there is a positional disorder between O1 and Cl2. Such disorder has been reported in a number of molybdenum complexes in which case the relationship of the subject atoms are *cis* configuration.[70-72]

The crystal packings of **9**–**12** are shown in Figure II-6. When the packing structures of each complexes were seen, laws that existed in the disorder and packing were observed. In **10** and **11**, which showed normal bond distances, the intermolecular interaction was not observed and the tendency, that the directions of the O1−Re1−Cl2 axis were not constant, was observed. On the other hand, in **9** and **12** which showed too long Re1−O1 distances and too short Re1−Cl2 distances, the intermolecular interaction (quinoline ring–quinoline ring (3.44(5) Å) and pyridine ring–pyridine ring (3.45(5) Å) intermolecular π−π stacking in **9**, and quinoline ring–quinoline ring (3.9 Å) π−π stacking in **12**) were observed. The tendency, that the directions of the O1−Re1−Cl2 axis were constant, was observed. From these tendencies, when the molecular are packed strongly by intermolecular interaction and the directions of the O1−Re1−Cl2 axis are constant, the influence on the stability of the crystal may be a little even if a part of molecular does packing in shape that O1 changes places into Cl2 on the axis. Therefore, it is presumed that the packing pattern would be a cause of the positional disorder, which is due to the exchange of O1 atom for Cl2 atom.

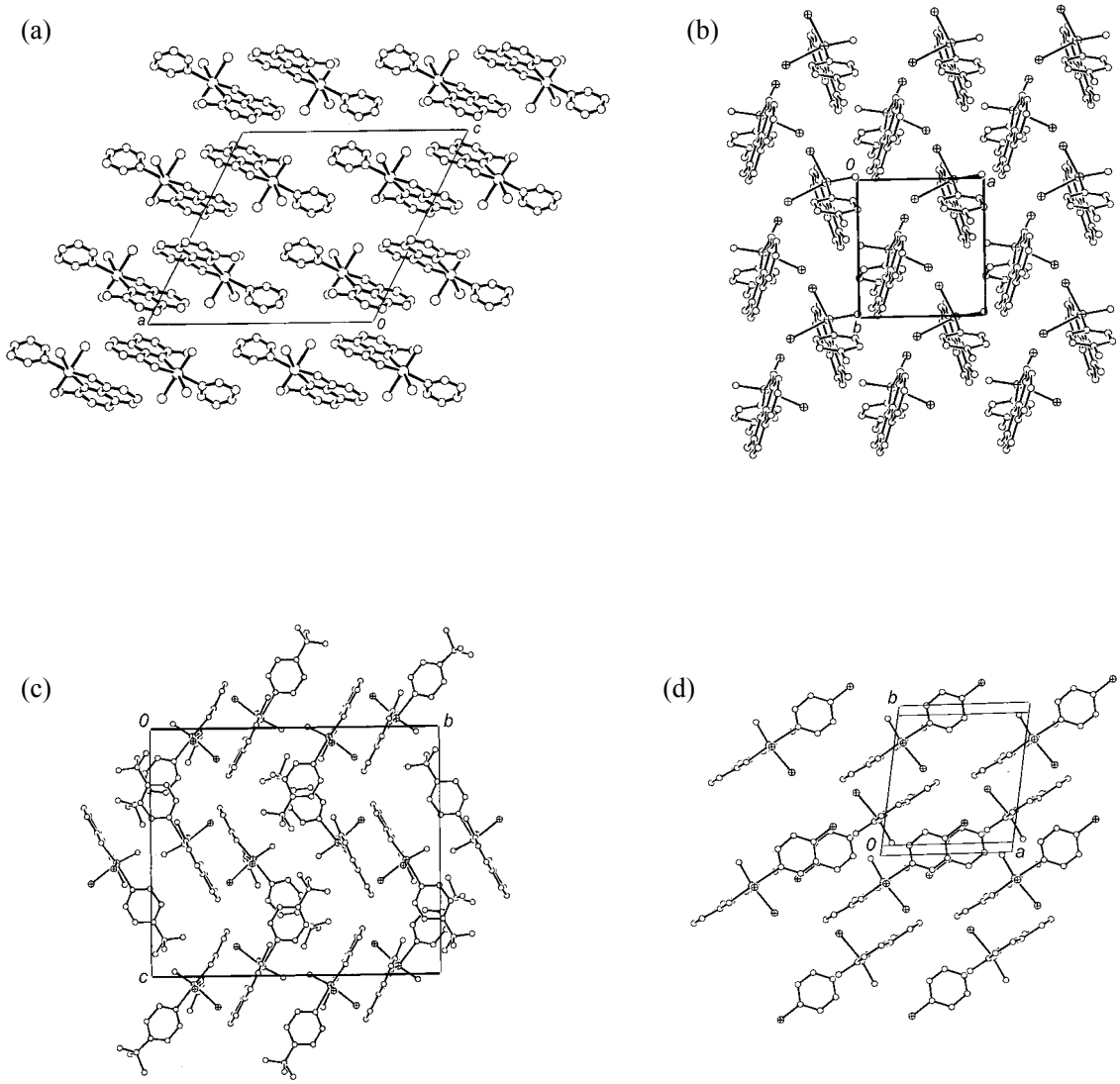

Figure II-6 Projection of crystal packing for [$ReOCl_2$(Hamq)(py)] **9** (a), [$ReOCl_2$(Hamq)(4-Mepy)] **10** (b), [$ReOCl_2$(Hamq)(4-*t*-Bupy)] **11** (c), and [$ReOCl_2$(Hamq)(4-Clpy)] **12** (d).

II-iv-ii. Crystal Structures of **5b**, **6**, **7**

[$ReCl_3$(aq)(PPh_3)] 5b An X-ray crystal analysis for **5b** revealed the presence of a complex molecule and a $C_6H_5CH_3$ molecule. A perspective drawing of only the complex molecule **5b** is shown in Figure II-7. The $C_6H_5CH_3$ molecule evaporated from the crystal during the X-ray measurement and then the crystal was broken slowly. Therefore, an X-ray crystal analysis for **5b** is not complete. The geometrical structure, however, was revealed and it was the same as reported one,[18] which did not include any $C_6H_5CH_3$ solvent. The coordination geometry around the rhenium atom is distorted octahedral with two nitrogen atoms from the asymmetrical didentate-*N*,*N* ligand, three chloride ions and one phosphorus atom from the PPh_3 ligand. The three chloride ions take facial configuration.

Referring to the reported data,[18] the Re1–N2 distance (1.760(9) Å) is significantly shorter than that of **1** (2.000(4) Å). Further, the Re1–N2–C8 angle (129.6(8)°) is somewhat larger than the corresponding angles of the complex with the amido-type Haq.[15] Therefore, it is suggested that N2 amine group is fully deprotonated and the Re1–N2 bond has a double bond character (imide).[15,73]

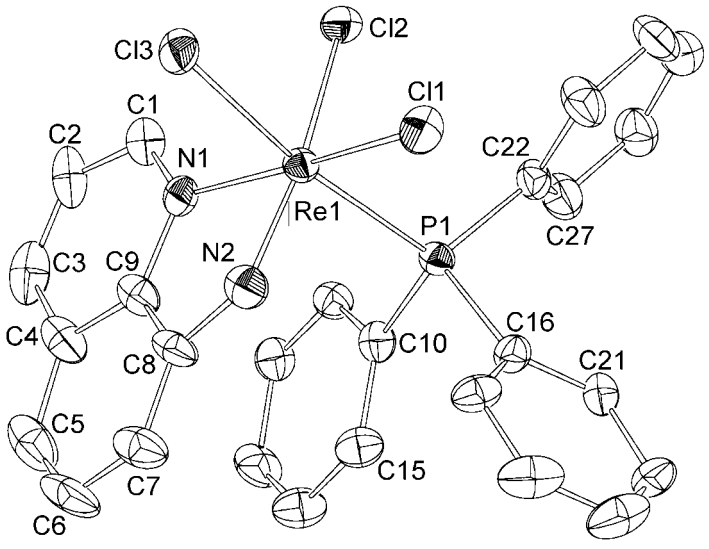

Figure II-7 An ORTEP view of [$ReCl_3$(Haq)(PPh_3)] **5b** with numbering scheme. Hydrogen atoms have been omitted for clarity

[ReOX$_2$(Haq)(L')] 6 (X = Cl, L' = OPPh$_3$), **7** (X = Br, L' = PPh$_3$)　An X-ray crystal analysis for **6** revealed also its geometrical structure, and its perspective drawing is shown in Figure II-8. Selected bond distances and angles are given in Table II-7. The coordination geometry of **6** is similar to the PPh$_3$ coordinated complex **1**, but different from the deoxo complex **5b**. The coordination geometry around rhenium atom is distorted octahedral. The oxo ligand and aromatic amido nitrogen atom N2 lie in the *trans* position, whereas the heterocyclic nitrogen atom N1 and one bromine atom Br1, and the

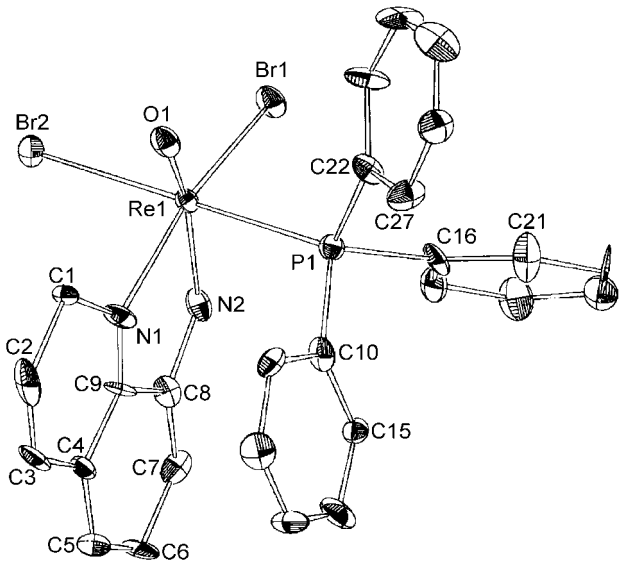

Figure II-8　An ORTEP view of [ReOBr$_2$(Haq)(PPh$_3$)] **6** with numbering scheme. Hydrogen atoms have been omitted for clarity.

Table II-7　Selected bond distances (Å) and angles (°) for [ReOBr$_2$(Haq)(PPh$_3$)] **6**

Re1–O1	1.70(2)	Re1–N1	2.19(2)
Re1–N2	1.98(3)	Re1–P1	2.437(9)
Re1–Br1	2.479(3)	Re1–Br2	2.620(4)
O1–Re1–N1	89.7(10)	N2–Re1–N1	69.3(10)
O1–Re1–P1	86.6(7)	N2–Re1–P1	87.7(7)
O1–Re1–Br1	107.7(6)	N2–Re1–Br1	93.3(7)
O1–Re1–Br2	94.1(7)	N2–Re1–Br2	91.8(7)
O1–Re1–N2	158.4(9)	N1–Re1–Br1	162.6(7)
P1–Re1–Br2	179.2(2)	N1–Re1–P1	88.4(7)
N1–Re1–Br2	92.0(6)	P1–Re1–Br1	91.5(2)
Br1–Re1–Br2	88.0(1)	Re1–N2–C8	123(1)

phosphorus atom and another bromine atom Br2 occupy the *trans* positions, respectively. Though the detail discussion could not be done because of the low quality of crystal for X-ray analysis, the Re=O double bond looks like long similarly to **1**.

The ORTEP drawing of **7** shows a disorder of the aq moiety (outline and solid line) as shown in Figure II-9. Selected bond distances and angles are given in Table II-8. The relation between these two types of structures is enantiomer. In the corresponding methylquinolinylamido complexes **3** and **4**, the disorders were not observed. Therefore, it is presumed that the obtaining the crystals suitable for X-ray analysis depend on whether the quinoline ring has a methyl group or not. The coordination geometry in itself is similar to the corresponding methylquinolinylamido complexes **3** and **4**. The coordination geometry around rhenium atom is distorted octahedral. The oxo ligand and the $OPPh_3$ ligand lie in the *trans* position (axial direction), whereas two nitrogen atoms from the asymmetrical didentate-*N*,*N* ligand and two halogen atoms form the equatorial plane. However, the details could not be discussed, since the crystals for analysis were low quality and the *R* values was large.

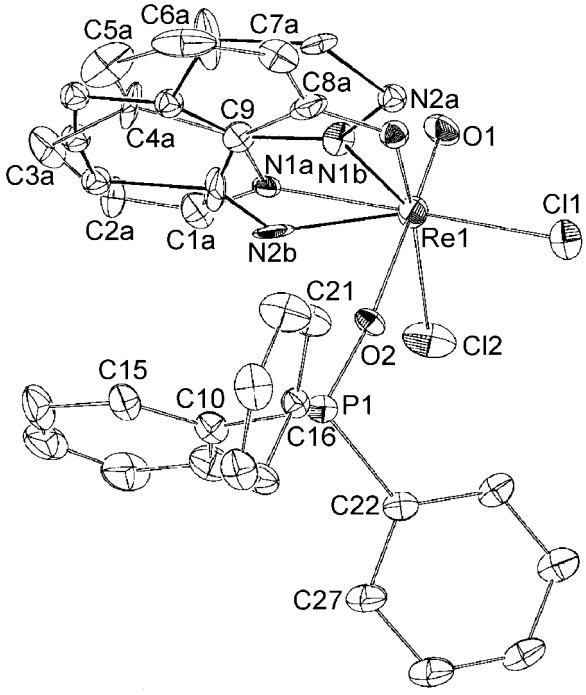

Figure II-9 An ORTEP view of $[ReOCl_2(Haq)(OPPh_3)]$ **7** with numbering scheme. Outline and solid line show disorder in aq moiety. Hydrogen atoms have been omitted for clarity.

Table II-8 Selected bond distances (Å) and angles (°) for [$ReOCl_2(Haq)(OPPh_3)$] **7**

Re1–O1	1.651(9)	Re1–O2	2.171(8)
Re1–N1a, b	2.07(3),[a] 1.88(5)[b]	Re1–N2a, b	2.03(2),[a] 2.13(6)[b]
Re1–Cl1	2.365(4)	Re1–Cl2	2.398(5)
O1–Re1–N1a, b	98.2(7),[a] 98(1)[b]	O2–Re1–N1a, b	80.3(6),[a] 81(1)[b]
O1–Re1–N2a, b	100.7(6),[a] 93(1)[b]	O2–Re1–N2a, b	81.0(5),[a] 83(1)[b]
O1–Re1–Cl1	98.6(4)	O2–Re1–Cl1	86.9(1)
O1–Re1–Cl2	96.0(4)	O2–Re1–Cl2	83.5(2)
O1–Re1–O2	177.4(4)	N1a, b–Re1–Cl1	155.1(7),[a] 110(1)[b]
N2a, b–Re1–Cl2	163.1(5),[a] 74(1)[b]	N1a, b–Re1–N2a, b	75(1),[a] 79(1)[b]
N1a, b–Re1–Cl2	104.4(7),[a] 150(1)[b]	N2a, b–Re1–Cl1	83.4(8),[a] 162.7(7)[b]
Cl1–Re1–Cl2	92.0(2)	Re1–N2a, b–C8	123(4),[a] 106(8)[b]

[a] The bond distance or bond angle of the respectable for the disordered quinolinylamide ring a.

[b] The bond distance or bond angle of the respectable for the disordered quinolinylamide ring b.

II-v. Spectroscopic Properties

IR and far-IR Spectra The IR spectral patterns of **1** and **2** are very similar to each other, and those of **3** and **4**, which have the same geometrical structure in X-ray analysis, are also similar to each other (Figure II-10, Table II-9). For **3** and **4**, the strong IR bands, which are characteristic of the Re=O stretching vibration, are observed in 973 and 972 cm^{-1} (Table II-9), respectively, which are in the normal region (1000–940 cm^{-1}) for the analogous oxorhenium(V) complexes.[74] On the other hand, **1** and **2** exhibit the strong bands at 908 and 915 cm^{-1}, respectively, in the lower wavenumber side (Table II-9). Since the lower wavenumber shift supports the long Re=O bond observed by X-ray crystal analysis, the Re=O distance in **2** may be similar to that in **1**. Accordingly, it is suggested that the structure of **2**, whose single crystals suitable for X-ray analysis could not be obtained, is similar to that of **1**. The aforesaid remark is provided from the fact that **4** was formed from **2**, as well as **3** was formed from **1**. Except for the strong IR band due to Re=O bond, the large differences between the PPh_3 coordinated complexes and the $OPPh_3$ coordinated complexes are observed in ca. 1150, 1120, and 725 cm^{-1} (Figure II-10). These bands, which are only observed in the $OPPh_3$ coordinated complexes, seem to be arisen from the $OPPh_3$ ligand, because the free $OPPh_3$ ligand exhibits the bands at 1190, 1120, and 722 cm^{-1}, respectively. Indeed, the O=P vibration of coordinated $OPPh_3$ was observed in

1140–1150 cm^{-1} in other oxorhenium complexes with $OPPh_3$.[52,53] Only one characteristic band is observed in the region of over 3300 cm^{-1} (Table II-9). This band is assigned to N–H bond and this supports that the amine group of amq ligand is partially deprotonated and the Re–N (amido) bond has a multiple bonding character between single and double bonds.

In the far-IR spectra of the methylquinolinylamido complexes (Figure II-11, Table II-9), for **1** and **3**, two strong bands are observed around 300 cm^{-1} (**1**, 334 and 270 cm^{-1}; **3**, 316 and 280 cm^{-1}). They are assigned to the Re–Cl stretching vibration by referring to the literature.[16,17] The lower value is indicative of the Re–Cl bond in the position *trans* to the PPh_3 (in **1**) or amido of the amq ligand (in **3**). Although no strong bands are observed in **2** and **4** at < 400 cm^{-1}, it is reasonable to assume that two relatively week bands at 224 and 202 cm^{-1} for **2** and 231 and 210 cm^{-1} for **4** are due to the Re–Br stretching vibration mode by considering the reduced mass (Table II-9).

The IR spectral patterns of the quinolinylamido complexes **7** and **8** are similar to each other and the corresponding methylquinolinylamido complexes **3** and **4** (Figure II-12, Table II-9). Therefore, the coordination geometry of **8**, which could not be obtained by the X-ray analysis because of low crystal quality, would be the same as that of the corresponding complexes **3**, **4**, and **7**. The IR spectral pattern of **6** is also similar to the corresponding methylquinolinylamido complexes **1** and **2**. The strong IR bands of the Re=O bond in **7** and **8** are observed in 968 cm^{-1} (Table II-9) which are in the normal region (1000–940 cm^{-1}) for the analogous oxorhenium(V) complexes.[74] On the other hand, **6** exhibit the IR bands at 909 cm^{-1} in the lower wavenumber side as in **1** and **2**. Therefore, the Re=O double bond distance of **6**, which could not be obtained from structural data because of low crystal quality, is expected to be long similarly to **1**. Except for the strong IR band due to Re=O bond, characteristic one N–H band and the differences between the PPh_3 coordinated complexes and the $OPPh_3$ coordinated complexes are also observed, as in the methylquinolinylamido complexes (Figure II-12, Table II-9). In the quinolinylamido complexes mixture **5a**, though the spectral pattern in the region of 1700 to 1000 cm^{-1} is similar to complex **6**, two pairs of weak bands which are assigned to the Re=O double bond (951 and 901 cm^{-1}) and the N–H bond (3336 and 3199 cm^{-1}) are observed (Table II-9). Therefore, **5a** may be the mixture of **5** and its geometrical isomers. On the other hand, the spectral pattern of the imido complex **5b** does not show the band of the Re=O double bond and N–H bond. This agrees with the fact that the structure of **5b** did not have any Re=O double bonds and the N–H bonds.

Table II-9 Selected IR and far-IR spectral data

Complex	IR (ν/cm^{-1})[a]			far-IR (ν/cm^{-1})[a]
	Re=O	N–H	P=O	Re–X (X = Cl or Br)
$[ReOCl_2(Hamq)(PPh_3)]$ **1**	908 (vs)	3292 (s)	—	334 (vs) 270 (vs)
$[ReOBr_2(Hamq)(PPh_3)]$ **2**	915 (vs)	3254 (m)	—	224 (s) 202 (w)
$[ReOCl_2(Hamq)(OPPh_3)]$ **3**	973 (vs)	3316 (m)	1151 (vs)	316 (vs) 280 (vs)
$[ReOBr_2(Hamq)(OPPh_3)]$ **4**	972 (vs)	3311 (m)	1147 (vs)	231 (m) 202 (w)
quinolinylamido complexes mixture **5a**	951 (w) 901 (w)	3336 (w) 3199 (w)	—	(351 (m) 320 (m) 301 (m) 280 (w) 268 (m))
$[ReCl_3(aq)(PPh_3)]$ **5b**	—	—	—	320 (s) 300 (m) 284 (s)
$[ReOBr_2(Haq)(PPh_3)]$ **6**	909 (vs)	3192 (m)	—	237 (w) 202 (m)
$[ReOCl_2(Haq)(OPPh_3)]$ **7**	968 (vs)	3307 (m)	1151 (vs)	326 (m) 276 (m)
$[ReOBr_2(Haq)(OPPh_3)]$ **8**	968 (vs)	3292 (m)	1147 (vs)	245 (m) 199 (m)
$[ReOCl_2(Hamq)(py)]$ **9**	940 (vs)	3326 (s)	—	324 (vs) 277 (vs)
$[ReOCl_2(Hamq)(4\text{-Mepy})]$ **10**	947 (vs)	3326 (s)	—	330 (s) 264 (s)
$[ReOCl_2(Hamq)(4\text{-}t\text{-Bupy})]$ **11**	938 (vs)	3292 (s)	—	332 (s) 261 (s)
$[ReOCl_2(Hamq)(4\text{-Clpy})]$ **12**	940 (m)	3289 (m)	—	325 (s)

[a] vs, very strong; s, strong; m, medium; w, weak.

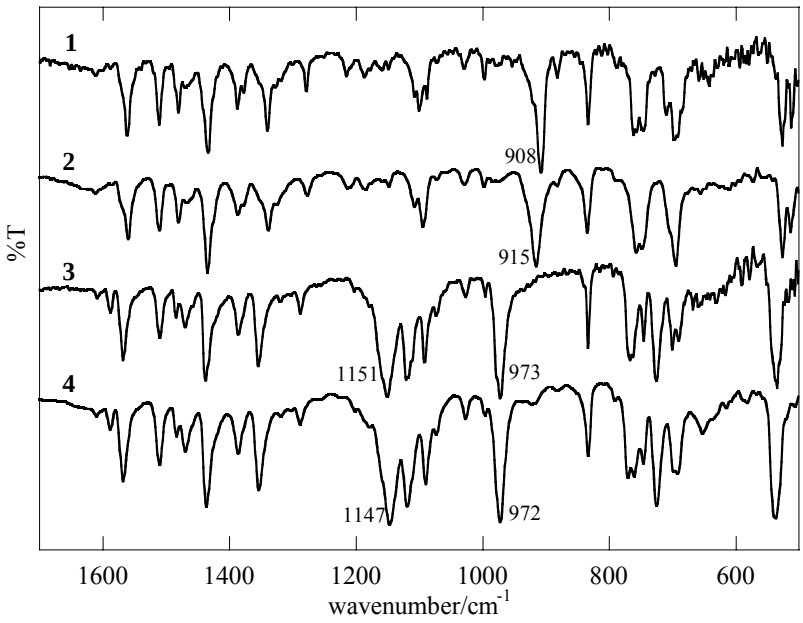

Figure II-10 IR spectra of $[ReOCl_2(Hamq)(PPh_3)]$ **1**, $[ReOBr_2(Hamq)(PPh_3)]$ **2**, $[ReOCl_2(Hamq)(OPPh_3)]$ **3**, and $[ReOBr_2(Hamq)(OPPh_3)]$ **4**.

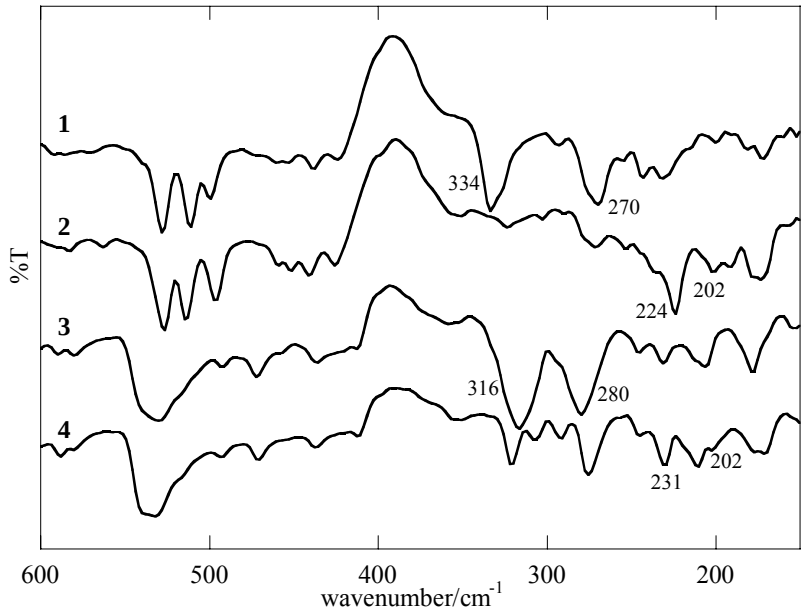

Figure II-11 Far-IR spectra of $[ReOCl_2(Hamq)(PPh_3)]$ **1**, $[ReOBr_2(Hamq)(PPh_3)]$ **2**, $[ReOCl_2(Hamq)(OPPh_3)]$ **3**, and $[ReOBr_2(Hamq)(OPPh_3)]$ **4**.

In the far-IR spectra of the quinolinylamido complexes, the Re–Cl stretching vibration bands are not so clear such as the methylquinolinylamido complexes **1** and **3**, but they are assigned in the region of 330–270 cm^{-1} (Figure II-13, Table II-9). No strong band is also observed in the bromo complexes **6** and **8** at < 400 cm^{-1}. It is reasonable to assume that two relatively week bands at 237 and 202 cm^{-1} for **6** and 245 and 199 cm^{-1} for **8** are due to the Re–Br stretching vibration mode by considering the reduced mass, as in the amq complexes.

The IR spectra of the complexes **9**–**12** with pyridine derivatives were shown in Figure II-14. The strong IR bands of the Re=O are observed in 947–938 cm^{-1} (Table II-9), which are in the normal region for the analogous oxorhenium(V) complexes.[74] Therefore the Re=O double bond distances of **9** and **12**, which were observed as unusual long values because of low crystal quality and disorder, are expected to be normal length, in truth. Except for the strong IR band due to Re=O bond, characteristic one N–H band is observed in 3326–3289 cm^{-1} (Table II-9). This only one band suggests that the amine group of amq ligand is partially deprotonated and the Re–N (amido) bond has a multiple bonding character between single and double bonds.

In the far-IR spectra of the pyridine coordinated complex, the Re–Cl stretching vibration bands of **9**–**11** are observed as two very strong bands (277–261 cm^{-1} and 332–324 cm^{-1}) (Figure II-15, Table II-9). These values are close to chloro complexes **1** and **3**. On the other hand, in **12**, one strong band assigned to Re–Cl vibration was observed close to other complexes with pyridine derivatives (325 cm^{-1}). The second band around 270 cm^{-1}, however, could not be assigned because there are many middle intensity bands.

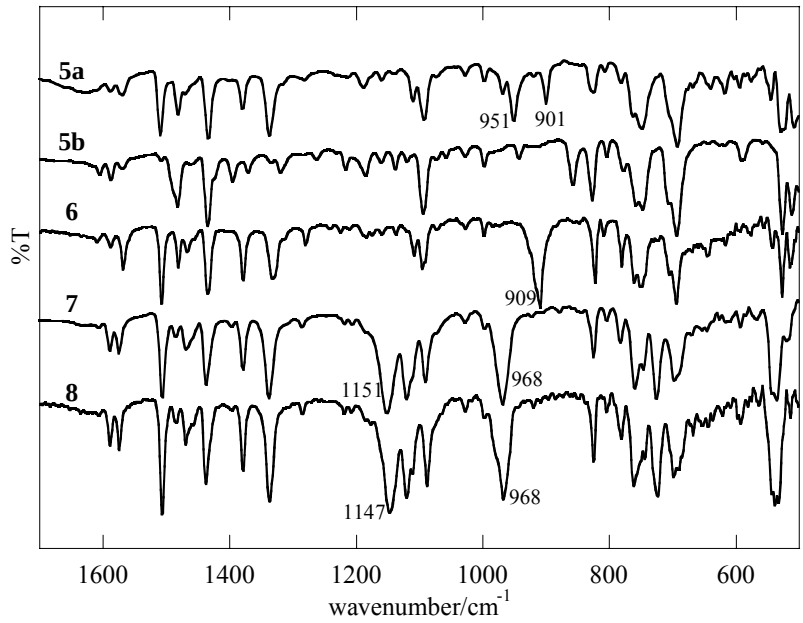

Figure II-12 IR spectra of quinolinylamido complexes mixture **5a**, [$ReCl_3$(aq)(PPh_3)] **5b**, [$ReOBr_2$(Haq)(PPh_3)] **6**, [$ReOCl_2$(Haq)($OPPh_3$)] **7**, and [$ReOBr_2$(Haq)($OPPh_3$)] **8**.

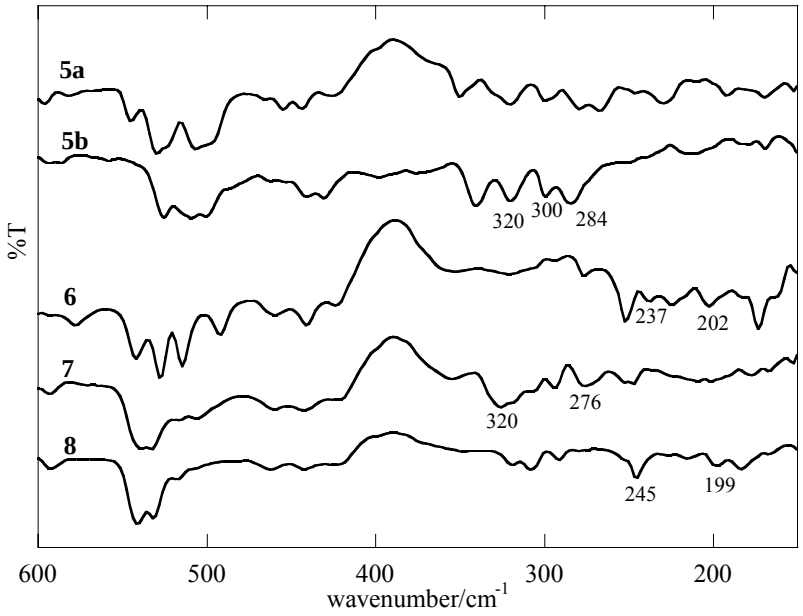

Figure II-13 Far-IR spectra of quinolinylamido complexes mixture **5a**, [$ReCl_3$(aq)(PPh_3)] **5b**, [$ReOBr_2$(Haq)(PPh_3)] **6**, [$ReOCl_2$(Haq)($OPPh_3$)] **7**, and [$ReOBr_2$(Haq)($OPPh_3$)] **8**.

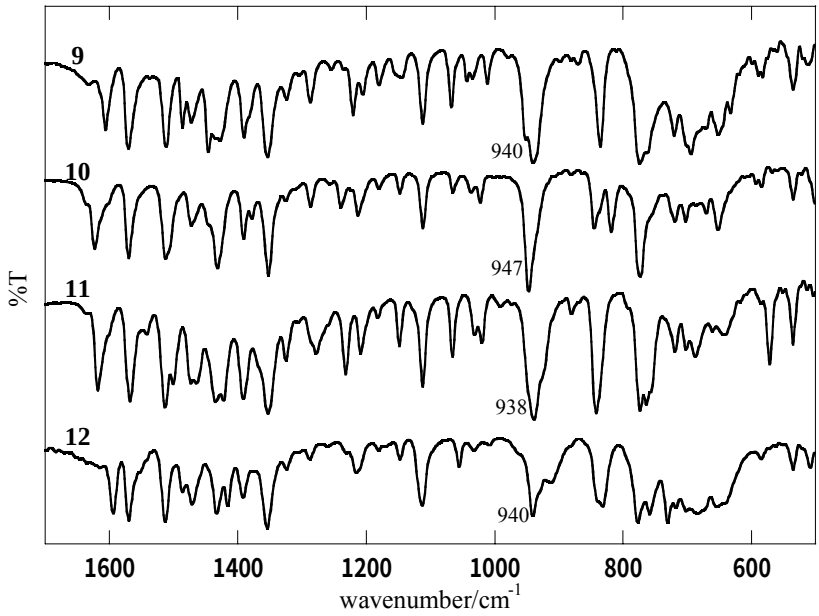

Figure II-14 IR spectra of [$ReOCl_2$(Hamq)(py)] **9**, [$ReOCl_2$(Hamq)(4-Mepy)] **10**, [$ReOCl_2$(Hamq)(4-*t*-Bupy)] **11**, and [$ReOCl_2$(Hamq)(4-Clpy)] **12**

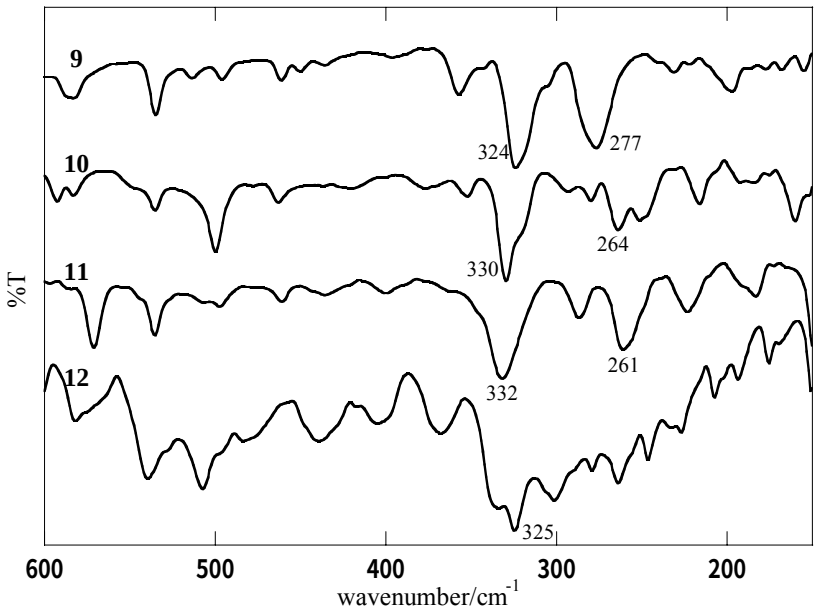

Figure II-15 Far-IR spectra of [$ReOCl_2$(Hamq)(py)] **9**, [$ReOCl_2$(Hamq)(4-Mepy)] **10**, [$ReOCl_2$(Hamq)(4-*t*-Bupy)] **11**, and [$ReOCl_2$(Hamq)(4-Clpy)] **12**

Electronic Absorption and Diffuse Reflectance Spectra The electronic absorption spectra of complexes **1**–**11** were measured by using CH_2Cl_2 solution in different concentrations (1.0×10^{-3}, 1.0×10^{-4}, and 1.0×10^{-5} mol dm^{-3}) (Figures II-16–II-21). The solid state diffuse reflectance (DR) spectra of complexes **1**–**11** were also measured. The absorption and DR spectral data are summarized in Tables II-10 and II-11, respectively. The absorption spectra of **1** exhibit concentration dependence (Figure II-16). That is to say, the peak intensity at 445 nm increases with increasing the concentration of **1**. By considering the results of ^{31}P NMR (vide infra), it is expected that the reason of the concentration dependence would be the release of monodentate ligand PPh_3 in solution. Indeed, when the excess of PPh_3 was added to the solution of **1** (1.0×10^{-4} mol dm^{-3}), a new intense band was appeared at 436 nm and the spectral patterns were dramatically changed with increasing the concentration of PPh_3 (Figure II-17). The spectrum curving pattern of **1** with excess PPh_3 (1.0×10^{-1} mol dm^{-3}) is similar to that of solid state DR spectrum (Figure II-17). This suggest that **1** keeps metal center-ligand (PPh_3) bond and a six-coordinated state under high PPh_3 concentration condition, while **1** releases PPh_3 from metal center and changes to the five-coordinated state under low PPh_3 concentration condition. Thus, the equilibrium Eq. II-9 will apply in **1**. Generally, in high oxidation state complexes with the multiple

$$[ReOCl_2(Hamq)(PPh_3)]\ \mathbf{1} \rightleftharpoons [ReOCl_2(Hamq)] + PPh_3 \quad \text{(II-9)}$$

bonding ligands, the sixth coordination bond becomes weak. However, such an easy releases of PPh_3 in the concentration region (1.0×10^{-3}–1.0×10^{-5} mol dm^{-3}) are rare for oxorhenium(V) complexes with PPh_3 and it is very interesting property from the standpoint of applying for catalyst. The absorption spectral patterns of the bromo complex **2** also show concentration dependence similar to those of **1** except for the increased in molar absorptivity in whole. On the other hand, the absorption spectra of **3** (Figure II-18) and **4** showed little concentration dependence apparently ranging in concentration from 1.0×10^{-3} to 1.0×10^{-5} mol dm^{-3}. When following in the wake of **1**, the excess of $OPPh_3$ was added to the solution of **3** (1.0×10^{-4} mol dm^{-3}), a new intense band was appeared at 392 nm and the spectral patterns were dramatically changed similarly to **1** with PPh_3 (Figure II-19). The

$$[ReOCl_2(Hamq)(OPPh_3)]\ \mathbf{3} \rightleftharpoons [ReOCl_2(Hamq)] + OPPh_3 \quad \text{(II-10)}$$

equilibrium Eq. II-10 will apply in **3**. The low concentration (1.0×10^{-5} mol dm^{-3}) spectral pattern of **1** and **3** are about the same. This result supports the Eqs. II-9 and II-10 that these complexes release the monodentate ligand and have the same five-coordinated state $[ReOCl_2(Hamq)]$ in solution state

(Scheme II-5). The absorption spectra of the complexes **9**–**11** with pyridine derivatives show obvious concentration dependence and the low concentration spectral pattern of **9** was similar to that of **1** and **3** (Figure II-20). This suggests that **9** also have the same five-coordinated state [$ReOCl_2$(Hamq)] as **1** and **3** in solution (Scheme II-5). The pyridine concentration dependence was measured by using excess of py and 1.0×10^{-4} mol dm^{-3} of **1** in stead of **9** (Figure II-21), because the metal–ligand (py) interaction is observed and the equilibrium of **9** (Eq. II-11) does not heavily lean to right in 1.0×10^{-4} mol dm^{-3} different from **1** and **3**. These concentration dependence spectra revealed that the equiliburium constant of the metal–ligand bond for **9** is larger than that for **1** by two orders of magnitude.

$$[ReOCl_2(Hamq)(py)]\ \mathbf{9} \rightleftharpoons [ReOCl_2(Hamq)] + py \qquad (II\text{-}11)$$

Scheme II-5

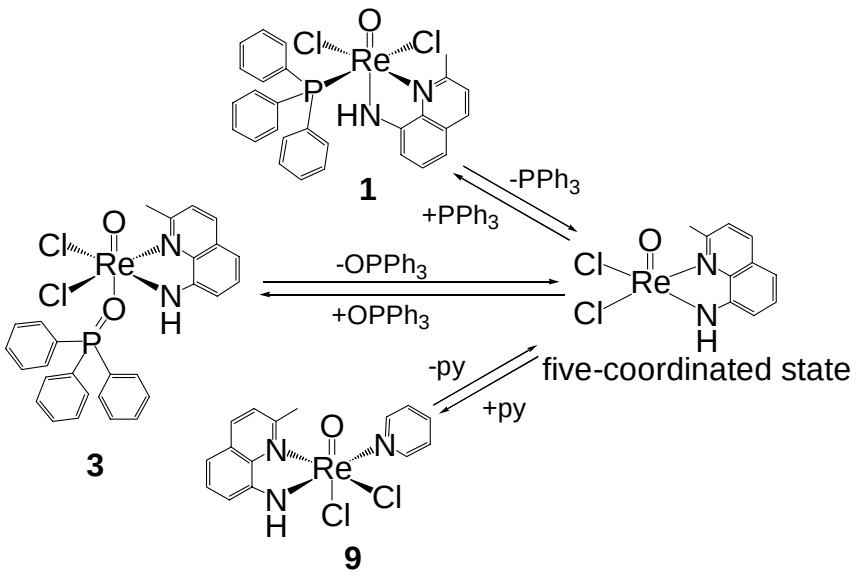

Table II-10 Absorption and reflectance spectral data of **1**–**8**

	Concentration (mol dm^{-3})	Absorption and diffuse reflectance maxima nm (ε/mol^{-1} dm^3 cm^{-1})			
1	1.0×10^{-3}	329 (4.4×10^3)	342 (4.7×10^3)	365 (3.6×10^3)	445 (2.2×10^3)
	1.0×10^{-4}	330 (5.0×10^3)	342 (5.4×10^3)	366 (4.0×10^3)	452 (1.9×10^3)
	1.0×10^{-5}	330 (5.0×10^3)	342 (5.4×10^3)	361 (4.0×10^3)	452 (1.8×10^3)
	DR	452	524 (sh)	617 (sh)	
2	1.0×10^{-3}	328 (5.0×10^3)	343 (4.9×10^3)	372 (4.0×10^3)	448 (2.4×10^3)
	1.0×10^{-4}	331 (5.5×10^3)	344 (5.7×10^3)	372 (4.7×10^3)	462 (1.7×10^3)
	1.0×10^{-5}	330 (5.4×10^3)	344 (5.7×10^3)	372 (4.7×10^3)	462 (1.6×10^3)
	DR	459	524 (sh)	602	
3	1.0×10^{-3}	332 (4.4×10^3)	342 (4.8×10^3)	365 (3.6×10^3)	453 (1.6×10^3)
	1.0×10^{-4}	330 (4.7×10^3)	342 (5.1×10^3)	371 (3.7×10^3)	462 (1.6×10^3)
	1.0×10^{-5}	330 (4.9×10^3)	342 (5.1×10^3)	364 (3.8×10^3)	457 (1.7×10^3)
	DR	442 (sh)	518		
4	1.0×10^{-3}	332 (5.4×10^3)	344 (5.7×10^3)	371 (4.7×10^3)	462 (1.6×10^3)
	1.0×10^{-4}	332 (5.8×10^3)	344 (6.1×10^3)	372 (5.0×10^3)	464 (1.5×10^3)
	1.0×10^{-5}	331 (5.1×10^3)	344 (5.9×10^3)	372 (4.8×10^3)	464 (1.5×10^3)
	DR	448	518 (sh)		
5a	1.0×10^{-3}	434			
	1.0×10^{-4}	436			
	1.0×10^{-5}	441			
	DR	446	521 (sh)		
5b	1.0×10^{-3}	362 (6.9×10^3)	400 (4.9×10^3 sh)	474 (1.2×10^3 sh)	
	1.0×10^{-4}	360 (7.2×10^3)	400 (5.1×10^3 sh)	474 (1.2×10^3 sh)	
	1.0×10^{-5}	360 (7.2×10^3)	400 (5.1×10^3 sh)	474 (1.2×10^3 sh)	
	DR	370	395	450	
6	1.0×10^{-3}	446 (5.9×10^3)			
	1.0×10^{-4}	446 (4.6×10^3)			
	1.0×10^{-5}	457 (3.4×10^3)			
	DR	457			
7	1.0×10^{-3}	326 (2.8×10^3)	340 (2.9×10^3)	374 (2.8×10^3)	460 (2.0×10^3 sh)
	1.0×10^{-4}	325 (3.5×10^3)	340 (3.4×10^3)	360 (2.7×10^3)	459 (2.1×10^3)
	1.0×10^{-5}	325 (4.0×10^3)	337 (3.8×10^3)	361 (2.8×10^3)	461 (2.3×10^3)
	DR	431	524		
8	1.0×10^{-3}	323 (3.2×10^3)	340 (3.1×10^3)	385 (3.4×10^3)	472 (2.0×10^3 sh)
	1.0×10^{-4}	325 (4.1×10^3)	340 (3.9×10^3)	371 (3.6×10^3)	462 (2.3×10^3)
	1.0×10^{-5}	326 (4.6×10^3)	336 (4.4×10^3)	367 (3.6×10^3)	466 (2.4×10^3)
	DR	437	518		

Table II-11 Absorption and reflectance spectral data of **9**–**11**

	Concentration (mol dm^{-3})	Absorption and diffuse reflectance maxima nm (ε/mol^{-1} dm^3 cm^{-1})
9	1.0×10^{-3}	328 (4.3×10^3) 400 (4.9×10^3) 530 (1.3×10^3 sh) 710 (1.2×10^2)
	1.0×10^{-4}	330 (4.4×10^3) 342 (4.4×10^3) 380 (3.8×10^3)
	1.0×10^{-5}	330 (4.5×10^3) 342 (4.7×10^3) 365 (3.6×10^3) 442 (1.7×10^3)
	DR	424 535 728 (sh)
10	1.0×10^{-3}	404 (5.1×10^3) 520 (1.5×10^3 sh) 720 (1.3×10^2)
	1.0×10^{-4}	393 (4.2×10^3) 420 (3.8×10^3)
	1.0×10^{-5}	328 (4.2×10^3) 342 (4.3×10^3) 370 (3.4×10^3) 455 (1.9×10^3 sh)
	DR	435 536 728
11	1.0×10^{-3}	404 (5.0×10^3) 520 (1.4×10^3) 710 (1.2×10^2)
	1.0×10^{-4}	396 (4.4×10^3)
	1.0×10^{-5}	329 (4.2×10^3) 342 (4.2×10^3) 371 (3.4×10^3) 450 (2.0×10^3)
	DR	435 560 (sh) 740 (sh)

The spectral patterns of the quinolinylamido complexes **5a**, **6**, **7**, and **8** also show concentration dependence. The sample for measurement of **5a** was prepared on the assumption that the molecular weight of **5a** is the same as that of **5**. The spectral shift pattern of **5a** (shift from 434 to 441 nm) is similar to that of **6** (shift from 446 to 457 nm) (Table II-10). Therefore, it is suggested that **5a**, in solution, does not retain the structure of solid state and **5** ([$ReOCl_2$(Haq)(PPh_3)]) may be formed mixture when it precipitate. In the spectra of **7** and **8** in dilute solution, the new peaks appear at 461 and 466 nm, respectively (Table II-10). On the other hand, the deoxo complex **5b** does not show concentration dependence. Since the absorption spectral pattern agrees with the DR spectral pattern of **5b**, it is assumed that **5b** retains its structure in solution state.

For **1**, **3**, and **9**, Figures II-17, 19, and 21 show dramatically changing bands at ca. 400 nm. These bands can be attributed to the charge-transfer (CT) band between metal center and coordinated monodentate ligand. In previous reports,[14] the bands, which are observed in the region of 350–250 nm, were assigned to the CT band of amide to metal center. Therefore, in the present cases, the bands observed in 345–325 nm are assumed to CT band of amide.

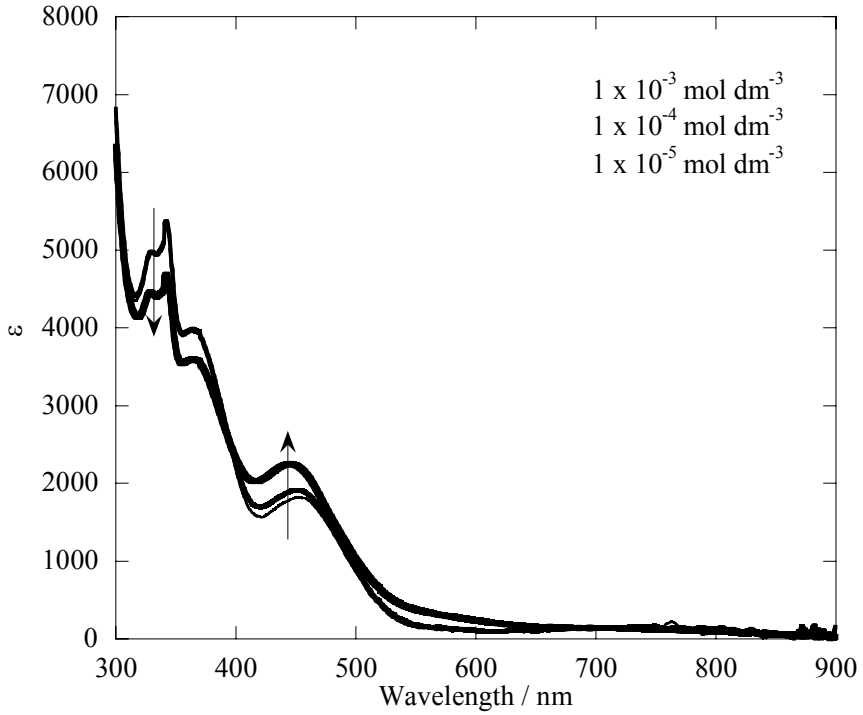

Figure II-16 Electronic absorption spectra of $[ReOCl_2(Hamq)(PPh_3)]$ **1** in some concentration conditions in CH_2Cl_2.

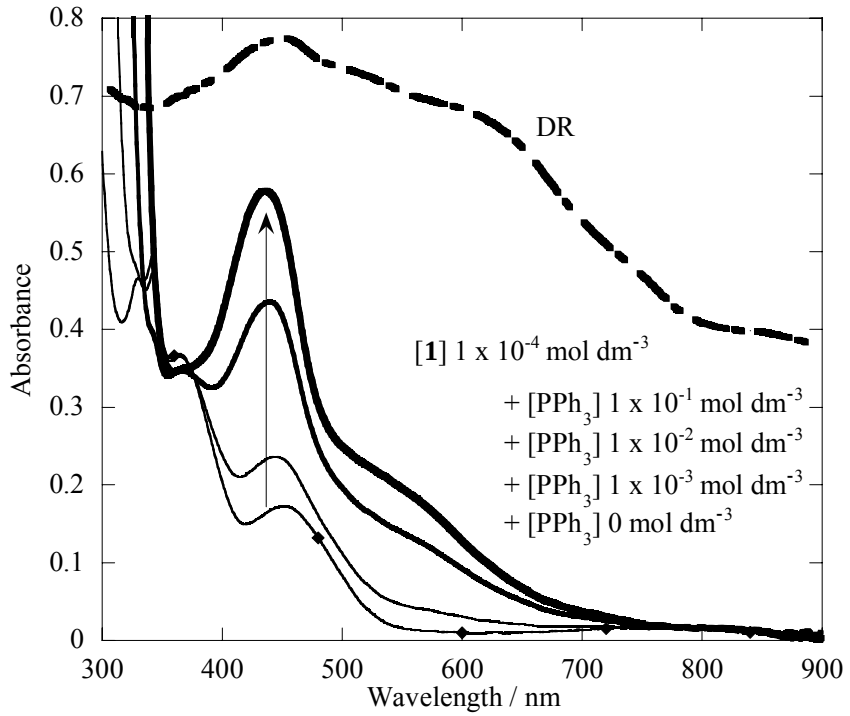

Figure II-17 PPh_3 concentration dependence of 1×10^{-4} mol dm^{-3} of **1** in CH_2Cl_2.

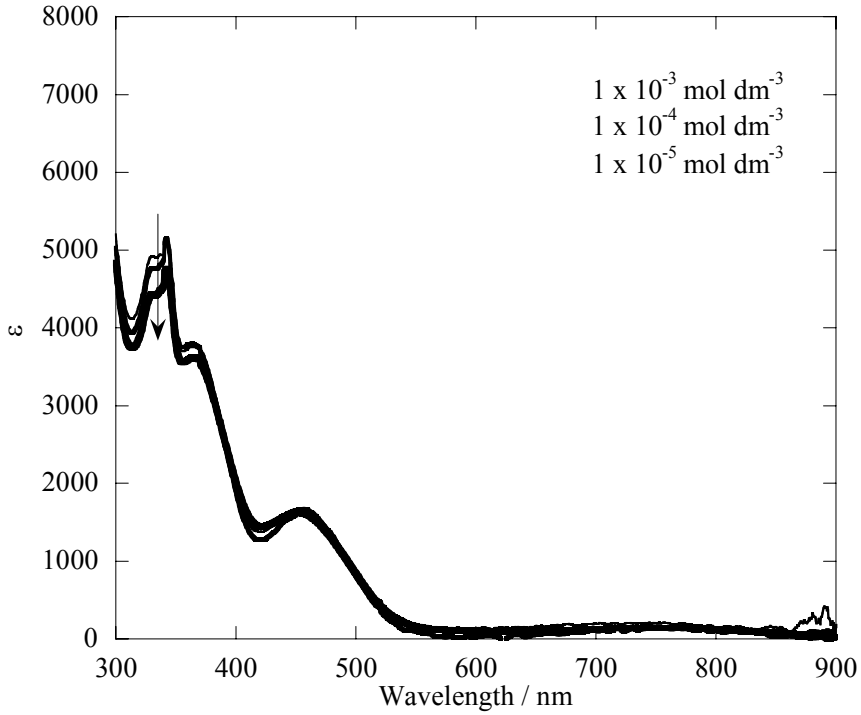

Figure II-18 Electronic absorption spectra of $[ReOCl_2(Hamq)(OPPh_3)]$ **3** in some concentration conditions in CH_2Cl_2.

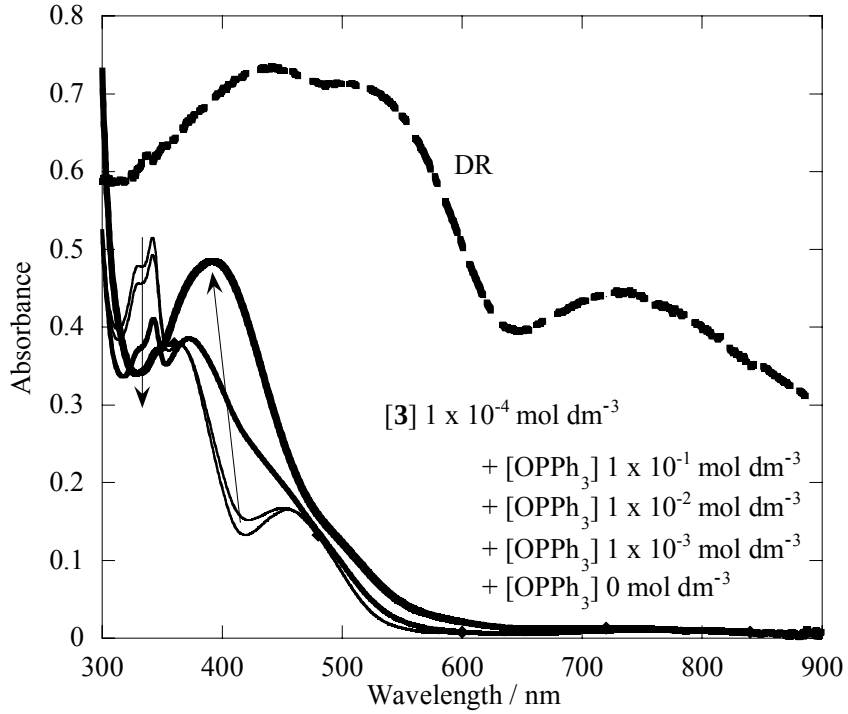

Figure II-19 $OPPh_3$ concentration dependence of 1×10^{-4} mol dm^{-3} of **3** in CH_2Cl_2.

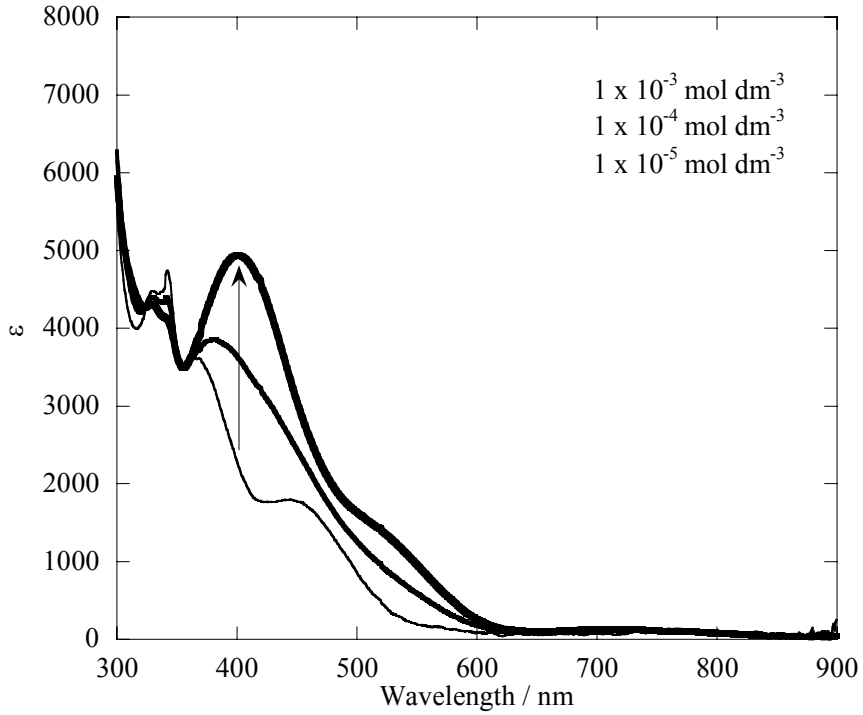

Figure II-20 Electronic absorption spectra of $[ReOCl_2(Hamq)(py)]$ **9** in some concentration conditions in CH_2Cl_2.

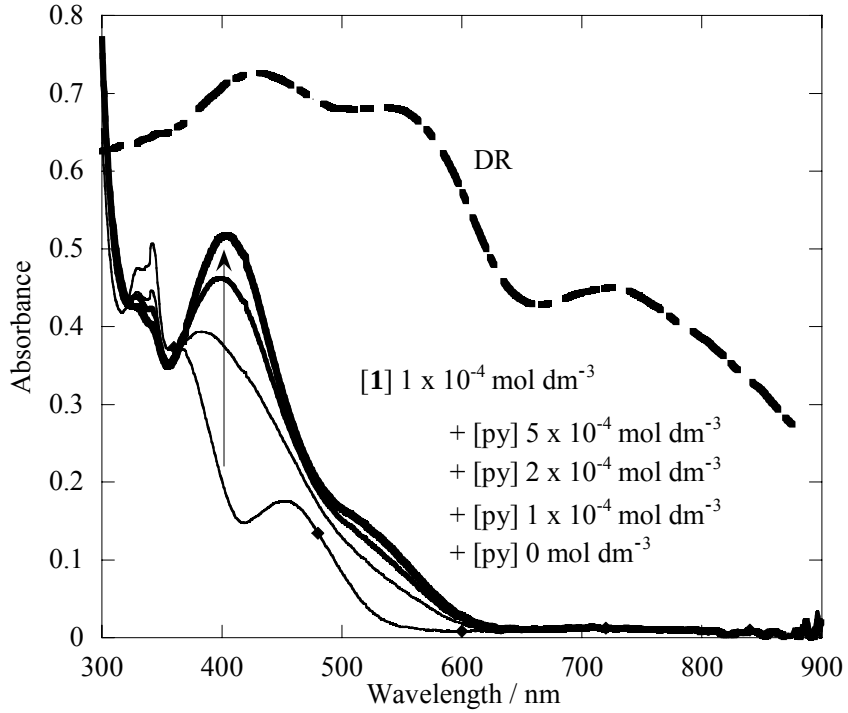

Figure II-21 py concentration dependence of 1×10^{-4} mol dm^{-3} of **1** in CH_2Cl_2.

$^{31}P\{^{1}H\}$ NMR and CP-MAS NMR Spectra The $^{31}P\{^{1}H\}$ NMR chemical shifts exhibit at δ -7.1 – -7.6 for the PPh_3 coordinated complexes **1**, **2**, **5a**, and **6**, and δ 26.8 – 28.5 for the $OPPh_3$ coordinated complexes **3**, **4**, **7**, and **8** in $CDCl_3$ solution. They are close to the values of the free PPh_3 (δ -7.4) and $OPPh_3$ (δ 27.4) ligands (Table II-12). These results indicate that these complexes release PPh_3 or $OPPh_3$ in solution state as expected in the electronic absorption spectra. On the other hand, the $^{31}P\{^{1}H\}$ NMR chemical shift of the imido complex **5b** is observed in δ -26.8 and shows the retention of Re–P bond. The fact that the retention of Re–P bond was observed in the $^{31}P\{^{1}H\}$ NMR spectra agrees with the result which was observed in the electronic absorption spectra. Since the complexes **1**–**8** except **5b** do not retain their structures in solution state, the measurements of the $^{31}P\{^{1}H\}$ CP-MAS NMR spectra in solid state, corresponding to the $^{31}P\{^{1}H\}$ NMR spectra in solution state, were carried out. The $^{31}P\{^{1}H\}$ CP-MAS NMR spectra for the $OPPh_3$ coordinated complexes **3**, **4**, **7**, and **8** exhibit many sharp signals in relatively sparse number of integration (Figure II-22). Changing spin rate (Figure II-23) establishes distinction between many spinning-sideband and one main signal (δ 38.4 for **3**, 39.7 for **4**, 38.1 for **7**, and 40.0 for **8**). On the other hand, the $^{31}P\{^{1}H\}$ CP-MAS NMR spectra for the PPh_3 coordinated complexes **1**, **2**, **5a**, and **6** show very broad signals and could not be assigned. Although the reason of broadening is unclear, I presume that this broadening probably comes from some quadrupole effect of rhenium (I = 5/2). In the PPh_3 coordinated complexes, the phosphorus atom bounds to the rhenium atom directly. On the other hand, the oxygen atom exists between the phosphorus and rhenium atoms in the $OPPh_3$ coordinated complexes. Therefore, the $OPPh_3$ coordinated complexes are not affected by the quadrupole effect as in the PPh_3 coordinated complexes, and show sharp signals. A similar tendency was also observed for their precursors. The free PPh_3 and $OPPh_3$ ligands show sharp signals, whereas the oxorhenium(V) precursors $[ReOX_3(PPh_3)_2]$ (X = Cl or Br) show broad signals (Figure II-24). The sharp signal at about δ 40 in **1** is expected to come from **3**, which is slightly introduced as the impurity. The difference in chemical shift from **3** is expected to attribute to incomplete phase adjustment by very broad signals. Consequently, it was elucidated that the $^{31}P\{^{1}H\}$ CP-MAS NMR spectra would be used for discrimination that there is the direct Re–P bond or not. Additionally, the $^{31}P\{^{1}H\}$ spectra also supported the fact that the structures of complexes **1**–**8** except **5b** are not retained in solution.

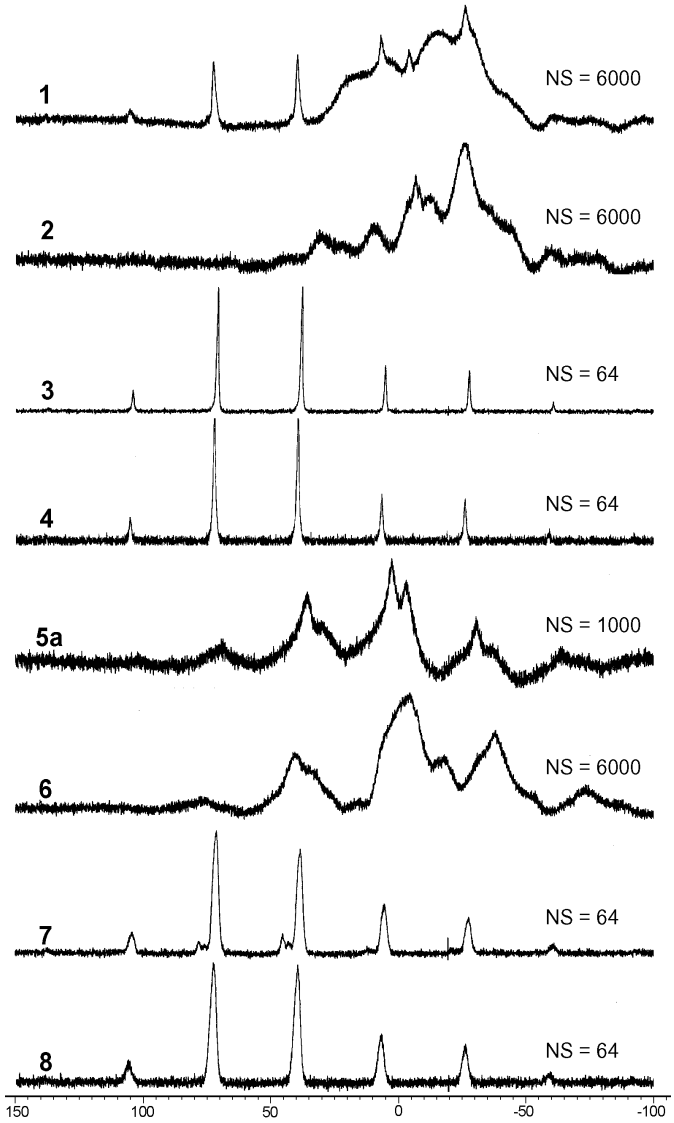

Figure II-22 $^{31}P\{^{1}H\}$ CP-MAS spectra (spinning rate; 8000 Hz) of complexes **1**–**8** except **5b** (NS: number of scans).

Table II-12 $^{31}P\{^{1}H\}$ NMR and $^{31}P\{^{1}H\}$ CP-MAS spectral data of complexes **1**–**8**

Complex	$^{31}P\{^{1}H\}$ NMR	$^{31}P\{^{1}H\}$ CP-MAS
$[ReOCl_2(Hamq)(PPh_3)]$ **1**	-7.6	impossible to be assigned
$[ReOBr_2(Hamq)(PPh_3)]$ **2**	-7.5	impossible to be assigned
$[ReOCl_2(Hamq)(OPPh_3)]$ **3**	28.4	38.4
$[ReOBr_2(Hamq)(OPPh_3)]$ **4**	27.7	39.7
quinolinylamido complexes mixture **5a**	-7.1	impossible to be assigned
$[ReCl_3(aq)(PPh_3)]$ **5b**	-26.8	–
$[ReOBr_2(Haq)(PPh_3)]$ **6**	-7.3	impossible to be assigned
$[ReOCl_2(Haq)(OPPh_3)]$ **7**	28.5	38.1
$[ReOBr_2(Haq)(OPPh_3)]$ **8**	26.8	40.0

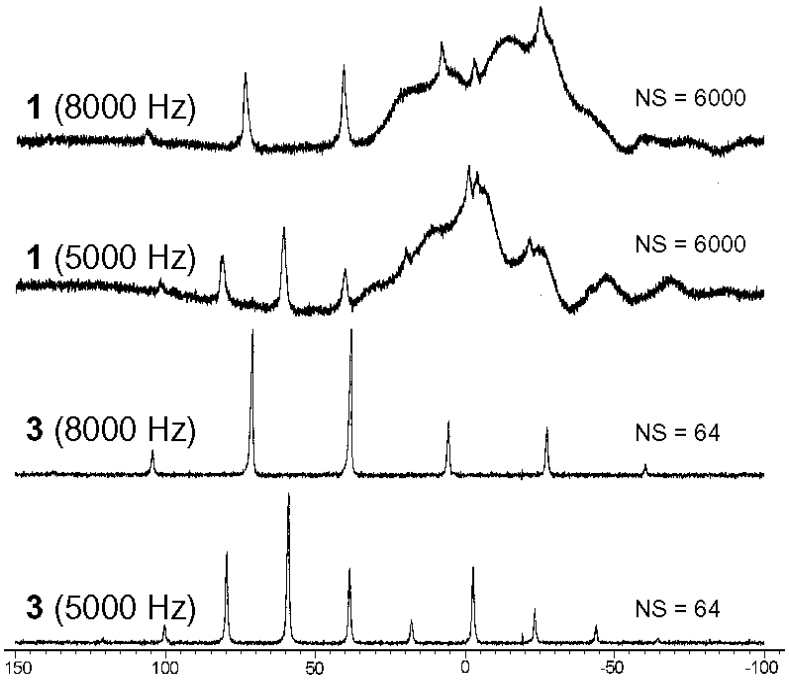

Figure II-23 $^{31}P\{^{1}H\}$ CP-MAS spectra of **1** and **3** measured in two types of spinning rate (8000 and 5000 Hz).

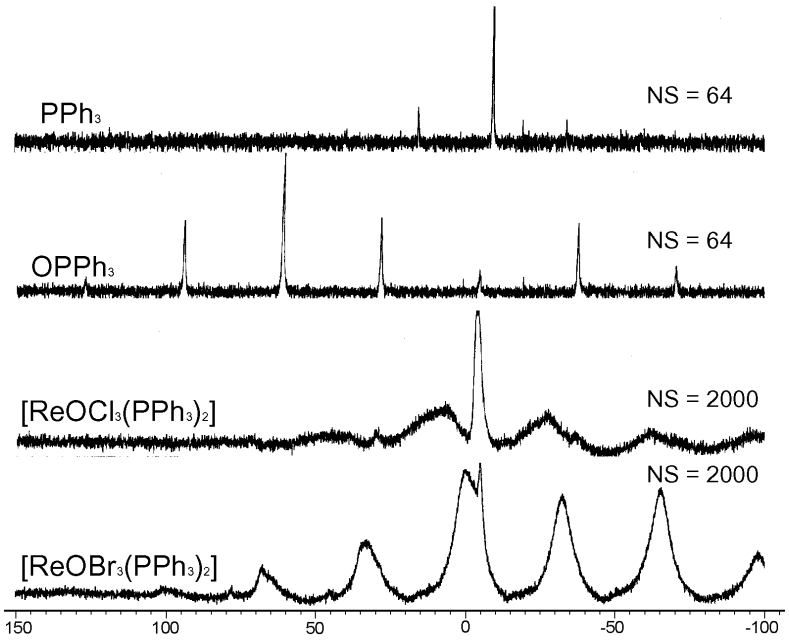

Figure II-24 $^{31}P\{^{1}H\}$ CP-MAS spectra (spinning rate; 8000 Hz) of precursors.

II-vi. OAT Catalytic Reactivity of 1

The OAT catalytic reaction by using dioxo intermediate state on reactive site is widely reported in the methylated oxorhenium(V) complexes, which are the five-coordinated structures and have reactive site.[28-32] In the case of the quinolinylamido complexes, though **1** has no reactive sites in solid state, the vacant site, which could be used for the catalytic reaction, was obtained by releasing the monodentate ligand in solution, as mentioned above. Therefore, the OAT catalytic reactivity of **1** from pyO or 2,6-lutidine-*N*-oxide (2,6-Me_2pyO) to PPh_3 (Eq. II-12) were investigated. It was monitored by ^1H

$$PPh_3 + pyO \xrightarrow{\mathbf{1}} OPPh_3 + py \qquad \text{(II-12)}$$

NMR spectra (Figure II-25). The control experiments of the reaction between 2,6-Me_2pyO and PPh_3 without **1** showed no reaction. As a result of reaction with **1**, it revealed that **1** has OAT catalytic property. In the case of 2,6-Me_2pyO, the reaction was nearly finished, though in the case of pyO, the reaction was incomplete. This incomplete reaction in the case of pyO would be caused by the formation of pyridine coordinated complex [$ReOCl_2$(Hamq)(py)] **9** by stronger interaction between rhenium reactive site and by-product py as observed in electronic absorption spectra, different from the weaker interaction between metal center and bulky 2,6-Me_2py ligand. This result anticipates that

Scheme II-6

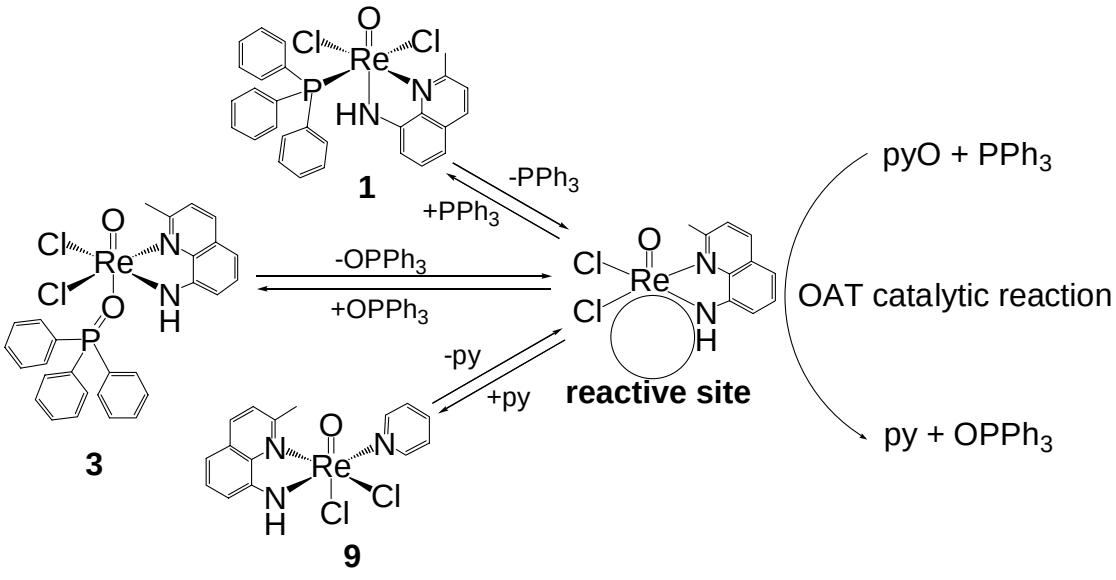

the OAT catalytic reaction of Hamq complexes would occur on the characteristic reactive site similarly to the literatures (Scheme II-6).[28-32] The reactivity of Hamq complexes is rare for non-methylated oxorhenium(V) complexes and its application to OAT catalyst is very interesting.[27] However, the number of OAT catalytic cycles of **1** was about 10 times only. After the reaction, the catalyst **1** showed decomposition to $[pyO]^+[ReO_4]^-$ and H_3amqCl (Eq. II-13). Therefore, the development of a new stabilized complex will be required for the improvement of catalytic activity of quinolinylamido complexes.

$$[ReOCl_2(Hamq)(PPh_3)] + pyO \xrightarrow{H_2O} [Hpy]^+[ReO_4]^- + H_3amqCl + OPPh_3 + HCl \quad (II\text{-}13)$$

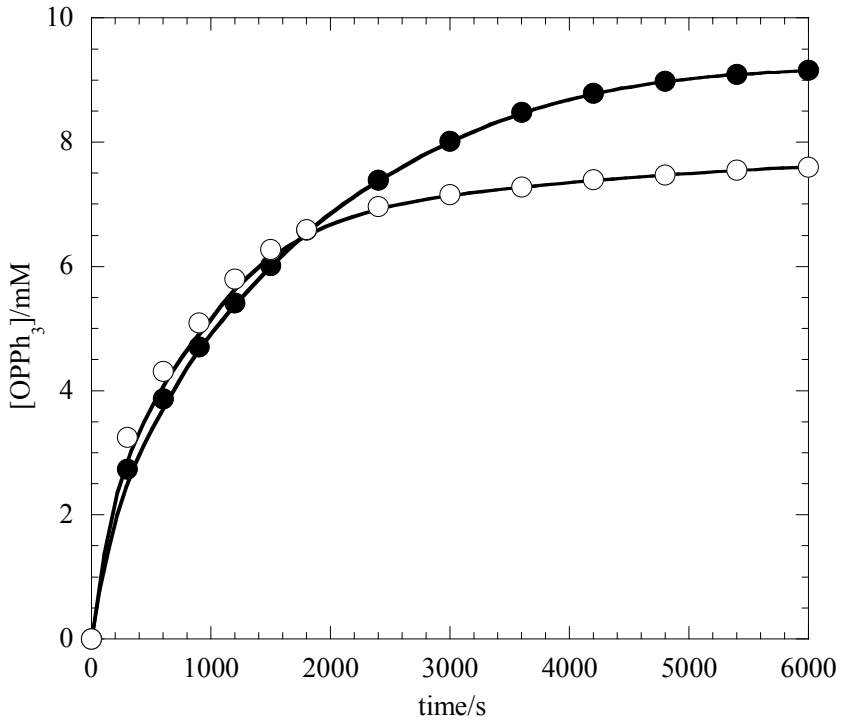

Figure II-25 OAT catalytic reaction of **1** monitored by ^1H NMR spectra in $CDCl_3$: PPh_3 1×10^{-2} mol dm^{-3}: oxygen donor 1×10^{-2} mol dm^{-3} (open circle, pyO; closed circle, 2,6-Me_2pyO): **1** 1×10^{-3} mol dm^{-3}.

II-vii. Conclusion

The reactions of the oxorhenium(V) precursors $[ReOX_3(PPh_3)_2]$ (X = Cl or Br) with the asymmetrical didentate-*N*,*N* ligands 8-aminoquinoline derivatives (H_2amq or H_2aq) in the $CH_2Cl_2/C_6H_5CH_3$ mixed solvent gave the quinolinylamido complexes $[ReOX_2(HL)(PPh_3)]$ (L = amq, X = Cl **1**; L = amq, X = Br **2**; L = aq, X = Br **6**). These complexes were characterized by X-ray crystal analyses and IR, far-IR, electronic absorption, diffuse reflectance, $^{31}P\{^1H\}$ NMR, and $^{31}P\{^1H\}$ CP-MAS NMR spectra. The results of these analyses showed that these complexes have easy replacement property, namely, the PPh_3 ligand was released easily in solution. On the other hand, in the synthesis of $[ReOCl_2(Haq)(PPh_3)]$ **5**, the quinolinylamido complexes mixture **5a** and the deoxo complex $[ReCl_3(aq)(PPh_3)]$ **5b** were obtained depending on the reaction time instead of **5**. The results of the spectroscopic properties revealed that **5a** has concentration dependence, while **5b** does not have that property.

The $OPPh_3$ coordinated complexes $[ReOX_2(HL)(OPPh_3)]$ (L = amq, X = Cl **3**; L = amq, X = Br **4**; L = aq, X = Cl **7**; L = aq, X = Br **8**) were synthesized by using the replacement property of the PPh_3 coordinated complexes. That is to say, they were synthesized by the ligand substitution of PPh_3 for $OPPh_3$. The pyridine coordinated complexes $[ReOCl_2(Hamq)(L)]$ (L = py, **9**; 4-Mepy, **10**; 4-*t*-Bupy, **11**; 4-Clpy, **12**) were also synthesized by using this interesting property in **1**. The results of the electronic absorption spectra showed that these complexes also have easy replacement property, namely, the $OPPh_3$ or pyridine derivatives ligands were released in solution. The results of the X-ray crystal analyses revealed that the changes of the coordination geometry around the oxorhenium(V) core accompanied substitution reactions of PPh_3 to $OPPh_3$ or pyridine derivatives. These structural changes were also supported by the spectroscopic properties.

The OAT catalytic reactivity of **1** from pyO or 2,6-lutidine-*N*-oxide (2,6-Me_2pyO) to PPh_3 were investigated by using the easy replacement reaction observed in the oxorhenium(V) complexes. Eventually, the complex was decomposed but it showed about 10 cycles. The OAT catalytic property is rare for the non-methylated oxorhenium(V) complexes and it is very interesting from the viewpoint of application for catalyst.

References

1 J. H. Espenson, X. Shan, D. W. Lahti, T. M. Rockey, B. Saha, and A. Ellern, *Inorg. Chem.*, **40**, 6717 (2001).

2 S. Fortin and A. L. Beauchamp, *Inorg. Chem.*, **39**, 4886 (2000).

3 S. Fortin and A. L. Beauchamp, *Inorg. Chem.*, **40**, 105 (2001).

4 S. Bélanger and A. L. Beauchamp, *Acta Crystallogr., Sect. C*, **55**, 517 (1999).

5 M. Papachristou, I. C. Pirmettis, C. Tosukalas, D. Papagiannopoulou, C. Raptopoulou, A. Terzis, C. I. Stassinopoulou, E, Chiotellis, M. Pelecanou, and M. Papadopoulos, *Inorg. Chem.*, **42**, 5778 (2003).

6 J. H. Jung, T. A. Albright, D. M. Hoffman, and T. R. Lee, *J. Chem. Soc., Dalton Trans.*, 4487 (1999).

7 J. H. Jung, J. S. Park, D. M. Hoffman, and T. R. Lee, *Polyhedron*, **20**, 2129 (2001).

8 S. D. Orth, J. Barrera, M. Sabat, and W. D. Harman, *Inorg. Chem.*, **33**, 3026 (1994).

9 S. D. Orth, J. Barrera, M. Sabat, and W. D. Harman, *Inorg. Chem.*, **32**, 594 (1993).

10 H. Luo, I. Setyawati, S. J. Rettig, and C. Orvig, *Inorg. Chem.*, **34**, 2287 (1995).

11 J. Chatt and G. A. Rowe, *J. Chem. Soc.*, 4019 (1962).

12 J. Chatt, J. D. Garforth, N. P. Johnson, and G. A. Rowe, *J. Chem. Soc.*, 1012 (1964).

13 J. Chatt, J. R. Dilworth, and G. J. Leigh, *J. Chem. Soc., A*, 2240 (1970).

14 F. Refosco, F. Tisato, G. Bandoli, C. Bolzati, A. Moresco, and M. Nicolini, *J. Chem. Soc., Dalton Trans.*, 605 (1993).

15 M. T. Ahmet, B. Coutinho, J. R. Dilworth, J. R. Miller, S. J. Parrott, Y, Zheng, M. Harman, M. B. Hursthouse, and A. Malik, *J. Chem. Soc., Dalton Trans.*, 3041 (1995).

16 G. Bandoli, A. Dolmella, T. I. A. Gerber, J. Perils, and J. G. H. du Preez, *Inorg. Chim. Acta*, **303**, 24 (2000).

17 G. Bandoli, T. I. A. Gerber, J. Perils, and J. G. H. du Preez, *Inorg. Chim. Acta*, **278**, 96 (1998).

18 Y. Miyashita, N. Mahboob, S. Tsuboi, Y. Yamada, K. Fujisawa, and K. Okamoto, *Acta Crystallogr., Sect. C*, **57**, 558 (2001).

19 J. C. Bryan, R. E. Stenkamp, T. H. Tulip, and J. M. Mayer, *Inorg. Chem.*, **26**, 2283 (1987).

20 Y. Wang and J. H. Espenson, *Inorg. Chem.*, **41**, 2266 (2002).

21 M. M. Abu-Omer, E. H. Appelman, and J. H. Espenson, *Inorg. Chem.*, **35**, 7751 (1996).

22 H. R. Tetzlaff and J. H. Espenson, *Inorg. Chem.*, **38**, 881 (1999).

23 M. D. Eager and J. H. Espenson, *Inorg. Chem.*, **38**, 2533 (1999).

24 J. H. Espenson and D. T. Y. Yiu, *Inorg. Chem.*, **39**, 4113 (2000).

25 L. D. McPherson, M. Drees, S. I. Khan, T. Strassner, and M. M. Abu-Omar, *Inorg. Chem.*, **43**, 4036 (2004).

26 R. Huang and J. H. Espenson, *Inorg. Chem.*, **40**, 994 (2001).

27 J. Arias, C. R. Newlands, and M. M. Abu-Omar, *Inorg. Chem.*, **40**, 2185 (2001).

28 K. A. Brittingham and J. H. Espenson, *Inorg. Chem.*, **40**, 2730 (2001).

29 M. M. Abu-Omer and J. H. Espenson, *Inorg. Chem.*, **34**, 6239 (1995).

30 N. Koshino and J. H. Espenson, *Inorg. Chem.*, **42**, 5735 (2003).

31 G. Lente and J. H. Espenson, *Inorg. Chem.*, **39**, 4809 (2000).

32 Y. Cai, A. Ellern, and J. H. Espenson, *Inorg. Chem.*, **44**, 2560 (2005).

33 A. K. Yudin and B. Sharpless, *J. Am. Chem. Soc.*, **119**, 11536 (1997).

34 A. Deloffre, S. Halut, L. Salles, J. M. Brégeault, J. R. Gregorio, B. Denise, and H. Rudler, *J. Chem. Soc., Dalton Trans.*, 2897 (1999).

35 K. P. Gable and E. C. Brown, *Organometallics*, **19**, 944 (2000).

36 W. A. Herrmann, R. M. Kratzer, H. Ding, W. R. Thiel, and H. Glas, *J. Organomet. Chem.*, **555**, 293 (1998).

37 J. H. Espenson, *Coord. Chem. Rev.*, **249**, 329 (2005).

38 M. J. Sabater, M. E. Domine, and A. Corma, *J. Catal.*, **210**, 192 (2002).

39 N. P. Johnson, C. J. L. Lock, and G. Wilkinson, *Inorg. Synth.*, **9**, 145 (1967).

40 N. P. Johnson, C. J. L. Lock, and G. Wilkinson, *J. Chem. Soc.*, 1054 (1964).

41 D. E. Grove and G. Wilkinson, *J. Chem. Soc., A*, 1224 (1966).

42 A. Altomare, M. Burla, M. Camalli, G. Cascarano, C. Giacovazzo, A. Guagliardi, and G. Polidori, *J. Appl. Crystallogr.*, **27**, 435 (1994).

43 M. C. Burla, M. Camalli, G. Cascarana, C. Giacovazzo, G. Polidori, R. Spagna, and D. Viterbo, *J. Appl. Crystallogr.*, **22**, 389 (1989).

44 P. T. Beurskens, G. Admiraal, G. Beurskens, W. P. Bosman, R. de Gelder, R. Israel, and J. M. M. Smits, The DIRDIF-94 Program System, Technical Report of the Crystallography Laboratory, University of Nijmegen, The Netherlands (1994).

45 teXsan. Single Crystal Structure Analysis Software, Version 1.10b. Molecular Structure Corporation, The Woodlands, TX, USA (1999).

46 CrystalCrear, J. W. Pflugrath, *Acta Crystallogr*., *Sect*. *D*, **55**, 1718 (1999).

47 H.-F. Fan, Structure Analysis Programs with Intelligent Control, Rigaku Corporation, Tokyo, Japan (1991).

48 P. T. Beurskens, G. Admiraal, G. Beurskens, W. P. Bosman, R. de Gelder, R. Israel, and J. M. M. Smits, The DIRDIF-99 Program System, Technical Report of the Crystallography Laboratory, University of Nijmegen, The Netherlands (1999).

49 CrystalStructure 3.10: Crystal Structure Analysis Package, Rigaku and Rigaku/MSC, 2000-2002.

50 CrystalStructure 3.5.1: Crystal Structure Analysis Package, Rigaku and Rigaku/MSC, 2000-2003.

51 M. M. Abu-Omar and S. I. Khan, *Inorg*. *Chem*., **37**, 4979 (1998).

52 L. Hansen, E. Alessio, M. Iwamoto, P. A. Marzilli, and L. G. Marzilli, *Inorg*. *Chim*. *Acta*, **240**, 413 (1995).

53 G. Battistuzzi, M. Cannio, M. Saladini, and R. Battistuzzi, *Inorg*. *Chim*. *Acta*, **320**, 178 (2001).

54 I. Chakraborty, S. Bhattacharyya, S. Banerjee, B. K. Dirghangi, and A. Chakravorty, *J*. *Chem*. *Soc*., *Dalton Trans*., 3747 (1999).

55 S. Bélanger and A. L. Beauchamp, *Inorg*. *Chem*., **35**, 7836 (1996).

56 S. Bélanger and A. L. Beauchamp, *Inorg*. *Chem*., **36**, 3640 (1997).

57 J. M. Botha, K. Umakoshi, Y. Sasaki, and G. J. Lamprecht, *Inorg*. *Chem*., **37**, 1609 (1998).

58 C. Bolzati, F. Tisato, F. Refosco, G. Bandoli, and A. Dolmella, *Inorg*. *Chem*., **35**, 6221 (1996).

59 J. M. Mayer, D. L. Thorn, and T. H. Tulip, *J*. *Am*. *Chem*. *Soc*., **107**, 7454 (1985).

60 T. I. A. Gerber, J. Bruwer, G. Bandoli, J. Perils, and J. G. H. du Preez, *J*. *Chem*. *Soc*., *Dalton Trans*., 2189 (1995).

61 J. R. Dilworth, D. V. Griffithe, S. J. Parrott, and Y. Zheng, *J*. *Chem*. *Soc*., *Dalton Trans*., 2931 (1997).

62 G. Bandoli, A. Dolmella, T. I. A. Gerber, J. Perils, and J. G. H. du Preez, *Inorg*. *Chim*. *Acta*, **294**, 114 (1999).

63 X. Chen, F. J. Femia, J. W. Babich, and J. Zubieta, *Inorg*. *Chim*. *Acta*, **308**, 80 (2000).

64 T. Głowiak, W. K. Rybak, and A. Skarżyńska, *Polyhedron*, **19**, 2667 (2000).

65 A. Imai, Master Thesis, University of Tsukuba (2004).

66 X. Chen, F. J. Femia, J. W. Babich, and J. Zubieta, *Inorg*. *Chim*. *Acta*, **306**, 113 (2000).

67 S. Bhattacharyya, S. Banerjee, B. K. Dirghangi, M. Memon, and A. Chakravorty, *J*. *Chem*. *Soc*., *Dalton Trans*., 155 (1999).

68 Y. Yamada, K. Fujisawa, and K. Okamoto, *Bull*. *Chem*. *Soc*. *Jpn*., **73**, 2067 (2000).

69 Y. Yamada, K. Fujisawa, and K. Okamoto, *Bull*. *Chem*. *Soc*. *Jpn*., **73**, 2297 (2000).

70 V. N. Nemykin and P. Basu, *Inorg*. *Chem*., **44**, 7494 (2005).

71 V. A. Ung, S. M. Couchman, J. C. Jeffery, J. A. McCleverty, M. D. Ward, F. Totti, and D. Gatteschi, *Inorg*. *Chem*., **38**, 365 (1999).

72 P. J. Desrochers, K. W. Nebesny, M. J. LaBarre, S. E. Lincoln, T. M. Loehr, and J. H. Enemark, *J*. *Am*. *Chem*. *Soc*., **113**, 9193 (1991).

73 F. Refosco, F. Tisato, A. Moresco, and G. Bandoli, *J*. *Chem*. *Soc*., *Dalton Trans*., 3475 (1995).

74 J. O'Neil, S. Wilson, and J. Katzenellenbogen, *Inorg*. *Chem*., **33**, 319 (1994).

Chapter III. Characterization and OAT Catalytic Reactivity of Oxorhenium(V) Complexes with 2-Methylquinolin-8-ylamide and Catecholate Derivatives

III-i. Introduction

As described in Chapter II, it revealed that the quinolinylamido complex $[ReOCl_2(Hamq)(PPh_3)]$ **1** has the interesting property, i.e., easy releasing property of the monodentate ligand. Moreover, the OAT catalytic property for **1** was observed by using the releasing property. Although the OAT catalytic property using the vacant sixth coordination site is sometimes observed in the methylated oxorhenium(V) complexes,[1-4] the non-methylated oxorhenium(V) complexes having the catalytic property is rare. However, the lifetime of catalyst **1** was only 10 cycles and the decomposition to perrhenate(VII) was observed. Therefore, in this chapter, catechol derivatives (catechol, H_2cat; tetrachlorocatechol, H_2Cl_4cat; tetrabromocatechol, H_2Br_4cat) were introduced in the quinolinylamido complex **1** for stabilizing the complex by chelate effect, instead of two chloride ions, and the catecholato derivatives coordinated complexes $[ReO(X_4cat)(Hamq)(PPh_3)]$ (X = H, **13**; Cl, **14**; Br, **15**) were synthesized (Scheme III-1). If the multiple bonding character between quinolinylamide and metal center keeps after the substitution reaction of two chloride ions with catechol derivatives, the releasing property of the monodentate ligand would also be kept. Then, it is expected that the stability for the OAT catalytic reaction in the catechol derivatives introduced complexes **13**–**15** would be improved. Actually, the ligand exchange reaction of **14** with $OPPh_3$ and pyridine derivatives (4-Mepy, 4-*t*-Bupy) by using the releasing property gave new substituted complexes $[ReO(Cl_4cat)(Hamq)(L)]$ (L = $OPPh_3$, **16**; 4-Mepy, **17**; 4-*t*-Bupy, **18**). The structures of these complexes were determined by X-ray

Scheme III-1

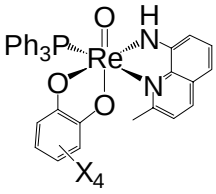

$[ReO(X_4cat)(Hamq)(PPh_3)]$

X = H; **13**
X = Cl; **14**
X = Br; **15**

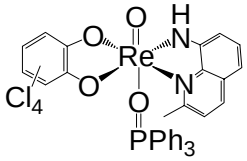

$[ReO(Cl_4cat)(Hamq)(OPPh_3)]$ **16**

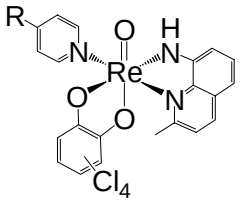

$[ReO(Cl_4cat)(Hamq)(4\text{-}R\text{-}py)]$

R = Me (4-Mepy); **17**
R = *t*-Bu (4-*t*-Bupy); **18**

crystal analysis and these complexes were characterized by spectroscopic measurements. The OAT catalytic reactivity and the catalytic cycle of **14** were also investigated from the viewpoint of reaction kinetics.

III-ii. Experimental

Materials

$[ReOCl_2(Hamq)(PPh_3)]$ **1** was prepared in Chapter II. Tetrachlorocatechol monohydrate ($H_2Cl_4cat·H_2O$), tetrabromocatechol (H_2Br_4cat), 4-*t*-buthylpyridine (4-*t*-Bupy), and 4-cyanopyridine-*N*-oxide (4-CNpyO) were purchased from Aldrich Chemical Co., Inc. 4-Methylpyridine (4-Mepy), pyridine-*N*-oxide (pyO), and 4-methylpyridine-*N*-oxide (4-MepyO) were purchased from Tokyo Kasei Kogyo Co., Ltd. The other materials were purchased from Wako Pure Chemical Ind., Ltd. All the chemicals were used without further purification.

Syntheses of Complexes

$[ReO(cat)(Hamq)(PPh_3)]$ 13. To a solution containing catechol (H_2cat) (33.5 mg, 0.304 mmol) in the mixed solvent of $(CH_3)_2CO$ (50 cm^3) and H_2O (2 cm^3) was added the quinolinylamido complex $[ReOCl_2(Hamq)(PPh_3)]$ **1** (209 mg, 0.301 mmol). The mixture was neutralized with NaOH aqueous solution (0.4 mol dm^{-3}) and it was stirred for 30 min. After insoluble materials were filtered off, the filtrate was concentrated to 5 cm^3 under vacuum. The resulting dark brown precipitate was collected by filtration and washed with H_2O and $(C_2H_5)_2O$. Yield 158 mg, 71%. Anal. Found: C, 55.98; H, 4.02; N, 3.68%. $[ReO(C_6H_4O_2)(C_{10}H_9N_2)P(C_6H_5)_3]$ requires C, 55.96; H, 3.87; N, 3.84%. IR (KBr) 3340m (N–H) and 917s, 905s (Re=O) cm^{-1}. $^{31}P\{^1H\}$ NMR δ -7.6.

$[ReO(Cl_4cat)(Hamq)(PPh_3)]$ 14. To a solution containing $H_2Cl_4cat·H_2O$ (78.0 mg, 0.293 mmol) in the mixed solvent of $(CH_3)_2CO$ (45 cm^3) and H_2O (5 cm^3) was added **1** (199 mg, 0.287 mmol). The mixture was stirred for 1 h. After insoluble materials were filtered off, the filtrate was concentrated to 5 cm^3 under vacuum. The resulting brown precipitate was collected by filtration and washed with H_2O. Yield 209 mg, 84%. The precipitate was recrystallized from $(CH_3)_2CO$ to yield the dark brown pillar

crystals suitable for X-ray analysis. Anal. Found: C, 46.45; H, 2.80; N, 3.18%. $[ReO(C_6Cl_4O_2)(C_{10}H_9N_2)P(C_6H_5)_3]$ requires C, 47.07; H, 2.79; N, 3.23%. IR (KBr) 3341m (N–H) and 936s (Re=O) cm^{-1}. $^{31}P\{^1H\}$ NMR δ -4.2.

$[ReO(Br_4cat)(Hamq)(PPh_3)]$ 15. To a solution containing H_2Br_4cat (62.3 mg, 0.146 mmol) in the mixed solvent of $(CH_3)_2CO$ (25 cm^3) and H_2O (2 cm^3) was added **1** (99.9 mg, 0.144 mmol). The mixture was neutralized with NaOH aqueous solution (0.4 mol dm^{-3}) and it was stirred for 15 min. After insoluble materials were filtered off, the filtrate was concentrated to 5 cm^3 under vacuum. The resulting brown precipitate was collected by filtration and washed with H_2O. The brown powder was redissolved in the mixed solvent of $(CH_3)_2CO$ and H_2O, and the solution was concentrated to 5 cm^3 under vacuum. The resulting brown precipitate was recollected by filtration and washed with H_2O. Yield 104 mg, 68%. Anal. Found: C, 39.29; H, 2.57; N, 2.59%. $[ReO(C_6Br_4O_2)(C_{10}H_9N_2)P(C_6H_5)_3]$ requires C, 39.06; H, 2.31; N, 2.68%. IR (KBr) 3334m (N–H) and 945s, 923s (Re=O) cm^{-1}. $^{31}P\{^1H\}$ NMR δ -4.3.

$[ReO(Cl_4cat)(Hamq)(OPPh_3)]$ 16. To a solution containing $[ReO(Cl_4cat)(Hamq)(PPh_3)]$ **14** (104 mg, 0.120 mmol) in the mixed solvent of $(CH_3)_2CO$ (25 cm^3) and C_7H_{16} (15 cm^3) was added excess of $OPPh_3$ (331 mg, 1.19 mmol). The mixture was stirred for 15 min. After insoluble materials were filtered off, the filtrate was concentrated to 3 cm^3 under vacuum. The resulting brown precipitate was collected by filtration and washed with the mixed solvent of C_6H_{14}/ C_2H_5OH (5/1). Yield 86.8 mg, 82%. The precipitate was recrystallized from $(CH_3)_2CO/C_7H_{16}$ (1/1) to yield the dark brown plate crystals suitable for X-ray analysis. Anal. Found: C, 46.12; H, 2.87; N, 3.12%. $[ReO(C_6Cl_4O_2)(C_{10}H_9N_2)OP(C_6H_5)_3]$ requires C, 46.22; H, 2.74; N, 3.17%. IR (KBr) 3372m (N–H), 1142s (P=O), and 960s (Re=O) cm^{-1}. $^{31}P\{^1H\}$ NMR δ 28.9.

$[ReO(Cl_4cat)(Hamq)(4\text{-}Mepy)]$ 17. To a solution containing $[ReO(Cl_4cat)(Hamq)(PPh_3)]$ **14** (100 mg, 0.115 mmol) in the mixed solvent of $(CH_3)_2CO$ (15 cm^3) and C_2H_5OH (35 cm^3) was added excess of 4-Mepy (109 mg, 1.17 mmol) in the mixed solvent of $(CH_3)_2CO$ (3 cm^3) and C_2H_5OH (7 cm^3). The mixture was stirred for 1 h. After insoluble materials were filtered off, the filtrate was concentrated to 8 cm^3 under vacuum. The brown suspension was cooled on ice bath and the resulting precipitate was collected by filtration. The brown precipitate was washed with cold C_2H_5OH. Yield 45.0 mg, 56%. The precipitate was recrystallized from $(CH_3)_2CO$/ C_2H_5OH (1/2) to yield the dark

brown block crystals suitable for X-ray analysis. Anal. Found: C, 38.03; H, 2.28; N, 5.99%. [ReO($C_6Cl_4O_2$)($C_{10}H_9N_2$)(C_6H_7N)] requires C, 37.84; H, 2.31; N, 6.02%. IR (KBr) 3248m (N–H) and 942s (Re=O) cm^{-1}.

[ReO(Cl_4cat)(Hamq)(4-*t*-Bupy)] 18. To a solution containing [ReO(Cl_4cat)(Hamq)(PPh_3)] **14** (100 mg, 0.115 mmol) in the mixed solvent of $(CH_3)_2CO$ (15 cm^3) and C_2H_5OH (35 cm^3) was added excess of 4-*t*-Bupy (159 mg, 1.18 mmol) in the mixed solvent of $(CH_3)_2CO$ (3 cm^3) and C_2H_5OH (7 cm^3). The mixture was stirred for 1 h. After insoluble materials were filtered off, the filtrate was concentrated to 5 cm^3 under vacuum. The brown suspension was cooled on ice bath and the resulting precipitate was collected by filtration. The brown precipitate was washed with cold C_2H_5OH and H_2O. Yield 36.0 mg, 42%. The precipitate was recrystallized from CH_2Cl_2/$C_6H_5CH_3$ (2/1) to yield the dark brown plate crystals suitable for X-ray analysis. Anal. Found: C, 40.75; H, 3.34; N, 5.36%. [ReO($C_6Cl_4O_2$)($C_{10}H_9N_2$)($C_9H_{13}N$)] requires C, 40.55; H, 3.00; N, 5.68%. IR (KBr) 3298br (N–H) and 938s (Re=O) cm^{-1}.

Measurements

Elemental analyses (C, H, N) were performed by the Research Facility Center for Science and Technology or Department of Chemistry of the University of Tsukuba. IR spectra were recorded as KBr pellets on a JASCO FT/IR-550 spectrometer in the range of 4000–400 cm^{-1} and far-IR spectra were recorded as Nujol mull method in the range of 650–50 cm^{-1} at room temperature. The electronic absorption spectra were recorded with a JASCO V-560 spectrophotometer or a JASCO CT-10TP multichannel spectrophotometer. The diffuse reflectance spectra were recorded on a JASCO V-570 spectrophotometer equipped with an integrating sphere apparatus (JASCO ISN-470). The ^1H and $^{31}P\{^1H\}$ NMR spectra were obtained on a BRUKER AVANCE 600 spectrometer or BRUKER AVANCE 500 spectrometer with $SiMe_4$ as an internal reference and PPh_3 as an external reference respectively (in $CDCl_3$ PPh_3 resonates at δ -7.42 with respect to 85% H_3PO_4 in D_2O).[5]

Crystallography

Single crystals of **14**, **16**, **17**, and **18** were used for data collection on a Rigaku Mercury CCD area detector with graphite-monochromatized MoKα (0.71069 Å) radiation. The intensity data were

collected to a maximum 2θ value of 55° at 296 K. An empirical absorption correction was applied. Data were collected and were processed using CrystalClear.[6] The crystal data and experimental parameters are listed in Table III-1.

The positions of most non-hydrogen atoms of **14** and **17** were determined by direct methods (SIR92[7] in **14** and SIR97[8] in **17**) and some remaining atoms positions were found by successive difference Fourier techniques.[9] The positions of most non-hydrogen atoms of **16** and **18** were determined by heavy-atom Patterson methods (PATTY[10] in **16** and **18**) and some remaining atoms positions were found by successive difference Fourier techniques.[9] The structures were refined by full-matrix least-squares techniques using anisotropic thermal parameters for non-hydrogen atoms. For **14**, **16**, **17**, and **18**, all the hydrogen atoms were included in the refinement but constrained to ride on the atoms (C–H = N–H = 0.95 Å, U(H) = 1.2U(C, N)). The calculations on **14**, **16**, **17**, and **18** were performed using the CrystalStructure crystallographic software package.[11]

Table III-1 Crystal data and experimental parameters for [ReO(Cl_4cat)(Hamq)(PPh_3)]·$(CH_3)_2CO$ **14**·$(CH_3)_2CO$, [ReO(Cl_4cat)(Hamq)($OPPh_3$)] **16**, [ReO(Cl_4cat)(Hamq)(4-Mepy)] **17**, and [ReO(Cl_4cat)(Hamq)(4-*t*-Bupy)]·$C_6H_5CH_3$ **18**·$C_6H_5CH_3$

	14·$(CH_3)_2CO$	**16**	**17**	**18**·$C_6H_5CH_3$
Formula	$C_{37}H_{30}Cl_4N_2O_4PRe$	$C_{34}H_{24}Cl_4N_2O_4PRe$	$C_{22}H_{16}Cl_4N_3O_3Re$	$C_{32}H_{30}Cl_4N_3O_3Re$
Formula weight	925.65	883.57	698.41	832.63
Cryst. system	triclinic	triclinic	monoclinic	triclinic
Space group	*P*-1 (No. 2)	*P*-1 (No. 2)	*C*2/c (No. 15)	*P*-1 (No. 2)
a, Å	9.244(3)	9.9241(2)	17.326(3)	9.6619(8)
b, Å	11.851(8)	11.84500(10)	15.161(2)	10.4842(7)
c, Å	17.204(5)	15.3422(2)	18.543(3)	16.2744(11)
α, °	77.653(5)	71.750(3)		91.840(3)
β, °	84.442(8)	87.326(4)	106.007(2)	94.458(3)
γ, °	84.711(7)	74.144(4)		100.999(4)
V, Å^3	1827.5(9)	1646.11(4)	4681.8(12)	1611.5(2)
Z	2	2	8	2
D_{calc}, g cm^{-3}	1.682	1.782	1.982	1.716
μ (Mo Kα), cm^{-1}	37.04	41.07	56.80	41.41
Reflections collected	14490	26614	30598	25990
Unique reflections	8018	7412	5426	7244
R_{int}	0.026	0.023	0.073	0.022
Observations ($I > 3\sigma(I)$)	7370	6987	3756	6530
Variable parameters	472	439	314	418
R[a]	0.034	0.028	0.074	0.032
R_w[b]	0.099	0.081	0.120	0.095
GOF	0.955	1.006	1.678	1.002

[a] $R = \Sigma||F_o| - |F_c||/\Sigma|F_o|$. [b] $R_w = [\Sigma w(F_o^2 - F_c^2)^2/\Sigma w(F_o^2)^2]^{1/2}$, where $w = 1/\sigma^2(F_o^2)$.

III-iii. Syntheses

III-iii-i. [ReO(X_4cat)(Hamq)(PPh_3)] (X = H, **13**; Cl, **14**; Br, **15**)

The complexes with catecholate were obtained from the following way. To a solution containing catechol derivatives (H_2X_4cat; X = H, Cl, Br) in $(CH_3)_2CO/H_2O$ mixed solvent were added the quinolinylamido complex [$ReOCl_2$(Hamq)(PPh_3)] **1** and stirred. After concentrating this solution until the precipitate appeared, the precipitated catecholato complexes [ReO(X_4cat)(Hamq)(PPh_3)] (X = H, **13**; Cl, **14**; Br, **15**) were collected and washed with H_2O. In these complexes, the two chloride ions were substituted with didentate catechol derivatives (Eq. III-1). In the course of synthesis of **13**, the reddish brown by-product

$$[ReOCl_2(Hamq)(PPh_3)]\ \mathbf{1} + H_2X_4cat \longrightarrow [ReO(X_4cat)(Hamq)(PPh_3)]\ (\mathbf{13}–\mathbf{15}) + 2HCl \quad \text{(III-1)}$$

was obtained. This by-product was assumed to be the de-quinolinylamido complex [ReOCl(cat)(PPh_3)$_2$] by elemental analysis and spectroscopic analyses.[12] Though further details about the by-product only in the case of non-substituted catechol are unclear, it may be attributable to an electronic effect. In other words, the higher electron donating ligand in **13** makes an electron density on metal center increase. Then the bond strength between rhenium and quinolinylamide may become weak, and the quinolinylamide ligand may be released. The existence of chloride ion and PPh_3 in the reaction system may support the formation of the by-product.

III-iii-ii. [ReO(Cl_4cat)(Hamq)(L)] (L = $OPPh_3$, **16**; 4-Mepy, **17**; 4-*t*-Bupy, **18**)

The tetrachlorocatecholato complex [ReO(Cl_4cat)(Hamq)(PPh_3)] **14** also had concentration dependence similarly to complex **1** in electronic absorption spectra (vide infra). Therefore, the releasing property of the monodentate ligand PPh_3 is expected. The substitution reactions of PPh_3 for $OPPh_3$ or pyridine derivatives were studied by using the releasing property. As a result of the substitution reaction, $OPPh_3$, 4-Mepy, or 4-*t*-Bupy coordinated complexes ([ReO(Cl_4cat)(Hamq)($OPPh_3$)] **16**, [ReO(Cl_4cat)(Hamq)(4-Mepy)] **17**, or [ReO(Cl_4cat)(Hamq)(4-*t*-Bupy)] **18**) were obtained (Eqs. III-2 and III-3). On the other hand, in the case of py and 4-CNpy, the substituted complexes were not isolated. When the Hammett σ was minus, the substitution reaction was observed from the viewpoint of Hammett substitution constants (CNpy,

0.66; py, 0.00; 4-Mepy, -0.12; 4-*t*-Bupy, -0.17).[13] That is to say, the nucleophilicity would be the key thing of the substitution reaction.

$$[ReO(Cl_4cat)(Hamq)(PPh_3)]\ \mathbf{14} + OPPh_3 \longrightarrow [ReO(Cl_4cat)(Hamq)(OPPh_3)]\ \mathbf{16} + PPh_3 \quad \text{(III-2)}$$

$$[ReO(Cl_4cat)(Hamq)(PPh_3)]\ \mathbf{14} + \text{4-R-py} \longrightarrow [ReO(Cl_4cat)(Hamq)(\text{4-R-py})]\ \mathbf{17}(R = Me),\ \mathbf{18}\ (R = t\text{-Bu}) + PPh_3$$

$$\not\longrightarrow [ReO(Cl_4cat)(Hamq)(\text{4-R-py})]\ (R = H, CN) + PPh_3 \quad \text{(III-3)}$$

III-iv. Crystal Structures of 14, 16–18

[ReO(Cl$_4$cat)(Hamq)(PPh$_3$)] 14 An X-ray crystal analysis for **14** revealed the presence of a complex molecule and an $(CH_3)_2CO$ molecule. A perspective drawing of the complex molecule **14** is shown in Figure III-1 and its selected bond distances and angles are listed in Table III-2. The coordination geometry around rhenium atom is distorted octahedral with three oxygen atoms of the oxo ligand and catecholate ligand, two nitrogen atoms from the quinolinylamide ligand, and one phosphorus atom from the PPh_3 ligand. Different from the precursor complex **1**, the *trans* position to the oxo ligand is occupied by the oxygen atom of the catecholate ligand. This coordination geometry of **14** follows the tendency of oxorhenium(V) complexes that oxygen atom usually lies in the *trans* position to the oxo ligand. The same tendency was observed in other catecholato complexes.[12,14-19]

The Re1–N1 distance (2.210(3) Å) in **14** (Table III-2) is a little longer than those of the quinolinylamido complexes observed in the previous chapter are. This extension of the bond distance would be attributed to the *trans* influence of the PPh_3. The Re1–N2 distance (1.960(4) Å) and the Re1–N2–C8 angle (118.2(3)°) are similar to the corresponding distance and angle in the quinolinylamido complexes observed in the previous chapter. Therefore, it is suggested that the N2 amine group is also partially deprotonated and the Re1–N2 bond has a multiple bonding character (amide). Though the Re1–O1 distance (1.695(3) Å) is shorter than that of **1**, it is normal as double bonds in oxorhenium(V) complexes.[16-29] The Re1–O3 distance (2.126(3) Å) is longer than the Re1–O2 distance (2.026(2) Å) (Table III-2), and it lies at the long end of the range found for the Re–O

(catecholate or phenolate) distances (1.96–2.10 Å).[12,17,29,30] This long bond distance would exhibit the *trans* influence of the Re1–N2 (amide) bond. The tendency that the equatorial ligands are displaced away from the Re=O group (0.133(1) Å) was observed, in analogy with that observed in the previous chapter. Moreover, the bite angles of two didentate ligands (N1–Re1–N2, 79.0(1)°; O2–Re1–O3, 75.9(1)°) deviate from 90° (Table III-2). These deviations are responsible for the distorted octahedral structure. In this crystal structure (Figure III-2), **14** adopts the conformation that the phenyl rings of

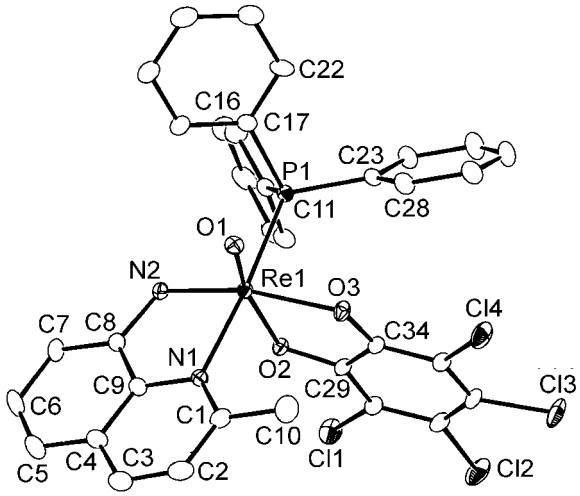

Figure III-1 An ORTEP view of [ReO(Cl_4cat)(Hamq)(PPh_3)] **14** with numbering scheme. Hydrogen atoms have been omitted for clarity.

Table III-2 Selected bond distances (Å) and angles (°) for [ReO(Cl_4cat)(Hamq)(PPh_3)] **14**

Re1–O1	1.695(3)	Re1–O2	2.026(2)
Re1–O3	2.126(3)	Re1–N1	2.210(3)
Re1–N2	1.960(4)	Re1–P1	2.456(1)
O1–Re1–O3	89.9(1)	O2–Re1–O3	75.9(1)
O1–Re1–N1	94.3(1)	O2–Re1–N1	87.9(1)
O1–Re1–N2	106.3(1)	O2–Re1–N2	87.9(1)
O1–Re1–P1	88.3(1)	O2–Re1–P1	90.98(8)
O1–Re1–O2	165.8(1)	N1–Re1–P1	173.7(1)
O3–Re1–N2	163.3(1)	O3–Re1–N1	96.0(1)
O3–Re1–P1	89.70(8)	N1–Re1–N2	79.0(1)
N2–Re1–P1	94.8(1)	Re1–N2–C8	118.2(3)

PPh_3 avoid the catecholate ring, and the intramolecular π–π stacking interaction is not observed unlike **1**. The crystal packing shows no intermolecular π–π interaction between the rings of **14** (Figure III-3). Although the $(CH_3)_2CO$ molecule is also incorporated in the crystal packing, it does not participate in any intermolecular interactions.

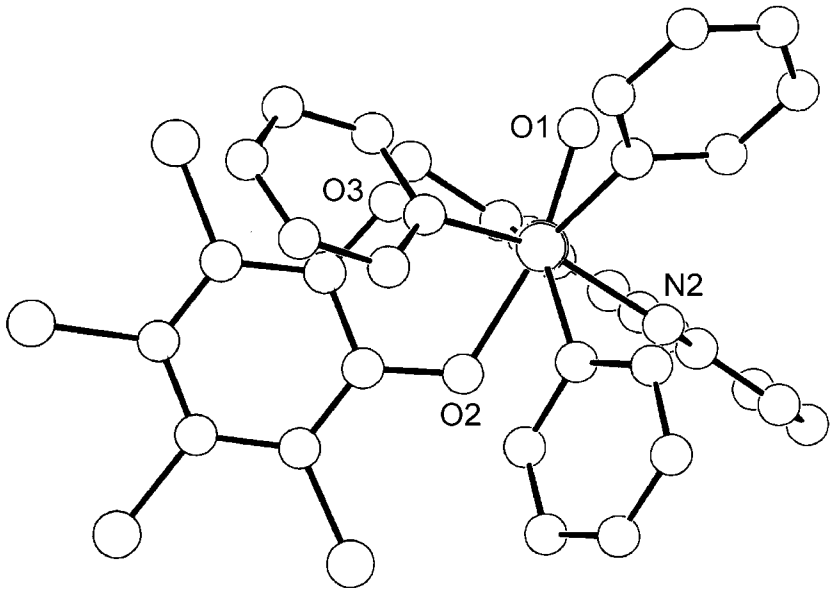

Figure III-2 Crystal structure of [ReO(Cl_4cat)(Hamq)(PPh_3)] **14** viewed from P–Re axis.

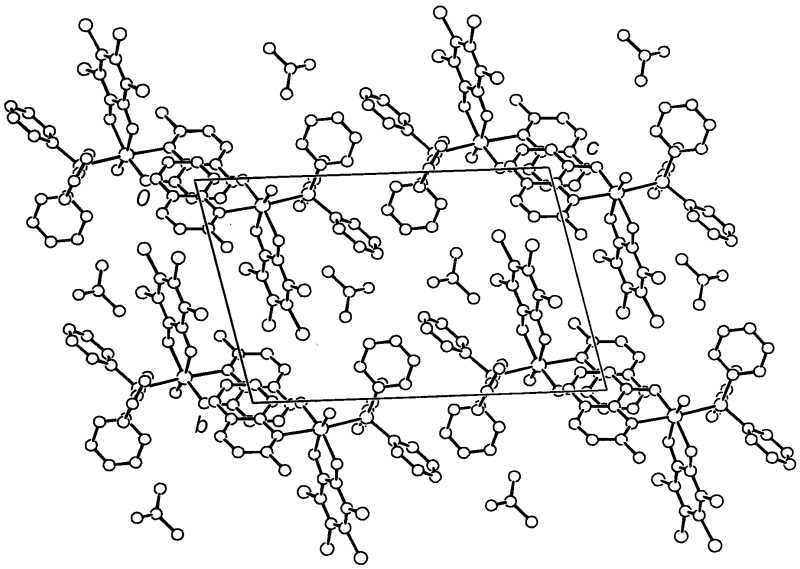

Figure III-3 Projection of crystal packing for [ReO(Cl_4cat)(Hamq)(PPh_3)]·$(CH_3)_2CO$ **14**·$(CH_3)_2CO$.

[ReO(Cl$_4$cat)(Hamq)(OPPh$_3$)] 16 An X-ray crystal analysis for **16** revealed the presence of only a complex molecule. A perspective drawing of the complex molecule **16** is shown in Figure III-4 and its selected bond distances and angles are listed in Table III-3. The coordination geometry around rhenium atom is distorted octahedral with four oxygen atoms of the oxo ligand, the $OPPh_3$ ligand, and catecholate ligand, and two nitrogen atoms from the quinolinylamide ligand. Though the coordination geometry, that the *trans* position to the oxo ligand is occupied by oxygen atom of the $OPPh_3$ ligand, is different from that of precursor complex **14**, this coordination geometry also follows the tendency of oxorhenium(V) complexes that oxygen atom usually lies in the *trans* position to the oxo ligand.

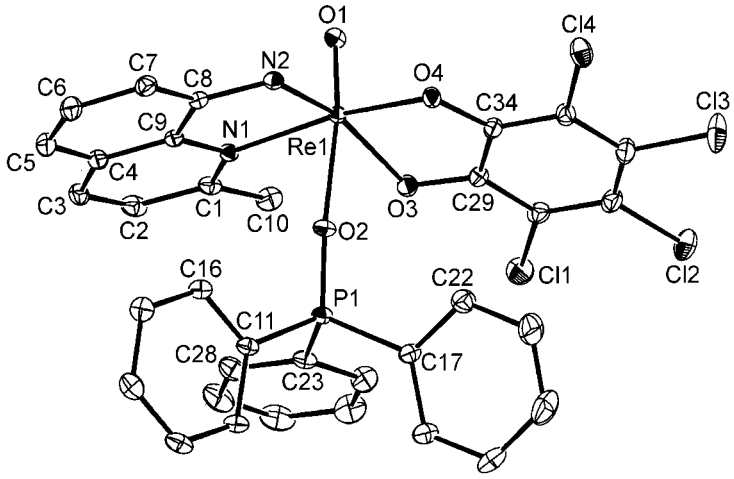

Figure III-4 An ORTEP view of [ReO(Cl$_4$cat)(Hamq)(OPPh$_3$)] **16** with numbering scheme. Hydrogen atoms have been omitted for clarity.

Table III-3 Selected bond distances (Å) and angles (°) for [ReO(Cl$_4$cat)(Hamq)(OPPh$_3$)] **16**

Re1–O1	1.681(3)	Re1–O2	2.249(2)
Re1–O3	2.031(2)	Re1–O4	1.993(3)
Re1–N1	2.148(3)	Re1–N2	1.967(2)
O1–Re1–O3	99.9(1)	O2–Re1–O3	77.62(9)
O1–Re1–O4	103.0(1)	O2–Re1–O4	88.0(1)
O1–Re1–N1	91.4(1)	O2–Re1–N1	78.0(1)
O1–Re1–N2	102.5(1)	O2–Re1–N2	80.7(1)
O1–Re1–O2	168.3(1)	O3–Re1–N2	157.6(1)
O4–Re1–N1	164.7(1)	O3–Re1–O4	80.68(9)
O3–Re1–N1	102.11(9)	O4–Re1–N2	93.0(1)
N1–Re1–N2	78.7(1)	Re1–N2–C8	118.4(2)

Different from **14**, the equatorial ligands bond distances (Re1–O3, 2.031(2); Re1–O4, 1.993(3); Re1–N1, 2.148(3); Re1–N2, 1.967(2) Å) are normal in comparison with the reported oxorhenium(V) complexes (Table III-3).[12,17,28-32] The Re1–O1 distance (1.681(3) Å) is also normal as double bonds in the oxorhenium(V) complexes.[16-29] On the other hand, the Re1–O2 distance (2.249(2) Å) is unusually long as Re–O single bond distance. This distance in **16** is about 0.12 Å longer than the Re–O ($OPPh_3$) distance in **3** or **4**, and it is longer than the reported Re–O ($OPPh_3$) distances (2.07–2.19 Å),[14-16,33,34] except only one example [$ReO(Cl_4cat)_2(OPPh_3)$] (2.232(6) Å).[12] In this case, the unusually long bond distance was caused by the *trans* influence of an extremely short Re=O distance (1.576(8) Å). Therefore, the *trans* influence of the oxo ligand may be one cause for the unusually long distance in **16**, but there would be more. The oxygen atoms of the phosphine oxide in **3**, **4**, or above examples also occupy the *trans* position of the oxo ligand. The principal factor of the unusually long distance is still not clear, while the long distance would support the releasing property (vide infra). Two equatorial axis are bending largely (O4–Re1–N1, 164.7(1); O3–Re1–N2, 157.6(1)°) which caused by the bite angles of two didentate ligands, and as often observed in oxorhenium(V) systems, the equatorial ligand are displaced away from the Re=O group (0.319(1) Å) (Table III-3). In the crystal packing of **16**, the neighboring hetero ring parts (N1–C1–C2–C3–C4–C9) of the quinoline rings are overlapped, and the interplane distance is within the range of intermolecular π–π stacking (interplane distance = 3.353(6) Å, dihedral angle = 0°) (Figure III-5).[35,36]

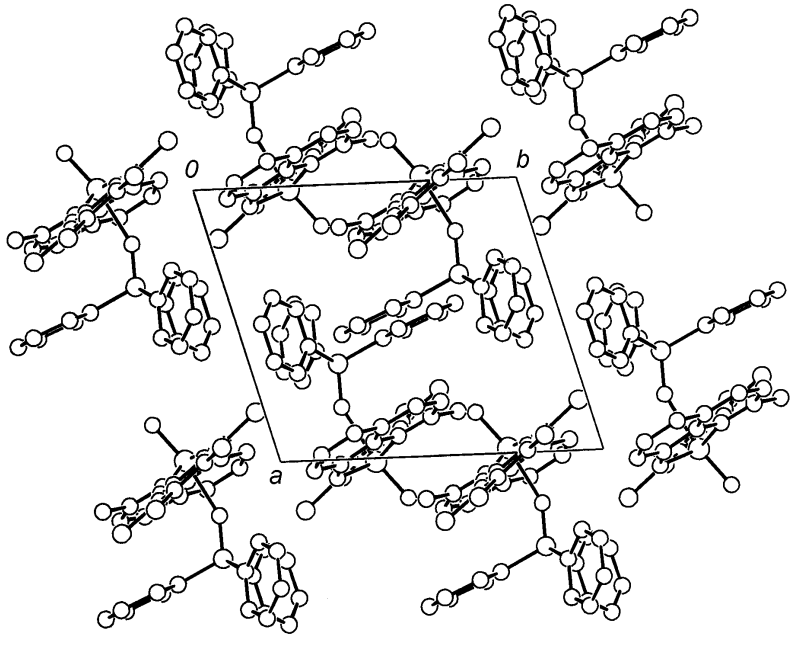

Figure III-5 Projection of crystal packing for [$ReO(Cl_4cat)(Hamq)(OPPh_3)$] **16**.

[ReO(Cl_4cat)(Hamq)(4-R-py)] (R = Me, 17; *t*-Bu, 18) An X-ray crystal analysis for **17** revealed the presence of only a complex molecule, while an X-ray crystal analysis for **18** revealed the presence of a complex molecule and a $C_6H_5CH_3$ molecule. Though the difference in crystal packing between **17** and **18** was observed, the coordination geometries around rhenium(V) center were roughly the same each other. A perspective drawing of the complex molecule **17** is shown in Figure III-6 representatively and the selected bond distances and angles of **17** and **18** are listed in Table III-4. The coordination geometry around rhenium atom is distorted octahedral with three oxygen atoms of the oxo ligand and catecholate ligand, and three nitrogen atoms from the quinolinylamide ligand and pyridine derivatives. The *trans* position to the oxo ligand is occupied by the oxygen atom of catecholate ligand similarly to **14**, and this coordination geometry follows the tendency of oxorhenium(V) complexes that oxygen atom usually lies in the *trans* position to the oxo ligand.

Reflecting the similar coordination geometry with **14**, the Re1–O3 distances (**17**, 2.15(1); **18**, 2.155(3) Å) shown in Table III-4 are also longer than the reported Re–O (catecholate or phenolate) distances.[12,17,29,30] On the other hand, the Re1–N2 distance (1.89(2) Å) in **17** is shorter than the reported Re–N (amide) distances.[5,28,37] This short bond would be cause of the long Re1–O3 distance. The Re1–N3 distance of **18** is 0.04 Å shorter than that of **17** in spite of the steric hindrance in 4-position. In this case, the difference in bond distances would be controlled by the nucleophilicity of pyridine derivatives. These Re–N (py) distances (Table III-4) are shorter than that in **10** or **11**, which was affected by the *trans* influence of the amide ligand, and they are within the reported Re-N (heterocyclic) distances (2.11–2.17 Å).[22-24,38,39] The each Re1–O1 distance (**17**, 1.65(1); **18**, 1.678(3) Å) is normal as double bonds in the oxorhenium(V) complexes.[16-29] As often reported in oxorhenium(V) systems, the bending of axis bond angles and the displacing away of equatorial ligands from the Re=O group are also observed in **17** (0.182(8) Å) and **18** (0.176(2) Å) (Table III-4). The crystal packing of **17** shows intermolecular π–π stacking interaction between the neighboring quinoline rings (interplane distance = 3.31(3) Å, dihedral angle = 0°) (Figure III-7 (a)). On the other hand, the crystal packing of **18** shows not only the quinoline ring–quinoline ring intermolecular π–π stacking interaction (interplane distance = 3.371(7) Å, dihedral angle = 0°) but also the quinoline ring–$C_6H_5CH_3$ ring π–π stacking (interplane distance = 3.85(2) Å, dihedral angle = 18.7(3)°) (Figure III-7 (b)).[35,36]

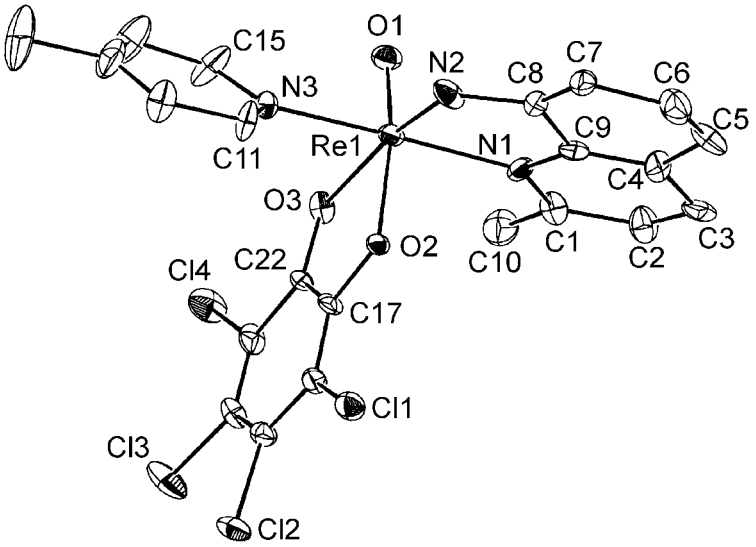

Figure III-6 An ORTEP view of [ReO(Cl_4cat)(Hamq)(4-Mepy)] **17** with numbering scheme. Hydrogen atoms have been omitted for clarity. The numbering scheme of **18** is the same as that of **17**.

Table III-4 Selected bond distances (Å) and angles (°) for [ReO(Cl_4cat)(Hamq)(4-Mepy)] **17** and [ReO(Cl_4cat)(Hamq)(4-*t*-Bupy)] **18**

	17	**18**		**17**	**18**
Re1–O1	1.65(1)	1.678(3)	Re1–O2	2.00(1)	2.026(3)
Re1–O3	2.15 (1)	2.155(3)	Re1–N1	2.15(2)	2.164(3)
Re1–N2	1.89(2)	1.943(3)	Re1–N3	2.16(1)	2.121(4)
O1–Re1–O3	87.5(5)	86.6(1)	O2–Re1–O3	76.4(4)	76.0(1)
O1–Re1–N1	96.2(6)	95.7(1)	O2–Re1–N1	88.0(5)	87.3(1)
O1–Re1–N2	106.2(6)	105.6(2)	O2–Re1–N2	89.8(6)	91.8(1)
O1–Re1–N3	91.1(6)	92.7(3)	O2–Re1–N3	86.5(5)	86.5(1)
O1–Re1–O2	163.9(5)	162.6(1)	O3–Re1–N2	166.2(6)	167.6(1)
N1–Re1–N3	170.7(6)	169.6(1)	O3–Re1–N1	102.9(5)	102.5(1)
O3–Re1–N3	83.1(5)	84.0(1)	N1–Re1–N2	76.7(7)	78.9(1)
N2–Re1–N3	95.8(7)	93.0(1)	Re1–N2–C8	124(1)	119.3(3)

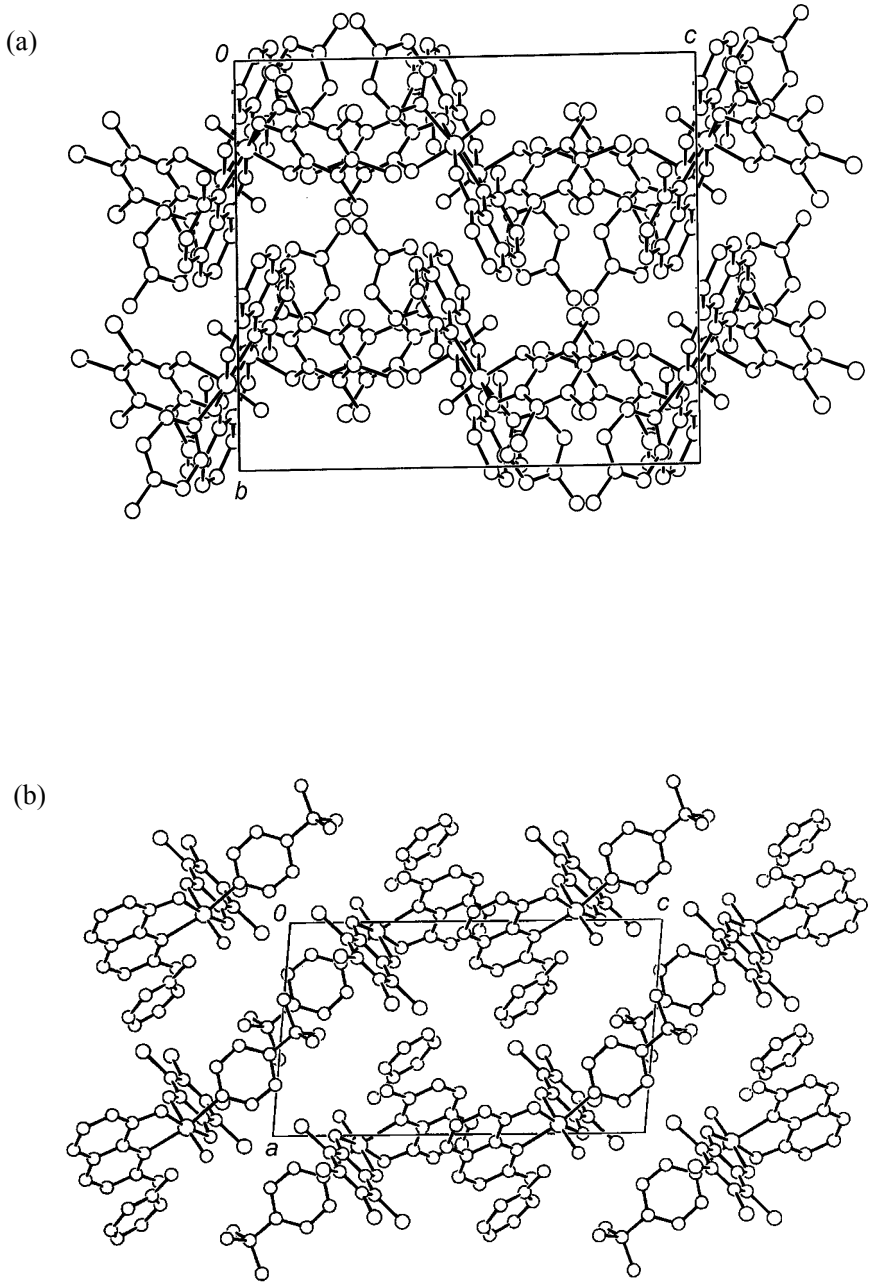

Figure III-7 Projection of crystal packing for [ReO(Cl_4cat)(Hamq)(4-Mepy)] **17** (a) and [ReO(Cl_4cat)(Hamq)(4-*t*-Bupy)]·$C_6H_5CH_3$ **18**·$C_6H_5CH_3$ (b).

III-v. Spectroscopic Properties

IR and far-IR Spectra The IR spectra of X_4cat complexes series (**13**–**15**) are shown in Figure III-8. The spectral data are summarized in Table III-5. The spectral patterns of three catecholato complexes **13**–**15** are similar to each other. Therefore, the coordination geometry of **13** and **15**, which could not be obtained by the X-ray analysis because of low crystal quality, would be analogously to that of **14**. The molecular formula of **13** and **15** were also supported by elemental analysis. Though it is not clear why the bands assigned to Re=O bond in **13** and **15** are split into two band, the Re=O bands of **14** appear in higher wavenumber than that of **13**. This blue shift may be due to the electrophilic effect of tetrachlorocatechol ligand.[12] That is to say, the acidity of metal center coordinated with tetrachlorocatechol is higher than that of metal center of **13** and the Re=O bond of **14** would be stronger than **13**. In the far-IR spectra, the bands assigned to Re–Cl bond are not observed in the region of 300 cm^{-1}. This result supports the substitution reaction from two chloride ions to catechol derivatives.

The IR spectra of the monodentate ligand substituted complexes **14**, **16**–**18** with tetrachlorocatecholate are shown in Figure III-9. In all cases the bands assigned to Re=O bond are observed in the normal region (1000–900 cm^{-1}) (Table III-5). The IR spectrum of $OPPh_3$ coordinated complex **16** shows new bands at 1142 ($\nu_{P=O}$), 1114, and 724 cm^{-1} (Figure III-8) similar to the $OPPh_3$ coordinated complexes **3**, **4**, **7**, and **8** observed in the previous chapter. Therefore, these bands are assigned to coordinated $OPPh_3$. In the complexes **17** and **18** with pyridine derivatives, the bands around 700 cm^{-1} arising from PPh_3 disappear and the bands assigned to alkyl substituent of pyridine derivatives appear at ca. 2970 cm^{-1}. The far-IR spectra of the monodentate ligand substituted series (**14**, **16**–**18**) also did not show strong bands assigned to Re–Cl bond.

Table III-5 Selected IR spectral data

Complex	IR (ν/cm^{-1})[a]		
	Re=O	N–H	P=O
[ReO(cat)(Hamq)(PPh_3)] **13**	905 (s), 917 (s)	3340 (w)	—
[ReO(Cl_4cat)(Hamq)(PPh_3)] **14**	936 (s)	3341 (w)	—
[ReO(Br_4cat)(Hamq)(PPh_3)] **15**	924 (s), 945 (s)	3340 (m)	—
[ReO(Cl_4cat)(Hamq)($OPPh_3$)] **16**	960 (s)	3372 (m)	1142 (s)
[ReO(Cl_4cat)(Hamq)(4-Mepy)] **17**	942 (s)	3248 (m)	—
[ReO(Cl_4cat)(Hamq)(4-*t*-Bupy)] **18**	938 (s)	3298 (w, br)	—

[a] s, strong; m, medium; w, weak; br, broad.

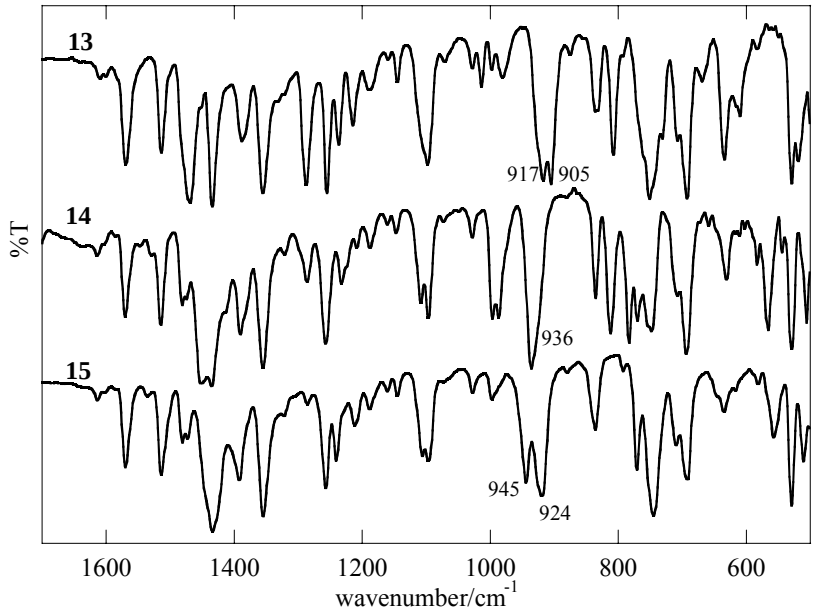

Figure III-8 IR spectra of [ReO(cat)(Hamq)(PPh_3)] **13**, [ReO(Cl_4cat)(Hamq)(PPh_3)] **14**, and [ReO(Br_4cat)(Hamq)(PPh_3)] **15**.

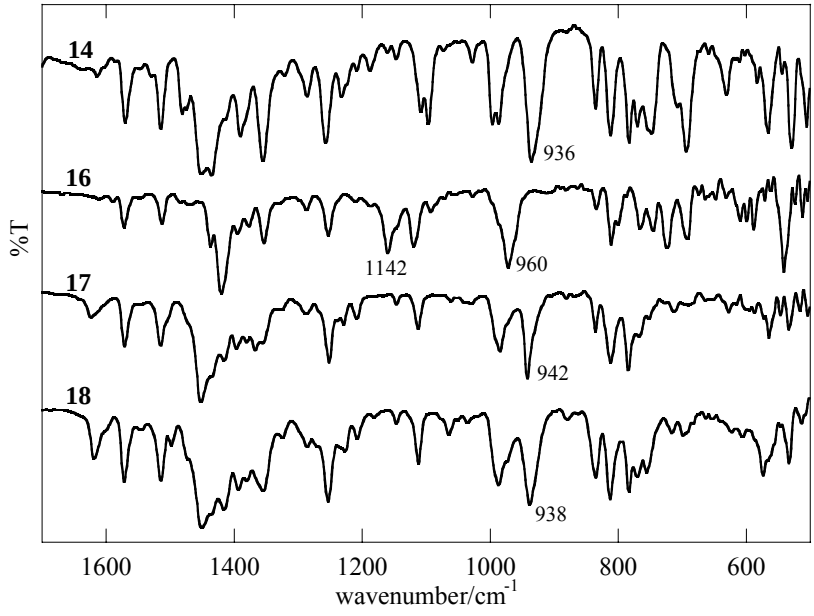

Figure III-9 IR spectra of [ReO(Cl_4cat)(Hamq)(PPh_3)] **14**, [ReO(Cl_4cat)(Hamq)($OPPh_3$)] **16**, [ReO(Cl_4cat)(Hamq)(4-Mepy)] **17**, and [ReO(Cl_4cat)(Hamq)(PPh_3)] **18**.

Electronic Absorption and Diffuse Reflectance Spectra The electronic absorption spectra of complexes **13**–**18** were measured by using CH_2Cl_2 solution in three different concentrations (1.0×10^{-3}, 1.0×10^{-4}, and 1.0×10^{-5} mol dm^{-3}). The solid state diffuse reflectance (DR) spectra of complexes **13**–**18** were also measured. The electronic spectra are shown in Figures III-10–III-18 and the spectral data are summarized in Table III-6. The spectral patterns of non-substituted catecholato coordinated complex **13** do not show the concentration dependence in this concentration conditions (1.0×10^{-3}–1.0×10^{-5} mol dm^{-3}) (Figure III-10). It is presumed that **13** is the five-coodinated state in this concentration conditions, because the spectral patterns of **13** are similar to that of low concentratiion condition (1.0×10^{-5} mol dm^{-3}) of **14** (vide infra). Actually, when the excess of PPh_3 was added to the solution of **13** (1.0×10^{-4} mol dm^{-3}), a new intense band is appeared at 399 nm (Figure III-11). From these spectra, the equilibrium constant K of **13** is 52 dm^3 mol^{-1} (Eq. III-4). On the other hand, the absorption spectral

$$[ReO(Cl_4cat)(Hamq)] + PPh_3 \underset{}{\overset{K}{\rightleftharpoons}} [ReO(Cl_4cat)(Hamq)(PPh_3)]\ \mathbf{14} \qquad \text{(III-4)}$$

patterns of **14** show concentration dependence as expected (Figure III-12). In other words, the increase of the peak intensity at 402 and 816 nm with increasing the concentration of **14** is observed. When the excess amount of PPh_3 was added to the solution of **14** (1.0×10^{-4} mol dm^{-3}), a similar spectral changing pattern is observed (Figure III-13). The spectrum curving pattern of **14** in high concentration condition (1.0×10^{-3} mol dm^{-3}) is similar to that of the solid state DR spectrum. Therefore, the concentration dependence observed in **14** would be due to the release or bonding of PPh_3 ligand similar to **1**. That is, **14** would keep metal center–ligand (PPh_3) bond and the six-coordinated state under high concentration condition, while **14** would release PPh_3 from metal center and changes to the five-coordinated state under low concentration condition (Scheme III-2). From these results, the band observed in 402 nm would be assigned to PPh_3–Re LMCT transition. The absorption spectral patterns of the tetrabromocatecholato complex **15** also show concentration dependence similar to those of **14** (Figure III-14). The equilibrium constants K of **14** and **15** are 1.0×10^4 dm^3 mol^{-1} and 2.4×10^4 dm^3 mol^{-1}, respectively (Eq. III-4). The equilibrium constant of **14** is 200 times larger than that of **13**. This difference is in accord with the higher electrophilicity of metal center due to the electrophilic effect of the tetrachlorocatechol ligand.

Scheme III-2

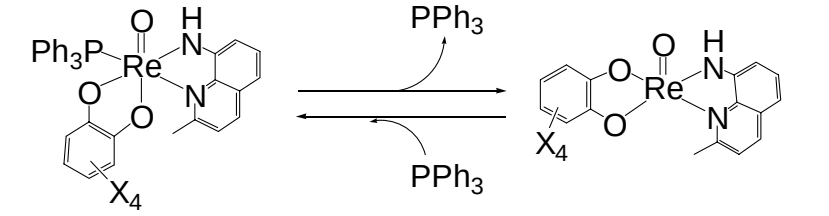

six-coordinated state five-coordinated state

Table III-6 Absorption and reflectance spectral data of **13**–**18**

	Concentration (mol dm^{-3})	Absorption and diffuse reflectance maxima nm (ε/mol^{-1} dm^3 cm^{-1})
13	1.0×10^{-3}	443 (2.5×10^3) 804 (69)
	1.0×10^{-4}	447 (2.6×10^3) 804 (69)
	1.0×10^{-5}	446 (2.5×10^3) 804 (89)
	DR	430 (sh) 528 828 858
14	1.0×10^{-3}	402 (7.1×10^3) 816 (6.6×10^2)
	1.0×10^{-4}	405 (4.9×10^3) 814 (3.8×10^2)
	1.0×10^{-5}	434 (2.9×10^3) 822 (1.6×10^2)
	DR	432 797 858
15	1.0×10^{-3}	401 (7.1×10^3) 812 (7.1×10^2)
	1.0×10^{-4}	403 (5.2×10^3) 809 (4.4×10^2)
	1.0×10^{-5}	440 (3.0×10^3) 806 (1.7×10^2)
	DR	429 805
16	1.0×10^{-3}	404 (5.8×10^3)
	1.0×10^{-4}	450 (2.6×10^3)
	1.0×10^{-5}	450 (2.5×10^3)
	DR	437 631 740 (sh)
17	1.0×10^{-3}	389 (6.5×10^3) 822 (3.8×10^2)
	1.0×10^{-4}	400 (4.3×10^3 sh) 470 (2.8×10^3 sh) 822 (2.3×10^2 sh)
	1.0×10^{-5}	447 (2.7×10^3)
	DR	422 540 (sh) 680 (sh) 842
18	1.0×10^{-3}	390 (7.2×10^3) 824 (7.1×10^2)
	1.0×10^{-4}	400 (4.9×10^3 sh) 470 (2.9×10^3 sh) 833 (2.4×10^2)
	1.0×10^{-5}	445 (2.8×10^3)
	DR	414 841

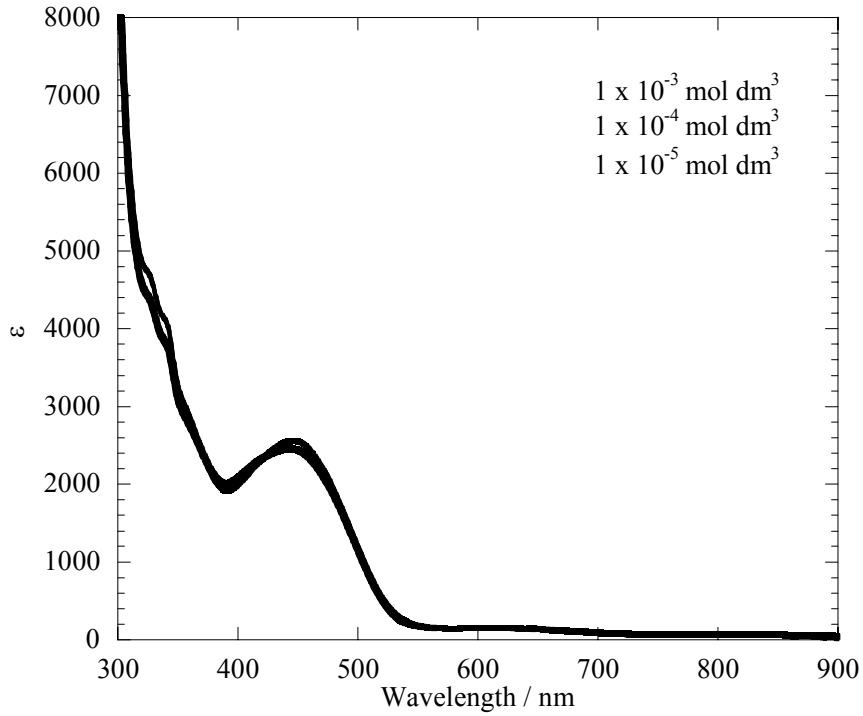

Figure III-10 Electronic absorption spectra of [ReO(cat)(Hamq)(PPh_3)] **13** in some concentration conditions in CH_2Cl_2.

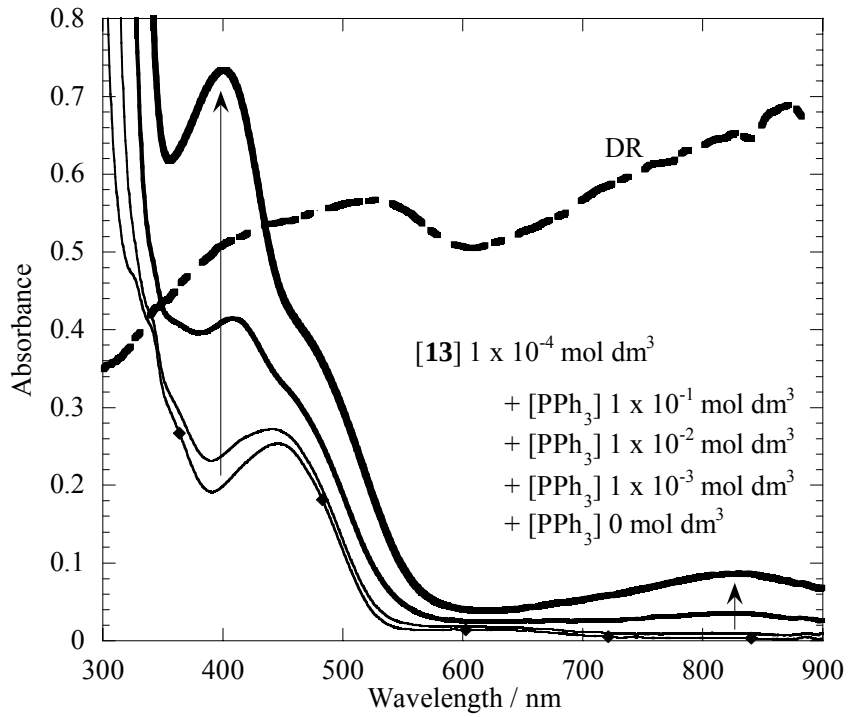

Figure III-11 PPh_3 concentration dependence of 1×10^{-4} mol dm^3 of **13** in CH_2Cl_2.

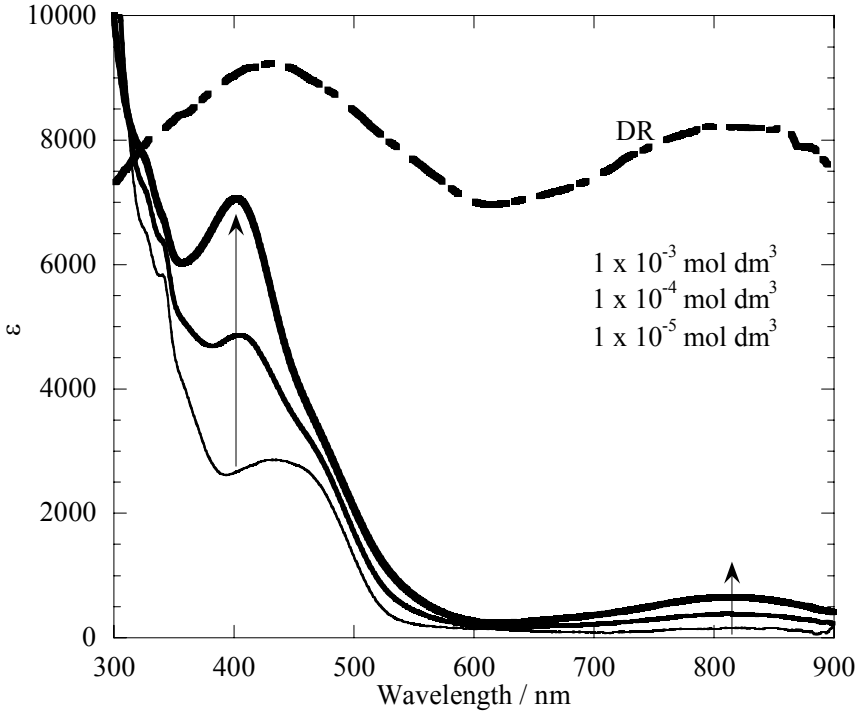

Figure III-12 Electronic absorption spectra of [ReO(Cl_4cat)(Hamq)(PPh_3)] **14** in some concentration conditions in CH_2Cl_2.

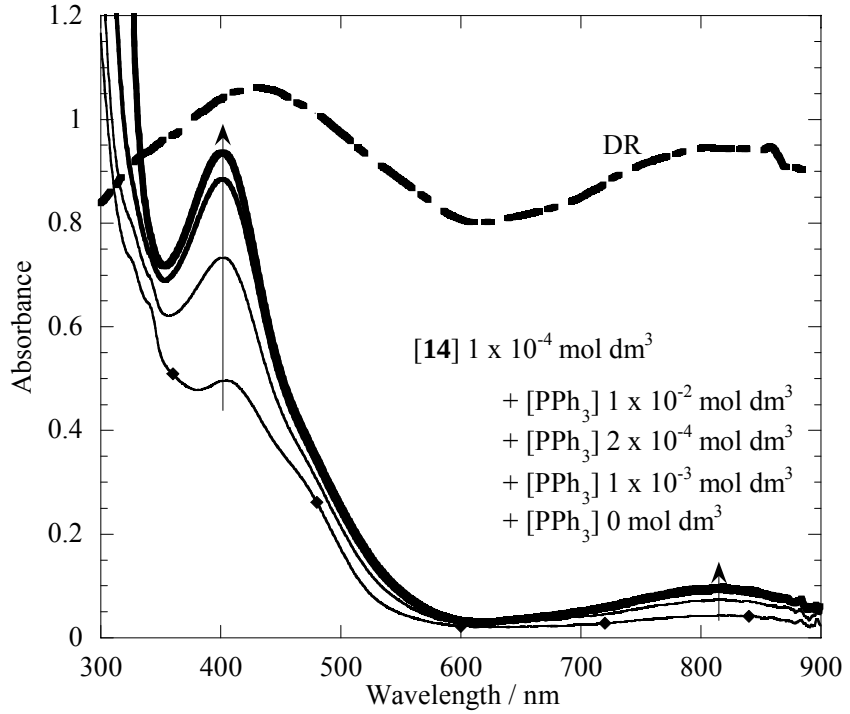

Figure III-13 PPh_3 concentration dependence of 1×10^{-4} mol dm^3 of **14** in CH_2Cl_2.

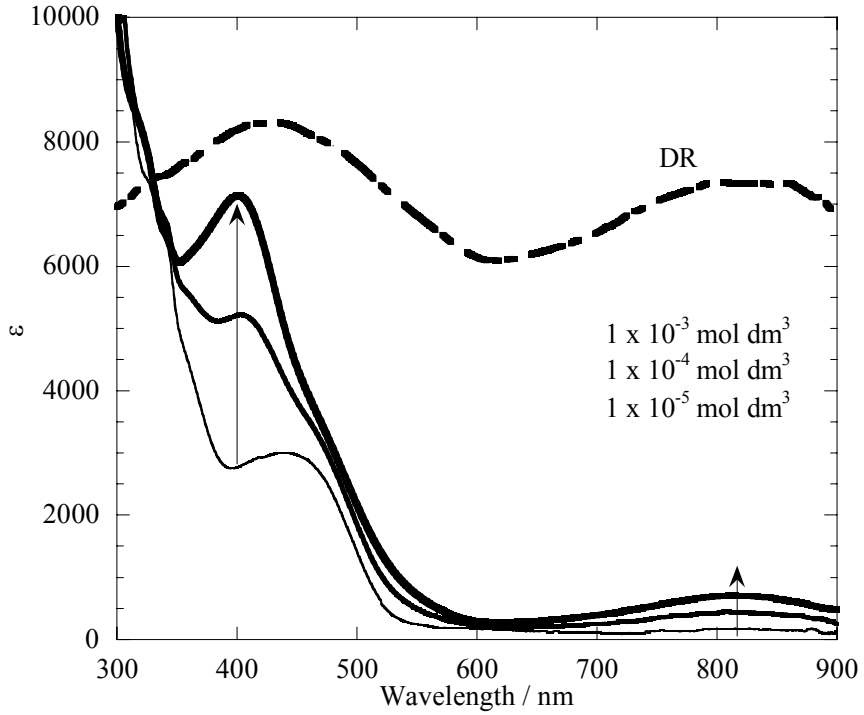

Figure III-14 Electronic absorption spectra of [ReO(Br_4cat)(Hamq)(PPh_3)] **15** in some concentration conditions in CH_2Cl_2.

The monodentate ligand substituted complexes **16**–**18** are also showed concentration dependence (Figures III-15–III-18). The change of the spectral patterns in $OPPh_3$ coordinated complex **16** is small distinct from **14** in this concentration conditions, while the addition of excess of $OPPh_3$ to 1.0×10^{-4} mol dm^{-3} of **16** shows the spectral changing pattern similarly to **14** (Figure III-16). Because the spectral patterns of low concentration condition (1.0×10^{-5} mol dm^{-3}) in **16**–**18** are very similar to that in **14**, the concentration dependence observed in **16**–**18** would be due to the releasing or bonding of monodentate ligands as **14**. The equilibrium constants *K* of **16**, **17**, and **18** are 5×10^2 dm^3 mol^{-1}, 2.0×10^4 dm^3 mol^{-1}, and 2.4×10^4 dm^3 mol^{-1}, respectively (Eq. III-4). The equilibrium constant of **16** is much smaller than those of **14**, **17**, and **18**. This may be caused by the difference in coordination geometry observed in X-ray crystal structure. Only **16**, the monodentate ligand $OPPh_3$ is occupied the *trans* position of the oxo ligand, and the Re–O ($OPPh_3$) distance in **16** was unusually long. Generally, in oxorhenium(V) complexes, the *trans* position of the oxo ligand is more active site than the *cis* position.[40]

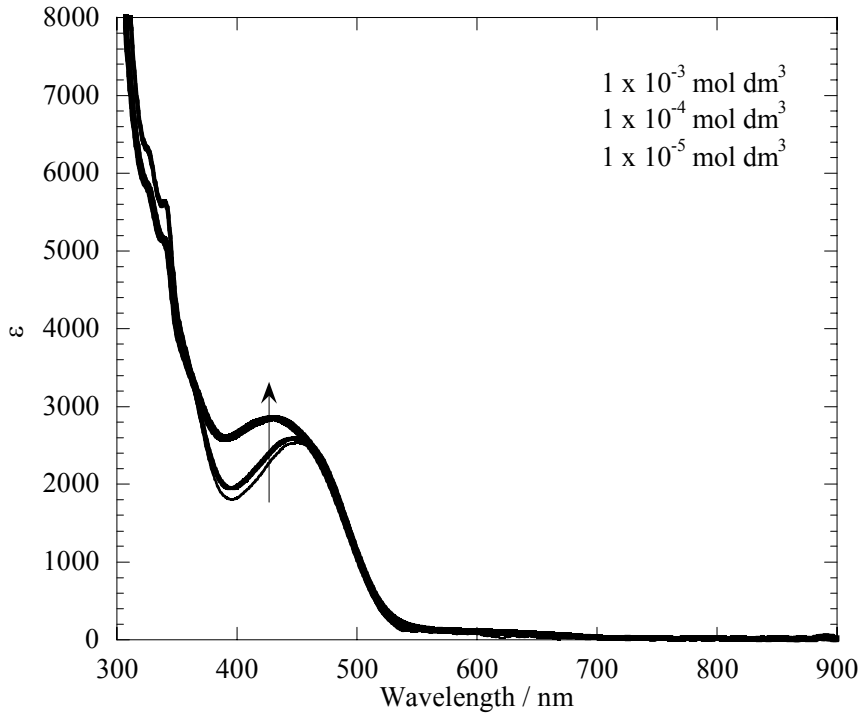

Figure III-15 Electronic absorption spectra of [ReO(Cl_4cat)(Hamq)($OPPh_3$)] **16** in some concentration conditions in CH_2Cl_2.

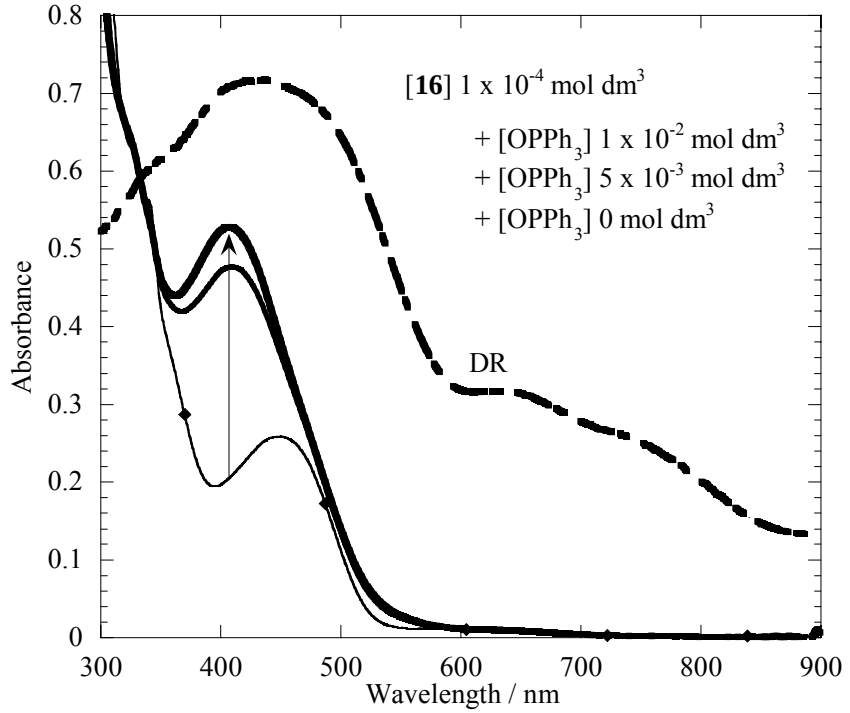

Figure III-16 $OPPh_3$ concentration dependence of 1×10^{-4} mol dm^3 of **16** in CH_2Cl_2.

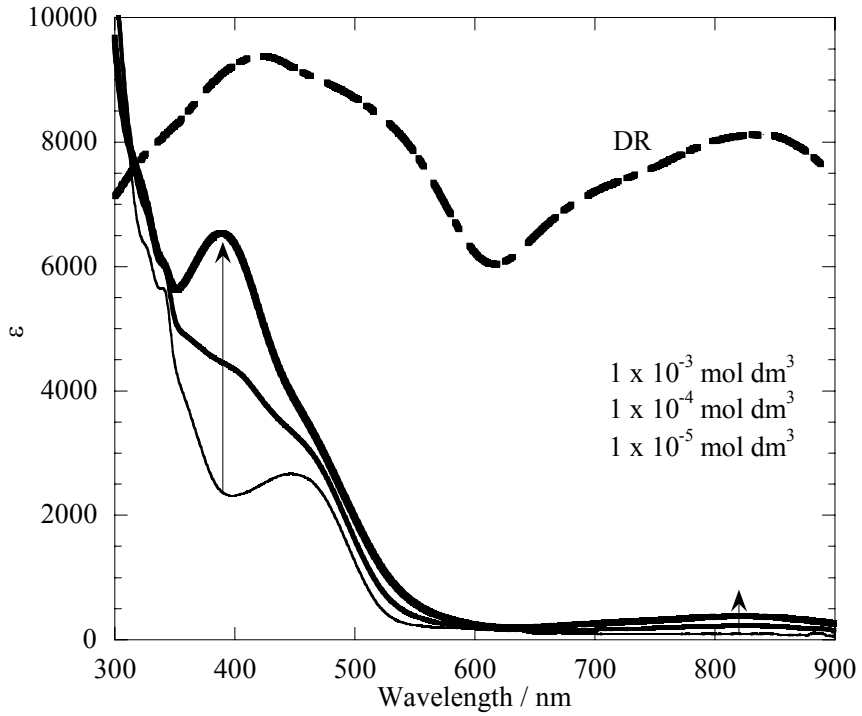

Figure III-17 Electronic absorption spectra of [ReO(Cl_4cat)(Hamq)(4-Mepy)] **17** in some concentration conditions in CH_2Cl_2.

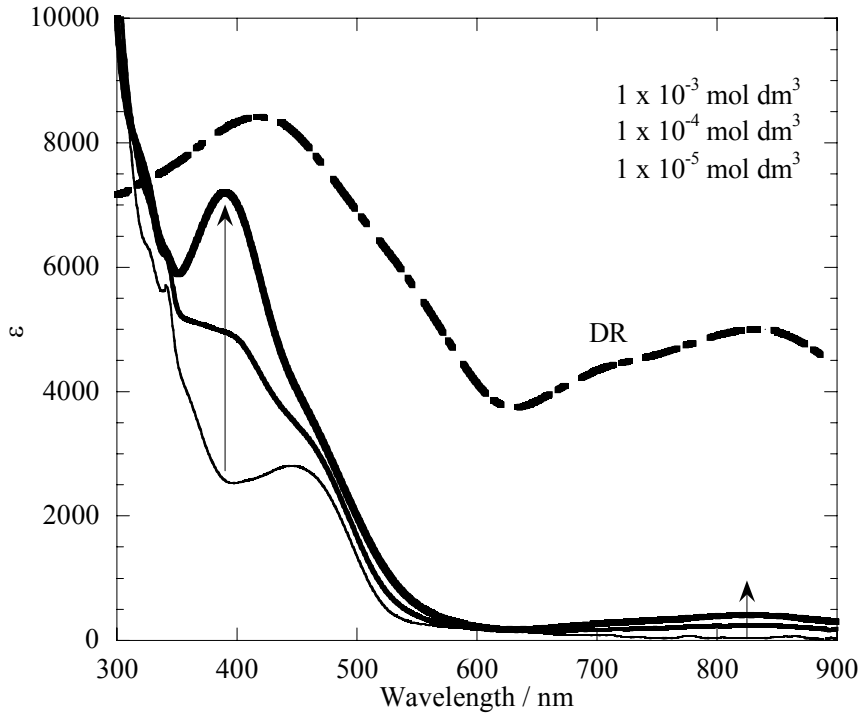

Figure III-18 Electronic absorption spectra of [ReO(Cl_4cat)(Hamq)(4-*t*-Bupy)] **18** in some concentration conditions in CH_2Cl_2.

$^{31}P\{^{1}H\}$ NMR Spectra The $^{31}P\{^{1}H\}$ NMR spectra of complexes **13**–**16** were measured by using PPh_3 as an external reference (δ -7.4) in $CDCl_3$ (Table III-7). The signals of PPh_3 in **14** (δ -4.2) and **15** (δ -4.3) are shifted from that in free PPh_3. These shifts are in agreement with the results of the electronic absorption spectra that the PPh_3 ligands would be approximately coordinated with metal center in measurement condition (ca. 2×10^{-3} mol dm^{-3}). On the other hand, the chemical shifts of **13** (δ -7.4) and **16** (δ 28.9), which showed lower equilibrium constant than **14** in electronic absorption spectra, are very similar to the chemical shift of free PPh_3 (δ -7.4) and $OPPh_3$ (δ 27.4), respectively. This suggests that **13** and **16** release PPh_3 or $OPPh_3$ in measurement condition as expected in electronic absorption spectra.

Table III-7 $^{31}P\{^{1}H\}$ NMR spectral data of complexes **13**–**16**

Complex	$^{31}P\{^{1}H\}$ NMR
[ReO(cat)(Hamq)(PPh_3)] **13**	-7.4
[ReO(Cl_4cat)(Hamq)(PPh_3)] **14**	-4.2
[ReO(Br_4cat)(Hamq)(PPh_3)] **15**	-4.3
[ReO(Cl_4cat)(Hamq)($OPPh_3$)] **16**	28.9

III-vi. OAT Catalytic Reactivity of 14

The quinolinylamido complex **1**, which has active site in solution, showed OAT catalytic activity (Chapter II). As a result of spectroscopic analysis, it was revealed that **14** also releases the monodentate ligand PPh_3 and has active site like **1** in solution. Therefore, the OAT catalytic reactivity from 2,6-lutidine-*N*-oxide (2,6-Me_2pyO) to PPh_3 were investigated (Eq. III-5). In this chapter,

$$PPh_3 + 2,6\text{-}Me_2pyO \xrightarrow{\mathbf{14}} OPPh_3 + 2,6\text{-}Me_2py \qquad \text{(III-5)}$$

2,6-Me_2pyO is used as a main oxygen donor, since the catalytic reaction product 2,6-Me_2py, which has steric substituent groups in 2- and 6-positions, would not act as an inhibitor by strong coordination to active site on metal center. The OAT catalytic reactions of the catecholato complex in Eq. III-5 were monitored by electronic absorption spectra, because the catalytic reaction progression of **14** was much faster than that of **1** (monitored by ^{1}H NMR), and the electronic absorption spectrum was more suitable for monitoring the reaction. The progression of reaction was obtained by converting absorbance to 2,6-Me_2pyO concentration according to Eq. III-6.

$$[2,6\text{-}Me_2pyO]_t = [2,6\text{-}Me_2pyO]_0 \frac{Abs_t - Abs_\infty}{Abs_0 - Abs_\infty} \qquad \text{(III-6)}$$

The control experiments of the reaction between 2,6-Me_2pyO and PPh_3 without **1** showed no reaction. Addition of oxygen donor 2,6-Me_2pyO, in the absence of PPh_3, the solution of **14** turned from orange to deep reddish-purple, which is catalytic active state. The electronic absorption spectrum of the active state showed a new intense band at 489 nm (Figure III-19). It is suggested that the active state would be dioxorhenium(VII) [$ReO_2(Cl_4cat)$(Hamq)], since the spectroscopic character is in agreement with dioxorhenium(VII) complexes.[21,41] The absorbance–time profile showed the decomposition of active state dioxorhenium(VII) complex in the condition of absence of PPh_3 and the solvent containing H_2O (Figure III-19). On the other hand, the catalysis proceeds normally as long as PPh_3 remains. This fact indicates that the recycling of **14** between its resting and active states prevents its decomposition during the catalytic stage. Namely, the rate of the reaction dioxo active states with PPh_3 is much faster than that of dioxo decomposition when there are enough PPh_3 (Scheme III-3). In practice, the band at 489 nm assigned to the dioxo intermediate is not observed on the catalytic stage, therefore it is anticipated that the dioxo intermediate is immediately consumed by PPh_3 after arisen.

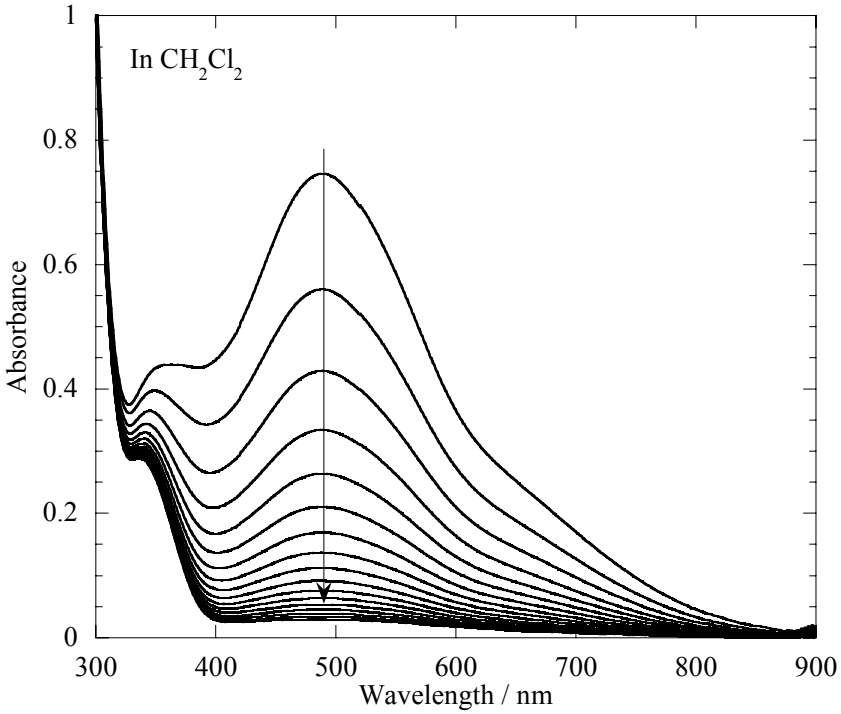

Figure III-19 The decrease of the absorbance of dioxorhenium intermediate (mixture of **14** (1×10^{-4} mol dm^{-3}) and 2,6-Me_2pyO (1×10^{-3} mol dm^{-3})) in CH_2Cl_2. The spectra are shown in 15 min interval.

Scheme III-3

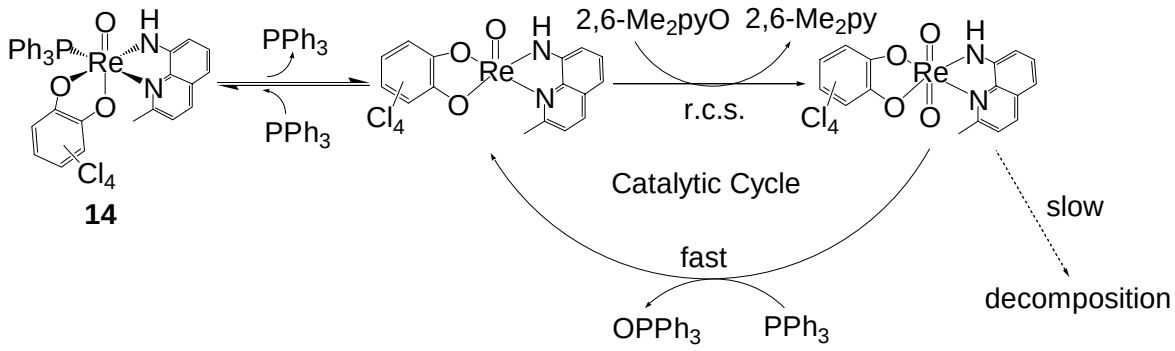

Figure III-20 shows the change of absorbance at 325 nm depending on reaction time to the end of reaction in the condition **14** (1×10^{-5} mol dm^{-3}), PPh_3 (1×10^{-2} mol dm^{-3}), and 2,6-Me_2pyO (1×10^{-2} mol dm^{-3}) in CH_2Cl_2. The catalytic reaction proceeds smoothly to the end of reaction. Therefore, it is suggested that the decomposition of complex dose not occur and the reaction product 2,6-Me_2py does not act as inhibiter to form 2,6-Me_2py substituted complex [ReO(Cl_4cat)(Hamq)(2,6-Me_2py)]. The catecholato complex **14** showed at least 1000 cycles without degradation of the catalytic property, although **1** showed only 10 cycles by decomposition of complex. As would be predicted, the

improvement of the stability of catalyst was achieved and **14** became better than **1** from the viewpoint of OAT catalyst. The initial rates are obtained from the concentration–time curve fitting with a least squares program by using the data from start to 60 s later (Table III-8).[4] Figure III-21 shows concentration of remained 2.6-Me_2pyO versus time curve when the initial concentrations of **14** are varied (4×10^{-5}, 2×10^{-5}, 1×10^{-5}, 0.5×10^{-5}, 0.25×10^{-5} mol dm^{-3}) and initial concentration of 2,6-Me_2pyO and PPh_3 are fixed to 1×10^{-2} mol dm^{-3} in CH_2Cl_2. The increase of slopes (initial rates) is observed with increase of the concentration of **14**. Since the slope of the log–log plot is 1.1 (Figure III-22), the reaction order of concentration of complex **14** is estimated to 1. In a similarly fashion, when the initial concentrations of 2,6-Me_2pyO are varied (4×10^{-5}, 2×10^{-5}, 1×10^{-5}, 0.5×10^{-5}, 0.25×10^{-5} mol dm^{-3}) and initial concentration of **14** and PPh_3 are fixed to 1×10^{-5} and 1×10^{-2} mol dm^{-3} in CH_2Cl_2, respectively, the initial rates increase with the concentration of 2,6-Me_2pyO (Figure III-23, Table III-8). The slope of the log–log plot is 0.96 (Figure III-24), therefore the reaction order of concentration of 2,6-Me_2pyO is estimated to 1. On the other hand, when the initial concentrations of the PPh_3 are varied (2×10^{-5}, 1×10^{-5}, 0.5×10^{-5} mol dm^{-3}) and initial concentration of **14** and 2,6-Me_2pyO are fixed to 1×10^{-5} and 1×10^{-2} mol dm^{-3} in CH_2Cl_2, respectively, the initial rates decrease with the concentration of PPh_3 as opposite to the case of above (Figure III-25, Table III-8). The slope of the log–log plot is -0.94 (Figure III-26), therefore the reaction order of concentration of PPh_3 is estimated to -1. From these reaction orders, the initial rate equation is determined as Eq. III-7.

$$v_0 = k_c \frac{[\mathbf{14}][2,6\text{-}Me_2pyO]}{[PPh_3]} \qquad \text{(III-7)}$$

Its form is further tested by a plot of all the values of v_0 against the composite concentration variable. The data are in agreement with this model, as shown in Figure III-27, and least-square fitting affords k_c = 1.8 s^{-1} at 23 ˚C in CH_2Cl_2. This total reaction rate constant of the OAT reaction, from 2,6-Me_2pyO to PPh_3 with **14** is near to the rate constant (k_c = 6.0 dm^3 mol^{-1} s^{-1}) with [MeReO(mtp)(PPh_3)], which is a typical methylated oxorhenium(V) complex with OAT catalytic property reported by Espenson et al.[4] The initial rate of **14** ($v_0 = 1.8 \times 10^{-5}$ mol dm^{-3} s^{-1}), however, will be about 30 times faster than that of [MeReO(mtp)(PPh_3)] ($v_0 = 6.0 \times 10^{-7}$ mol dm^{-3} s^{-1}) in an experimental condition (for example; catalyst (1×10^{-5} mol dm^{-3}), PPh_3 (1×10^{-2} mol dm^{-3}), and 2,6-Me_2pyO (1×10^{-2} mol dm^{-3})). Because the rate equation in **14** is different from that in [MeReO(mtp)(PPh_3)] ($v_0 = k_c$[2,6-Me_2pyO]^2[catalyst][PPh_3]$^{-1}$) (Eq. III-7).[4] The catalytic activity of **14** is an only example which could have comparable to that of the methylated oxorhenium(V) complex under certain condition to my knowledge.

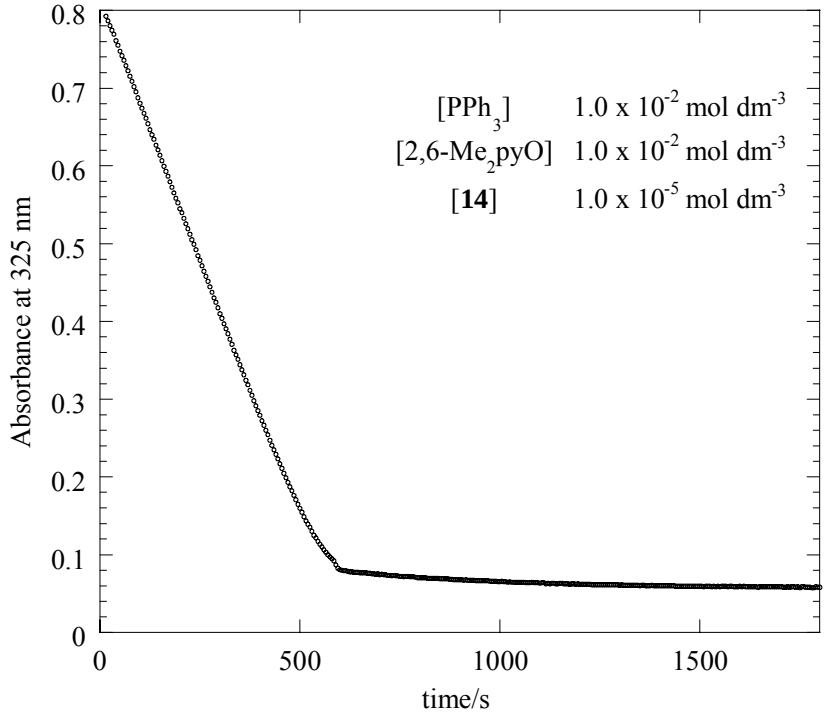

Figure III-20 Plot of absorbance versus time for OAT catalytic reaction of **14**. Conditions: **14** (1×10^{-5} mol dm^{-3}), PPh_3 (1×10^{-2} mol dm^{-3}), and 2,6-Me_2pyO (1×10^{-2} mol dm^{-3}) in CH_2Cl_2.

Table III-8 Initial reaction rate data for the oxidation of PPh_3 by luO catalyzed by **14**

[**14**] / 10^{-5} mol dm^{-3}	[PPh_3] / 10^{-2} mol dm^{-3}	[2,6-Me_2pyO] / 10^{-2} mol dm^{-3}	v_0 / 10^{-5} mol dm^{-3} s^{-1}
0.25	1.0	1.0	0.33
0.50	1.0	1.0	0.88
1.0	1.0	1.0	1.8
2.0	1.0	1.0	3.7
4.0	1.0	1.0	7.2
1.0	0.50	1.0	4.2
1.0	2.0	1.0	1.1
1.0	1.0	0.25	0.52
1.0	1.0	0.50	0.89
1.0	1.0	2.0	3.3
1.0	1.0	4.0	7.6

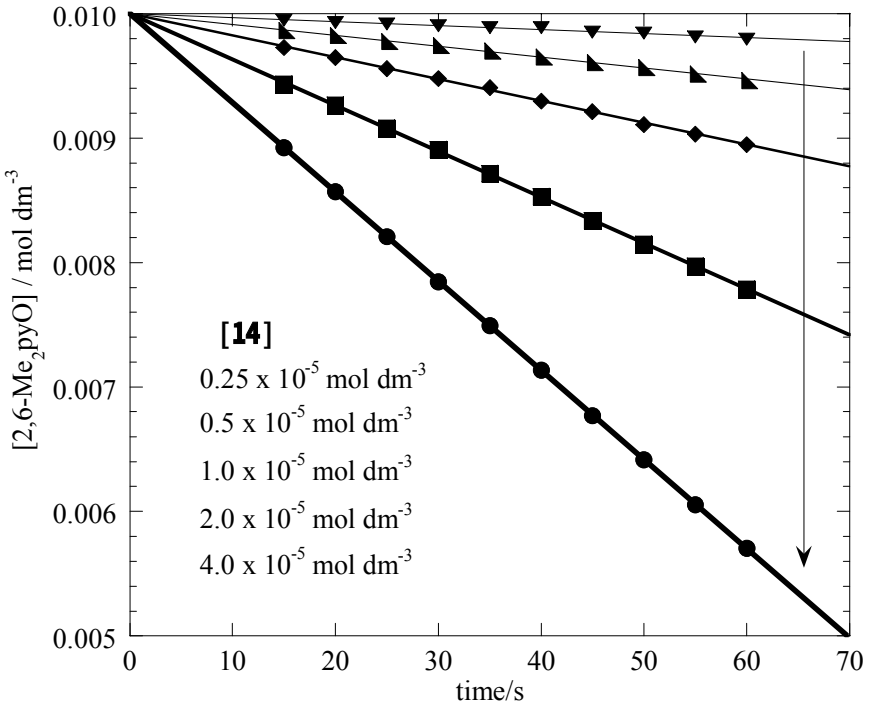

Figure III-21 Plots of concentration of remained 2,6-Me_2pyO versus time for OAT catalytic reaction of **14**. Conditions: [**14**] was varied with 1×10^{-2} mol dm^{-3} PPh_3 and 1×10^{-2} mol dm^{-3} 2,6-Me_2pyO in CH_2Cl_2.

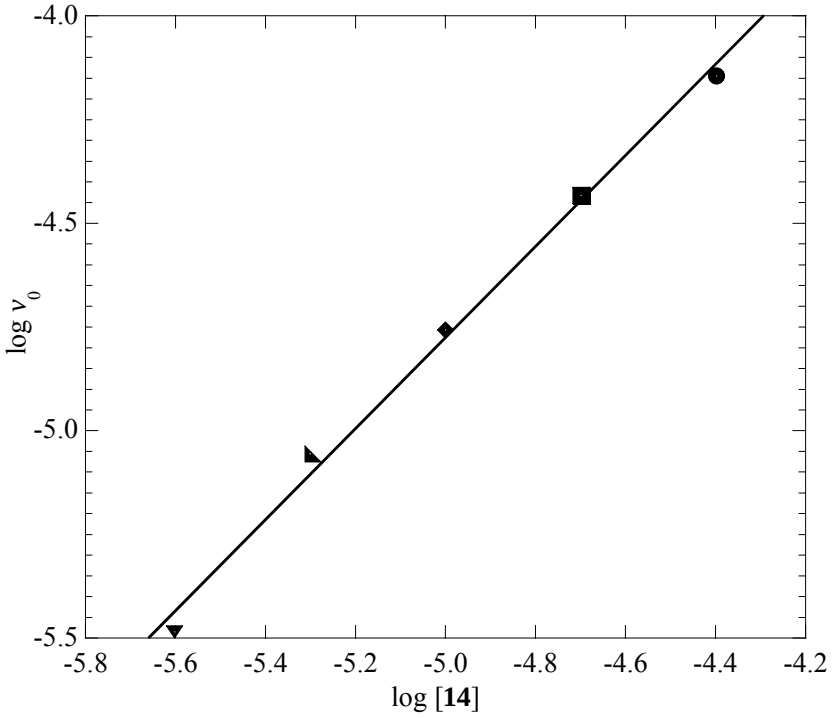

Figure III-22 The initial rates of reaction dependence on concentration of **14**, as shown on log-log scales. Conditions: **14** was varied with 1×10^{-2} mol dm^{-3} PPh_3 and 1×10^{-2} mol dm^{-3} 2,6-Me_2pyO in CH_2Cl_2.

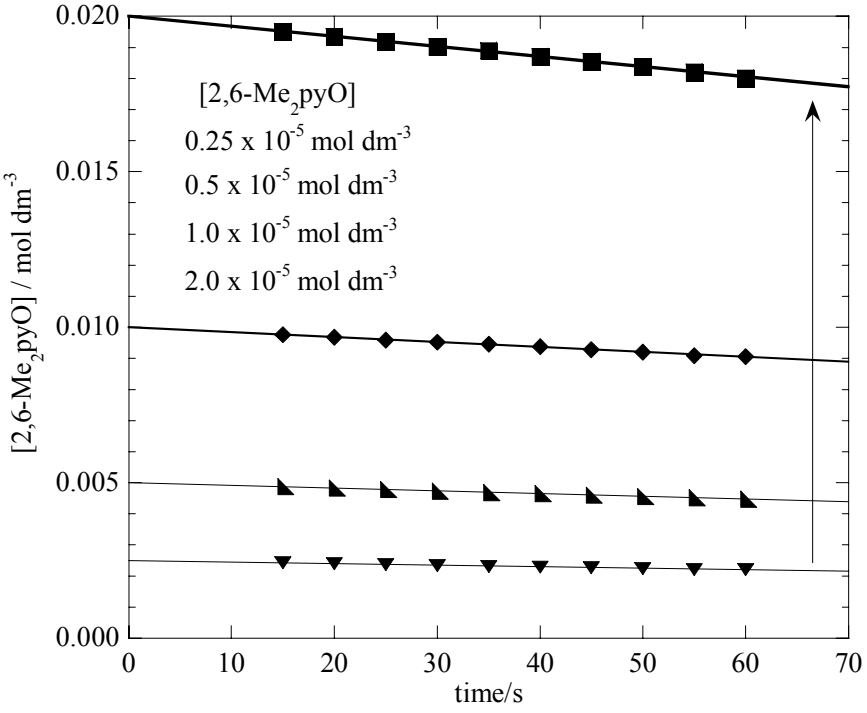

Figure III-23 Plots of concentration of remained 2,6-Me_2pyO versus time for OAT catalytic reaction of **14**. Conditions: [2,6-Me_2pyO] was varied with 1×10^{-5} mol dm^{-3} **14** and 1×10^{-2} mol dm^{-3} PPh_3 in CH_2Cl_2.

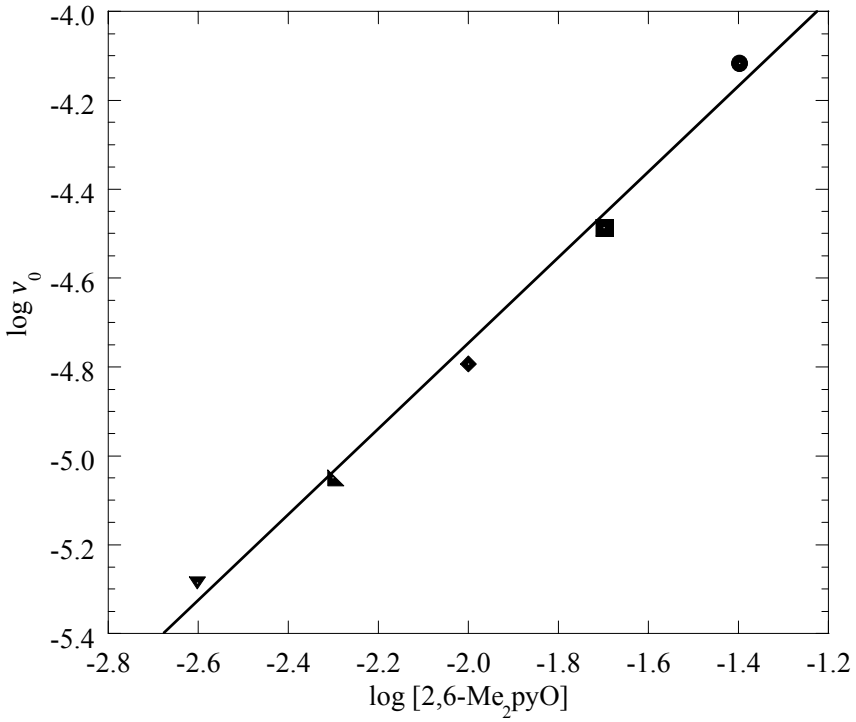

Figure III-24 The initial rates of reaction dependence on concentration of luO, as shown on log-log scales. Conditions: [2,6-Me_2pyO] was varied with 1×10^{-5} mol dm^{-3} **14** and 1×10^{-2} mol dm^{-3} PPh_3 in CH_2Cl_2.

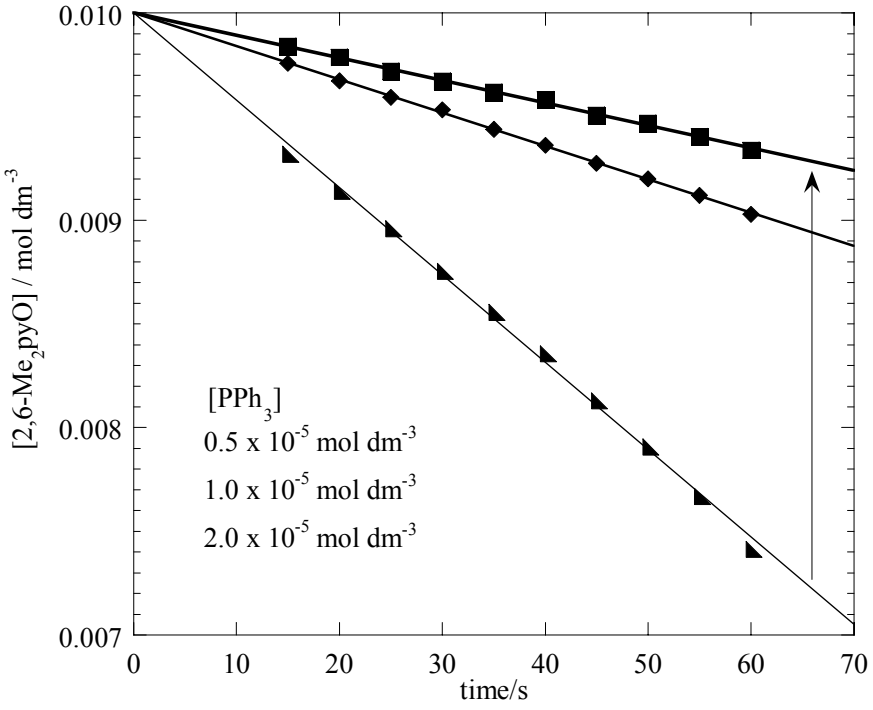

Figure III-25 Plots of concentration of remained 2,6-Me_2pyO versus time for OAT catalytic reaction of **14**. Conditions: [PPh_3] was varied with 1×10^{-5} mol dm^{-3} **14** and 1×10^{-2} mol dm^{-3} 2,6-Me_2pyO in CH_2Cl_2.

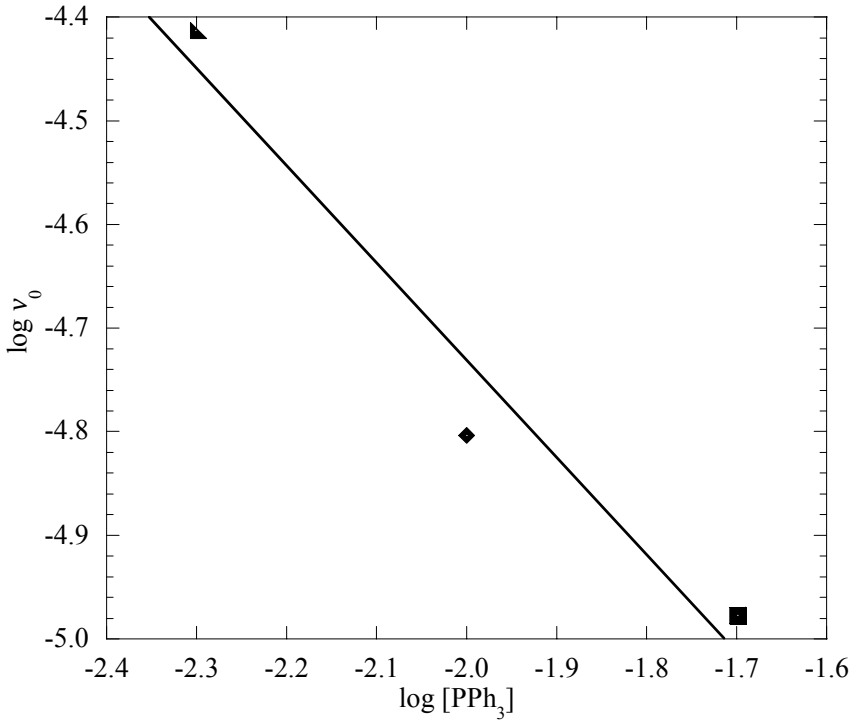

Figure III-26 The initial rates of reaction dependence on concentration of PPh_3, as shown on log-log scales. Conditions: [PPh_3] was varied with 1×10^{-5} mol dm^{-3} **14** and 1×10^{-2} mol dm^{-3} 2,6-Me_2pyO in CH_2Cl_2.

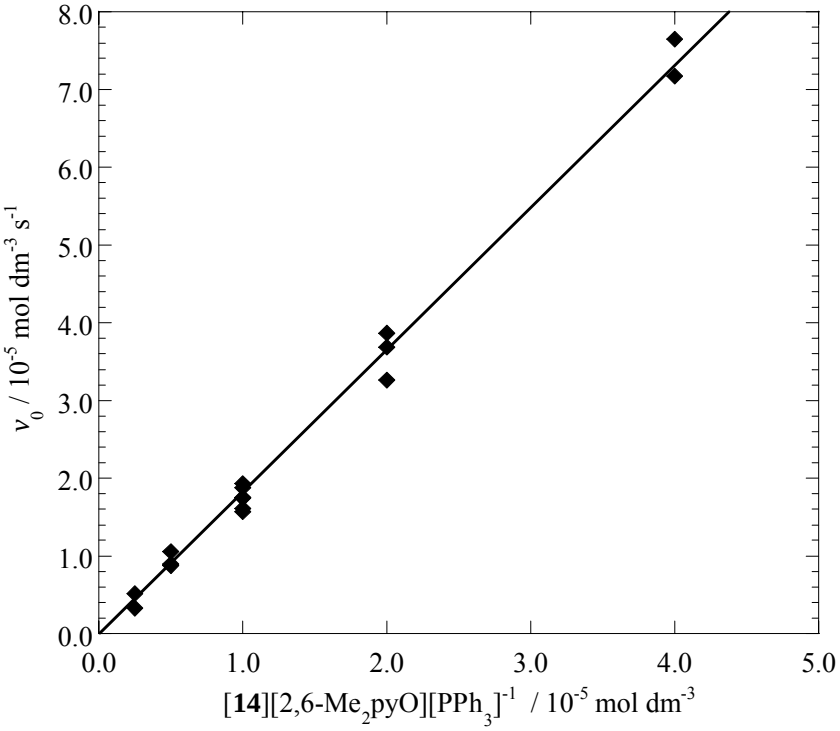

Figure III-27 The initial rates of reaction dependence on the combined concentration variable, as in Eq. III-7.

From the results of these measurements of OAT catalytic reactivity, the reaction cycle is supposed to Scheme III-4. In brief, it comprises the following steps: (1) **14** releases the PPh_3 ligand and forms the five-coordinated intermediate **A**; (2) **A** and 2,6-Me_2pyO form the 2,6-Me_2pyO coordinated intermediate **B**; (3) 2,6-Me_2py is released from **B**, to form the dioxo intermediate **C**; (4) **C** reacts with PPh_3 quite rapidly and forms **16**, without an influence on the rate; (5) $OPPh_3$ is released from **16** and return to **A**. The rate law for Scheme III-4 is derived from Eqs. III-8–III-10. Eq. III-11 is obtained by solving Eqs. III-8 and III-9. If the third step is assumed to the rate controlling step (r.c.s.) as with the literature,[4] the reaction rate is expressed as Eq. III-12. To attain correspondence between Eq. III-12 and Eq. III-7, the 2,6-Me_2pyO ([pyO]) denominator term in Eq. III-12 must be negligible, so that the equation simplifies to the first form in Eq. III-13. The rate constant in r.c.s. (k_3) is much smaller than k_{-2}, therefore the equation is further simplified to the final form in Eq. III-13.

$$[\mathbf{A}] = \frac{k_1[\mathbf{14}] + k_{-2}[\mathbf{B}]}{k_{-1}[PPh_3] + k_2[pyO]} \qquad \text{(III-8)}$$

$$[\mathbf{B}] = \frac{k_2[\mathbf{A}][pyO]}{k_{-2} + k_3} \qquad \text{(III-9)}$$

$$[\mathbf{C}] = k_3[\mathbf{B}] \qquad \text{(III-10)}$$

$$[\mathbf{B}] = \frac{k_1 k_2[\mathbf{14}][\text{pyO}]}{(k_{-1}k_{-2} + k_{-1}k_3)[\text{PPh}_3] + k_2 k_3[\text{pyO}]} \qquad \text{(III-11)}$$

$$v_0 = k_3[\mathbf{B}] = \frac{k_1 k_2 k_3[\mathbf{14}][\text{pyO}]}{(k_{-1}k_{-2} + k_{-1}k_3)[\text{PPh}_3] + k_2 k_3[\text{pyO}]} \qquad \text{(III-12)}$$

$$v_0 = \frac{k_1 k_2 k_3[\mathbf{14}][\text{pyO}]}{(k_{-1}k_{-2} + k_{-1}k_3)[\text{PPh}_3]}$$

$$\xrightarrow{(k_3 << k_{-2})} = \frac{k_1 k_2 k_3[\mathbf{14}][\text{pyO}]}{k_{-1}k_{-2}[\text{PPh}_3]} = K_1 K_2 k_3 \frac{[\mathbf{14}][\text{pyO}]}{[\text{PPh}_3]} \qquad \text{(III-13)}$$

Scheme III-4

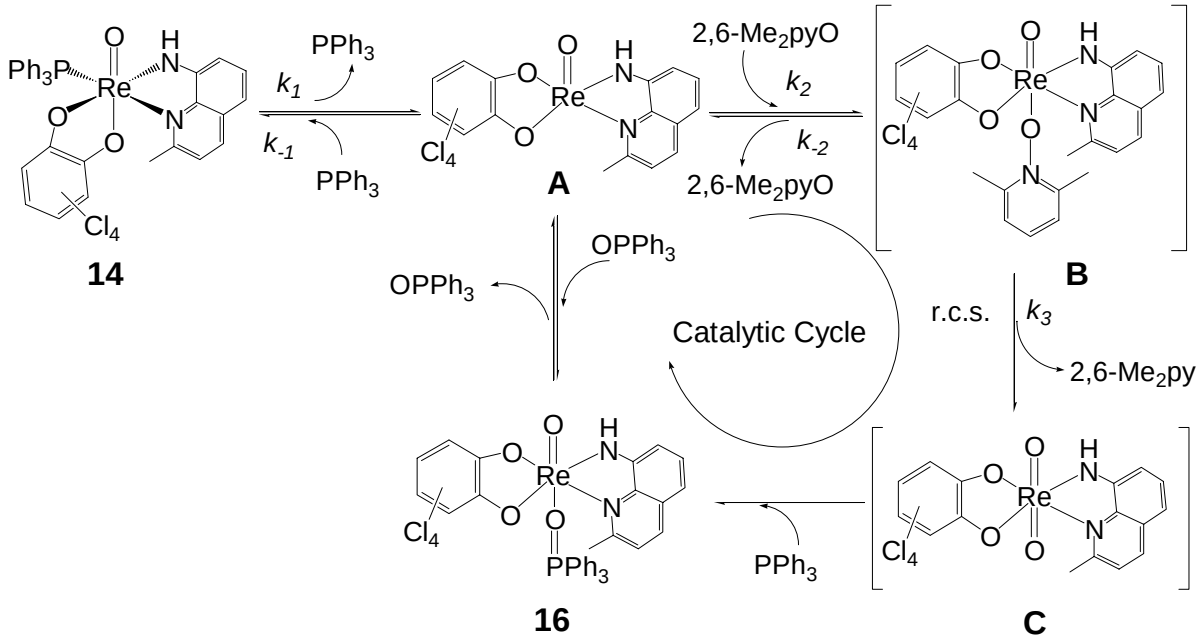

The OAT catalytic reaction is also measured by changing the oxygen donor from 2,6-Me_2pyO to pyO, 4-MepyO, and 4-CNpyO under the condition that the concentrations of **14**, PPh_3, and pyridine oxide derivatives are 1×10^{-5}, 1×10^{-2}, and 1×10^{-2} mol dm^{-3}, respectively (Figure III-28, Table III-9). As a result of the measurements, it is revealed that the reaction rate constants are increasing such as 2,6-Me_2pyO > pyO 4-Mepy > 4-CNpy. The difference in the rate constants between highest 2,6-Me_2pyO and 4-CNpyO are less than 4 times. On the other hand, in the case of

[MeReO(mtp)(PPh_3)][4], the difference in the rate constants between highest 4-MepyO and 4-CNpyO is more than 3000 times (Table III-9). That is to say, the influence of substituents on pyridine oxide derivatives in catalyst **14** is much smaller than that in [MeReO(mtp)(PPh_3)]. The difference in the substituent influence would be caused by the difference in a catalytic cycle. In the case of [MeReO(mtp)(PPh_3)], pyridine oxide derivatives are instrumental twice in a catalytic cycle. On the other hand, in the case of **14**, pyridine oxide derivatives are instrumental only once in a catalytic cycle.

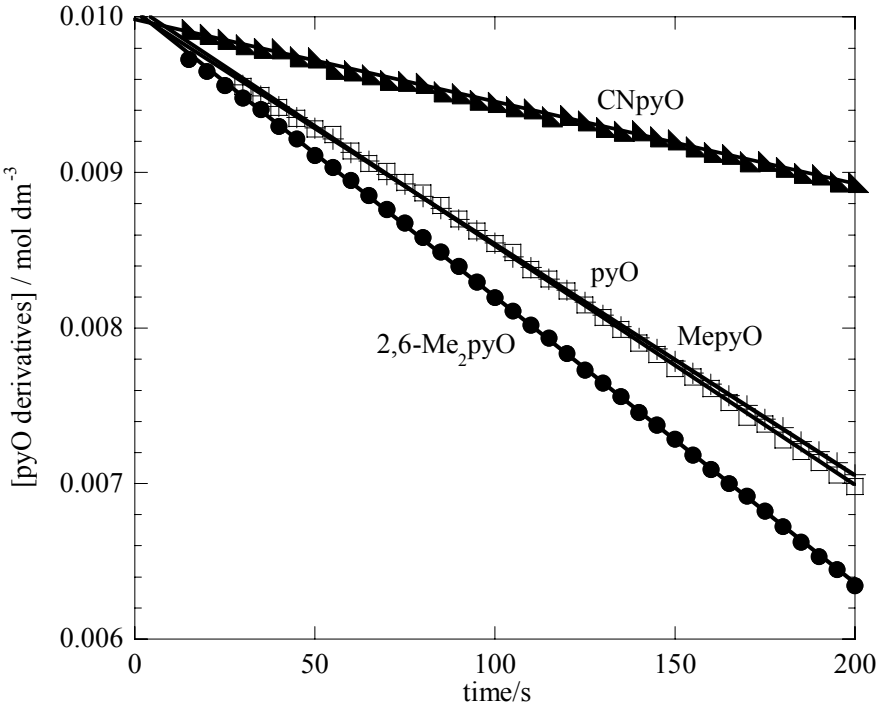

Figure III-28 Plots of concentration of remained pyO derivatives (2,6-Me_2pyO (circle), pyO (square), 4-MepyO (cross), 4-CNpyO (triangle)) versus time for OAT catalytic reaction of **14**. Conditions: 1×10^{-2} mol dm^{-3} **14**, 1×10^{-2} mol dm^{-3} PPh_3 and 1×10^{-2} mol dm^{-3} pyO derivatives in CH_2Cl_2.

Table III-9 Rate constants for the reaction between pyridine oxide derivatives and PPh_3, catalyzed by **14** and [MeReO(mtp)(PPh_3)]

pyO derivatives	k_c[a] / s^{-1}	k_c[a] (rel)	k_c[b] / dm^3 mol^{-1} s^{-1}	k_c[b] (rel)
2,6-Me_2pyO	1.8	1.2	6.0	4.9×10^{-3}
pyO	1.5	(1.0)	1.2×10^3	(1.0)
4-MepyO	1.5	1.0	1.5×10^4	12
4-CNpyO	0.53	0.35	4.0	3.3×10^{-3}

[a] The rate law $v = k_c$[**14**][pyO derivatives][PPh_3]$^{-1}$ defines k_c. [b] The catalyst is [MeReO(mtp)(PPh_3)] reported by Espenson et al.[4]

III-vii. Conclusion

The catecholate derivatives coordinated complexes **13**–**15** were synthesized by the reaction of **1** with catechol derivatives for improving the stability of the quinolinylamido complex **1**. The X-ray crystal analysis of **14** revealed the coordination geometry of tetrachlorocatecholato coordinated complex. The *trans* position to the oxo ligand was occupied by oxygen atom of catecholato ligand following the tendency of oxorhenium(V) complexes that oxygen atom usually lies in the *trans* position to the oxo ligand. From the results of spectroscopic studies, it was revealed that catecholato complexes **13**–**15** release the monodentate ligand PPh_3 in solution similarly to **1**. The substitution reactions of monodentate ligand were investigated and substituted complexes [ReO(Cl_4cat)(Hamq)(L)] (L = $OPPh_3$, **16**; 4-Mepy, **17**; 4-*t*-Bupy, **18**) were obtained by using this releasing property. The X-ray crystal analysis of **17** and **18** revealed that the *trans* position to the oxo ligand was also occupied by oxygen atom of catecholato ligand similarly to **14**. On the other hand, the *trans* position to the oxo ligand was occupied by oxygen atom of $OPPh_3$. These complexes showed concentration dependence in CH_2Cl_2. The OAT catalytic property of **14** was monitored by electronic absorption spectra and the rate equations, rate constants, and catalytic cycle schemes were investigated. As a result of the introducing didentate catecholate derivatives, the stability of the catalyst was significantly improved. That is, the total turnover number of **14** was at least 100 times greater than that of **1**. Furthermore, it was revealed that the OAT catalytic reaction rate of **14** was comparable with that of the methylated oxorhenium complex [MeReO(mtp)(PPh_3)]. When the oxygen donor was changed from 2,6-Me_2pyO to pyO, 4-MepyO, and 4-CNpyO, the noticeable substituent effect was not observed different from the case of Espenson's report.[3,4]

References

1 N. Koshino and J. H. Espenson, *Inorg. Chem.*, **42**, 5735 (2003).

2 Y. Cai, A. Ellern, and J. H. Espenson, *Inorg. Chem.*, **44**, 2560 (2005).

3 J. H. Espenson, *Coord. Chem. Rev.*, **249**, 329 (2005).

4 Y. Wang and J. H. Espenson, *Inorg. Chem.*, **41**, 2266 (2002).

5 F. Refosco, F. Tisato, G. Bandoli, C. Bolzati, A. Moresco, and M. Nicolini, *J. Chem. Soc., Dalton Trans.*, 605 (1993).

6 CrystalCrear, J. W. Pflugrath, *Acta Crystallogr., Sect. D*, **55**, 1718 (1999).

7 A. Altomare, M. Burla, M. Camalli, G. Cascarano, C. Giacovazzo, A. Guagliardi, and G. Polidori, *J. Appl. Crystallogr.*, **27**, 435 (1994).

8 A. Altomare, M. Burla, M. Camalli, G. Cascarano, C. Giacovazzo, A. Guagliardi, A. Moliterni, G. Polidori, and R. Spagna, *J. Appl. Crystallogr.*, **32**, 115 (1999).

9 P. T. Beurskens, G. Admiraal, G. Beurskens, W. P. Bosman, R. de Gelder, R. Israel, and J. M. M. Smits, The DIRDIF-99 Program System, Technical Report of the Crystallography Laboratory, University of Nijmegen, The Netherlands (1999).

10 P. T. Beurskens, G. Admiraal, G. Beurskens, W. P. Bosman, S. Garcia-Granda, R. O. Gould., J. M. M. Smits, and C. Smykalla, The DIRDIF Program System, Technical Report of the Crystallography Laboratory, University of Nijmegen, The Netherlands (1999).

11 CrystalStructure 3.5.1: Crystal Structure Analysis Package, Rigaku and Rigaku/MSC, 2000-2003.

12 C. F. Edwards, W. P. Griffith, A. J. P. White, and D. J. Williams, *J. Chem. Soc., Dalton Trans.*, 957 (1992).

13 The Chemical Society of Japan, KAGAKUBINRAN KISOHEN, 2nd ed.; Maruzen Co., Ltd.: Tokyo (1975).

14 M. M. Abu-Omar and S. I. Khan, *Inorg. Chem.*, **37**, 4979 (1998).

15 L. Hansen, E. Alessio, M. Iwamoto, P. A. Marzilli, and L. G. Marzilli, *Inorg. Chim. Acta*, **240**, 413 (1995).

16 G. Battistuzzi, M. Cannio, M. Saladini, and R. Battistuzzi, *Inorg. Chim. Acta*, **320**, 178 (2001).

17 G. Bandoli, A. Dolmella, T. I. A. Gerber, J. Perils, and J. G. H. du Preez, *Inorg. Chim. Acta*, **294**, 114 (1999).

18 T. Głowiak, W. K. Rybak, and A. Skarżyńska, *Polyhedron*, **19**, 2667 (2000).

19 A. Skarżyńska, W. K. Rybak, and T. Głowiak, *Polyhedron*, **20**, 2667 (2001).

20 J. R. Dilworth, D. V. Griffithe, S. J. Parrott, and Y. Zheng, *J. Chem. Soc., Dalton Trans.*, 2931 (1997).

21 J. Arias, C. R. Newlands, and M. M. Abu-Omar, *Inorg. Chem.*, **40**, 2185 (2001).

22 S. Bélanger and A. L. Beauchamp, *Inorg. Chem.*, **35**, 7836 (1996).

23 S. Bélanger and A. L. Beauchamp, *Inorg. Chem.*, **36**, 3640 (1997).

24 J. M. Botha, K. Umakoshi, Y. Sasaki, and G. J. Lamprecht, *Inorg. Chem.*, **37**, 1609 (1998).

25 C. Bolzati, F. Tisato, F. Refosco, G. Bandoli, and A. Dolmella, *Inorg. Chem.*, **35**, 6221 (1996).

26 J. M. Mayer, D. L. Thorn, and T. H. Tulip, *J. Am. Chem. Soc.*, **107**, 7454 (1985).

27 T. I. A. Gerber, J. Bruwer, G. Bandoli, J. Perils, and J. G. H. du Preez, *J. Chem. Soc., Dalton Trans.*, 2189 (1995).

28 M. T. Ahmet, B. Coutinho, J. R. Dilworth, J. R. Miller, S. J. Parrott, Y, Zheng, M. Harman, M. B. Hursthouse, and A. Malik, *J. Chem. Soc., Dalton Trans.*, 3041 (1995).

29 X. Chen, F. J. Femia, J. W. Babich, and J. Zubieta, *Inorg. Chim. Acta*, **308**, 80 (2000).

30 H. Luo, I. Setyawati, S. J. Rettig, and C. Orvig, *Inorg. Chem.*, **34**, 2287 (1995).

31 S. D. Orth, J. Barrera, M. Sabat, and W. D. Harman, *Inorg. Chem.*, **32**, 594 (1993).

32 S. D. Orth, J. Barrera, M. Sabat, and W. D. Harman, *Inorg. Chem.*, **33**, 3026 (1994).

33 P. Perez-Lourido, J. Romero, J. Garcia-Vazquez, A. Sousa, K. P. Maresca, D. J. Rose, and J. Zubieta, *Inorg. Chem.*, **37**, 3331 (1998).

34 B. Machura, M. Jaworska, and R. Kruszynski, *Polyhedron*, **24**, 267 (2005).

35 Y. Yamada, K. Fujisawa, and K. Okamoto, *Bull. Chem. Soc. Jpn.*, **73**, 2067 (2000).

36 Y. Yamada, K. Fujisawa, and K. Okamoto, *Bull. Chem. Soc. Jpn.*, **73**, 2297 (2000).

37 G. Bandoli, A. Dolmella, T. I. A. Gerber, J. Perils, and J. G. H. du Preez, *Inorg. Chim. Acta*, **303**, 24 (2000).

38 I. Chakraborty, S. Bhattacharyya, S. Banerjee, B. K. Dirghangi, and A. Chakravorty, *J. Chem. Soc., Dalton Trans.*, 3747 (1999).

39 S. Fortin and A. L. Beauchamp, *Inorg. Chem.*, **39**, 4886 (2000).

40 D. F. Shriver, P. W. Atkins, Inorganic Chemistry, Third edition; Oxford University Press: UK (2001).

41 M. M. Abu-Omar, L. D. McPherson, J. Arias, and V. M. Béreau, *Angew. Chem., Int. Ed.*, **39**, 4310 (2000).

Chapter IV. Structures and Properties of Stable Oxorhenium(V) Complexes with 2-Methyl-8-quinolinolate

IV-i. Introduction

The oxorhenium(V) complexes with quinolinylamide showed the unusual substitution property in the previous chapters. That is, the substitution reaction of monodentate ligand and OAT reaction were observed by using the property. Thus, to explore the effect of the coordinated atoms for characteristics of oxorhenium(V) complexes, the didentate-*N*,*O* ligand 8-hydroxy-2-methylquinoline (Hhmq), that the aromatic amine in 8-amino-2-methylquinoline was changed to aromatic alcohol, was chosen for ansymmetric didentate ligand. Generally, in high oxidation state complexes with multiple bonds, the sixth coordination bond becomes weaker by strong *trans* influence. In some cases, therefore, these complexes have the five-coordinated state.[1-5] However, the quinolinol oxygen atom could not make a multiple bond with metal center, even if the quinolinol is deprotonated and changed to quinolinolate. Furthermore, the phenolate oxygen atom in the quinolinolate ligand is hard base from the viewpoint of HSAB theory. The oxorhenium(V) complexes coordinated with hard base ligand, alcholate or chloride, tend to prefer the six-coordinated state,[6-8] while the oxorhenium(V) complexes coordinated with soft base ligand, alkyl or thiolate, tend to prefer the five-coordination state.[9-12] Therefore, it is expected that the reactivity of the quinolinolato complexes will be less than that of the quinolinylamido complexes.

In this chapter, the oxorhenium(V) complexes with quinolinolate $[ReOCl_2(hmq)(PPh_3)]$ **19**, which correspond to the quinolinylamido complex $[ReOCl_2(Hamq)(PPh_3)]$ **1**, is synthesized (Scheme IV-1). Additionally, the bisquinolinolato complex $[ReOCl(hmq)_2]$ **20** is synthesized. The structures of the obtained oxorhenium(V) complexes were determined by X-ray diffraction study and their spectrochemical properties are discussed. The structures and properties are compared with the reported

Scheme IV-1

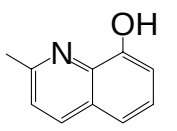

Hhmq

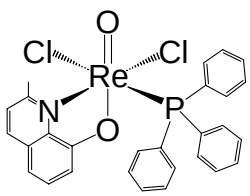

$[ReOCl_2(hmq)(PPh_3)]$ **19**

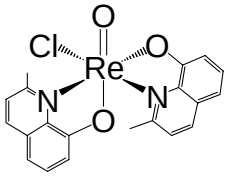

$[ReOCl(hmq)_2]$ **20**

complexes.[6,13,14] The substitution reactivity and OAT catalytic reactivity of **19** was also investigated.

IV-ii. Experimental

Materials

Rhenium was purchased from Soekawa Chemical Co., Ltd. 8-Hydoxy-2-methylquinoline (Hhmq) and pyridine-*N*-oxide (pyO) were purchased from Tokyo Kasei Kogyo Co., Ltd. The other materials were purchased from Wako Pure Chemical Ind., Ltd. All the chemicals were used without further purification. The starting material $[ReOCl_3(PPh_3)_2]$[15] was prepared according to the literature.

$[ReOCl_2(hmq)(PPh_3)]$ 19. To a suspension containing $[ReOCl_3(PPh_3)_2]$ (200 mg, 0.24 mmol) in $C_6H_5CH_3$ (40 cm^3) was added a solution containing an equimolar of Hhmq (39 mg, 0.24 mmol) in $C_6H_5CH_3$ (20 cm^3). The mixture was heated and stirred for 3.5 h, whereupon the color of the mixture turned from light-green to dark-brown. After cooling to room temperature, the solution was concentrated to ca. 5 cm^3 by vacuum line. The brownish green powder was collected by filtration and washed with $(C_2H_5)_2O$. Yield 129 mg, 78%. The obtained complex was recrystallized from $CH_2Cl_2/C_6H_5CH_3$ (5/1) to yield the brownish green crystals. A well-formed crystal of **19**·$C_6H_5CH_3$ was used for an X-ray analysis. Anal. Found: C, 48.20; H, 3.39; N, 2.14%. $[ReOCl_2(C_{10}H_8NO)P(C_6H_5)_3]$ requires C, 48.49; H, 3.34; N, 2.02%. IR (KBr) 961s(Re=O) cm^{-1}. far-IR (Nujol) 330s and 290s (Re–Cl) cm^{-1}. $^{31}P\{^1H\}$ NMR δ -21.0.

$[ReOCl(hmq)_2]$ 20. To a suspension containing $[ReOCl_3(PPh_3)_2]$ (204 mg, 0.245 mmol) in $C_6H_5CH_3$ (40 cm^3) was added a solution containing the Hhmq (85.3 mg, 0.536 mmol) in $C_6H_5CH_3$ (10 cm^3). The mixture was heated and stirred for 3 h, whereupon the color of the mixture turned from light-green to dark-green. After cooling to room temperature, the deep green powder was collected by filtration and washed with H_2O and $(C_2H_5)_2O$. Yield 71.5 mg, 53%. The obtained complex was recrystallized from $CH_2Cl_2/C_6H_5CH_3$ (2/1) to yield the deep green crystals. A well-formed crystal of **20** was used for an X-ray analysis. Anal. Found: C, 43.71; H, 3.05; N, 5.09%. $[ReOCl(C_{10}H_8NO)_2]$ requires C, 43.36; H, 2.91; N, 5.06%. IR (KBr) 969vs (Re=O) cm^{-1}. far-IR (Nujol) 318s (Re–Cl) cm^{-1}.

Measurements

Elemental analyses (C, H, N) were performed by the Research Facility Center for Science and Technology or Department of Chemistry of the University of Tsukuba. IR spectra were recorded as KBr pellets on a JASCO FT/IR-550 spectrometer in the range of 4000–400 cm^{-1} and far-IR spectra were recorded as Nujol mull method in the range of 650–50 cm^{-1} at room temperature. The electronic absorption spectra were recorded with a JASCO V-560 spectrophotometer. The diffuse reflectance spectra were recorded on a JASCO V-570 spectrophotometer equipped with an integrating sphere apparatus (JASCO ISN-470). The ^{1}H and $^{31}P\{^{1}H\}$ NMR spectra were obtained on a BRUKER AVANCE 600 spectrometer or BRUKER AVANCE 500 spectrometer with $SiMe_4$ as an internal reference and PPh_3 as an external reference respectively (in $CDCl_3$ PPh_3 resonates at δ -7.42 with respect to 85% H_3PO_4 in D_2O).[16] The electrochemical experiments were performed by a CW-50W voltammetry analyzer, Bioanalytical Systems, Inc. (BAS) using platinum-working electrode (BAS, Pt). An acetonitrile Ag/AgCl/Bu_4NClO_4 electrode (BAS, RE-5) and platinum wire were used as reference and auxiliary electrodes, respectively. The experiments were conducted by the complexes (0.001 mol dm^{-3}) in an acetonitrile solution of Bu_4NClO_4 (0.1 mol dm^{-3}) as a supporting electrolyte. Ferrocene (Fc) was used as an external reference.

Crystallography

Single crystals of **19** and **20** were used for data collection on a Rigaku Mercury CCD area detector with graphite-monochromatized MoKα (0.71069 Å) radiation. The intensity data were collected to a maximum 2θ value of 55° at 296 K. An empirical absorption correction was applied. Data were collected and were processed using CrystalClear.[17] The crystal data and experimental parameters are listed in Table IV-1.

The positions of most non-hydrogen atoms of **19** and **20** were determined by direct methods (SIR97[18] in **19** and SHELX97[19] in **20**) and some remaining atoms positions were found by successive difference Fourier techniques.[20] The structures were refined by full-matrix least-squares techniques using anisotropic thermal parameters for non-hydrogen atoms. For **19** and **20**, all the hydrogen atoms were included in the refinement but constrained to ride on the atoms (C–H = N–H = 0.95 Å, U(H) = 1.2U(C, N)). The calculations on **19** and **20** were performed using the CrystalStructure crystallographic software package.[21]

Table IV-1 Crystal data and experimental parameters for $[ReOCl_2(hmq)(PPh_3)]\cdot C_6H_5CH_3$ **19**$\cdot C_6H_5CH_3$ and $[ReOCl(Hamq)_2]$ **20**

	19$\cdot C_6H_5CH_3$	**20**
Formula	$C_{35}H_{31}Cl_2NO_2PRe$	$C_{20}H_{16}ClN_2O_3Re$
Formula weight	785.72	554.02
Cryst. system	monoclinic	triclinic
Space group	$P2_1/c$ (No. 14)	P-1 (No. 2)
a, Å	9.8021(4)	7.7073(2)
b, Å	14.7217(5)	9.2869(2)
c, Å	22.8506(10)	12.7456(4)
α, °		85.986(3)
β, °	102.1519(5)	85.950(3)
γ, °		84.680(3)
V, Å^3	3223.5(2)	904.24(4)
Z	4	2
D_{calc}, g cm^{-3}	1.619	2.035
μ (Mo Kα), cm^{-1}	40.18	68.94
Reflections collected	50978	14544
Unique reflections	7618	4068
R_{int}	0.030	0.021
Observations ($I > 3\sigma(I)$)	5562	3877
Variable parameters	410	260
R[a]	0.032	0.025
R_w[b]	0.083	0.067
GOF	1.007	1.008

[a] $R = \Sigma||F_o| - |F_c||/\Sigma|F_o|$. [b] $R_w = [\Sigma w(F_o^2 - F_c^2)^2/\Sigma w(F_o^2)^2]^{1/2}$, where $w = 1/\sigma^2(F_o^2)$.

IV-iii. Syntheses of $[ReOCl_2(hmq)(PPh_3)]$ (19) and $[ReOCl(hmq)_2]$ (20)

The monoquinolinolato complex $[ReOCl_2(hmq)(PPh_3)]$ **19** was obtained by the refluxing of the oxorhenium(V) precursor $[ReOCl_3(PPh_3)_2]$ with an equimolecular of 8-hydroxy-2-methylquinoline (Hhmq) ligand in $C_6H_5CH_3$ (Eq. IV-1). The substitution of a chloride ion and a PPh_3 for an oxygen

$$[ReOCl_3(PPh_3)_2] + Hhmq \xrightarrow[\Delta]{} [ReOCl_2(hmq)(PPh_3)]\ \mathbf{19} + HCl + PPh_3 \quad (IV\text{-}1)$$

atom and a nitrogen atom of ligand takes place in the course of the reaction. On the other hand, refluxing of the oxorhenium(V) precursor $[ReOCl_3(PPh_3)_2]$ with two equimolecular of Hhmq gave the bisquinolinolato complex $[ReOCl(hmq)_2]$ **20** (Eq. IV-2). It showed the difference in the reactivity

$$[ReOCl_3(PPh_3)_2] + 2Hhmq \xrightarrow[\Delta]{} [ReOCl(hmq)_2]\ \mathbf{20} + 2HCl + 2PPh_3 \quad (IV\text{-}2)$$

between the quinolinylamide with precursor and quinolinolate with precursor. When the precursor complex $[ReOCl_3(PPh_3)_2]$ was reacted with excess of H_2amq, the corresponding bisquinolinylamido complex $[ReOCl(Hamq)_2]$ was not isolated. In the case of **19**, the influence of the coordinated atom change from nitrogen ($[ReOCl_2(Hamq)(PPh_3)]$ **1**) to oxygen was not observed from the viewpoint of coordination geometry. On the other hand, the influence of the coordinated atom change appeared in the substitution reactivity. **19** did not show the substitution reaction from PPh_3 to $OPPh_3$ or pyridine derivatives (L) different from **1** (Eq. IV-3). It was only natural that the $OPPh_3$ substituted complex

$$[ReOCl_2(hmq)(PPh_3)]\ \mathbf{19} + L \xrightarrow{\times} [ReOCl_2(hmq)(L)] + PPh_3 \quad (IV\text{-}3)$$

$[ReOCl_2(hmq)(OPPh_3)]$ was not also obtained as a by-product in synthesis of **19** different from the case of **1**. This lowering of the substitution reactivity seems to be due to the tendency that **19** keeps the six-coordinated state. The reason of the keeping six-coordinated state would be caused by the quinolinolate oxygen character, which is hard base and could not make multiple bond with metal center.

IV-iv. Crystal Structures of 19, 20

[$ReOCl_2$(hmq)(PPh_3)] 19 An X-ray crystal analysis for **19** revealed the presence of a complex molecule and a $C_6H_5CH_3$ molecule in an asymmetric unit. A perspective drawing of the complex molecule **19** is shown in Figure IV-1 and its selected bond distances and angles are listed in Table IV-2. The coordination geometry around rhenium atom is distorted octahedral with the oxo ligand, one nitrogen atom and one oxygen atom from the asymmetrical didentate-*N*,*O* ligand, two chloride ions and one phosphorus atom from the PPh_3 ligand. The oxygen atom of hmq ligand lies in *trans* to the oxo ligand along the axial direction, whereas the heterocyclic nitrogen atom, which is another moiety of hmq ligand, phosphorus atom, and two *cis* chloride ions occupy the equatorial plane. The same coordination geometry was observed for the similar quinolinolate coordinated complexes and the corresponding quinolinylamido complex [$ReOCl_2$(Hamq)(PPh_3)] **1**.[6,14]

The Re1–O2 distance (1.969(3) Å) in **19** is shorter than those (2.010(7)–2.036(5) Å) in the similar complexes with quinolinolate derivatives (Table IV-2).[6,14] These reported quinolinolato complexes have electron-withdrawing group at 5- or 7-position and the shorter bond distance in **19** would be due to absence of electron-withdrawing group on the quinoline ring. The Re1–O1 distance (1.678(3) Å) is typical of the oxorhenium(V) complexes and the Re1–N1 distance (2.175(4) Å) is within the normal Re–N (heterocyclic) bond for oxorhenium(V) complexes (2.11–2.17 Å).[6,7,14,22-25] The Re1–Cl2 distance *trans* to the PPh_3 is 0.04 Å longer than the Re1–Cl1 distance *trans* to the quinoline nitrogen. This seems to be due to the *trans* influence of the phosphorous, as observed in the corresponding quinolinylamido complex **1** and other oxorhenium(V) complexes with phosphine ligands.[6,26,27] Although the Re1–P1 distance (2.486(1) Å) in **19** is 0.03 Å longer than that in **1** (2.455(1) Å), and this bond in **19** seems to be weaker than that in **1**, **19** did not show the releasing property. It may not be necessarily appropriate to suggest that the reactivity in solution corresponds to the bond strength in solid.

The O1–Re1–O2 angle (162.3(2)°) deviates from 180° for an ideal octahedral structure (Table IV-2). The principal distortions are the result of the bite angle of the didentate-*N*,*O* ligand (O2–Re1–N1; 76.6(1)°). The Re=O linkage significantly expands the angles to the equatorial ligands; the Cl1–Re1–O1, Cl2–Re1–O1, P1–Re1–O1, and N1–Re1–O1 angles are larger than the Cl1–Re1–O2, Cl2–Re1–O2, P1–Re1–O2, and N1–Re1–O2 angles, respectively. As a result, rhenium is displaced 0.1929(9) Å form the mean equatorial plane (N1, P1, Cl1, and Cl2).

The dihedral angle between the quinoline ring and one of the phenyl rings (13.2(2)°) means that the quinoline plate is nearly parallel to the phenyl, which is made from C11–C16. The distance between two planes is 3.473(9) Å. However, the O2–Re1–P1–C11 (86.1(2)°) and N1–Re1–P1–C11 (10.0(2)°) torsion angles are significantly different from the corresponding torsion angles (59.1(4) to 60.3(8)° and -14.4(3) to -15.8(4)°, respectively) in the reported analogous complexes.[14] This means that the C11–C16 phenyl ring position in **19** is not just above the quinoline ring, but it is over between the methyl group C10 and the edge of the quinoline ring C1 different from the reported analogous complexes whose phenyl ring is just above the quinoline ring.[14] The similar intramolecular CH–π stacking interaction between two planes was observed in the corresponding quinolinylamido complex **1** (interplane distance = 3.67(1) Å, dihedral angle = 22.7(2)°). Therefore, the difference in the intramolecular stacking style between **19** and the reported analogous complexes can be attributed to the presence of a substitution group. The crystal packing of **19** shows the intermolecular π–π stacking interaction (3.441(9) Å) between neighboring hetero ring parts (N1–C1–C2–C3–C4–C9) of the quinoline rings (Figure IV-2). Though the $C_6H_5CH_3$ molecular is also incorporated in the crystal packing, it does not participate in any intermolecular interactions.

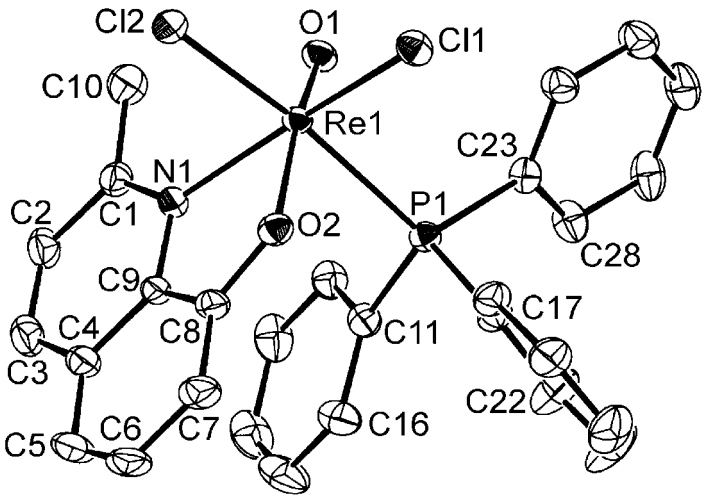

Figure IV-1 An ORTEP view of $[ReOCl_2(hmq)(PPh_3)]$ **19** with numbering scheme. Hydrogen atoms have been omitted for clarity.

Table IV-2 Selected bond distances (Å) and angles (°) for $[ReOCl_2(hmq)(PPh_3)]$ **19**

Re1–O1	1.678(3)	Re1–O2	1.969(3)
Re1–N1	2.175(4)	Re1–P1	2.486(1)
Re1–Cl1	2.341(1)	Re1–Cl2	2.380(1)
O1–Re1–N1	93.0(1)	O2–Re1–N1	76.6(1)
O1–Re1–P1	84.9(1)	O2–Re1–P1	81.2(1)
O1–Re1–Cl1	101.1(1)	O2–Re1–Cl1	90.5(1)
O1–Re1–Cl2	103.4(1)	O2–Re1–Cl2	90.4(1)
O1–Re1–O2	162.3(2)	N1–Re1–Cl1	165.6(1)
P1–Re1–Cl2	171.54(5)	N1–Re1–P1	92.0(1)
N1–Re1–Cl2	86.1(1)	P1–Re1–Cl1	92.45(4)
Cl1–Re1–Cl2	87.50(5)	Re1–O2–C8	119.4(3)

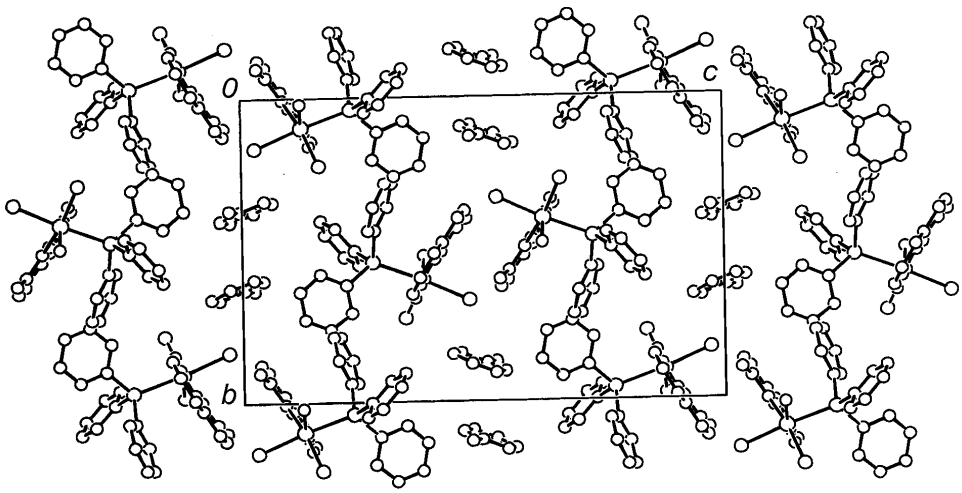

Figure IV-2 Projection of crystal packing for $[ReOCl_2(hmq)(PPh_3)]\cdot C_6H_5CH_3$ **19**$\cdot C_6H_5CH_3$.

[ReOCl(hmq)$_2$] 20 An X-ray crystal analysis for **20** revealed the presence of only a complex molecule, differing from that for **19**. A perspective drawing of the complex molecule **19** is shown in Figure IV-3 and its selected bond distances and angles are listed in Table IV-3. The coordination geometry around rhenium atom is distorted octahedral with the oxo ligand, two nitrogen and oxygen atoms from two asymmetrical didentate-*N*,*O* ligands, and one chloride ion. The oxo ligand and one phenolate oxygen atom O2 lie the *trans* position (axial direction), whereas the heterocyclic nitrogen atom N1, which is another moiety of the vertical hmq ligand, a nitrogen atom N2 and a oxygen atom O3 in another horizontal hmq ligand, and a chloride ion Cl1 occupy the equatorial plane. The *trans* position of the heterocyclic nitrogen atom N1 in the vertical hmq is occupied with phenolate oxygen atom O3 in horizontal hmq ligand and the *trans* position of the heterocyclic nitrogen atom N2 in the horizontal hmq is occupied with a chloride ion Cl1. This coordination geometry is the same as the two quinolinolate derivatives coordinated complex [ReO(OMe)(5-NH$_2$-8-hq)(5-NO$_2$-8-hq)],[6] whereas the coordination geometry of **20** is different from the case of similar two didentate-*N*,*O* ligands coordinated complex [ReOX(hoz)$_2$] (hoz; 2-(2'-hydroxyphenyl)-2-oxazoline, X = Cl, Br).[8,28] In the case of these reported complexes, the oxo ligand and one phenolate oxygen atom in the vertical hoz lie in the *trans* position similarly to **20**, on the contrary, the *trans* position of the heterocyclic nitrogen atom in the vertical hoz is occupied with heterocyclic nitrogen atom in the horizontal hoz. Though the correct reason of this difference is not clear, there are some differences between **20** and the hoz coordinated complexes. For example, the chelate ring sizes are different (the five membered ring in **20**, the six membered ring in hoz coordinated complexes) and Re–N distances (2.098(5)–2.045(5) Å) in the hoz coordinated complexes are shorter than the Re–N (heterocyclic) distances (2.10–2.17 Å) in the five membered ring of ligand containing oxorhenium(V) complexes.[6,7,14,22-25]

The Re–O (phenolate) distance (Re1–O2, 2.012(2) Å) in the *trans* position of the oxo ligand is longer than that in equatorial plane (Re1–O3, 1.969(3) Å) (Table IV-3). This longer Re1–O2 distance is consistent with the *trans* influence of the Re=O linkage. The same tendency was observed in the two quinolinolate derivatives coordinated complex [ReO(OMe)(5-NH$_2$-8-hq)(5-NO$_2$-8-hq)] (Re–O$_{ax}$, 2.077(6) Å; Re–O$_{eq}$, 1.975(5) Å).[6] The Re1–O1 distance (1.680(3) Å) is typical of the oxorhenium(V) complexes and the Re–N distances (2.192(3) and 2.168(3) Å) are also typical of Re–N (heterocyclic) bond.

The O1–Re1–O2 angle (163.6(1)°) deviates from 180° for an ideal octahedral structure (Table IV-3). The principal distortions are the result of the bite angles of the didentate-*N*,*O* ligands (O2–Re1–N1 = 76.2(1), O3–Re1–N2 = 80.3(1)°). The ligand donor atoms on equatorial plane are bent away from the

oxo ligand; the Cl1−Re1−O1, O3−Re1−O1, N1−Re1−O1, and N2−Re1−O1 angles are larger than the Cl1−Re1−O2, O3−Re1−O2, N1−Re1−O2, and N2−Re1−O2 angles, respectively. As a result, rhenium is displaced 0.226(1) Å form the mean equatorial plane (O3, N1, N2, and Cl1). Different from **19**, in two hmq coordinated complex **20**, the intramolecular interaction is not observed. The crystal packing of **20** showed two intermolecular interactions, which were the vertical quinoline ring−vertical quinoline ring (3.425(6) Å) and the horizontal quinoline ring−holizontal quinoline ring (3.532(6) Å) intermolecular π−π stacking interaction (Figure IV-4).

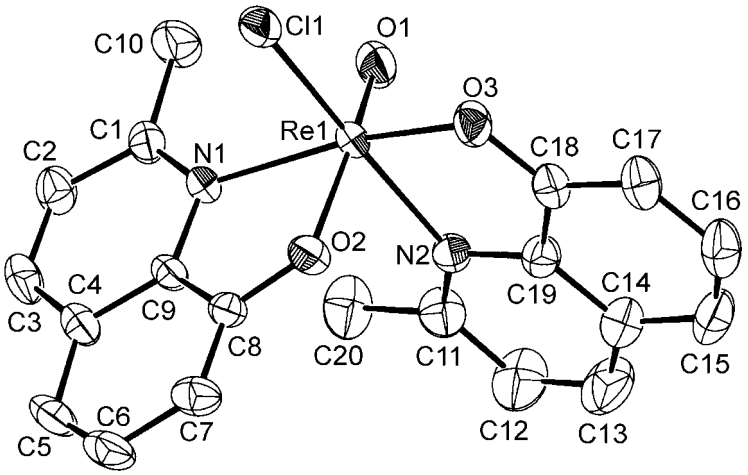

Figure IV-3 An ORTEP view of $[ReOCl(hmq)_2]$ **20** with numbering scheme. Hydrogen atoms have been omitted for clarity.

Table IV-3 Selected bond distances (Å) and angles (°) for $[ReOCl(hmq)_2]$ **20**

Re1−O1	1.680(3)	Re1−O2	2.012(2)
Re1−O3	1.969(3)	Re1−N1	2.192(3)
Re1−N2	2.168(3)	Re1−Cl1	2.364(1)
O1−Re1−O3	105.2(1)	O2−Re1−O3	87.5(1)
O1−Re1−N1	91.6(1)	O2−Re1−N1	76.2(1)
O1−Re1−N2	89.5(1)	O2−Re1−N2	82.4(1)
O1−Re1−Cl1	100.0(1)	O2−Re1−Cl1	90.08(7)
O1−Re1−O2	163.6(1)	O3−Re1−N1	163.2(1)
N2−Re1−Cl1	167.85(9)	O3−Re1−N2	80.3(1)
O3−Re1−Cl1	89.90(8)	N1−Re1−N2	101.2(1)
N1−Re1−Cl1	86.14(8)		

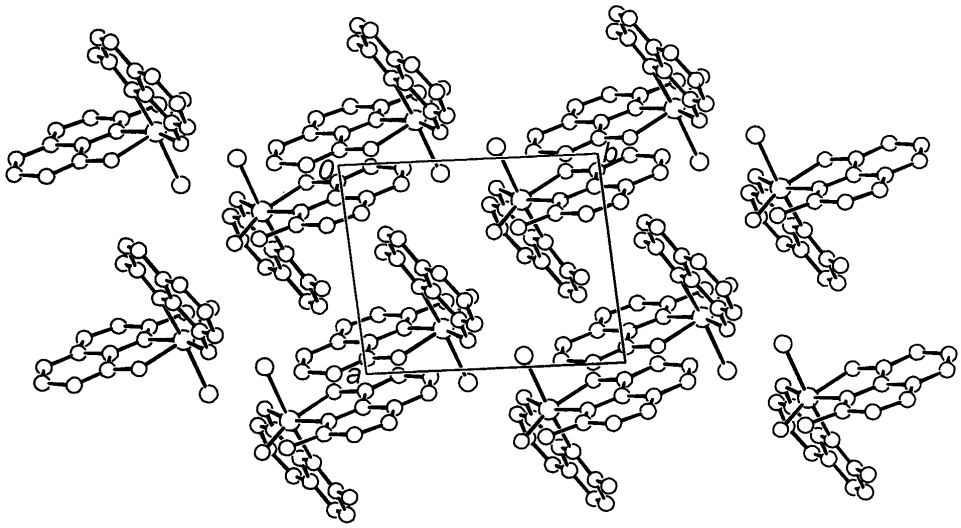

Figure IV-4 Projection of crystal packing for [ReOCl(hmq)$_2$] **20**.

IV-v. Properties

IR and far-IR Spectra Table IV-4 shows IR, far-IR, electronic absorption, diffuse reflectance (DR), and ^{31}P NMR spectral data for the present quinolinolato complexes **19** and **20**, and together with the reported complexes [ReOCl$_2$(5-X-7-Y-8-hq)(PPh$_3$)]. The IR spectra of **19** and **20** are shown in Figure IV-5. **19** and the corresponding complexes [ReOCl$_2$(5-X-7-Y-8-hq)(PPh$_3$)] showed similar IR spectral pattern to each other. The red shift of the strong IR band assigned to Re=O bond was observed in **19** (967 cm^{-1}) in comparison with [ReOCl$_2$(5-X-7-Y-8-hq)(PPh$_3$)] (976–981 cm^{-1}) (Table IV-4). This red shift may be due to the difference in the electrophilic effect of the substituent groups on the quinoline ring. The Re=O band in **20** (969 cm^{-1}) also appeared in the normal region for oxorhenium(V) complexes and similar to the Re=O band in the analogous bisquinolinolato complex [ReOCl(hq)$_2$][13] (967 cm^{-1}) and the two quinolinolate derivatives coordinated complex [ReO(OMe)(5-NH$_2$-8-hq)-(5-NO$_2$-8-hq)][6] (963 cm^{-1}). In Figure IV-5, in the region of over 3100 cm^{-1}, a characteristic N–H band observed in the quinolinylamido complexes is naturally disappeared in **19** and **20** (Table IV-4).

In the far-IR spectra (Figure IV-6, Table IV-4), the Re–Cl stretching vibration bands in **19** are observed as two strong bands (330 and 290 cm^{-1}). This result is in agreement with the results observed in the corresponding quinolinylamido complexes (Chapter II). The red shift which may be due to the electrophilic effect was observed again in the Re–Cl bands (**19** (330 and 290 cm^{-1}) < [ReOCl$_2$(5-X-7-Y-8-hq)(PPh$_3$)] (345–347 and 296–312 cm^{-1})).[6,14] On the other hand, the band in **20** is

observed as only one band (318 cm^{-1}) similar to the case of analogous bisquinolinolato complex $[ReOCl(hq)_2]$ (308 cm^{-1}).[13] These results support the X-ray analyses results, namely, in **19** which has two Re–Cl bonds, two Re–Cl bands were observed and in **20** which has only one Re–Cl bond, one Re–Cl band were observed.

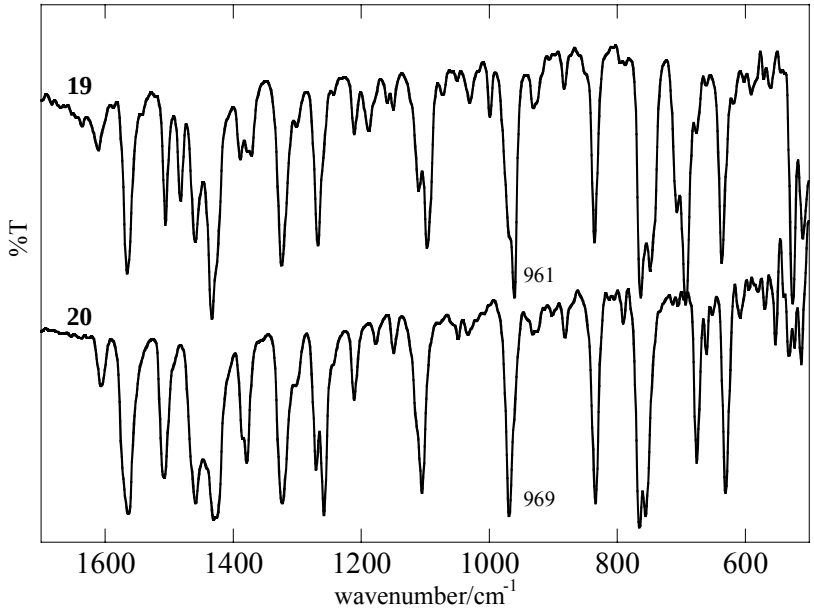

Figure IV-5 IR spectra of $[ReOCl_2(hmq)(PPh_3)]$ **19** and $[ReOCl(hmq)_2]$ **20**.

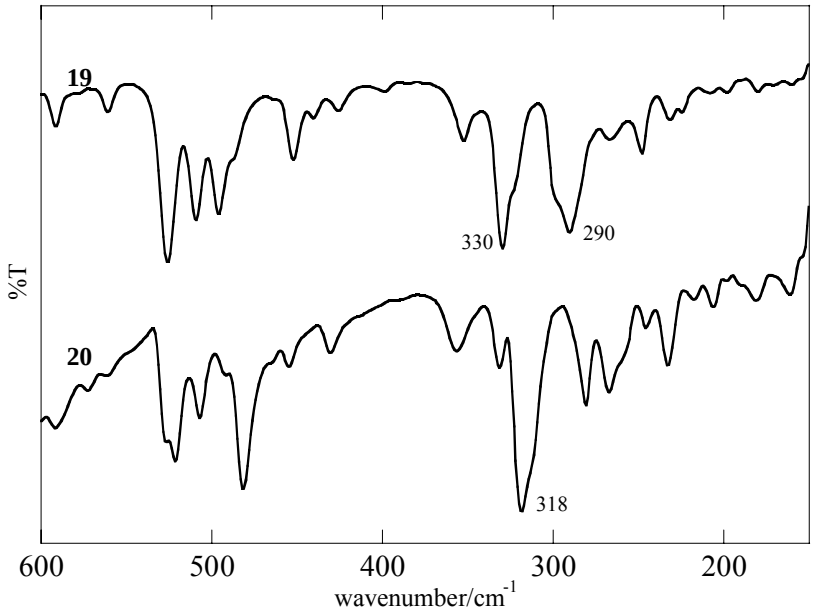

Figure IV-6 Far-IR spectra of $[ReOCl_2(hmq)(PPh_3)]$ **19** and $[ReOCl(hmq)_2]$ **20**.

Table IV-4 Spectrochemical data for $[ReOCl_2(hmq)(PPh_3)]$ **19**, $[ReOCl(hmq)_2]$ **20**, and the corresponding oxorhenium(V) complexes with hydroxyquinoline derivatives

complex	IR (KBr)	far-IR (Nujol)	electronic Abs (CH_2Cl_2)	DR (MgO)	^{31}P-NMR ($CDCl_3$)
	ν/cm^{-1}	ν/cm^{-1}	λ/nm ($\varepsilon/M^{-1}\ cm^{-1}$)	λ/nm	δ/ppm[a]
$[ReOCl_2(hmq)(PPh_3)]$ **19**	961s	330s, 290s	394 (6.7×10^3), 652 (2.9×10^2)	410, 646	-21.0
$[ReOCl(hmq)_2]$ **20**	969s	318s	399 (8.8×10^3), 684 (3.4×10^2)	427, 688, 723	-
$[ReOCl_2(5\text{-Cl-8-hq})(PPh_3)]$[b]	976s	345s, 296s	420 (8.9×10^3), 684(3.9×10^2)	431	-13.6
$[ReOCl_2(5\text{-Cl-7-Cl-8-hq})(PPh_3)]$[b]	981s	347s, 312s	420 (8.3×10^3), 693(3.6×10^2)	431	-14.0
$[ReOCl_2(5\text{-Cl-7-I-8-hq})(PPh_3)]$[b]	981s	347s, 310s	424 (8.1×10^3), 694(3.5×10^2)	433	-14.0
$[ReOCl_2(5\text{-Br-7-Br-8-hq})(PPh_3)]$[b]	981s	347s, 308s	423 (8.8×10^3), 694(3.7×10^2)	431	-14.0

[a] PPh_3 = -7.42 ppm. [b] ref 14.

Electronic Absorption and Diffuse Reflectance Spectra The electronic absorption spectra of complexes **19** and **20** were measured by using CH_2Cl_2 solution. The solid state diffuse reflectance (DR) spectra of **19** and **20** were also measured. The absorption and DR spectral data are summarized in Table IV-4. The absorption spectral pattern of each of the quinolinolato complexes **19** and **20** does not show concentration dependence different from the quinolinylamido complexes (Figures IV-7 and IV-8). The absorption spectral curving patterns of **19** and **20** are similar to those of solid state DR spectra. Therefore, **19** and **20** would keep the six-coordinated state in solution different from the quinolinylamido complexes. These complexes display a relatively weak band around 680 nm (Table IV-4). This band would be due to the ligand field transition ($5d_{xy} \rightarrow d_{yz, zx}$).[25] The shoulder observed in 460 nm in **19** assigned to Cl–Re CT transition is almost disappeared in **20** which has only one chloride ion (Figures IV-7 and IV-8).[16] On the other hand, the absorbance in the region of 320–420 nm, which assigned to other ligands (hmq and PPh_3) to rhenium CT transition, is increased in **20**. In particular, the absorbance around 350 nm in **20** is approximately double of that in **19**. Therefore this absorption may be originated in the quinolinolate ligand to rhenium CT band. This result is in agreement with the change of the number of the didentate ligands.

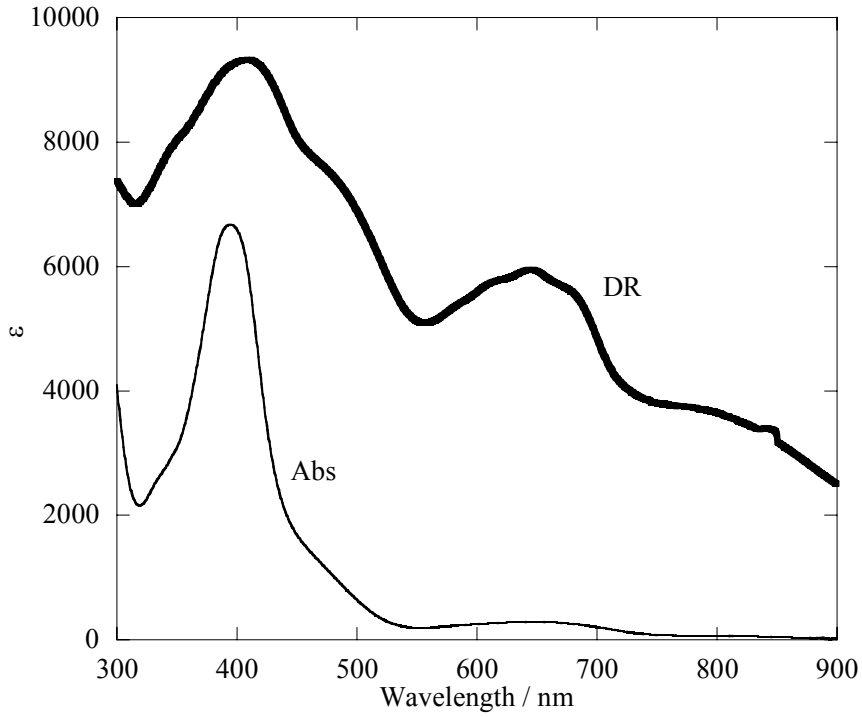

Figure IV-7 Electronic absorption (Abs) spectrum in CH_2Cl_2 and diffuse reflectance (DR) spectrum of $[ReOCl_2(hmq)(PPh_3)]$ **19**.

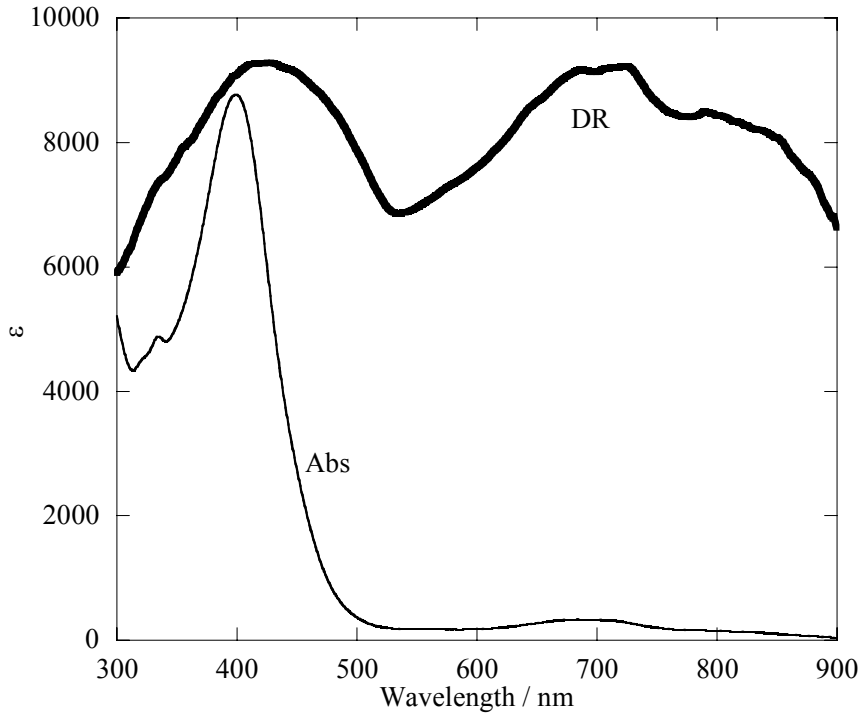

Figure IV-8 Electronic absorption (Abs) supectrum in CH_2Cl_2 and diffuse reflectance (DR) spectrum of [ReOCl(hmq)$_2$] **20**.

^{31}P{^{1}H} NMR Spectra The ^{31}P{^{1}H} NMR spectra of **19** is measured by using PPh_3 as an external reference (δ -7.4) in $CDCl_3$ (Table IV-4). The signal of PPh_3 in **19** (δ -21.0) is shifted from that of free PPh_3 different from the corresponding quinolinylamido complex **1**. This shift is in agreement with the results of the electronic absorption spectra indicating that **19** keeps the six-coordinated state, without releasing the PPh_3, in solution. This chemical shift is significantly different from those (δ -13.6 – -14.0) for the reported complexes [$ReOCl_2$(5-X-7-Y-8-hq)(PPh_3)].[14] This would be caused by the difference in electrophilicity on metal center. That is to say, in the oxorhenium(V) complexes with quinolinolate derivatives containing electron-withdrawing group [$ReOCl_2$(5-X-7-Y-8-hq)(PPh_3)], the electron density of metal center would be lowered, and the chemical shift of PPh_3, coordinated with metal center, would show downfield shift. On the other hand, in **19** containing electron-donating group, methyl, on quinolinolate derivatives, the electron density of metal center would be higher. Consequently, the chemical shift of PPh_3 would show upfield shift.

Cyclic Voltammetry As observed in the spectroscopic measurements, the quinolinolato complexes **19** and **20** are stable in solution. Therefore, the electrochemical property of **19** was

investigated by using a cyclic voltammetric technique. The cyclic voltammetry experiment using CH_3CN solution showed two redox waves at ca. +1 and ca. -1.5 V (vs Fc/Fc^+) for **19** and **20** (Figure IV-9). Their redox potentials with scan rate 100 mV s^{-1} are summarized in Table IV-5.[14] Each of the peaks at ca. +1 V, which are irreversible in **19** and quasi-reversible in **20**, is assigned to the redox process of $Re^{VI/V}$, whereas each of the peaks at ca. -1.5 V, which are irreversible in both complexes, is assigned to the redox process of $Re^{V/VI}$ (Figure IV-9).[14,25] The waves of **19** were observed in relatively negative region (ca. 0.15 V) in comparison with similar complexes $[ReOCl_2(5\text{-X-7-Y-8-hq})(PPh_3)]$ (Table IV-5). The negative shift of redox peaks agrees with the effect of substituent group on the quinoline ring as observed in other spectroscopic measurements. That is to say, in **19** which has electron-donating group on the quinoline ring, the metal center oxidation would be easier and the reduction would be more difficult than the reported complexes $[ReOCl_2(5\text{-X-7-Y-8-hq})(PPh_3)]$ which have electron-withdrawing group on the quinoline ring. Furthermore, the waves of **20** were observed in more negative region (ca. 0.19 V) in comparison with **19** (Table IV-5). It is expected that the shift would arise from the effect of electron-withdrawing or donating of ligands.

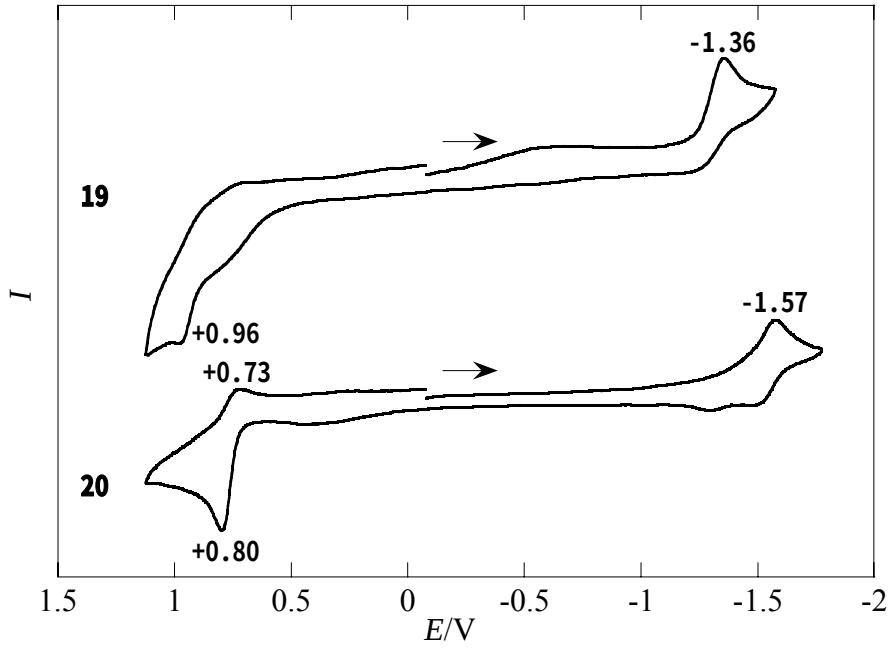

Figure IV-9 Cyclic voltammograms of complexes **19** and **20** in acetonitrile solution (0.1 mol dm^{-3} Bu_4NClO_4) at platinum electrode (*E*/V vs Fc/Fc^+ Scan rate 100 mV s^{-1}).

Table IV-5 Electrochemical data (E/V vs Fc/Fc^+) for oxorhenium complexes with quinolinolate ligands

Complex	$Re^{VI/V}$			$Re^{V/VI}$		
	$E^{\circ\prime}$	E_{pa}	E_{pc}	$E^{\circ\prime}$	E_{pa}	E_{pc}
$[ReOCl_2(hmq)(PPh_3)]$ **19**		+0.96				-1.36
$[ReOCl(hmq)_2]$ **20**	+0.77	+0.80	+0.73			-1.57
$[ReOCl_2(5\text{-Cl-8-hq})(PPh_3)]$[a]		+1.11 shoulder		-1.20	-1.24	-1.15
$[ReOCl_2(5\text{-Cl-7-Cl-8-hq})(PPh_3)]$[a]	+1.10	+1.14	+1.06	-1.15	-1.18	-1.11
$[ReOCl_2(5\text{-Cl-7-I-8-hq})(PPh_3)]$[a]	+1.08	+1.12	+1.03	-1.15	-1.18	-1.11
$[ReOCl_2(5\text{-Br-7-Br-8-hq})(PPh_3)]$[a]	+1.10	+1.14	+1.06	-1.15	-1.18	-1.11

[a] ref 14.

IV-vi Reactivity of 19

The OAT catalytic reactivity of **19** from 2,6-lutidine-*N*-oxide (2,6-Me_2pyO) to PPh_3 in Eq. IV-4 was investigated to compare with the reactivity of the corresponding quinolinylamido complex **1**. It was

$$PPh_3 + 2,6\text{-}Me_2pyO \xrightarrow{\mathbf{19}} OPPh_3 + 2,6\text{-}Me_2py \quad \text{(IV-4)}$$

monitored by ^1H NMR spectra (Figure IV-10) similarly to the case of **1**. As a result of reaction with **19**, it revealed that the OAT catalytic reactivity of **19** is much less than that of **1** which worked only 10 times as catalyst. By considering that **19** keeps the six-coordinated state and does not provide the vacant site for progress the catalytic reaction in solution as revealed in spectroscopic section, this less reactivity is the same as an expected result. It is anticipated that the complexes, which coordinated with hard base ligand and stabilized the six-coordinated state like **19**, are not suitable for catalyst.

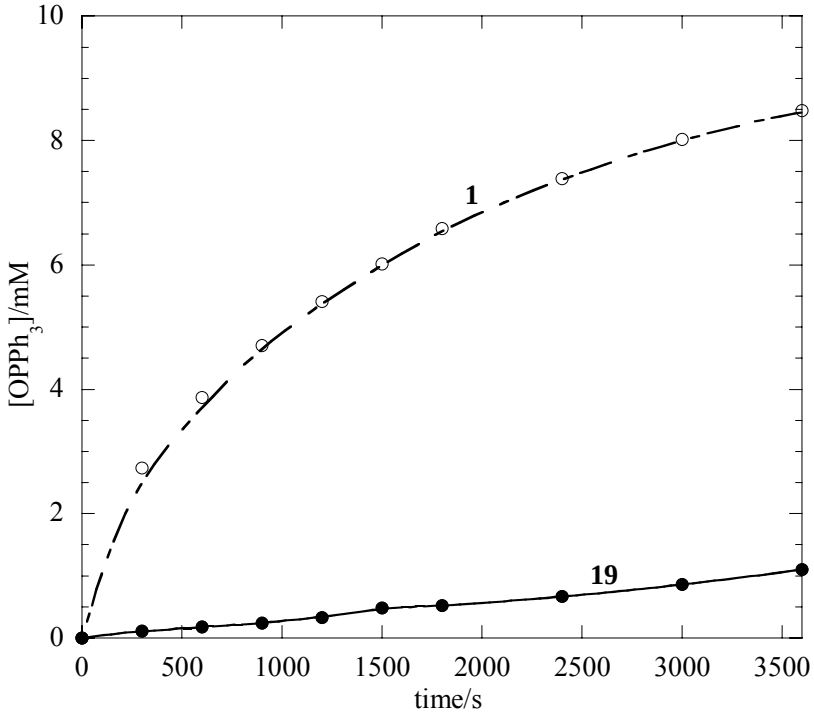

Figure IV-10 OAT catalytic reaction of **1** and **19** in $CDCl_3$: PPh_3 1×10^{-2} mol cm^{-3}: 2,6-Me_2pyO 1×10^{-2} mol cm^{-3}: complex 1×10^{-3} mol cm^{-3} (open circle, **1**; closed circle, **19**).

IV-vii. Conclusion

The reactions of the oxorhenium(V) precursors $[ReOCl_3(PPh_3)_2]$ with the asymmetrical didentate-*N*,*O* ligands 8-hydroxy-2-methylquinoline (Hhmq) in $C_6H_5CH_3$ gave the quinolinylamido complexes $[ReOCl_2(hmq)(PPh_3)]$ **19** or $[ReOCl(hmq)_2]$ **20** depending on the amounts of the Hhmq. These complexes were characterized by X-ray crystal analyses, cyclic voltammetry, and IR, far-IR, electronic absorption, diffuse reflectance, and $^{31}P\{^1H\}$ NMR spectra. The sixth coordination ligand would be tightly bound, because the phenolate oxygen atom of the quinolinolate ligand is hard base ligand and has no multiple bonding character. Therefore, low reactivity in the quinolinolato complex **19** was expected. Actually, the results of spectrochemical analyses showed that these complexes keep the six-coordinated state in solution different from the quinolinylamido complexes. **19** also did not show the substitution reactivity and OAT catalytic reactivity as expected from the results of spectroscopy and the tendency of the hard base ligand coordinated oxorhenium(V) complexes.

References

1 B. S. Lim, M. W. Willer, M. Miao, and R. H. Holm, *J. Am. Chem. Soc.*, **123**, 8343 (2001).

2 B. S. Lim, J. P. Donahue, and R. H. Holm, *Inorg. Chem.*, **39**, 263 (2000).

3 C. A. Goddard and R. H. Holm, *Inorg. Chem.*, **38**, 5389 (1999).

4 K. Kandasamy, H. B. Singh, R. J. Butcher, and J. P. Jasinski, *Inorg. Chem.*, **43**, 5704 (2004).

5 J. J. A. Cooney, M. D. Carducci, A. E. McElhaney, H. D. Selby, and J. H. Enemark, *Inorg. Chem.*, **41**, 7086 (2002).

6 X. Chen, F. J. Femia, J. W. Babich, and J. Zubieta, *Inorg. Chim. Acta*, **308**, 80 (2000).

7 J. M. Botha, K. Umakoshi, Y. Sasaki, and G. J. Lamprecht, *Inorg. Chem.*, **37**, 1609 (1998).

8 E. Shuter, H. R. Hoveyda, V. Karunaratne, S. J. Rettig, and C. Orvig, *Inorg. Chem.*, **35**, 368 (1996).

9 J. Jacob, I. A. Guzei, and J. H. Espenson, *Inorg. Chem.*, **38**, 1040 (1999).

10 X. Shan, A. Ellern, I. A. Guzei, and J. H. Espenson, *Inorg. Chem.*, **43**, 3854 (2004).

11 Y. Cai, A. Ellern, and J. H. Espenson, *Inorg. Chem.*, **44**, 2560 (2005).

12 P. Bouziotis, D. Papagiannopoulou, I. Pirmettis, M. Pelecanou, C. P. Raptopoulou, C. I. Stassinopoulou, A. Terzis, M. Friebe, H. Spies, M. Papadopoulos, and E. Chiotellis, *Inorg. Chim. Acta*, **320**, 174 (2001).

13 T. I. A. Gerber, J. Bruwer, G. Bandoli, J. Perils, and J. G. H. du Preez, *J. Chem. Soc., Dalton Trans.*, 2189 (1995).

14 A. Imai, Master Thesis, University of Tsukuba (2004).

15 N. P. Johnson, C. J. L. Lock, and G. Wilkinson, *Inorg. Synth.*, **9**, 145 (1967).

16 F. Refosco, F. Tisato, G. Bandoli, C. Bolzati, A. Moresco, and M. Nicolini, *J. Chem. Soc., Dalton Trans.*, 605 (1993).

17 CrystalCrear, J. W. Pflugrath, *Acta Crystallogr., Sect. D*, **55**, 1718 (1999).

18 A. Altomare, M. Burla, M. Camalli, G. Cascarano, C. Giacovazzo, A. Guagliardi, A. Moliterni, G. Polidori, and R. Spagna, *J. Appl. Crystallogr.*, **32**, 115 (1999).

19 G. M. Sheldrick, SHELX97 Program for Crystal Structure Refinement from Diffraction Data, University of Göttingen, Göttingen, Germany (1997).

20 P. T. Beurskens, G. Admiraal, G. Beurskens, W. P. Bosman, R. de Gelder, R. Israel, and J. M. M. Smits, The DIRDIF-99 Program System, Technical Report of the Crystallography Laboratory, University of Nijmegen, The Netherlands (1999).

21 CrystalStructure 3.5.1: Crystal Structure Analysis Package, Rigaku and Rigaku/MSC, 2000-2003.

22 S. Bélanger and A. L. Beauchamp, *Inorg. Chem.*, **35**, 7836 (1996).

23 S. Bélanger and A. L. Beauchamp, *Inorg. Chem.*, **36**, 3640 (1997).

24 S. Fortin and A. L. Beauchamp, *Inorg. Chem.*, **39**, 4886 (2000).

25 I. Chakraborty, S. Bhattacharyya, S. Banerjee, B. K. Dirghangi, and A. Chakravorty, *J. Chem. Soc., Dalton Trans.*, 3747 (1999).

26 S. Bhattacharyya, S. Banerjee, B. K. Dirghangi, M. Memon, and A. Chakravorty, *J. Chem. Soc., Dalton Trans.*, 155 (1999).

27 X. Chen, F. J. Femia, J. W. Babich, and J. Zubieta, *Inorg. Chim. Acta*, **306**, 113 (2000).

28 J. Arias, C. R. Newlands, and M. M. Abu-Omar, *Inorg. Chem.*, **40**, 2185 (2001).

Chapter V. Characterization and Reactivity of Oxorhenium(V) Complexes with 8-Quinolinethiolate and Catecholate Derivatives

V-i. Introduction

The influence on the properties of oxorhenium(V) complexes by changing of the substituent groups on 8-position of quinoline derivatives has been described in the previous chapters. In Chapters II and III, the quinolinylamido complexes, whose amide bond has the multiple bonding character, showed the releasing property of the monodentate ligand. This property was in agreement with the tendency that some oxorhenium(V) complexes coordinated with soft base ligand or multiple bonding character ligand prefer the five-coordinated state.[1-4] On the other hand, in Chapter IV, the quinolinolato complex, that the phenol part of quinolinol coordinated as 'hard base' phenolate, did not show the releasing property different from the quinolinylamido complexes. This result is also in agreement with the tendency that the oxorhenium(V) complexes coordinated with hard base ligand prefer the six-coordinated state.[5-7] Furthermore, the quinolinethiolato complex $[ReOCl_2(Sq)(PPh_3)]$ **21** was synthesized by introducing the didentate-*N*,*S* ligand 8-mercaptoquinoline (HSq), whose 8-position had thiol.[8] In oxorhenium(V) complexes coordinated with 'soft base' thiolate, some complexes with the five-coordinated geometry have been reported.[1-4] Therefore, the releasing property of the sixth coordinated ligand was expected for the quinolinethiolato complex **21**, but the high releasing property was not observed such as the quinolinylamido complexes from the results of the electronic absorption spectra and ^{31}P NMR spectra. On the other hand, the $OPPh_3$ substituted complex $[ReOCl_2(Sq)(OPPh_3)]$ **22** was obtained from the long time reaction between **21** and excess of $OPPh_3$. Therefore, it is assumed that **21** has a little releasing property.

In this chapter, the catechol derivatives (tetrachlorocatechol, H_2Cl_4cat; catechol, H_2cat) are introduced in the quinolinethiolato complex **21** for improving the releasing property, and then the quinolinethiolato complexes with catecholate derivatives $[ReO(X_4cat)(Sq)(PPh_3)]$ (X = Cl, **23**; H, **27**) were synthesized (Scheme V-1). Following Chapter III, the ligand exchange reaction of **23** and **27** with $OPPh_3$ and pyridine derivatives (py, 4-Mepy, 4-*t*-Bupy) were attempted. As a result of the substitution reaction, though $OPPh_3$ substituted complexes $[ReO(X_4cat)(Sq)(OPPh_3)]$ (X = Cl, H) were not isolated, the pyridine derivatives substituted complexes $[ReO(Cl_4cat)(Sq)(L)]$ (L = py, **24**; 4-Mepy, **25**; 4-*t*-Bupy, **26**) and [ReO(cat)(Sq)(L)] (L = py, **28**; 4-Mepy, **29**; 4-*t*-Bupy, **30**) were obtained. The structures of these complexes are determined by X-ray crystal analysis and these complexes are

characterized by spectroscopic measurements. In addition, the oxygen atom transfer (OAT) catalytic reactivity and the catalytic cycle of **23** and **27** are investigated.

Scheme V-1

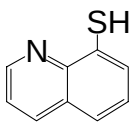

HSq

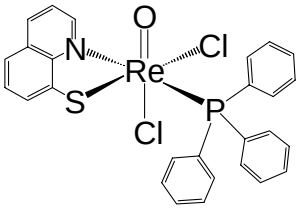

$[ReOCl_2(Sq)(PPh_3)]$ **21**

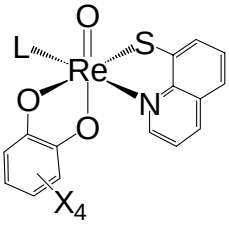

$[ReO(X_4cat)(Sq)(L)]$

X = Cl, L = PPh_3; **23**
X = Cl, L = py; **24**
X = Cl, L = 4-Mepy; **25**
X = Cl, L = 4-*t*-Bupy; **26**
X = H, L = PPh_3; **27**
X = H, L = py; **28**
X = H, L = 4-Mepy; **29**
X = H, L = 4-*t*-Bupy; **30**

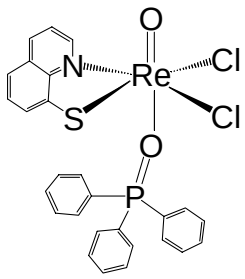

$[ReOCl_2(Sq)(OPPh_3)]$ **22**

V-ii. Experimental

Materials

Rhenium was purchased from Soekawa Chemical Co., Ltd. 8-Mercaptoquinoline hydrochloride (HSq·HCl) and 4-methylpyridine (4-Mepy) were purchased from Tokyo Kasei Kogyo Co., Ltd. Tetrachlorocatechol monohydrate ($H_2Cl_4cat·H_2O$), 4-*t*-buthylpyridine (4-*t*-Bupy), and triphenylphosphine oxide ($OPPh_3$) were purchased from Aldrich Chemical Co., Inc. The other materials were purchased from Wako Pure Chemical Ind., Ltd. All the chemicals were used without further purification. The starting material $[ReOCl_3(PPh_3)_2]$ was prepared according to the literature.[9]

$[ReOCl_2(Sq)(PPh_3)]$ 21. This complex was prepared according to the literature.[8] To a suspension containing $[ReOCl_3(PPh_3)_2]$ (2.03 g, 2.44 mmol) in CH_2Cl_2 (140 cm^3) and $C_6H_5CH_3$ (20 cm^3) was added a solution containing an equimolar HSq·HCl (486 mg, 2.46 mmol). The mixture was stirred for 1.5 h, whereupon the color of the mixture turned from light-green to dark-brown. After

insoluble materials were filtered off, the solution was concentrated to ca. 10 cm^3 by vacuum line. The dark brown powder was collected by filtration and washed with H_2O and $(C_2H_5)_2O$. Yield 1.42 g, 84%. The various data in obtained complex are in agreement with those in the literature.[8]

[$ReOCl_2$(Sq)($OPPh_3$)] 22. To a suspension containing **21** (20 mg, 0.029 mmol) in the mixed solvent of CH_2Cl_2 (15 cm^3) and $C_6H_5CH_3$ (7 cm^3) was added excess of $OPPh_3$ (35 mg, 0.12 mmol) and stirred for 10 min. The dark brown solution was filtered to remove insoluble materials and the filtrate was stood at room temperature to yield the green plate crystals. Yield 17 mg, 83%. The various data in obtained complex are in agreement with those in the literature.[8]

[ReO(Cl_4cat)(Sq)(PPh_3)] 23. To a solution containing $H_2Cl_4cat{\cdot}H_2O$ (82.8 mg, 0.311 mmol) in the mixed solvent of $(CH_3)_2CO$ (40 cm^3) and H_2O (3 cm^3) was added **21** (221 mg, 0.318 mmol). The mixture was stirred for 2 h, whereupon the color of the mixture turned from dark brown to greenish brown suspension. To the greenish brown suspension was added H_2O (10 cm^3), then further greenish brown powder was precipitated. The greenish brown precipitate was collected by filtration and washed with $(CH_3)_2CO/H_2O$ (6/4) mixed solvent. Yield 205 mg, 76%. The precipitate was recrystallized from $CH_2Cl_2/C_6H_5CH_3$ (2/1) to yield the dark green block crystals suitable for X-ray analysis. Anal. Found: C, 45.61; H, 2.49; N, 1.48%. [ReO($C_6Cl_4O_2$)(C_9H_6NS)P(C_6H_5)$_3$] requires C, 45.53; H, 2.43; N, 1.61%. IR (KBr) 946s (Re=O) cm^{-1}. $^{31}P\{^1H\}$ NMR δ -1.7.

[ReO(Cl_4cat)(Sq)(L)] (L = py, 24; 4-Mepy, 25; 4-*t*-Bupy, 26). To a solution containing [ReO(Cl_4cat)(Sq)(PPh_3)] **23** (100 mg, 0.116 mmol) in $C_6H_5CH_3$ (5 cm^3) was added excess of pyridine derivatives L (L = py, 108 mg: 1.36 mmol; 4-Mepy, 112 mg: 1.20 mmol; 4-*t*-Bupy, 154 mg: 1.14 mmol) in $C_6H_5CH_3$ (10 cm^3). The mixture was stirred for 19 h, whereupon the color of the mixture turned from dark green to brownish green suspension. The brownish green precipitate was collected by filtration and washed with H_2O and $(C_2H_5)_2O$. In **26**, the precipitate was recrystallized from $CH_2Cl_2/C_6H_5CH_3$ (2/1) to yield the brownish green plate crystals suitable for X-ray analysis.

Complex **24**; Yield: **24**·0.9 $C_6H_5CH_3$, 68.1 mg, 78%. Anal. Found: C, 41.00; H, 2.30; N, 3.59%. [ReO($C_6Cl_4O_2$)(C_9H_6NS)(C_5H_5N)]·0.9 $C_6H_5CH_3$ requires C, 40.01; H, 2.38; N, 3.64%. IR (KBr) 939s (Re=O) cm^{-1}.

Complex **25**; Yield: **25**, 53.5 mg, 65%. Anal. Found: C, 36.33; H, 1.97; N, 3.96%. [ReO($C_6Cl_4O_2$)(C_9H_6NS)(C_6H_7N)] requires C, 35.96; H, 1.87; N, 3.99%. IR (KBr) 940s (Re=O) cm^{-1}.

Complex **26**; Yield: **26**·$C_6H_5CH_3$, 68.2 mg, 70%. Anal. Found: C, 44.26; H, 3.13; N, 3.33%. $[ReO(C_6Cl_4O_2)(C_9H_6NS)(C_9H_{13}N)]\cdot C_6H_5CH_3$ requires C, 44.56; H, 3.26; N, 3.35%. IR (KBr) 948s (Re=O) cm^{-1}.

[ReO(cat)(Sq)(PPh_3)] 27. To a solution containing H_2cat (39.9 mg, 0.308 mmol) in the mixed solvent of $(CH_3)_2CO$ (40 cm^3) and H_2O (4 cm^3) was added **21** (202 mg, 0.290 mmol). The mixture was stirred for 1.5 h. After insoluble materials were filtered off, the filtrate was concentrated to 5 cm^3 under vacuum. The resulting dark brown precipitate was collected by filtration and washed with H_2O and $(CH_3)_2CO$. Yield 146 mg, 69%. Anal. Found: C, 53.93; H, 3.44; N, 1.89%. $[ReO(C_6H_4O_2)(C_9H_6NS)P(C_6H_5)_3]$ requires C, 54.09; H, 3.44; N, 1.91%. IR (KBr) 930s (Re=O) cm^{-1}. $^{31}P\{^1H\}$ NMR δ -0.1.

[ReO(cat)(Sq)(L)] (L = py, 28; 4-Mepy, 29; 4-*t*-Bupy, 30). To a solution containing [ReO(cat)(Sq)(PPh_3)] **27** (100 mg, 0.136 mmol) in $C_6H_5CH_3$ (7 cm^3) was added excess of pyridine derivatives L (L = py, 105 mg: 1.32 mmol; 4-Mepy, 128 mg: 1.37 mmol; 4-*t*-Bupy, 183 mg: 1.35 mmol) in $C_6H_5CH_3$ (8 cm^3). The mixture was stirred for 1 d, whereupon the color of the mixture turned from dark brown to brown suspension. The brown precipitate was collected by filtration and washed with H_2O and $(C_2H_5)_2O$. In **29**, the precipitate was recrystallized from $CH_2Cl_2/C_6H_5CH_3$ (2/1) to yield the brownish green plate crystals suitable for X-ray analysis.

Complex **28**; Yield: **28**, 54.2 mg, 74%. Anal. Found: C, 43.81; H, 2.68; N, 4.88%. $[ReO(C_6H_4O_2)(C_9H_6NS)(C_5H_5N)]$ requires C, 43.71; H, 2.76; N, 5.10%. IR (KBr) 943vs (Re=O) cm^{-1}.

Complex **29**; Yield: **29**, 65.1 mg, 84%. Anal. Found: C, 50.95; H, 3.78; N, 4.11%. $[ReO(C_6H_4O_2)(C_9H_6NS)(C_6H_7N)]\cdot C_6H_5CH_3$ requires C, 51.28; H, 3.84; N, 4.27%. IR (KBr) 941vs (Re=O) cm^{-1}.

Complex **30**; Yield: **30**, 56.7 mg, 68%. Anal. Found: C, 47.36; H, 3.63; N, 4.58%. $[ReO(C_6H_4O_2)(C_9H_6NS)(C_9H_{13}N)]$ requires C, 47.59; H, 3.83; N, 4.62%. IR (KBr) 950s (Re=O) cm^{-1}.

Measurements

Elemental analyses (C, H, N) were performed by Department of Chemistry of the University of Tsukuba. IR spectra were recorded as KBr pellets on a JASCO FT/IR-550 spectrometer in the range of 4000–400 cm^{-1} and far-IR spectra were recorded as Nujol mull method in the range of 650–50 cm^{-1} at

room temperature. The electronic absorption spectra were recorded with a JASCO V-560 spectrophotometer or a JASCO CT-10TP multichannel spectrophotometer. The diffuse reflectance spectra were recorded on a JASCO V-570 spectrophotometer equipped with an integrating sphere apparatus (JASCO ISN-470). The $^{31}P\{^{1}H\}$ NMR spectra were obtained on a BRUKER AVANCE 600 spectrometer or BRUKER AVANCE 500 spectrometer with PPh_3 as an external reference respectively (in $CDCl_3$ PPh_3 resonates at δ -7.42 with respect to 85% H_3PO_4 in D_2O).[10]

Crystallography

Single crystals of **23**, **26**, and **29** were used for data collection on a Rigaku Mercury CCD area detector with graphite-monochromatized MoKα (0.71069 Å) radiation. The intensity data were collected to a maximum 2θ value of 55° at 296 K. An empirical absorption correction was applied. Data were collected and were processed using CrystalClear.[11] The crystal data and experimental parameters are listed in Table V-1.

The positions of most non-hydrogen atoms of **23** and **29** were determined by direct methods (SIR97[12] in **23** and SHELX97[13] in **29**) and some remaining atoms positions were found by successive difference Fourier techniques.[14] The positions of most non-hydrogen atoms of **26** was determined by heavy-atom Patterson methods (PATTY)[15] and some remaining atoms positions were found by successive difference Fourier techniques.[14] The structures were refined by full-matrix least-squares techniques using anisotropic thermal parameters for non-hydrogen atoms except $C_6H_5CH_3$ part in **26**·$C_6H_5CH_3$. For **23**, **26**, and **29**, all the hydrogen atoms were included in the refinement but constrained to ride on the atoms (C–H = N–H = 0.95 Å, U(H) = 1.2U(C, N)). The calculations on **23**, **26**, and **29** were performed using the CrystalStructure crystallographic software package.[16]

Table V-1 Crystal data and experimental parameters for [ReO(Cl_4cat)(Sq)(PPh_3)] **23**, [ReO(Cl_4cat)(Sq)(4-*t*-Bupy)]·$C_6H_5CH_3$ **26**·$C_6H_5CH_3$, and [ReO(cat)(Sq)(4-Mepy)]·$C_6H_5CH_3$ **29**·$C_6H_5CH_3$

	23	**26**·$C_6H_5CH_3$	**29**·$C_6H_5CH_3$
Formula	$C_{33}H_{21}Cl_4NO_3PSRe$	$C_{31}H_{27}Cl_4N_2O_3SRe$	$C_{28}H_{25}N_2O_3SRe$
Formula weight	870.59	835.64	655.78
Cryst. system	monoclinic	triclinic	triclinic
Space group	*C*2/*c* (No. 15)	*P*-1 (No. 2)	*P*-1 (No. 2)
a, Å	20.9869(9)	9.6970(4)	6.1358(2)
b, Å	16.1987(5)	11.0224(4)	13.4472(2)
c, Å	19.4042(8)	14.9728(5)	16.2922(5)
α, °		87.435(4)	71.969(4)
β, °	105.4225(5)	86.239(4)	88.746(5)
γ, °		83.962(4)	85.484(5)
V, Å^3	6359.1(4)	1586.89(10)	1274.27(6)
Z	8	2	2
D_{calc}, g cm^{-3}	1.819	1.749	1.709
μ (Mo Kα), cm^{-1}	43.12	42.68	48.84
Reflections collected	50406	25646	20478
Unique reflections	7479	7155	5742
R_{int}	0.032	0.021	0.021
Observations ($I > 3.0\sigma(I)$)	5282	6646	5225
Variable parameters	418	363	341
R[a]	0.032	0.033	0.036
R_w[b]	0.081	0.098	0.103
GOF	1.020	1.015	1.003

[a] $R = \Sigma||F_o| - |F_c||/\Sigma|F_o|$. [b] $R_w = [\Sigma w(F_o^2 - F_c^2)^2/\Sigma w(F_o^2)^2]^{1/2}$, where $w = 1/\sigma^2(F_o^2)$.

V-iii. Syntheses

V-iii-i. [ReO(Cl_4cat)(Sq)(L)] (L = PPh_3, **23**; py, **24**; 4-Mepy, **25**; 4-*t*-Bupy, **26**)

The starting complex [$ReOCl_2$(Sq)(PPh_3)] **21** for the quinolinethiolato complexes with catecholate derivatives was obtained from the reaction of [$ReOCl_3(PPh_3)_2$] with 8-mercaptoquinoline hydrochloride (HSq·HCl) referring to the following literature.[8] The coordination geometry of the quinolinethiolato complex **21** in the crystal was different from that of the corresponding quinolinylamido complex **1** or quinolinolato complex **19**, which may be due to the *trans* influence of the thiolate sulfur atom. It is not much, however, in solution, a little releasing property was observed in **21**. Thus, a part of **21** may be able to be the five-coordinated state similarly to **1**. In Chapter III, the difference in the property in solution was observed between the quinolinylamido complexes with catecholate [ReO(cat)(Hamq)(PPh_3)] **13** and tetrachlorocatecholate [ReO(Cl_4cat)(Hamq)(PPh_3)] **14**, namely, the equilibrium constant of the rhenium−monodentate ligand PPh_3 interaction in **13** was much smaller (1/200) than that in **14**. On the other hand, the differences between the quinolinylamido complexes with tetrachlorocatecholate [ReO(Cl_4cat)(Hamq)(PPh_3)] **14** and tetrabromocatecholate [ReO(Br_4cat)(Hamq)(PPh_3)] **15** were small from the viewpoint of the property in solution. Therefore, the non-substituted catechol (H_2cat) and the tetrachlorocatechol (H_2Cl_4cat) were chosen for didentate ligand of the quinolinethiolato complexes.

The quinolinethiolato complex [ReO(Cl_4cat)(Sq)(PPh_3)] **23** corresponding to the quinolinylamido complex with tetrachlorocatecholate [ReO(Cl_4cat)(Hamq)(PPh_3)] **14** was obtained from the reaction of the starting complex **21** with equimolecular amount of tetrachlorocatechol monohydrate in $(CH_3)_2CO$ and H_2O mixed solvent. In **23**, the two chloride ions were substituted with the didentate tetrachlorocatecholate ligand in Eq. V-1 similarly to the quinolinylamido complex **14**, from the results of the various measurements (vide infra). By following the quinolinylamido complexes, the

$$[ReOCl_2(Sq)(PPh_3)]\ \mathbf{21} + H_2Cl_4cat \longrightarrow [ReO(Cl_4cat)(Sq)(PPh_3)]\ \mathbf{23} + 2HCl \quad \text{(V-1)}$$

substitution reactions from PPh_3 to $OPPh_3$ or pyridine derivatives (py, 4-Mepy, 4-*t*-Bupy) were investigated. As a result of the substitution reaction, the $OPPh_3$ substituted complex [ReO(Cl_4cat)(Sq)($OPPh_3$)] was not obtained different from the case of the quinolinylamido complex [ReO(Cl_4cat)(Hamq)($OPPh_3$)] **16**, even if **23** was stirred with excess of $OPPh_3$ (Eq. V-2). On the other

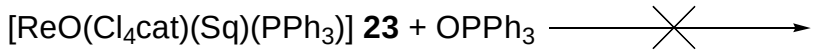

(V-2)

hand, the pyridine derivatives substituted complexes [ReO(Cl_4cat)(Sq)(L)] (L = py, **24**; 4-Mepy, **25**; 4-*t*-Bupy, **26**) were deposited selectively when the mixture of **23** and excess of pyridine derivatives were stirred for a long time in $C_6H_5CH_3$ (Eq. V-3). These pyridine derivatives substituted complexes **24**–**26** were not isolated when the CH_2Cl_2, which has higher solubility of complexes, was used for solvent. Therefore, it is expected that the low solubility of the substituted complexes **24**–**26** for $C_6H_5CH_3$ would be driving force of these substitution reaction.

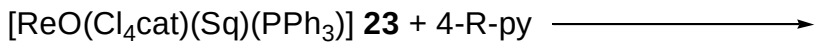

(V-3)

V-iii-ii. [ReO(cat)(Sq)(L)] (L = PPh_3, **27**; py, **28**; 4-Mepy, **29**; 4-*t*-Bupy, **30**)

As in the case of **23**, the quinolinethiolato complex with catecholate [ReO(cat)(Sq)(PPh_3)] **27** was obtained from the reaction of the starting complex **21** with equimolecular amount of catechol (H_2cat) in $(CH_3)_2CO$ and H_2O mixed solvent. In **27**, the two chloride ions were substituted with the didentate catecholate ligand in Eq. V-4 similarly to the corresponding quinolinylamido complex **13** or quinolinethiolato complex **23**. The substitution reactions from PPh_3 to $OPPh_3$ or pyridine derivatives (py, 4-Mepy, 4-*t*-Bupy) were also investigated in **27**. The $OPPh_3$ substituted complex [ReO(cat)(Sq)($OPPh_3$)] was not obtained in analogy with **23** (Eq. V-5), whereas the pyridine derivatives substituted complexes [ReO(cat)(Sq)(L)] (L = py, **28**; 4-Mepy, **29**; 4-*t*-Bupy, **30**) were obtained (Eq. V-6).

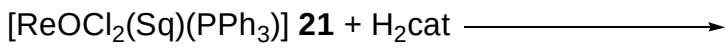

(V-4)

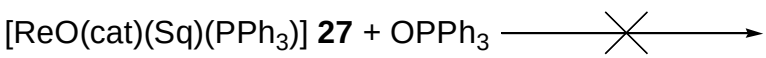

(V-5)

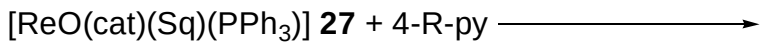

(V-6)

V-iv. Crystal Structures of 23, 26, 29

[ReO(Cl_4cat)(Sq)(PPh_3)] 23 An X-ray crystal analysis for **23** revealed the presence of only a complex molecule. A perspective drawing of the complex molecule **23** is shown in Figure V-1 and its selected bond distances and angles are listed in Table V-2. The coordination geometry around rhenium atom is distorted octahedral with three oxygen atoms of the oxo ligand and the catecholato ligand, one nitrogen atom and one sulfur atom from the quinolinethiolate ligand, and one phosphorus atom from the PPh_3 ligand. Some five-coordinated state complexes were reported in oxorhenium(V) complexes, which have several sulfur atoms as coordination ligand.[4,17] Therefore, there was a possibility that **23** could have the five-coordinated state, though it was the six-coordinated state complex, practically. It is anticipated that the only one sulfur atom in **23** may be not enough to be the five-coordinated state permanently. The coordination geometry of the tetrachlorocatecholato complex **23** keeps that of the precursor complex **21** except that coordination atoms changed from two chloride ions to tetrachlorocatecholate oxygen atoms, and the *trans* position to the oxo ligand is occupied by oxygen atom of catecholato ligand in the same manner as the corresponding quinolinylamido complex [ReO(Cl_4cat)(Hamq)(PPh_3)] **14**. This coordination geometry of **23** follows the tendency of oxorhenium(V) complexes that oxygen atom usually lies in the *trans* position to the oxo ligand.[18-24]

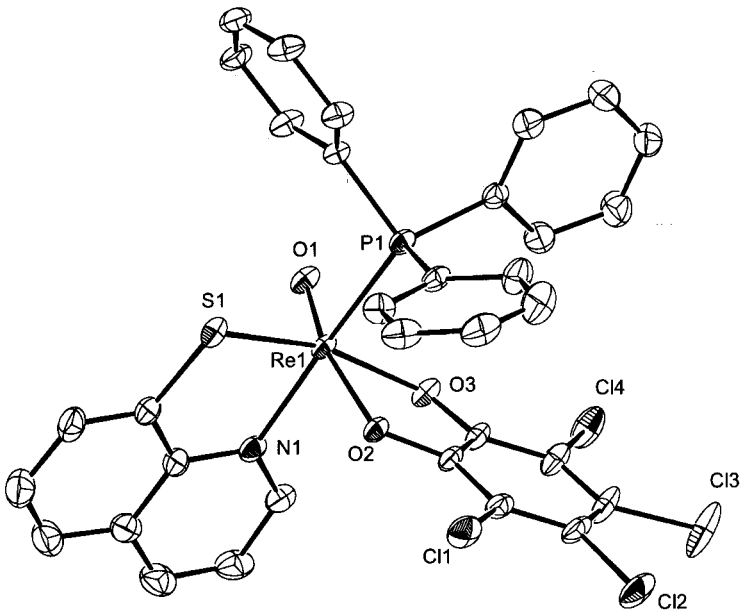

Figure V-1 An ORTEP view of [ReO(Cl_4cat)(Sq)(PPh_3)] **23** with numbering scheme. Hydrogen atoms have been omitted for clarity.

The Re1–O3 bond *trans* to the sulfur atom (2.130(3) Å) is significantly longer than the Re1–O2 bond *trans* to the oxo oxygen (2.012(4) Å) (Table V-2). This difference would be a result of a stronger *trans* influence of the sulfur atom as the analogously to the case of **14**. Indeed, the analogous *trans* influence of the sulfur atom is observed in **21** and **22**.[8] The Re1–O1 distance (1.686(4) Å) is normal as double bonds in the oxorhenium(V) complexes.[6,7,21-31] The Re1–N1 (2.154(4) Å) and Re1–S1 (2.291(1) Å) distances are also within the reported Re–N (heterocyclic) (2.11–2.17 Å)[6,30-33] and Re–S (thiolate) (2.27–2.33 Å)[1,8,34] distances, respectively. The O1–Re1–O2 angle (164.3(2)°) deviates from 180° for an ideal octahedral structure. The principal distortions are the result of the bite angles of the didentate ligands quinolinethiolate (S1–Re1–N1; 82.9(1)°) and catecholate (O2–Re1–O3; 75.9(1)°) (Table V-2). The rhenium atom is located 0.217(2) Å above the equatorial plane formed by one catecholate oxygen, one quinoline nitrogen, one thiolate sulfur, and phosphorus atoms. In this crystal structure (Figure V-2), **23** adopts the conformation that the phenyl rings of PPh_3 avoid the catecholate ring similarly to **14**, and the intramolecular π–π stacking interaction is not observed. On the other hand, in the crystal packing of **23** (Figure V-3), the neighboring a part of the quinoline rings (C4–C5–C6–C7–C8–C9) are overlapped, and the interplane distance is within the range of intermolecular π–π stacking (interplane distance = 3.55(1) Å, dihedral angle = 0.1(2)°).

Table V-2 Selected bond distances (Å) and angles (°) for [ReO(Cl_4cat)(Sq)(PPh_3)] **23**

Re1–O1	1.686(4)	Re1–O2	2.012(4)
Re1–O3	2.130(3)	Re1–S1	2.291(1)
Re1–N1	2.154(4)	Re1–P1	2.466(1)
O1–Re1–O3	89.0(2)	O2–Re1–O3	75.9(1)
O1–Re1–S1	104.2(1)	O2–Re1–S1	91.3(1)
O1–Re1–N1	97.6(2)	O2–Re1–N1	86.2(2)
O1–Re1–P1	91.5(1)	O2–Re1–P1	85.98(9)
O1–Re1–O2	164.3(2)	O3–Re1–S1	164.9(1)
N1–Re1–P1	170.1(1)	O3–Re1–N1	88.3(2)
O3–Re1–P1	95.6(1)	S1–Re1–N1	82.9(1)
S1–Re1–P1	91.24(5)		

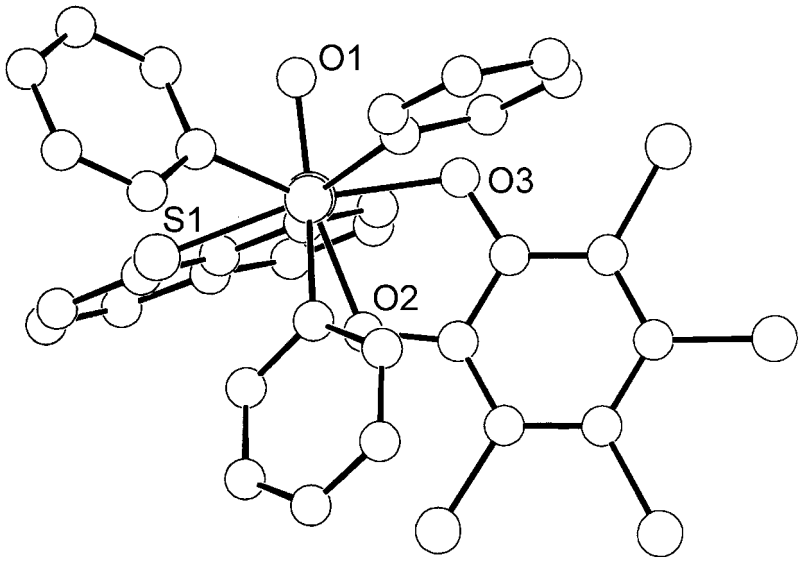

Figure V-2 Crystal structure of [ReO(Cl_4cat)(Sq)(PPh_3)] **23** viewed from P–Re axis.

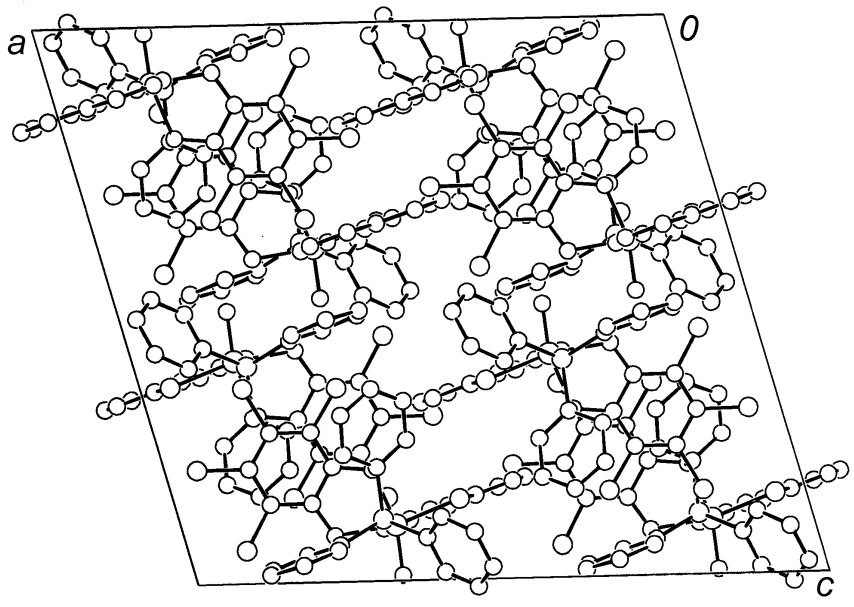

Figure V-3 Projection of crystal packing for [ReO(Cl_4cat)(Sq)(PPh_3)] **23**.

[ReO(Cl$_4$cat)(Sq)(4-*t*-Bupy)] 26 and [ReO(cat)(Sq)(4-Mepy)] 29 The structures of the complexes **26** and **29** were also determined by X-ray crystal analyses. In each case, they revealed the presence of a complex molecule and a $C_6H_5CH_3$ molecule. The perspective view of the complex molecules **26** and **29** are shown in Figures V-4 and V-5, respectively, as well as the selected bond distances and angles are listed in Tables V-3 and V-4. The coordination geometry of **26** and **29** are similar to the corresponding quinolinylamido complexes [ReO(Cl$_4$cat)(Hamq)(4-*t*-Bupy)] **18** and [ReO(Cl$_4$cat)(Hamq)(4-Mepy)] **17**, respectively, except for the change of the coordination atom from amide nitrogen to thiolate sulfur.

All bond distances, except the Re1−O3 distance, and all angles around rhenium atom for **26** and **29** are nearly the same as each other (Tables V-3 and V-4). The Re1−O2 and Re1−O3 distances in **26** (2.012(3) and 2.128(3) Å), which are slightly longer than the distances in **29** (1.999(3) and 2.100(4) Å), may be caused by the substituent effect on the catecholate ligand. Actually, these bond distances in the tetrachlorocatecholato complex **26** are very similar to those in the tetrachlorocatecholato complex **23** (2.012(4) and 2.130(3) Å). The Re1−N1 distances in **26** and **29** are approximately the same as each other (2.117(3) Å) (Tables V-3 and V-4), whereas their distances are 0.04 Å shorter than that in **23** (2.154(4) Å). This difference would arise from the *trans* influence of the PPh_3. The same tendency was observed in the corresponding quinolinylamido complexes **14**, **17**, and **18**. The Re−O1 distances in **26** and **29** (1.687(3) and 1.697(4) Å, respectively) are typical of double bonds in the oxorhenium(V) complexes.[6,7,21-31] The Re1−S1 distances in **26** and **29** are approximately the same as each other (2.303(1) and 2.303(2) Å, respectively). The Re1−S1 distances are similar to that in **23**, and they are also within the reported Re−S (thiolate) distances (2.27−2.33 Å).[1,8,34] The distortions of **26** and **29** are principally the result of the bite angles of the didentate ligands quinolinethiolate (S1−Re1−N1; 83.41(9) and 83.8(1)°, respectively) and catecholate (O2−Re1−O3; 76.8(1) and 76.9(1)°) (Tables V-3 and V-4). As often reported in oxorhenium(V) systems, the displacing away of the equatorial ligands from the Re=O group are also observed in **26** (0.195(1) Å) and **29** (0.246(2) Å). The intramolecular interaction was not observed in **26** and **29** similarly to the corresponding quinolinylamido complexes **17** and **18**. The crystal packing of **26** shows intermolecular π−π stacking interaction between the neighboring quinoline rings (interplane distance = 3.430(6) Å, dihedral angle = 0°) (Figure V-6 (a)). On the other hand, the crystal packing of **29** also shows the pyridine ring−pyridine ring intermolecular π−π stacking interaction (interplane distance = 3.59(1) Å, dihedral angle = 0°) (Figure V-6 (b)). In both case, though the $C_6H_5CH_3$ molecule is also incorporated in the crystal packing, it does not participate in any intermolecular interactions.

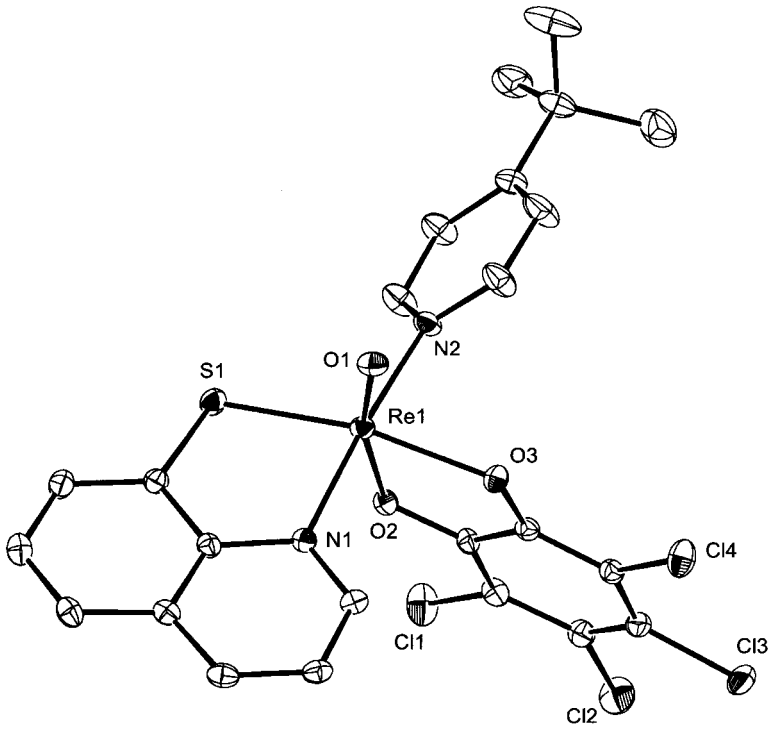

Figure V-4 An ORTEP view of [ReO(Cl_4cat)(Sq)(4-*t*-Bupy)] **26** with numbering scheme. Hydrogen atoms have been omitted for clarity.

Table V-3 Selected bond distances (Å) and angles (°) for [ReO(Cl_4cat)(Sq)(4-*t*-Bupy)] **26**

Re1–O1	1.687(3)	Re1–O2	2.012(3)
Re1–O3	2.128(3)	Re1–S1	2.303(1)
Re1–N1	2.117(3)	Re1–N2	2.158(3)
O1–Re1–O3	89.4(1)	O2–Re1–O3	76.8(1)
O1–Re1–S1	102.8(1)	O2–Re1–S1	91.54(8)
O1–Re1–N1	96.3(1)	O2–Re1–N1	89.8(1)
O1–Re1–N2	89.3(1)	O2–Re1–N2	84.1(1)
O1–Re1–O2	165.0(1)	O3–Re1–S1	166.81(8)
N1–Re1–N2	173.7(1)	O3–Re1–N1	90.3(1)
O3–Re1–N2	86.7(1)	S1–Re1–N1	83.41(9)
S1–Re1–N2	98.4(1)		

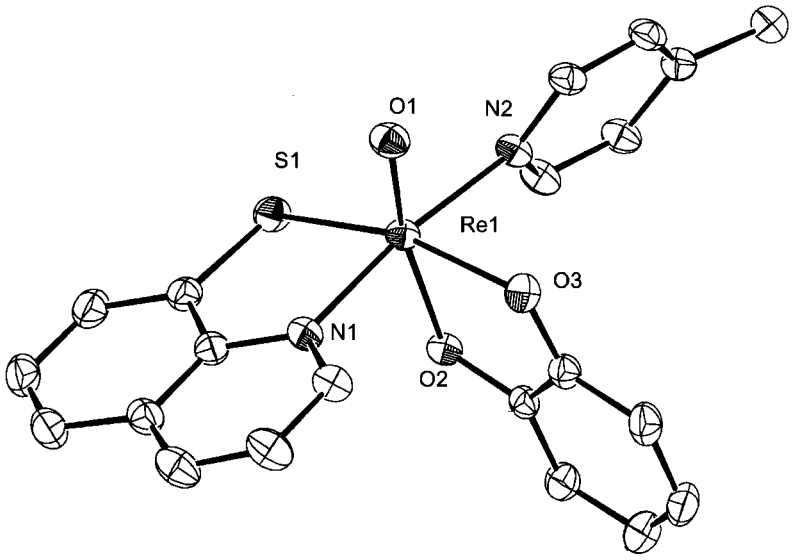

Figure V-5 An ORTEP view of [ReO(cat)(Sq)(4-Mepy)] **29** with numbering scheme. Hydrogen atoms have been omitted for clarity.

Table V-4 Selected bond distances (Å) and angles (°) for [ReO(cat)(Sq)(4-Mepy)] **29**

Re1–O1	1.697(4)	Re1–O2	1.999(3)
Re1–O3	2.100(4)	Re1–S1	2.303(2)
Re1–N1	2.117(5)	Re1–N2	2.160(5)
O1–Re1–O3	91.8(2)	O2–Re1–O3	76.9(1)
O1–Re1–S1	104.2(1)	O2–Re1–S1	87.3(1)
O1–Re1–N1	96.1(2)	O2–Re1–N1	86.9(1)
O1–Re1–N2	90.7(2)	O2–Re1–N2	85.6(1)
O1–Re1–O2	168.4(2)	O3–Re1–S1	163.4(1)
N1–Re1–N2	171.9(1)	O3–Re1–N1	90.2(2)
O3–Re1–N2	85.2(2)	S1–Re1–N1	83.8(1)
S1–Re1–N2	98.8(1)		

(a)

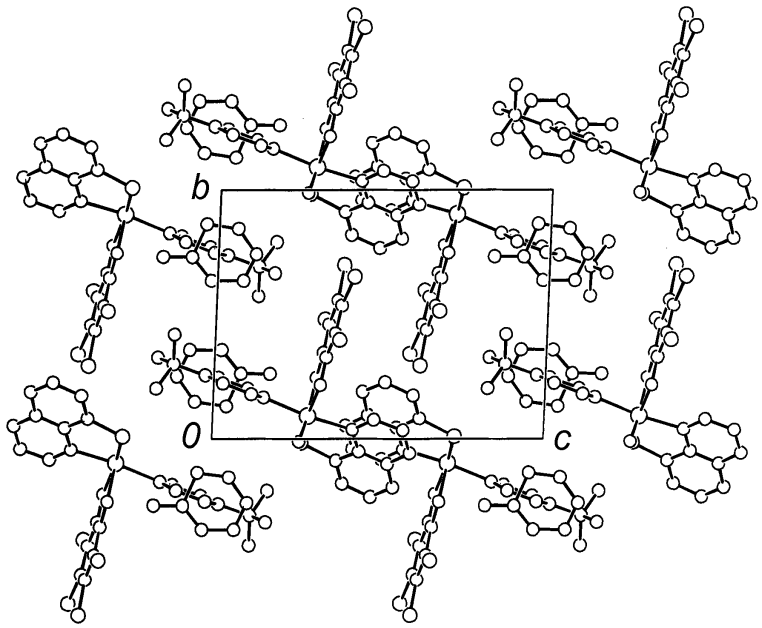

(b)

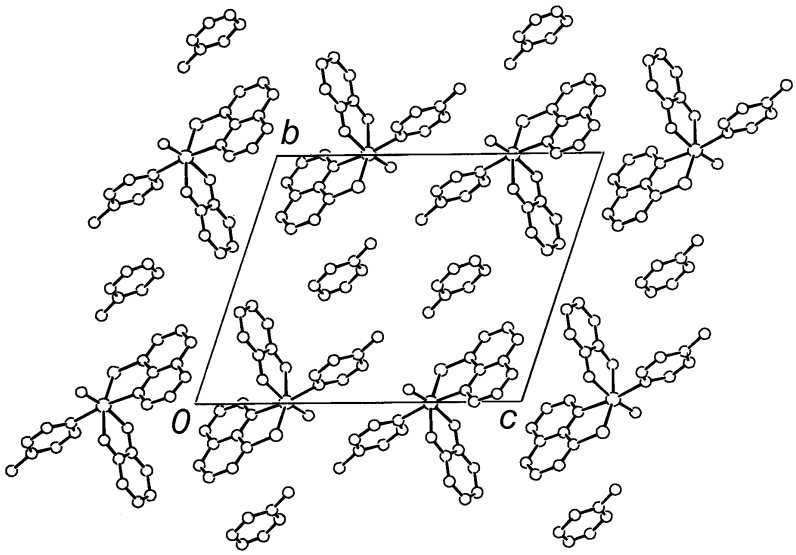

Figure V-6 Projection of crystal packing for [ReO(Cl_4cat)(Sq)(4-*t*-Mepy)]·$C_6H_5CH_3$ **26**·$C_6H_5CH_3$ (a) and [ReO(cat)(Sq)(4-Mepy)]·$C_6H_5CH_3$ **29**·$C_6H_5CH_3$ (b).

V-v. Spectroscopic Properties

IR and far-IR Spectra The IR spectra of the quinolinethiolato complexes with tetrachlorocatecholate series (**23**–**26**) and the quinolinethiolato complexes with catecholate series (**27**–**30**) are shown in Figures V-7 and V-8, respectively. The spectral patterns were similar to each other in each series except the band at ca. 1090 cm^{-1} which arises from PPh_3 (Figures V-7 and V-8). Therefore, the coordination geometry of the complexes, which could not be obtained by the X-ray analysis because of low crystal quality, would be similar to that of the corresponding complexes. That is to say, the coordination geometry of [ReO(Cl_4cat)(Sq)(py)] **24** and [ReO(Cl_4cat)(Sq)(4-Mepy)] **25** are similar to [ReO(Cl_4cat)(Sq)(4-*t*-Bupy)] **26**, and the coordination geometry of [ReO(cat)(Sq)(PPh_3)] **27**, [ReO(cat)(Sq)(py)] **28**, and [ReO(cat)(Sq)(4-*t*-Bupy)] **30** are similar to [ReO(cat)(Sq)(4-Mepy)] **29**. The molecular formulas of the complexes, whose structures were not determined by X-ray analysis, were also supported by elemental analysis. The strong IR bands, which are characteristic of the Re=O stretching vibration, are observed in ca. 940 cm^{-1}. The Re=O band of **23** in Figure V-7, which has electron-withdrawing group on the catecholate ligand, appeared in higher wavenumber than that of **27** in Figure V-8 similarly to the relationship between **14** and **13**. This blue shift may be due to the electrophilic effect of the tetrachlorocatechol ligand.[19] On the other hand, in the pyridine derivatives coordinated series (**24**–**26**, **28**–**30**), the differences of Re=O band as observed in above were not observed. In far-IR spectra, the bands assigned to Re–Cl bond are not observed in the region of ca. 300 cm^{-1}. This result supports the substitution reaction from two chlorine atoms to catechol derivatives.

Electronic Absorption and Diffuse Reflectance Spectra The electronic absorption spectra of complexes **23**–**30** were measured by using CH_2Cl_2 solution in different concentrations (1.0×10^{-3}, 1.0×10^{-4}, and 1.0×10^{-5} mol dm^{-3}). The solid state diffuse reflectance (DR) spectra of complexes **23**–**30** were also measured. The absorption and DR spectral data are summarized in Table V-5. The absorption spectral patterns of **23** in Figure V-9 show little concentration dependence in these concentration conditions different from the corresponding quinolinylamido complex [ReO(Cl_4cat)-(Hamq)(PPh_3)] **14**. As a result of the comparison with the absorption spectral patterns of the other quinolinethiolato complexes (vide infra) and the similarity with the solid state DR spectral pattern in **23**, it is believed that **23** keeps the six-coordinated state approximately in these concentration conditions. The equilibrium constant K of **23** could not be determined because of the measuring limit ($K >> 10^5$ dm^3 mol^{-1}) (Eq. V-7). This was unexpected result because some oxorhenium(V) complexes

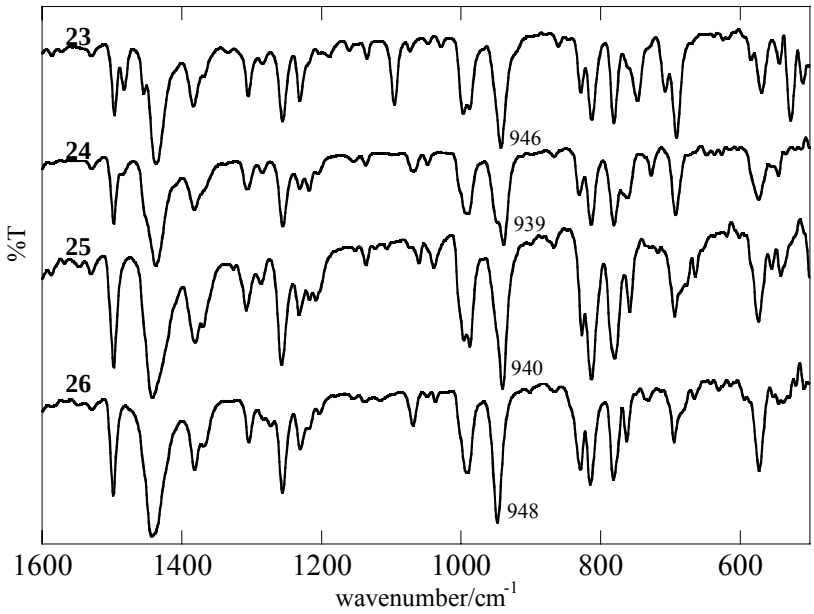

Figure V-7 IR spectra of [ReO(Cl_4cat)(Hamq)(PPh_3)] **23**, [ReO(Cl_4cat)(Hamq)(py)] **24**, [ReO(Cl_4cat)(Hamq)(4-Mepy)] **25**, and [ReO(Cl_4cat)(Hamq)(4-*t*-Bupy)] **26**.

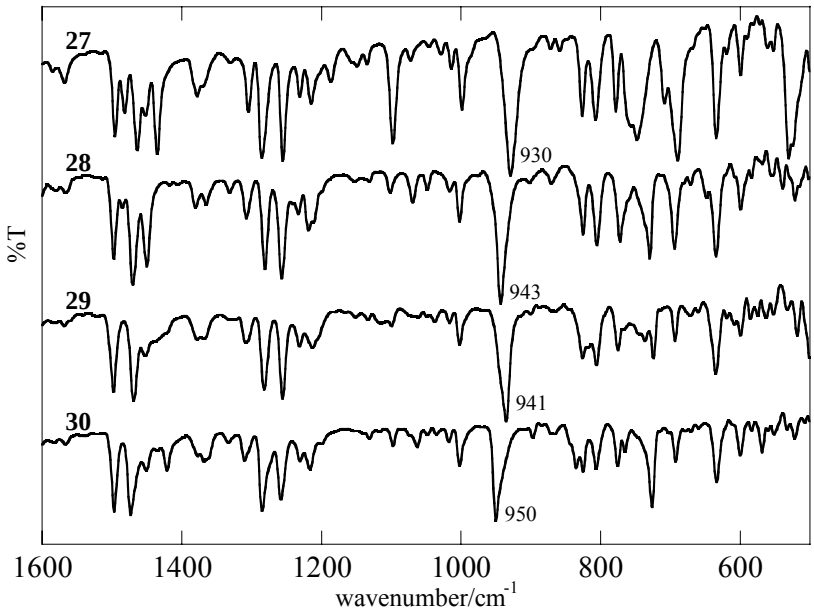

Figure V-8 IR spectra of [ReO(cat)(Hamq)(PPh_3)] **27**, [ReO(cat)(Hamq)(py)] **28**, [ReO(cat)(Hamq)(4-Mepy)] **29**, and [ReO(cat)(Hamq)(4-*t*-Bupy)] **30**.

$$[ReO(X_4cat)(Sq)] + L \underset{}{\overset{K}{\rightleftharpoons}} [ReO(X_4cat)(Sq)(L)]\ (\mathbf{23}–\mathbf{30}) \qquad (V\text{-}7)$$

with soft base ligand such as thiolate were reported as the five-coordination geometry.[17,22,34,35] Thus, it was anticipated that **23** would easily have the five-coordinated state by releasing the monodentate ligand PPh_3 in solution. On the other hand, the spectral patterns of the quinolinethiolato complexes **24**–**26** with tetrachlorocatecholate and pyridine derivatives showed the concentration dependence in the concentration conditions (1.0×10^{-3}–1.0×10^{-5} mol dm^{-3}) (Figures V-10–V-12, respectively). That is to say, the increase of the peak intensity at ca. 370 and ca. 700 nm with increasing the concentration of **24**–**26** was observed (Table V-5). The band observed in ca. 700 nm would be assigned to d–d transition ($5d_{xy} \rightarrow d_{yz, zx}$) and the band observed in ca. 370 nm would be assigned to py–Re LMCT transition from these results.[10,35] The complexes **24**–**26** seem to keep metal center–ligand (pyridine derivatives) bond and the six-coordinated state under higher concentration condition (> 10^{-4} mol dm^{-3}), while they release pyridine derivatives from metal center and changes to the five-coordinated state under lower concentration condition (< 10^{-4} mol dm^{-3}). Though the equilibrium constants *K* of **24**–**26** could not be determined exactly because of the measuring limit, the equilibrium constants *K* of these complexes are estimated ca. 10^6 dm^3 mol^{-1} (Eq. V-7). The equilibrium constants of the complex **14** with PPh_3 ($K = 1.0 \times 10^4$ dm^3 mol^{-1}) and the complexes **17** and **18** with pyridine derivatives ($K = 2.0 \times 10^4$, **17**; 2.4×10^4, **18** dm^3 mol^{-1}) are similar to each other. On the other hand, in the quinolinethiolato complexes with tetrachlorocatecholate series, the equilibrium constant of the complex **23** with PPh_3 ($K >> 10^5$ dm^3 mol^{-1}) is larger than those of the complexes **24**–**26** with pyridine derivatives (ca. 10^6 dm^3 mol^{-1}). The slow substitution reaction in **23** observed in syntheses is probably attributable to the tendency that the equilibrium constants of the complex **23** with PPh_3 is larger than *K* of the complexes **24**–**26** with the pyridine derivatives.

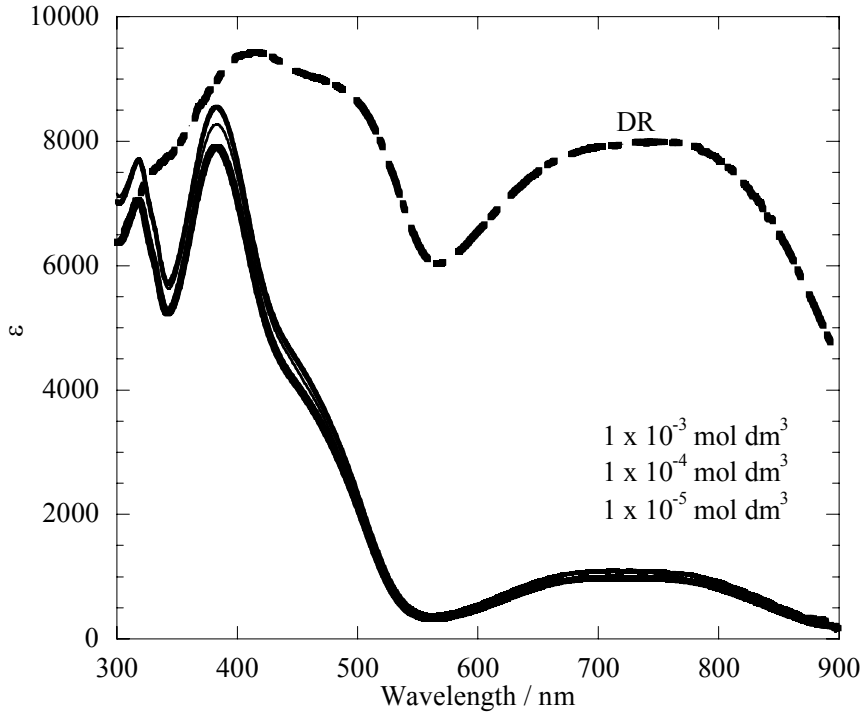

Figure V-9 Electronic absorption spectra of [ReO(Cl_4cat)(Sq)(PPh_3)] **23** in some concentration conditions in CH_2Cl_2.

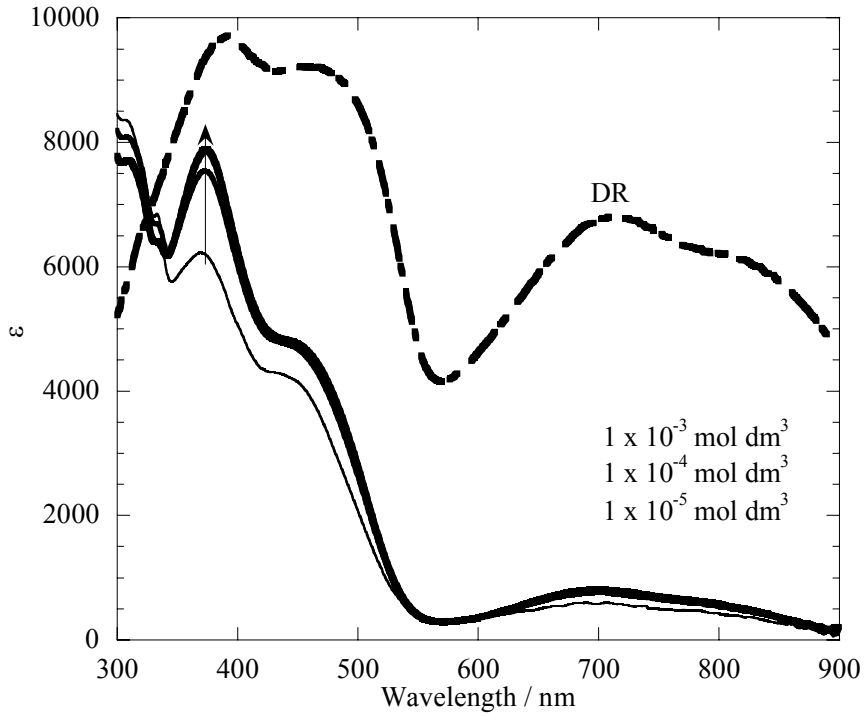

Figure V-10 Electronic absorption spectra of [ReO(Cl_4cat)(Sq)(py)] **24** in some concentration conditions in CH_2Cl_2.

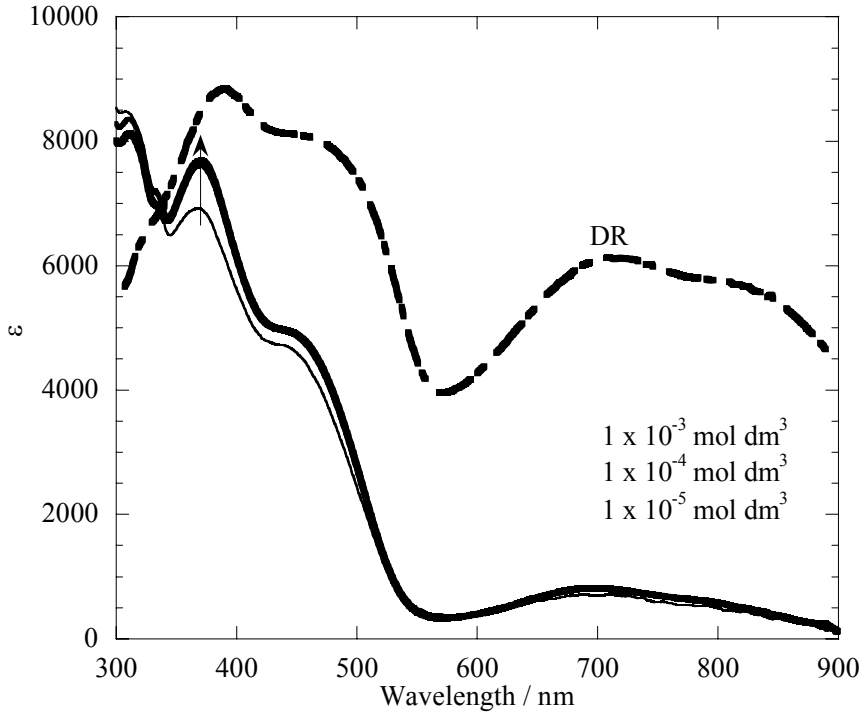

Figure V-11 Electronic absorption spectra of [ReO(Cl_4cat)(Sq)(4-Mepy)] **25** in some concentration conditions in CH_2Cl_2.

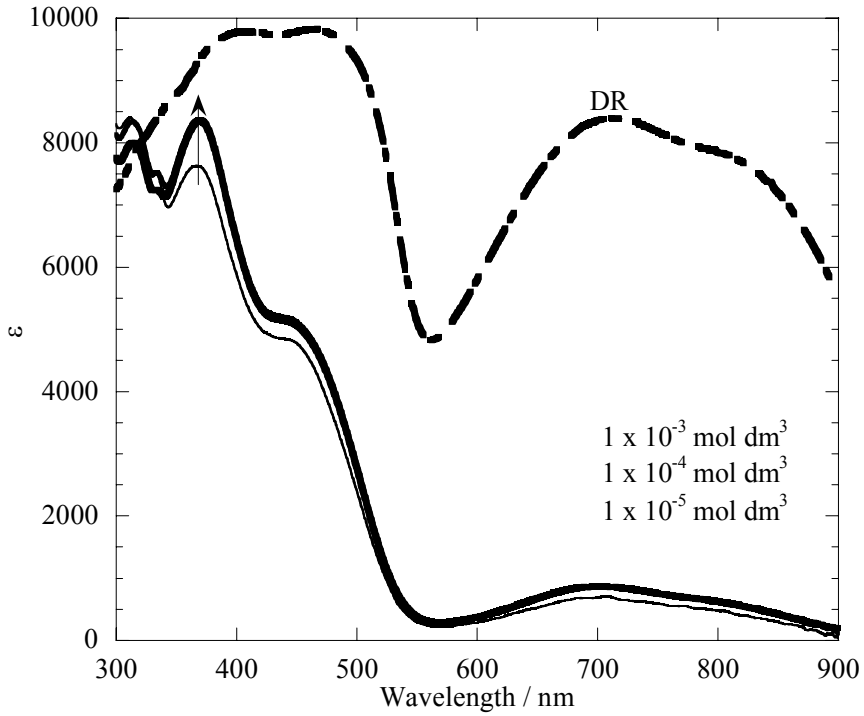

Figure V-12 Electronic absorption spectra of [ReO(Cl_4cat)(Sq)(4-*t*-Bupy)] **25** in some concentration conditions in CH_2Cl_2.

Table V-5 Absorption and reflectance spectral data of **23**–**30**

	Concentration (mol dm^{-3})	Absorption and diffuse reflectance maxima nm (ε/mol^{-1} dm^3 cm^{-1})
23	1.0×10^{-3}	383 (7.9×10^3) 465 (3.6×10^3 sh) 716 (9.8×10^2)
	1.0×10^{-4}	383 (8.6×10^3) 465 (4.0×10^3 sh) 713 (1.1×10^3)
	1.0×10^{-5}	383 (8.3×10^3) 465 (3.8×10^3 sh) 716 (1.0×10^3)
	DR	413 495 (sh) 660 (sh) 756
24	1.0×10^{-3}	373 (8.8×10^3) 460 (4.6×10^3 sh) 697 (8.0×10^2)
	1.0×10^{-4}	373 (7.5×10^3) 460 (4.5×10^3 sh) 702 (7.5×10^2)
	1.0×10^{-5}	369 (6.2×10^3) 455 (4.0×10^3 sh) 706 (6.0×10^3)
	DR	392 455 708 820 (sh)
25	1.0×10^{-3}	371 (7.7×10^3) 460 (4.7×10^3 sh) 697 (8.2×10^2)
	1.0×10^{-4}	371 (7.6×10^3) 460 (4.7×10^3 sh) 694 (8.0×10^2)
	1.0×10^{-5}	369 (6.9×10^3) 460 (4.4×10^3 sh) 689 (7.1×10^2)
	DR	392 480 (sh) 719 820 (sh)
26	1.0×10^{-3}	369 (8.4×10^3) 460 (4.9×10^3 sh) 700 (8.7×10^2)
	1.0×10^{-4}	368 (8.4×10^3) 460 (4.9×10^3 sh) 700 (8.5×10^2)
	1.0×10^{-5}	366 (7.6×10^3) 455 (4.7×10^3 sh) 709 (8.0×10^2)
	DR	402 467 708 825 (sh)
27	1.0×10^{-3}	372 (7.1×10^3) 460 (3.7×10^3 sh) 722 (9.8×10^2)
	1.0×10^{-4}	373 (6.5×10^3) 460 (3.5×10^3 sh) 721 (8.1×10^2)
	1.0×10^{-5}	374 (4.5×10^3) 455 (2.9×10^3 sh) 704 (3.9×10^2)
	DR	395 (sh) 490 725 (sh) 844
28	1.0×10^{-3}	378 (4.5×10^3) 455 (3.4×10^3 sh) 721 (4.5×10^2)
	1.0×10^{-4}	390 (4.0×10^3) 450 (3.2×10^3 sh)
	1.0×10^{-5}	401 (3.5×10^3) 455 (2.9×10^3 sh)
	DR	401 480 (sh) 708 805 (sh)
29	1.0×10^{-3}	368 (4.9×10^3) 450 (3.5×10^3 sh) 717 (4.8×10^2)
	1.0×10^{-4}	367 (4.4×10^3) 445 (3.4×10^3 sh) 717 (3.2×10^2)
	1.0×10^{-5}	395 (3.2×10^3) 440 (2.9×10^3 sh)
	DR	405 468 725 835 (sh)
30	1.0×10^{-3}	371 (5.6×10^3) 445 (4.0×10^3 sh) 723 (6.1×10^2)
	1.0×10^{-4}	370 (5.1×10^3) 445 (3.7×10^3 sh) 724 (3.7×10^2)
	1.0×10^{-5}	388 (3.6×10^3) 445 (3.1×10^3 sh)
	DR	380 445 723 835 (sh)

In the quinolinethiolato complex **27** with catecholate and PPh_3, the concentration dependence was observed under 10^{-3} mol dm^{-3} (Figure V-13). As in the case of other complexes, the band observed in 722 nm would be assigned to d–d transition ($5d_{xy} \rightarrow d_{yz, zx}$) and the band observed in 372 nm would be assigned to PPh_3–Re LMCT transition.[10,35] The equilibrium constant of **27** (ca. 1×10^5 dm^3 mol^{-1}) was determined by the spectra that the lowest concentration condition spectrum (1.0×10^{-5} mol dm^{-3}) in **28** was applied for the spectrum of the five-coordinated state. The quinolinethiolato complexes (**28**–**30**) with catecholate and pyridine derivatives also showed the concentration dependence in this concentration conditions (1.0×10^{-3}–1.0×10^{-5} mol dm^{-3}) (Figures V-14–V-16, respectively). The two bands which glow with concentration at ca. 720 and ca. 370 nm would be assigned to d–d transition ($5d_{xy} \rightarrow d_{yz, zx}$) and py–Re LMCT transition, respectively.[10,35] The equilibrium constants of **28**–**30** (ca. 1×10^3 dm^3 mol^{-1}) were determined by the absorption spectra. The spectra, which were added the excess of free pyridine derivatives to each complex, were applied for the spectra of the six-coordinated state. The equilibrium constants of the quinolinethiolato complexes **23**–**26** with tetrachlorocatecholate are more than three orders of magnitude larger than *K* of the corresponding quinolinethiolato complexes **27**–**30** with catecholate. These differences suggest that the influence of the substituent group on catechol ligand appear in the electrophilicity of metal center as observed in the relationship between the quinolinylamido complex with tetrachlorocatecholate [ReO(Cl_4cat)(Hamq)(PPh_3)] **14** and the quinolinylamido complex with catecholate [ReO(cat)(Hamq)(PPh_3)] **13**. The equilibrium constants of the quinolinethiolato complexes **23** ($K >> 10^5$ dm^3 mol^{-1}) and **27** (ca. 1×10^5 dm^3 mol^{-1}) are more than three orders of magnitude larger than *K* of the corresponding quinolinylamido complexes **14** ($K = 1.0 \times 10^4$ dm^3 mol^{-1}) and **13** ($K = 52$ dm^3 mol^{-1}). From these results, the lower OAT catalytic property of the quinolinethiolato complex **23** is expected.

$^{31}P\{^1H\}$ NMR Spectra The $^{31}P\{^1H\}$ NMR spectra of **23** and **27** were measured by using PPh_3 as an external reference (δ -7.4) in $CDCl_3$. The chemical shift of PPh_3 in **23** (δ -1.7) and **27** (δ -0.1) are shifted from that of free PPh_3. These shifts coincide with the results of the electronic absorption spectra, that is, the PPh_3 ligands would keep the bond with metal center in measurement condition (ca. 2×10^{-3} mol dm^{-3}). These shifts from free PPh_3 were larger than the case of corresponding quinolinylamido complexes **14** (δ -4.2) and **13** (δ -7.4). It is assumed that the cause of the difference in the extent of shift may be less of the coordination condition of phosphorus atom in the six-coordinated state complex than the releasing property of PPh_3 from metal center. This agrees with the result of electronic absorption spectra.

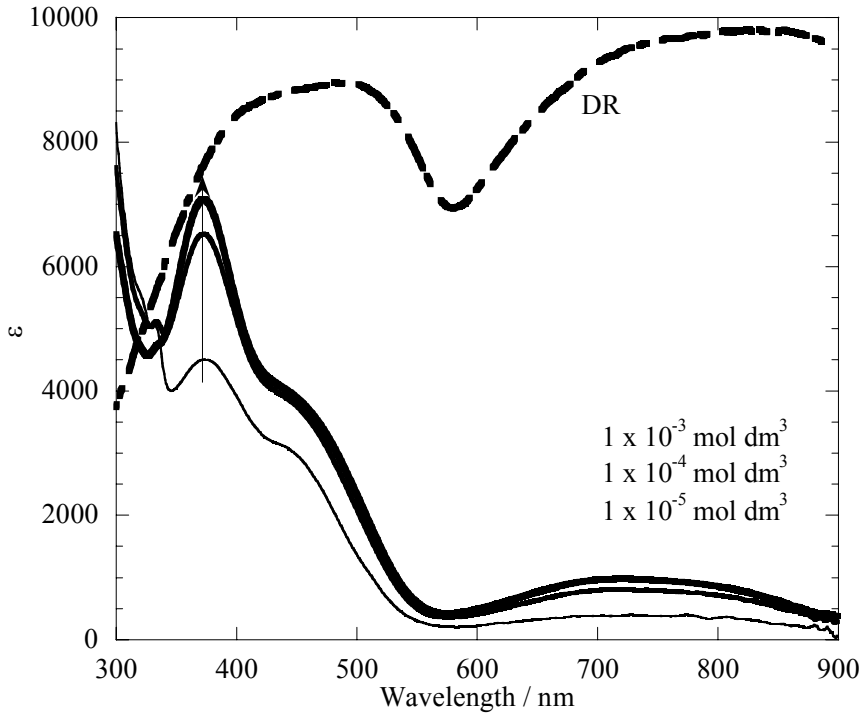

Figure V-13 Electronic absorption spectra of [ReO(cat)(Sq)(PPh_3)] **27** in some concentration conditions in CH_2Cl_2.

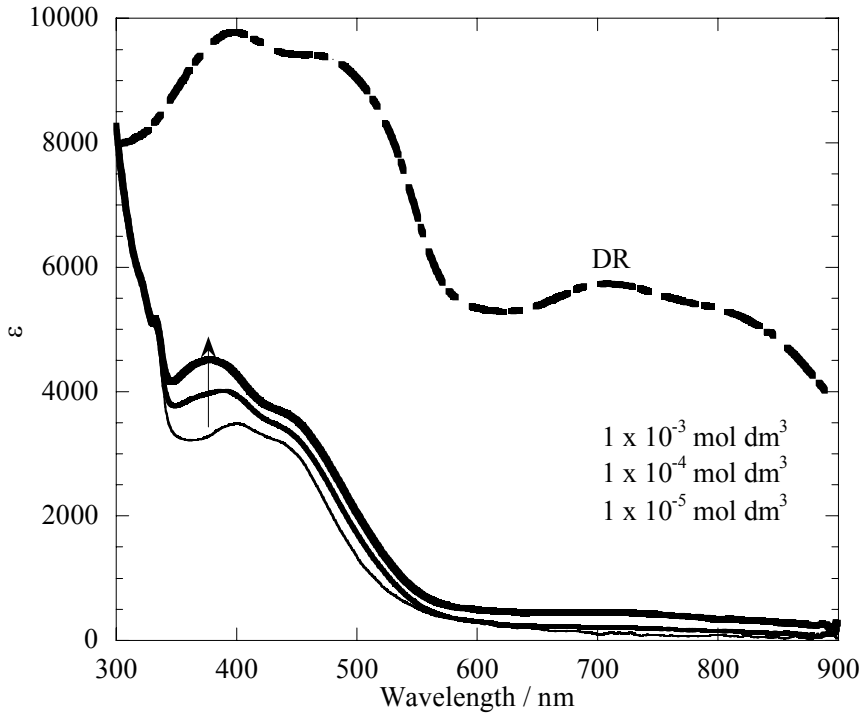

Figure V-14 Electronic absorption spectra of [ReO(cat)(Sq)(py)] **28** in some concentration conditions in CH_2Cl_2.

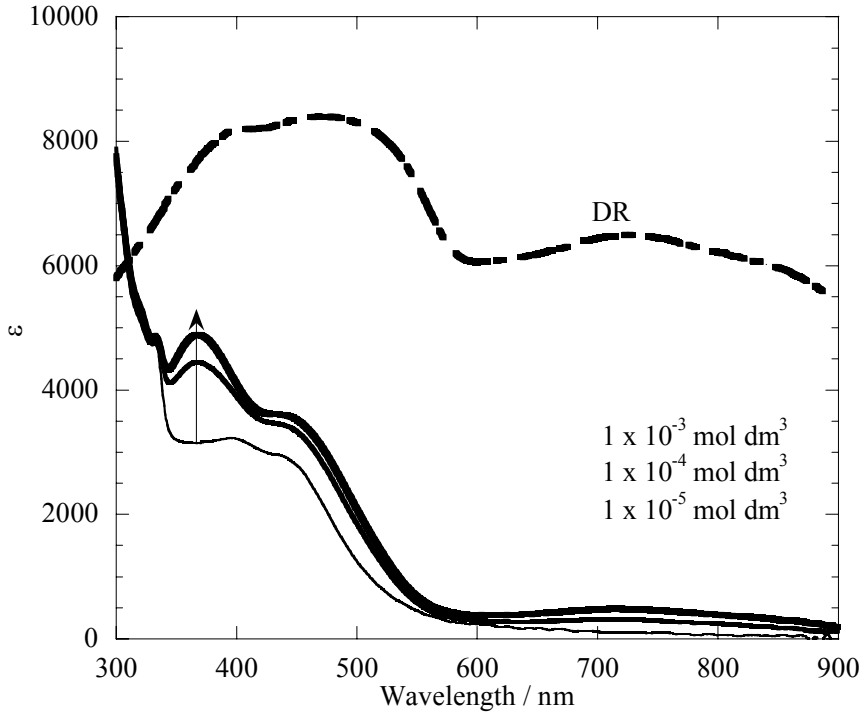

Figure V-15 Electronic absorption spectra of [ReO(cat)(Sq)(4-Mepy)] **29** in some concentration conditions in CH_2Cl_2.

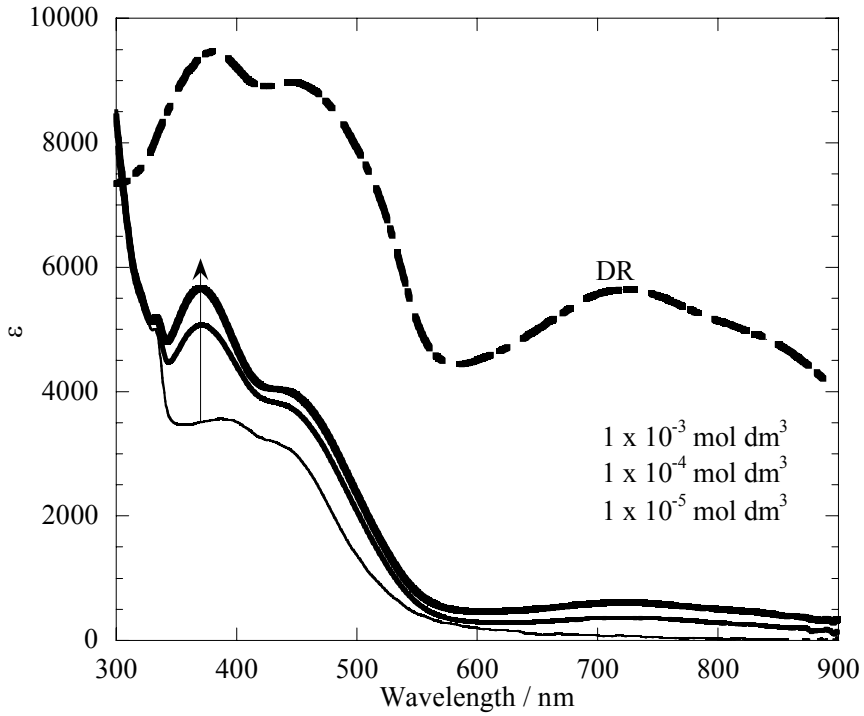

Figure V-16 Electronic absorption spectra of [ReO(cat)(Sq)(4-*t*-Bupy)] **30** in some concentration conditions in CH_2Cl_2.

V-vi. OAT Catalytic Reactivity of 23, 27

Though the quinolinethiolato complex with tetrachlorocatecholate [ReO(Cl_4cat)(Sq)(PPh_3)] **23** showed lesser releasing property than the corresponding quinolinylamido complex **14**, the OAT catalytic reactivity of **23** from 2,6-lutidine-*N*-oxide (2,6-Me_2pyO) to PPh_3 in Eq. V-8 was studied analogously to that of **14**. The OAT catalytic reactions of **23** were monitored by electronic absorption

$$PPh_3 + 2,6\text{-}Me_2pyO \xrightarrow{catalyst} OPPh_3 + 2,6\text{-}Me_2py \qquad (V\text{-}8)$$

spectra in CH_2Cl_2 at 23 ˚C (Eq. V-8). The progression of reaction was obtained by converting absorbance to 2,6-Me_2pyO concentration according to Eq. V-9.

$$[2,6\text{-}Me_2pyO]_t = [2,6\text{-}Me_2pyO]_0 \frac{Abs_t - Abs_\infty}{Abs_0 - Abs_\infty} \qquad (V\text{-}9)$$

When oxygen donor 2,6-Me_2pyO was added to the solution of **23** without PPh_3, the color gradually turned from orange to dark purple, which is catalytic active state. The electronic absorption spectrum of the active state showed new intense peak at 505 nm and new shoulder at 600 nm (Figure V-17). From the new intense band at 505 nm which is characteristic band for dioxorhenium(VII), the active state would be dioxorhenium(VII) [ReO_2(Cl_4cat)(Sq)] in analogy with **14**.[28,36] In the change of active state spectra with time in **23**, two major differences from that in **14** were observed. First, the formation of active state in **14** was too fast to measure the formation process, whereas the active state of **23** gradually formed by spending about 30 min (Figure V-17). Second, the active state of **14** showed slow decomposition in the PPh_3 absence condition, whereas the active state of **23** was more stable and the decomposition was not observed during one night. From the slow formation and stability of active state, though the catalytic lifetime in **23** would be expected to be greater than that in **14**, the catalytic reaction rate in **23** would be expected to be slower than that in **14**.

The progress of the OAT catalytic reaction in **23** was traced by the observation of the change of absorbance at 310 nm in a cell with a 1 mm optical path different from the case of **14** (observed in 325 nm in a cell with a 1 cm optical path). This modification was caused by the change of concentration of the catalyst complex **23** from 10^{-5} mol dm^{-3} to 10^{-4} mol dm^{-3} order. In this condition, the influence of the absorbance of the catalyst becomes large at 325 nm. Therefore, 310 nm, where absorbance is largely contributed by the absorbance of 2,6-Me_2pyO, was selected for monitoring wavelength. The OAT catalytic reaction was measured under a variety of the concentration conditions. Then the initial

rates (v_0) were obtained from the concentration–time curve fitting with least squares program. The data, when the extent of reaction was from 10 to 20%, were used for fitting (Table V-6), since the absorbance change in early phase of catalytic reaction was instable. This instability may be due to the absorbance change of catalyst or insufficiency of diffusion of reaction solution by using a thin cell (1 mm).[37] As a result of the measurement, the initial rates were proportional to the concentrations of the catalyst **23** and 2,6-Me_2pyO, whereas the initial rate was inversely proportional to the concentration of PPh_3. Therefore, the initial rate equation is determined as Eq. V-10. Its form is further tested by a plot of all the values of v_0 against the composite concentration variable. The data are in agreement with this model, as shown in Figure V-18, and least-square fitting affords $k_c = 3.1 \times 10^{-2}$ s^{-1} at 23 ˚C in CH_2Cl_2. Therefore, the reaction cycle is supposed to Scheme V-2 analogously to the case of **14**, whereas the total reaction rate constant of the OAT reaction, from 2,6-Me_2pyO to PPh_3 with **23**, was 60 times smaller than **14**. This lower reactivity would be caused by the slow formation and stability of active state as expected in above.

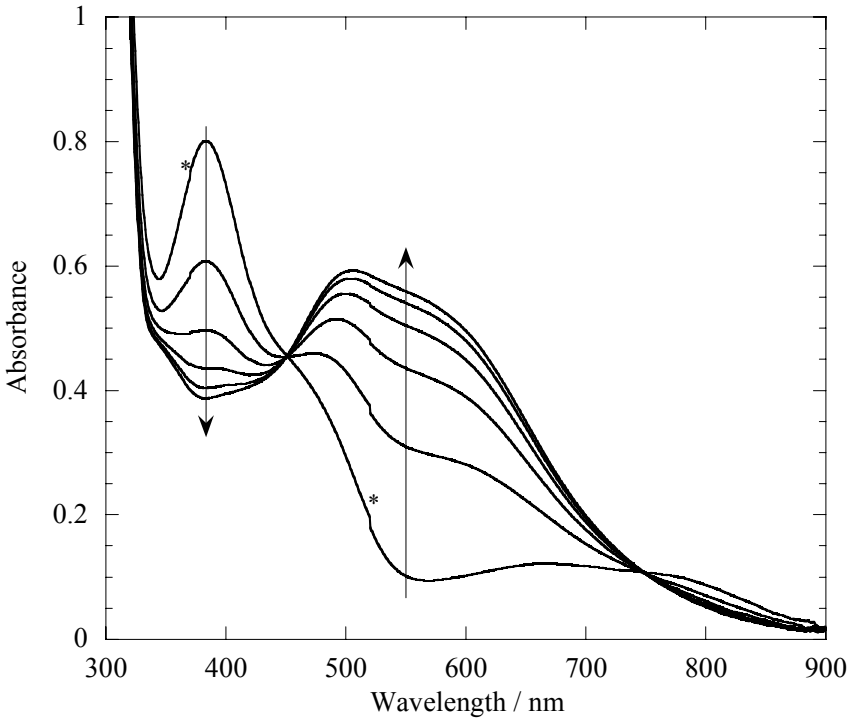

Figure V-17 The increase of the absorbance of dioxorhenium intermediate (mixture of **23** (1×10^{-4} mol dm^{-3}) and 2,6-Me_2pyO (1×10^{-2} mol dm^{-3})) in CH_2Cl_2. The spectra are shown in 5 min interval. *: Artifact

Table V-6 Initial reaction rate data for the oxidation of PPh_3 by 2,6-Me_2pyO catalyzed by **23**

[**23**] / 10^{-4} mol dm^{-3}	[PPh_3] / 10^{-2} mol dm^{-3}	[2,6-Me_2pyO] / 10^{-2} mol dm^{-3}	v_0 / 10^{-5} mol dm^{-3} s^{-1}
0.50	1.0	1.0	0.18
1.0	1.0	1.0	0.34
2.0	1.0	1.0	0.66
4.0	1.0	1.0	1.2
1.0	0.50	1.0	0.50
1.0	2.0	1.0	0.18
1.0	1.0	0.50	0.13
1.0	1.0	2.0	0.58

$$v_0 = k_c \frac{[\text{catalyst}][2,6\text{-Me}_2\text{pyO}]}{[PPh_3]} \qquad \text{(V-10)}$$

Scheme V-2

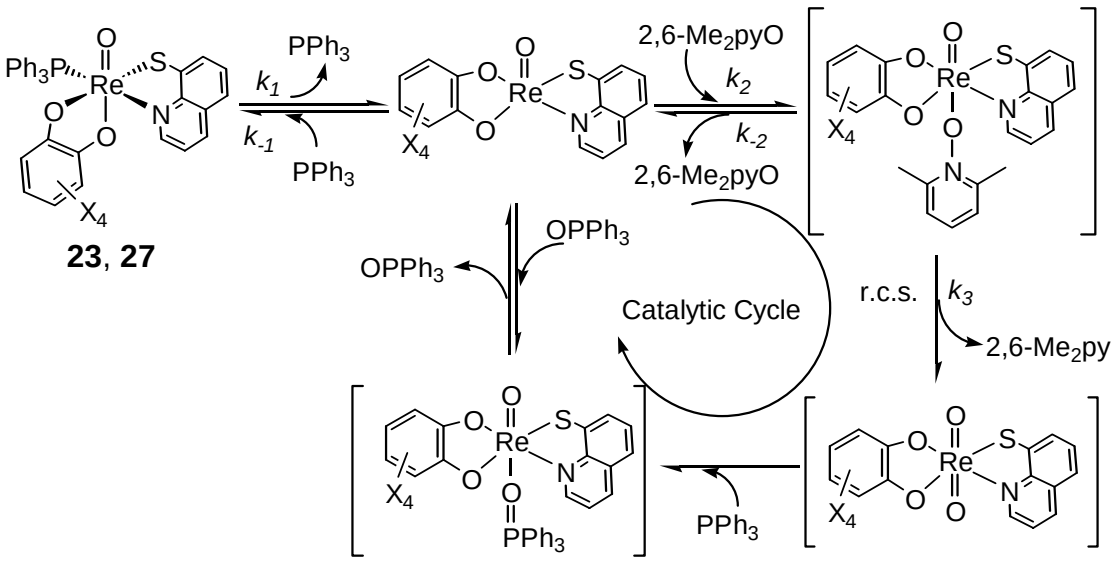

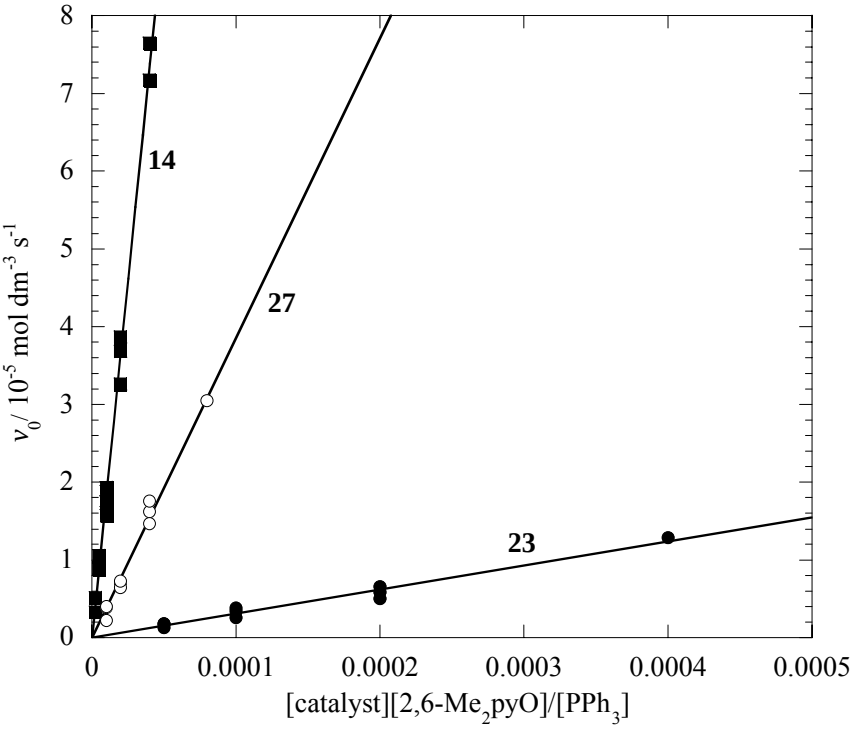

Figure V-18 The initial rates of reaction dependence on combined concentration variable, as in Eq. V-10 (**14**, closed square; **23**, closed circle; **27**, open circle).

Additionally, the OAT catalytic reactivity of the quinolinethiolato complex with non-substituted catecholate [ReO(cat)(Sq)(PPh_3)] **27** was investigated, since **27** showed higher releasing property than **23**, and higher catalytic reactivity was expected. The OAT catalytic reactions from 2,6-Me_2pyO to PPh_3 were monitored by electronic absorption spectra in CH_2Cl_2 at 23 ˚C, and the progression of reaction was obtained by converting absorbance to 2,6-Me_2pyO concentration according to Eq. V-9 analogously to the previous studies (**14** and **23**).

When oxygen donor 2,6-Me_2pyO was added to the solution of **27** without PPh_3, the color turned from orange to dark purple which is catalytic active state, within 1 min. The electronic absorption spectrum of the active state showed new intense peak at 477 nm which is characteristic band for dioxorhenium(VII).[28,36] Therefore, the active state would be dioxorhenium(VII) [ReO_2(cat)(Sq)] in analogy with **14** or **23**. Though the higher catalytic property is expected from the faster formation of active state, the active state of **27** was also stable similar to **23**.

The progress of the OAT catalytic reaction in **27** was traced by the observation of the change of absorbance at 325 nm in cell with a 1 cm optical path. The OAT catalytic reaction was measured under a variety of the concentration conditions, and the initial rates (v_0) were obtained from the concentration–time curve fitting with least squares program (Table V-7). As a result of the

Table V-7 Initial reaction rate data for the oxidation of PPh_3 by 2,6-Me_2pyO catalyzed by **27**

[**27**] / 10^{-5} mol dm^{-3}	[PPh_3] / 10^{-2} mol dm^{-3}	[2,6-Me_2pyO] / 10^{-2} mol dm^{-3}	v_0 / 10^{-5} mol dm^{-3} s^{-1}
1.0	1.0	1.0	0.38
2.0	1.0	1.0	0.70
4.0	1.0	1.0	1.6
8.0	1.0	1.0	3.1
2.0	0.50	1.0	1.8
1.0	2.0	1.0	0.40
1.0	1.0	0.50	0.22
1.0	1.0	2.0	15

measurement, the initial rates were proportional to the concentrations of the catalyst **27** and 2,6-Me_2pyO, whereas the initial rate was inversely proportional to the concentration of PPh_3 similarly to the cases of **14** and **23**. Therefore, the initial rate equation is determined as Eq. V-10, and the data are in agreement with this model, as shown in Figure V-18. The least-square fitting affords $k_c = 0.38$ s^{-1} at 23 ˚C in CH_2Cl_2. Then, the reaction cycle is supposed to Scheme V-2 analogously to the case of **14** and **23**. The total reaction rate constant, from 2,6-Me_2pyO to PPh_3 with **27** ($k_c = 0.38$ s^{-1}), was about 12 times higher than **23** ($k_c = 3.1 \times 10^{-2}$ s^{-1}). On the other hand, k_c in **27** was about 5 times lower than that in **14** ($k_c = 1.8$ s^{-1}). The total rate constants, from 2,6-Me_2pyO to PPh_3, of the quinolinethiolato complexes **23** ($k_c = 3.1 \times 10^{-2}$ s^{-1}) and **27** ($k_c = 0.38$ s^{-1}) are lower than that of the methylated oxorhenium(V) complex [MeRe(mtp)(PPh_3)] ($k_c = 6.0$ dm^3 mol^{-1} s^{-1}).[37] The initial rate of **27** ($v_0 = 3.8 \times 10^{-6}$ mol dm^{-3} s^{-1}), however, will be about 6 times faster than that of [MeReO(mtp)(PPh_3)] ($v_0 = 6.0 \times 10^{-7}$ mol dm^{-3} s^{-1}) in an experimental condition (for example; catalyst (1×10^{-5} mol dm^{-3}), PPh_3 (1×10^{-2} mol dm^{-3}), and 2,6-Me_2pyO (1×10^{-2} mol dm^{-3})).[37] Even in the case of **23**, whose total rate constant was 200 times lower than that of the methylated oxorhenium(V) complex, the initial rate ($v_0 = 3.1 \times 10^{-7}$ mol dm^{-3} s^{-1}) will be near to the case of [MeReO(mtp)(PPh_3)].[37] The discrepancies of the relationship between k_c and v_0 are caused by the difference in the rate equations (quinolinethiolato complexes, $v_0 = k_c$[2,6-Me_2pyO][catalyst][PPh_3]$^{-1}$; [MeReO(mtp)(PPh_3)], $v_0 = k_c$[2,6-Me_2pyO]^2-[catalyst][PPh_3]$^{-1}$). This means that the initial rates of quinolinethiolato complexes are a match for the methylated oxorhenium(V) complex, in low concentration condition.

From the viewpoint of catalytic reactivity, the quinolinethiolato complexes **23** and **27** were inferior to the quinolinylamido complex **14**, whereas **23** and **27** are far superior to **14** or other oxorhenium(V) complexes with OAT catalytic reactivity from the standpoint of the stability of active state. The decomposition of catalytic active state (dioxorhenium(VII)), in the absent of PPh_3, was also observed

in the methylated oxorhenium(V) complexes.[28,36-38] Therefore, it could be said that the quinolinethiolato complexes **23** and **27** have a long lifetime, and it is easier to treatment than **14** or other oxorhenium(V) complexes with OAT catalytic reactivity.

V-vii. Conclusion

The catecholato derivatives coordinated complexes [ReO(Cl_4cat)(Sq)(PPh_3)] **23** and [ReO(cat)(Sq)(PPh_3)] **27** were synthesized by the reaction of [$ReOCl_2$(Sq)(PPh_3)] **21** with catechol derivatives for improving the releasing property. From the substitution reaction, though the pyridine derivatives substituted complexes [ReO(Cl_4cat)(Sq)(L)] **24**–**26** and [ReO(cat)(Sq)(L)] **28**–**30** were obtained, $OPPh_3$ substituted complexes were not isolated different from the quinolinylamido complex. The X-ray crystal analyses of [ReO(Cl_4cat)(Sq)(PPh_3)] **23**, [ReO(Cl_4cat)(Sq)(4-Mepy)] **26**, and [ReO(cat)(Sq)(4-Mepy)] **29** revealed that the coordination geometries of them are similar to those of the corresponding quinolinylamido complexes [ReO(Cl_4cat)(Hamq)(PPh_3)] **14**, [ReO(Cl_4cat)(Hamq)(4-*t*-Bupy)] **18**, and [ReO(Cl_4cat)(Hamq)(4-Mepy)] **17**. From the results of spectroscopic studies, it was revealed that the quinolinethiolate complexes **23**–**30** with catecholate derivatives have the releasing property in solution though weaker than the quinolinylamido complexes with catecholate derivatives. The OAT catalytic properties of **23** and **27** were monitored by electronic absorption spectra, and the reaction path would be the same as that of **14**. The total reaction rate constants (k_c) in quinolinethiolato complexes **23** and **27** were smaller than that in quinolinylamido complex **14**, whereas the stabilities of active state in **23** and **27** were dominant over that in **14** or other oxorhenium(V) complexes with OAT catalytic reactivity. Therefore, it would be said that the stability of the active state in the quinolinethiolato complexes is significant characteristic.

References

1 J. Jacob, I. A. Guzei, and J. H. Espenson, *Inorg. Chem.*, **38**, 1040 (1999).

2 Y. Cai, A. Ellern, and J. H. Espenson, *Inorg. Chem.*, **44**, 2560 (2005).

3 P. Bouziotis, D. Papagiannopoulou, I. Pirmettis, M. Pelecanou, C. P. Raptopoulou, C. I. Stassinopoulou, A. Terzis, M. Friebe, H. Spies, M. Papadopoulos, and E. Chiotellis, *Inorg. Chim. Acta*, **320**, 174 (2001).

4 X. Shan, A. Ellern, I. A. Guzei, and J. H. Espenson, *Inorg. Chem.*, **43**, 3854 (2004).

5 E. Shuter, H. R. Hoveyda, V. Karunaratne, S. J. Rettig, and C. Orvig, *Inorg. Chem.*, **35**, 368 (1996).

6 J. M. Botha, K. Umakoshi, Y. Sasaki, and G. J. Lamprecht, *Inorg. Chem.*, **37**, 1609 (1998).

7 X. Chen, F. J. Femia, J. W. Babich, and J. Zubieta, *Inorg. Chim. Acta*, **308**, 80 (2000).

8 A. Imai, Master Thesis, University of Tsukuba (2004).

9 N. P. Johnson, C. J. L. Lock, and G. Wilkinson, *Inorg. Synth.*, **9**, 145 (1967).

10 F. Refosco, F. Tisato, G. Bandoli, C. Bolzati, A. Moresco, and M. Nicolini, *J. Chem. Soc., Dalton Trans.*, 605 (1993).

11 CrystalCrear, J. W. Pflugrath, *Acta Crystallogr., Sect. D*, **55**, 1718 (1999).

12 A. Altomare, M. Burla, M. Camalli, G. Cascarano, C. Giacovazzo, A. Guagliardi, A. Moliterni, G. Polidori, and R. Spagna, *J. Appl. Crystallogr.*, **32**, 115 (1999).

13 G. M. Sheldrick, SHELX97 Program for Crystal Structure Refinement from Diffraction Data, University of Göttingen, Göttingen, Germany (1997).

14 P. T. Beurskens, G. Admiraal, G. Beurskens, W. P. Bosman, R. de Gelder, R. Israel, and J. M. M. Smits, The DIRDIF-99 Program System, Technical Report of the Crystallography Laboratory, University of Nijmegen, The Netherlands (1999).

15 P. T. Beurskens, G. Admiraal, G. Beurskens, W. P. Bosman, S. Garcia-Granda, R. O. Gould., J. M. M. Smits, and C. Smykalla, The DIRDIF Program System, Technical Report of the Crystallography Laboratory, University of Nijmegen, The Netherlands (1999).

16 CrystalStructure 3.5.1: Crystal Structure Analysis Package, Rigaku and Rigaku/MSC, 2000-2003.

17 D. W. Lahti and J. H. Espenson, *J. Am. Chem. Soc.*, **123**, 6014 (2001).

18 M. M. Abu-Omar and S. I. Khan, *Inorg. Chem.*, **37**, 4979 (1998).

19 C. F. Edwards, W. P. Griffith, A. J. P. White, and D. J. Williams, *J. Chem. Soc., Dalton*

Trans., 957 (1992).

20 L. Hansen, E. Alessio, M. Iwamoto, P. A. Marzilli, and L. G. Marzilli, *Inorg*. *Chim*. *Acta*, **240**, 413 (1995).

21 G. Bandoli, A. Dolmella, T. I. A. Gerber, J. Perils, and J. G. H. du Preez, *Inorg*. *Chim*. *Acta*, **294**, 114 (1999).

22 G. Battistuzzi, M. Cannio, M. Saladini, and R. Battistuzzi, *Inorg*. *Chim*. *Acta*, **320**, 178 (2001).

23 T. Głowiak, W. K. Rybak, and A. Skarżyńska, *Polyhedron*, **19**, 2667 (2000).

24 A. Skarżyńska, W. K. Rybak, and T. Głowiak, *Polyhedron*, **20**, 2667 (2001).

25 C. Bolzati, F. Tisato, F. Refosco, G. Bandoli, and A. Dolmella, *Inorg*. *Chem*., **35**, 6221 (1996).

26 T. I. A. Gerber, J. Bruwer, G. Bandoli, J. Perils, and J. G. H. du Preez, *J*. *Chem*. *Soc*., *Dalton Trans*., 2189 (1995).

27 J. R. Dilworth, D. V. Griffithe, S. J. Parrott, and Y. Zheng, *J*. *Chem*. *Soc*., *Dalton Trans*., 2931 (1997).

28 J. Arias, C. R. Newlands, and M. M. Abu-Omar, *Inorg*. *Chem*., **40**, 2185 (2001).

29 J. M. Mayer, D. L. Thorn, and T. H. Tulip, *J*. *Am*. *Chem*. *Soc*., **107**, 7454 (1985).

30 S. Bélanger and A. L. Beauchamp, *Inorg*. *Chem*., **35**, 7836 (1996).

31 S. Bélanger and A. L. Beauchamp, *Inorg*. *Chem*., **36**, 3640 (1997).

32 S. Fortin and A. L. Beauchamp, *Inorg*. *Chem*., **39**, 4886 (2000).

33 I. Chakraborty, S. Bhattacharyya, S. Banerjee, B. K. Dirghangi, and A. Chakravorty, *J*. *Chem*. *Soc*., *Dalton Trans*., 3747 (1999).

34 J. T. Goodman and T. B. Rauchfuss, *Inorg*. *Chem*., **37**, 5040 (1998).

35 J. T. Goodman, S. Inomata, and T. B. Rauchfuss, *J*. *Am*. *Chem*. *Soc*., **118**, 11647 (1996).

36 M. M. Abu-Omar, L. D. McPherson, J. Arias, and V. M. Béreau, *Angew*. *Chem*., *Int*. *Ed*., **39**, 4310 (2000).

37 Y. Wang and J. H. Espenson, *Inorg*. *Chem*., **41**, 2266 (2002).

38 J. H. Espenson, *Coord*. *Chem*. *Rev*., **249**, 329 (2005).

Chapter VI. Summary

Oxorhenium(V) compounds have received much attention widely from nuclear pharmacy, biology, and industry. In order to accelerate the application of the oxorhenium(V) complexes to useful nuclear pharmacy or catalyst, the study in these fields has required structural information such as stereoselective coordination, spectroscopic properties, and reactivity including stability and catalytic property. In this context, the controlling of coordination geometry and the application of unusual reactivity to catalyst have been studied by using asymmetrical didentate ligands quinoline derivatives. It was revealed that the change of the substituent groups on the 8-position of quinoline derivatives influences the reactivity, and the change of other parts, except for the oxo ligand and didentate quinoline derivatives, affect the coordination geometry.

In Chapter II, the didentate-*N*,*N* ligands 8-aminoquinoline derivatives (H_2amq or H_2aq) were used as an asymmetrical ligand. The quinolinylamido complexes showed concentration dependence in electronic absorption spectra. As results of spectroscopic measurements, it was revealed that the quinolinylamido complexes have releasing property in solution. Though many oxorhenium(V) complexes have been investigated so far, few complexes have higher releasing property of the monodentate ligand than the present complexes. The substitution reactions from the PPh_3 to $OPPh_3$ or pyridine derivatives were performed by using the easy releasing property. The results of the X-ray crystal analyses revealed that the changes of the coordination geometry around the oxorhenium(V) core accompanied substitution reactions of PPh_3 to $OPPh_3$ or pyridine derivatives. The OAT catalytic reactivity from pyridine oxide derivatives to PPh_3 was also observed by using the replacement property. Though the catalyst lifetime was short, the OAT catalytic property is rare for the non-methylated oxorhenium(V) complexes. The catalytic property on the non-methylated oxorhenium(V) complexes is very interesting from the viewpoint of application for catalyst.

In Chapter III, the catecholate derivatives were introduced in the quinolinylamido complex obtained in Chapter II. From the spectroscopic measurements, it was revealed that catecholato coordinated complexes also release the monodentate ligand PPh_3 in solution. The substitution reaction was also observed. The coordination geometries of the obtained complexes were determined by the X-ray crystal analyses and the various spectroscopic results. The OAT catalytic reactivity of the quinolinylamido complex with tetrachlorocatecholate was improved from the viewpoint of catalyst lifetime. This improvement would be due to the stabilization of the quinolinylamido complex by the chelate effect of catecholate.

In Chapter IV, the didentate-*N*,*O* ligand 8-hydroxy-2-methylquinoline (Hhmq) was used as an asymmetrical didentate ligand, instead of the didentate-*N*,*N* ligand 8-amino-2-methylquinoline in the previous chapters. The coordination geometries of the quinolinolato complexes were determined by the X-ray crystal analyses and they were characterized by the various spectroscopic results. The results of spectroscopic analyses showed that these complexes keep the six-coordinated state in solution. The quinolinolato complex did not show the substitution reactivity and OAT catalytic reactivity as expected from the results of spectroscopy.

In Chapter V, the quinolinethiolato complexes with catecholate derivatives were synthesized from the reaction between the didentate-*N*,*S* ligand 8-quinolinethiolate (Sq) containing complex and catecholate derivatives similar to the quinolinylamido complexes with catecholate derivatives. The releasing property of the quinolinethiolato complexes with catecholate derivatives was weaker than the corresponding quinolinylamido complexes, but it was improved in comparison with the starting quinolinethiolate complex. The substitution reaction was observed as expected from the releasing property. The coordination geometries of the obtained complexes were determined by the X-ray crystal analyses and the various spectroscopic results. The OAT catalytic reactivity of quinolinethiolato complex with tetrachlorocatecholate was weaker than that of the corresponding quinolinylamido complex. The slow progression of catalytic cycle would be caused by the slow formation of the catalytic active state, which may be dioxo state. In contrast, the stability of the catalytic active state in the quinolinethiolato complex with tetrachlorocatecholate was much superior to that in the corresponding quinolinylamido complex.

The influence, which is caused by the change of the coordination atom (*N*, *O*, *S*) on 8-position of quinoline derivatives, was observed in the structures. The coordination geometry of the quinolinylamido complex $[ReOCl_2(Hamq)(PPh_3)]$ **1** and the quinolinolato complex $[ReOCl_2(hmq)(PPh_3)]$ **19** (the *trans* position to the oxo ligand was occupied by amide or phenolate) was different from that of the quinolinethiolato complex $[ReOCl_2(Sq)(PPh_3)]$ **21** (the *trans* position to the oxo ligand was occupied by chloride). This difference may be caused by the *trans* influence of the thiolate ligand in **21**. Namely, the strong *trans* influence between the oxo ligand and thiolate ligand may make difficult to keep the *trans* position each other. In the measurements of electronic absorption spectra, the influence of the difference in the didentate ligand was also observed. The quinolinylamido complexes series and the quinolinethiolato complexes series showed the concentration dependence, whereas the quinolinolato complex did not show the concentration dependence. This tendency was reflected in the reactivity of complexes. That is, the substitution reaction and OAT catalytic reaction

were observed in the quinolinylamido complexes and the quinolinethiolato complexes. On the other hand, the substitution reaction and OAT catalytic reaction were not observed in the quinolinolato complex. The distinction of the reactivity may be caused by the tendency that the oxorhenium(V) complexes with soft base ligand prefer to have the five-coordinated state, whereas the oxorhenium(V) complexes with hard base ligand prefer to keep the six-coordinated state.

The asymmetrical didentate ligand, quinoline derivatives, introduced complexes showed various stereoselective coordinations with the corresponding monodentate ligands. The revealed stereoselectivity would be useful for the design of the radiopharmaceuticals or other functional compounds. The most important result of introducing the asymmetrical didentate ligand was the high releasing property, which was not observed in other oxorhenium(V) complexes and the OAT catalytic reactivity. In particular, the OAT catalytic property of the catecholato complexes showed high performance. The OAT catalytic reaction rate of the quinolinylamido complex **14** with tetrachlorocatecholate was comparable with that of the methylated oxorhenium(V) complex [MeReO(mtp)(PPh_3)] in some conditions, and the stability of the catalytic active state in the quinolinethiolato complexes **23** and **27** with catecholate derivatives was far superior to that of the methylated oxorhenium(V) complex. From these results, the design of the non-methylated oxorhenium(V) complexes, which are superior to the methylated oxorhenium(V) complexes from the viewpoint of the OAT catalytic reaction rate and the stability, will be expected.

List of Publication

1 T. Ohashi, Y. Miyashita, Y. Yamada, K. Fujisawa, and K. Okamoto, "Selective Formation and Characterization of Oxorhenium(V) Complexes with 2-Methylquinolin-8-ylamido (Hamq). Interconversion between [$ReOX_2$(Hamq)(PPh_3)] and [$ReOX_2$(Hamq)($OPPh_3$)] (X = Cl, Br)", *Bull*. *Chem*. *Soc*. *Jpn*., **76**, 1199-1205 (2003).

2 Y. Miyashita, T. Ohashi, A. Imai, N. Amir, K. Fujisawa, and K. Okamoto, "Syntheses, Structures, and Properties of Oxorhenium(V) Complexes with 2-, 5-, and/or 7-Substituted 8-Quinolinolato Ligands", *Sci*. *Technol*. *Adv*. *Mater*., **6**, 660-666 (2005).

3 Y. Miyashita, T. Ohashi, A. Imai, N. Amir, K. Fujisawa, and K. Okamoto, "Dichlorooxo(quinoline-8-thiolato-κ^2N,S)(triphenylphosphine oxide-κO)rhenium(V) Acetone Solvate", *Acta Crystallogr*., *Sect*. *C*, **61**, m476-m478 (2005).

4 T. Ohashi, Y. Miyashita, N. Amir, K. Fujisawa, and K. Okamoto, "Oxygen Atom Transfer Catalytic Property of Oxorhenium(V) Complexes with 2-Methylquinolin-8-ylamide and Tetrachlorocatecholate", to be submitted.

Other

1 Y. Matsunaga, K. Fujisawa, N Ibi, M. Fujita, T. Ohashi, N. Amir, Y. Miyashita, K. Aika, Y. Izumi, and K. Okamoto, "Sulfur K-edge Extended X-ray Absorption Fine Structure Spectroscopy of Homoleptic Thiolato Complexes with Zn(II) and Cd(II)", *J*. *Inorg*. *Biochem*., **100**, 239-249 (2006).

Acknowledgment

The author wishes to express his deepest appreciation to Professor Ken-ichi Okamoto for his expert guidance and constant warm encouragement during his research work. Under his guidance, the author could learn much about the coordination chemistry and the other related fields. He is deeply grateful to Dr. Yoshitaro Miyashita for his helpful discussion and cordial support. He would also like to express his cordial gratitude to Dr. Kiyoshi Fujisawa for his precious advice and warm encouragement. He wants to express his thanks to Dr. Nagina Amir for her kind guidance to my English skill and valuable comments. He is very grateful to Dr. Yasunori Yamada for his much precious advice. He is also grateful to Mrs. Youko Koizumi for her warm assistance. He is grateful to Dr. Mitsuharu Fujita and Dr. Yuki Matsunaga for their warm assistance and their supports for his life in Tsukuba. He gives thanks to all the members of Inorganic Chemistry Laboratory for their kind help and excellent cooperation.

Finally, he wants to express his deep thanks to his parents and sister for their usual moral support, and this thesis is devoted to them.

February, 2006

Tetuya Ohashi